NASA-CR-164,297

NASA-CR-164297
19810014660

COLLEGE OF ENGINEERING

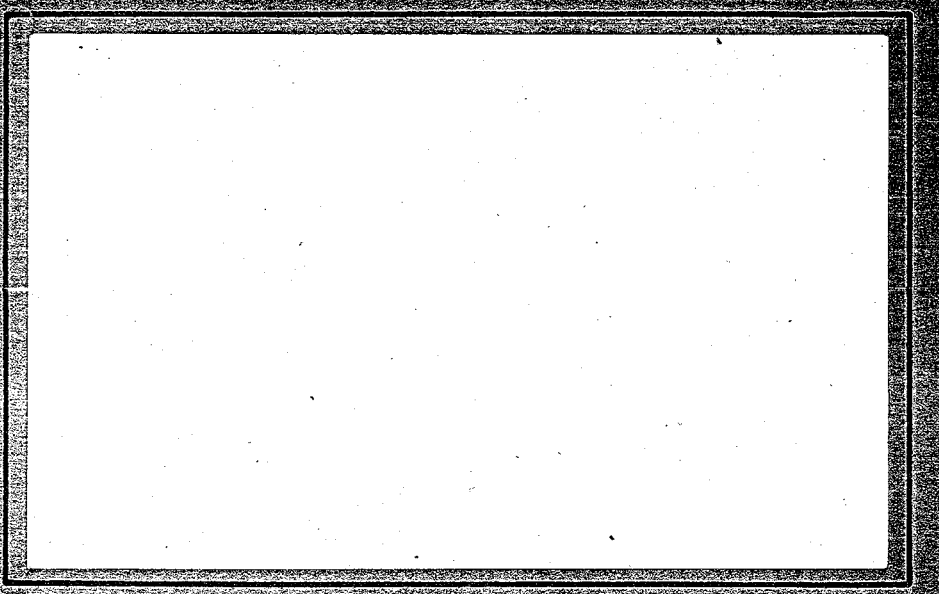

LIBRARY COPY
OCT 24 1992
LANGLEY RESEARCH CENTER
LIBRARY, NASA
HAMPTON, VIRGINIA

VIRGINIA POLYTECHNIC INSTITUTE AND STATE UNIVERSITY

NF01745

BLACKSBURG, VIRGINIA

DISPLAY 13/2/1

81N23193** ISSUE 14 PAGE 1882 CATEGORY 24 RPT#: NASA-CR-164297

VPI-E-81-3 CNT#: NCC2-71 NSG-2038 81/03/00 47 PAGES UNCLASSIFIED DOCUMENT

UTTL: Creep and creep rupture of laminated graphite/epoxy composites TLSP: Ph.D. Thesis. Final Report, 1 Oct. 1979 - 30 Sep. 1980

AUTH: A/DILLARD, D. A.; B/MORRIS, D. H.; C/BRINSON, H. F. PAA: A/(Missouri Univ., Rolla)

CORP: Virginia Polytechnic Inst. and State Univ., Blacksburg. CSS: (Dept. of Engineering Science and Mechanics.) AVAIL.NTIS

SAP: HC A03/MF A01

CIO: UNITED STATES

MAJS: /*CREEP RUPTURE STRENGTH/*CREEP TESTS/*GRAPHITE-EPOXY COMPOSITES/* LAMINATES/*MATHEMATICAL MODELS/*SHEAR STRESS

MINS: / FAILURE ANALYSIS/ FATIGUE (MATERIALS)

ABA: E.D.K.

ABS: An incremental numerical procedure based on lamination theory is developed to predict creep and creep rupture of general laminates. Existing unidirectional creep compliance and delayed failure data is used to develop analytical models for lamina response. The compliance model is based on a procedure proposed by Findley which incorporates the power law for creep into a nonlinear constitutive relationship. The matrix octahedral shear stress is assumed to control the stress interaction

ENTER: MORE

4BI

College of Engineering
Virginia Polytechnic Institute and State University
Blacksburg, VA 24061

VPI-E-81-3 March 1981

CREEP AND CREEP RUPTURE OF LAMINATED GRAPHITE/EPOXY COMPOSITES

by

Dillard, D. A.*, Research Associate
Morris, D. H., Associate Professor
Brinson, H. F., Professor

Department of Engineering Science and Mechanics
Virginia Polytechnic Institute and State University
Blacksburg, VA 24061

Prepared for:

National Aeronautics and Space Administration
Grant No. NASA-NSG 2038
Materials and Physical Sciences Branch
Ames Research Center
Moffett Field, CA 94035

*Now Assistant Professor of Engineering Mechanics, University of Missouri, Rolla, Missouri.
(This report is essentially the Ph.D. Dissertation of D. A. Dillard.)

N81-23193#

BIBLIOGRAPHIC DATA SHEET	1. Report No. VPI-E-81-3	2.	3. Recipient's Accession No.

4. Title and Subtitle
Creep and Creep Rupture of Laminated Graphite/Epoxy Composites

5. Report Date
March 1981

6.

7. Author(s)
Dillard, D. A., Morris, D. H., and Brinson, H. F.

8. Performing Organization Rept. No.

9. Performing Organization Name and Address
Department of Engineering Science and Mechanics
Virginia Polytechnic Institute and State University
Blacksburg, VA 24061

10. Project/Task/Work Unit No.

11. Contract/Grant No.
NCC 2-71

12. Sponsoring Organization Name and Address
NASA-Ames
Materials Science and Applications Office
Ames Research Center, 240-3
Moffett Field, CA 94035

13. Type of Report & Period Covered 10/1/79 to 9/30/80 - Final

14.

15. Supplementary Notes

16. Abstracts
See page i

17. Key Words and Document Analysis. 17a. Descriptors
Graphite/Epoxy, laminates, non-linear viscoelasticity, creep testing, creep rupture, accelerated characterization

17b. Identifiers/Open-Ended Terms

17c. COSATI Field/Group

18. Availability Statement	19. Security Class (This Report)	21. No. of Pages
Distribution unlimited	UNCLASSIFIED	228
	20. Security Class (This Page) UNCLASSIFIED	22. Price

FORM NTIS-35 (REV. 10-73) ENDORSED BY ANSI AND UNESCO. THIS FORM MAY BE REPRODUCED USCOMM-DC 8265-P74

ABSTRACT

Laminated fiber reinforced composite materials such as Graphite/Epoxy are generally designed using elastic considerations. Although graphite fibers are essentially elastic, the epoxy matrix behaves in a viscoelastic manner. The resulting Graphite/Epoxy composite material exhibits creep and delayed failures. Time dependent processes which are quite slow at room temperature are accelerated by higher temperatures and other factors. Assuming the applicability of the Time Temperature Superposition Principle (TTSP) concept, short term experimental creep compliance and creep rupture data should be useful in predicting the long term behavior of laminates at lower temperatures. Such an accelerated characterization procedure should have an impact on the design of laminated composite structures where combinations of temperature, moisture content, applied stress level, and duration of load application may necessitate the use of a time dependent analysis.

An incremental numerical procedure based on lamination theory is developed to predict creep and creep rupture of general laminates. Existing unidirectional creep compliance and delayed failure data is used to develop analytical models for lamina response. The compliance model is based on a procedure proposed by Findley which incorporates the power law for creep into a nonlinear constitutive relationship. The matrix octahedral shear stress is assumed to control the stress interaction effect. A modified superposition principle is used to account for the varying stress level effect on the creep strain. The lamina failure model is based on a modification of the Tsai-Hill

theory which includes the time dependent creep rupture strength. A linear cumulative damage law is used to monitor the remaining lifetime in each ply.

Creep compliance and delayed failure data is presented for several general laminates along with the numerical predictions. Typical failure zone pictures are also given. The compliance predictions for matrix dominated laminates indicate reasonable agreement with the experimental data at various stress levels. Predictions for fiber dominated laminates are erroneously bounded by lamination theory assumptions. Failure predictions are of the right magnitude but are not in exact agreement. Reasons for these discrepancies are presented, along with recommendations for improving the models and the numerical procedure.

ACKNOWLEDGEMENTS

The authors are deeply indebted to the contributions of many individuals who have helped make this work possible. Special acknowledgement is appropriate for the financial support of the National Aeronautics and Space Administration through Grant NASA-NSG 2038. The authors are deeply grateful to Dr. H. G. Nelson of NASA-Ames for his support and for his many helpful discussions. The suggestions of Dr. Linda Clements of NASA-Ames are also appreciated. The assistance of laboratory assistants Andrea Bertolotti and Joe Mensch has been invaluable in this endeavor and is greatly appreciated.

The authors are especially indebted to Mrs. Peggy Epperly for her excellent typing through numerous stages of this work and to Mrs. Karen Martinez for inking the figures.

TABLE OF CONTENTS

LIST OF TABLES

LIST OF PLATES

LIST OF FIGURES

Chapter 1

INTRODUCTION

The use of fiber reinforced materials is a concept that dates back at least to the use of straw in sundried Egyptian bricks. In the past two decades, however, there has been intense new interest in the use of relatively strong, stiff fibers as reinforcement in an otherwise weak and compliant matrix. Glass, boron, graphite, kevlar, and other fibers have been used in either chopped or continuous filament form with a variety of matrix materials including epoxy, polyester and aluminum.

Chopped fiber composites have been injection molded to form panels and more intricate shapes such as automobile grills. Continuous filaments impregnated with resin have been wound around mandrels to produce lightweight pressure vessels, missile cases, and struts for spacecraft, as well as more domestic items such as golf clubs, fishing rods, and bicycle frames. Continuous filaments may be arranged in unidirectional plies or woven into a coarse cloth, each of which are then impregnated with resin. These prepreg laminae may be stacked at various fiber angles and thermally cured in autoclaves to produce stiff, lightweight panels, spars, and fairings. Fabrication of other structural components by other techniques is also possible.

The term "advanced composites" has been applied to such continuous filament systems as boron/epoxy and graphite/epoxy (Gr/Ep) to distinguish them as much stronger and stiffer materials than other composite material systems. Advanced composites provide the strength

and stiffness of structural metals at a fraction of the weight. Primarily because of cost and performance among all continuous filament composites, graphite/epoxy currently finds the most wide-spread use and is the material of primary interest in the present study.

While the current applications of graphite/epoxy are primarily limited to high performance military aircraft and spacecraft, and a few consumer products in the area of sports equipment, there is much interest in introducing this material into other areas. Possible applications to the transportation industry support substantial current interest. The great potential for composite materials is derived from its reduced weight, improved fatigue resistance, greater design flexibility for tailoring material properties to meet design requirements, reduced manufacturing costs and fabrication scrap, and improved dimensional stability due to lower thermal expansion. There are, however, many unknowns still concerning the use of this "new" material system. The current literature abounds in work in the area of characterization, analysis, and design of composite materials.

Our interest lies in studying time dependent viscoelastic stress-strain response of polymer based composite materials and developing techniques to predict the long term creep and creep rupture properties based on short term testing. Such accelerated characterization procedures are of obvious practical value to the designer, who cannot afford to wait for the results of a 10 year test in designing a product for a similar intended service life. While graphite fibers have been shown to be essentially elastic, the epoxy matrix, as with most polymers, exhibits significant viscoelastic response [38,82]. Because

the response of a general laminate is governed by the matrix properties, as well as the fiber properties, it is important that the laminate be considered as a viscoelastic material.

For many applications, composite structures can still be designed with linear elastic analysis. However, there are applications where environmental effects and duration of applied loads require that the viscoelastic aspects of the material response be taken into account to insure long term structural integrity [45a,b,c]. The identification and analysis of these situations provided the impetus for the current investigation.

Previous Efforts

The present work is a continuation of a collaborative effort with the Materials Science and Applications Office of NASA - Ames Research Center and the ESM Department of Virginia Polytechnic Institute and State University. The thrust of the project has been to develop techniques which can give long range strength predictions for general laminates. While most of the work deals with graphite/epoxy, it is expected that the procedures developed will be applicable to laminated composites made with other material systems as well.

An accelerated characterization was proposed by Brinson [9] of VPI & SU to predict the long term response of general laminated composite materials based on a minimal amount of material testing. The procedure was based primarily upon the time-temperature superposition principle (TTSP) which utilizes short term data to predict long term results. The work at VPI & SU has been to pursue the development of

this method to verify assumptions made, obtain data to use with the technique, and to determine and correct any problem areas with the procedure. A great deal of data has been collected for the graphite/epoxy material system, and substantial progress has been made in time dependent characterization.

The VPI & SU investigations have been directed at viscoelastic behavior and creep ruptures, while the NASA - Ames counterpart has studied the effects of environment and fatigue on Gr/Ep materials. See [63,74,75].

Because the VPI & SU work spans several years of research and several different batches of material, much of the data previously obtained was not directly applicable to the current material. Because of variations from batch to batch, and because the properties within a given batch have been shown to be highly dependent on the thermal conditioning [38], there is not as much applicable data available as might be expected from such extensive testing. The author's contention is that many of the problems encountered in characterizing composite behavior are due in part to the variability of the properties from one batch to the next--even when made of the same materials and by the same manufacturer. The current work is no exception and this has posed a great deal of difficulty in interpreting the existing data.

The Accelerated Characterization Procedure

The accelerated characterization procedure proposed by Brinson [9] is summarized in Fig. 1.1. To characterize a new orthotropic, viscoelastic material system, a limited number of tests would be

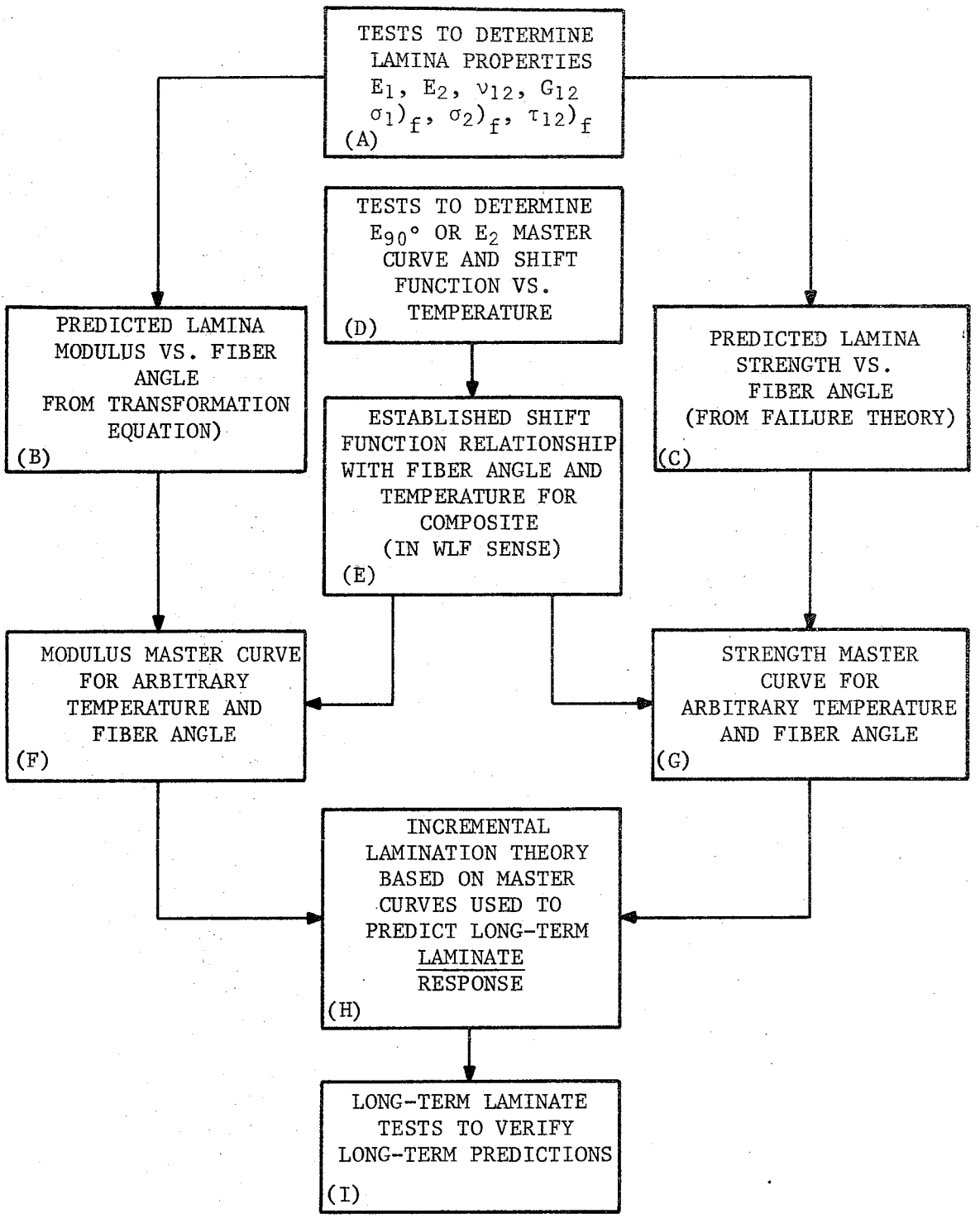

Fig. 1.1 Flow chart of the proposed procedures for laminate accelerated characterization and failure prediction.

conducted with the material to determine ramp loaded static moduli and strengths (A). Creep tests would also be conducted to determine an E_2 master curve and shift function as a function of temperature (D). Transformation equations could be used to transform the moduli in the material principal coordinate system to any arbitrary fiber angle (B,F). It has been found [82] that the shift function is essentially independent of the fiber angle (E). A time independent failure theory can be used to predict static ramp loaded strength of a lamina under an arbitrary stress state (C). Based on the assumption that the strength master curves have the same shape as the moduli master curves, strength master curves may be generated for arbitrary stress states and temperatures (G). An incremental lamination theory approach would be developed to incorporate the measured lamina properties into an analysis procedure capable of predicting the time dependent behavior of a general laminate at an arbitrary temperature and subject to a given stress state (H). Thus with only a minimum of testing of a material system, it is expected that long range predictions of strength and compliance for general laminates could be made. Finally, long term testing should be performed to verify the validity of the procedure (I).

Many of the ideas incorporated in Fig. 1.1 have already been verified and a great deal of data has been gathered for the graphite/epoxy unidirectional material. The original work for the accelerated characterization procedure can be found with supporting data in Brinson, Morris, and Yeow [9] and Yeow, Morris, and Brinson [84]. Yeow and Brinson [83] have reported on a comparison of shear

characterization methods. Morris, Yeow, and Brinson [55] have reported the viscoelastic behavior of the principal compliance matrix of the Gr/Ep lamina. Griffith, Morris, and Brinson have investigated the nonlinear aspects of the creep compliance [39] and creep rupture of unidirectional laminates [40].

Outline of Current Efforts

Much of the characterization of lamina properties has been completed in prior efforts as discussed above. A primary focus of the current work was an attempt to integrate this unidirectional information into an analysis procedure for a general laminate. A numerical method was developed to predict the compliance of a general laminate based on the nonlinear compliances of a single lamina. The Tsai-Hill failure theory was modified for time-dependent strengths and used to predict delayed ply failures in the laminate. Experimental compliance data for several laminates was taken to investigate the nonlinear characteristics of laminates and to check the validity of the numerical procedure. Delayed failures were obtained for each of a variety of laminates tested. Compliance and failure predictions were compared with the experimental data.

Chapter 2 discusses some background concepts and assumptions used in the current analysis. Chapter 3 details the development of a compliance model as used in the numerical procedure. A discussion of the failure model is found in Chapter 4. Chapter 5 provides a development of the numerical procedure. Presentation of the experimental technique is given in Chapter 6, along with details of the

material system. Chapter 7 expresses the results and comparisons of the experimental and numerical investigations. Conclusions and recommendations are found in Chapter 8.

Chapter 2

BACKGROUND INFORMATION

Comments on Terminology

Prior to discussing the main features of the present endeavor, it is worthwhile to clarify the terminology used herein. The term laminate refers to the bonded assemblage of several single plies or laminae into a panel. Laminate properties refer to the properties of the assemblage, while lamina properties refer to the properties of a single ply. For practical reasons, a single ply would be very difficult to test. Thus lamina properties are determined from testing unidirectional laminates, composed, in our case, of sixteen .0052" thick plies. Lamina properties are assumed to be equivalent to those obtained from a unidirectional laminate.

Because the fibers are much stiffer than the matrix, the fiber properties tend to control the response of a lamina in the fiber direction. Thus the compliance in the fiber direction is said to be a fiber dominated property. Also, in a uniaxial test along the fiber direction, the transverse strain is closely tied to the axial strain. Thus the Poisson's ratio effect, or S_{12} term of the compliance matrix is also considered fiber dominated unless there has been significant degradation of the matrix. On the other hand, the compliances in shear and transverse to the fiber direction are referred to as matrix dominated properties because they are closely tied to the matrix response.

The coordinate system convention used for fiber reinforced lamina is well standardized and is illustrated in Fig. 2.1. The x-y coordinates are referred to as global coordinates. The 1-2 coordinates are referred to as the local coordinates or the principal directions of the lamina and the 1 direction is parallel to the fiber orientation.

Balanced laminates are those which for every ply at an angle θ to some reference axis, there is also an identical ply at an angle $-\theta$. These reference axes are the principal axes of a balanced laminate. Symmetric laminates are those in which the laminae orientations form a mirror-image about the laminate midplane.

Orthotropic Constitutive Relations

The primary application of laminated composites is as flat or shallow panels loaded by in-plane loads in a state of plane stress. As such, the linear elastic constitutive relation for an anisotropic material may be simplified from the most general expression,

$$\varepsilon_{ij} = S_{ijk\ell}\,\sigma_{k\ell} \qquad i,j,k,\ell = 1,2,3 \tag{2.1}$$

ε_{ij} = strain tensor

$S_{ijk\ell}$ = 81 term compliance tensor

$\sigma_{k\ell}$ = stress tensor

to the reduced form applicable to orthotropic lamina under plane stress situations ($\sigma_3 = \tau_{23} = \tau_{13} = 0$) [48],

$$\begin{Bmatrix} \varepsilon_1 \\ \varepsilon_2 \\ \gamma_{12} \end{Bmatrix} = \begin{bmatrix} S_{11} & S_{12} & 0 \\ S_{21} & S_{22} & 0 \\ 0 & 0 & S_{66} \end{bmatrix} \begin{Bmatrix} \sigma_1 \\ \sigma_2 \\ \tau_{12} \end{Bmatrix} \tag{2.2}$$

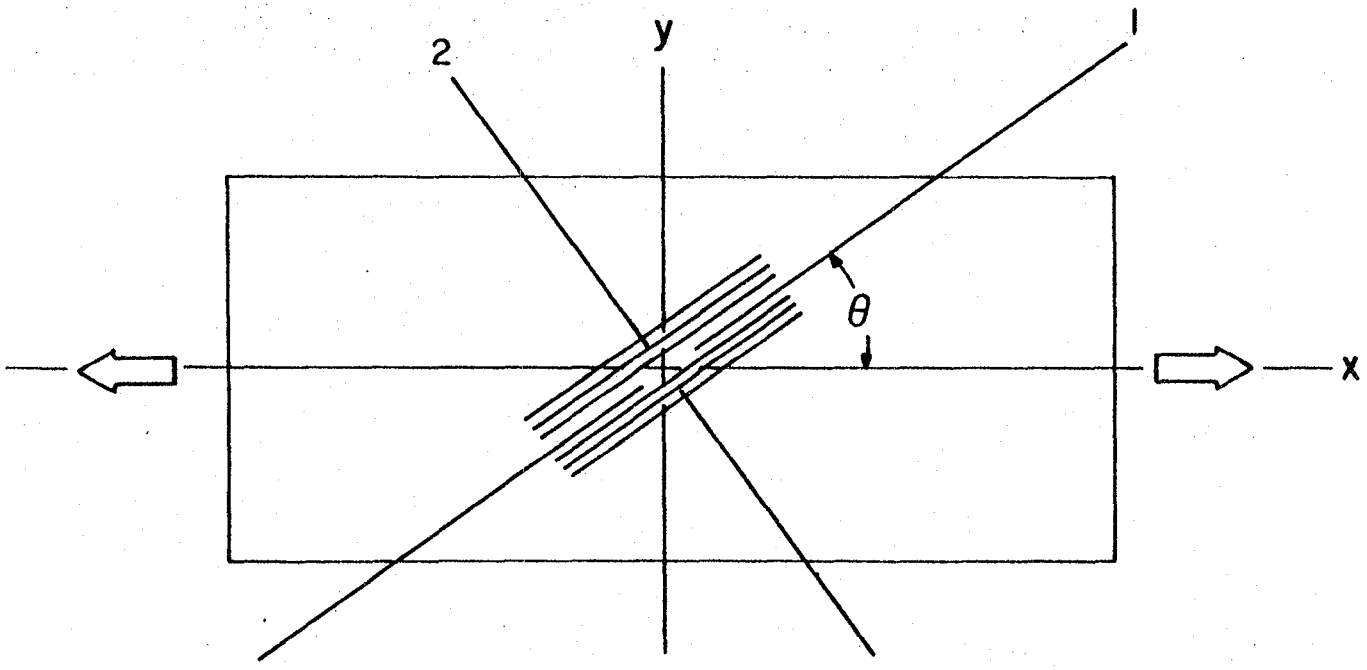

Fig. 2.1 Coordinate system and fiber angle, θ, as used in transformation equations.

or

$$\{\varepsilon\} = [S]\{\sigma\}$$

where

$\varepsilon_1, \varepsilon_2$ = in-plane normal strains

$\gamma_{12} = 2\varepsilon_{12}$ = in-plane engineering shear strain

S = reduced compliance matrix

σ_1, σ_2 = in-plane normal stresses

τ_{12} = in-plane shear stress

The components of the compliance matrix may be expressed in terms of the engineering material constants as,

$$S_{11} = 1/E_{11}$$

$$S_{22} = 1/E_{22}$$

$$S_{12} = S_{21} = -\nu_{12}/E_{11} = -\nu_{21}/E_{22}$$

$$S_{66} = 1/G_{12}$$

The strains may be transformed between local and global coordinates by,

$$\{\varepsilon\}_{12} = [T_2]\{\varepsilon\}_{xy} \quad \text{or} \quad \{\varepsilon\}_{xy} = [T_2]^{-1}\{\varepsilon\}_{12} \tag{2.3}$$

and the stresses by

$$\{\sigma\}_{12} = [T_1]\{\sigma\}_{xy} \quad \text{or} \quad \{\sigma\}_{xy} = [T_1]^{-1}\{\sigma\}_{12} \tag{2.4}$$

where the transformation matrices are given by,

$$[T_1] = \begin{bmatrix} m^2 & n^2 & 2mn \\ n^2 & m^2 & -2mn \\ -mn & mn & m^2-n^2 \end{bmatrix} \qquad [T_2] = \begin{bmatrix} m^2 & n^2 & mn \\ n^2 & m^2 & -mn \\ -2mn & 2mn & m^2-n^2 \end{bmatrix}$$

$m = \cos\theta$ $\qquad$ $n = \sin\theta$

The compliance matrix developed in the material principal coordinates can also be transformed to the global coordinates,

$$\{\varepsilon\}_{xy} = [T_2]^{-1}\{\varepsilon\}_{12} = [T_2]^{-1}[S][T_1]\{\sigma_{xy}\}$$

$$\text{or } [\bar{S}] = [T_2]^{-1}[S][T_1] \tag{2.5}$$

Alternatively, the constitutive relations may be expressed in terms of a reduced stiffness matrix

$$\{\sigma\}_{12} = [Q]\{\varepsilon\}_{12} \tag{2.6}$$

$$\text{where } [Q] = [S]^{-1}$$

Similarly, the stiffness matrix can be transformed to the global coordinate system by

$$[\bar{Q}] = [T_1]^{-1}[Q][T_2] \tag{2.7}$$

Experimentally, S_{11} and S_{22} are obtained from uniaxial tests (normally tension tests) on specimens cut parallel and perpendicular to the fiber direction of a unidirectional laminate, respectively. S_{11} and S_{22} are determined from axially mounted strain gages (or other deformation measuring devices). S_{12} (= S_{21}) may be determined from a transversely mounted gage on either specimen. S_{66} has been determined by a variety of techniques including rail shear, picture frame specimens, and off-axis tensile specimens. Chamis and Sinclair [16] have proposed the use of a 10° off-axis unidirectional specimen to measure the shear compliance. Yeow and Brinson [83] made a study of several methods for determining shear properties and have concluded that this 10° specimen is the best configuration for measuring shear properties.

Use of an electrical strain gage rosette on the off axis specimen allows determination of the shear strain. The shear compliance may then be computed directly. Alternatively, $\bar{S}_{11}$, as determined from an axially mounted strain gage on an off axis specimen, may be used to calculate the shear compliance. Expanding the first term of Eq. 2.5 yields

$$\bar{S}_{11} = S_{xx} = \cos^4\theta\, S_{11} + \sin^4\theta\, S_{22} + \cos^2\theta \sin^2\theta\, (2S_{12} + S_{66})$$

Knowing $\bar{S}_{11}$, one can solve for the shear compliance, S_{66}, in terms of S_{11}, S_{22}, S_{12}, and θ.

Lamination Theory

Classical laminated plate theory is an important tool in the analysis of laminated composite materials. The basic assumption of this theory is that lines normal to the laminate mid-plane remain straight and normal to the mid-plane after loading. This implies that there are no interlaminar shear deformations or stresses. While this is a valid assumption for interior regions of well bonded panels, it cannot be physically correct near free edges of the plate where interlaminar stresses must occur to maintain equilibrium. However, it may be shown that these regions are very localized [48]. The assumption of no interlaminar deformations may break down in specimens which have undergone large deformations or when failure is imminent. This theory is widely used, however, and it was felt that it would be adequate for the present analysis. Because all the laminates studied herein are symmetric about the mid-plane, only in-plane deformations result from in-plane loads and vice versa. Thus, only the in-plane

stiffness matrix is developed because out-of-plane deformations and loads are not considered.

To compute the constitutive properties of a laminate, the stiffness matrices for each contributing ply are transformed into the global x-y coordinates and combined to provide the total laminate stiffness

$$[A] = \sum_{k=1}^{K} [\bar{Q}]^k t_k \tag{2.8}$$

where [A] is the laminate stiffness matrix

K is the number of plies

$[\bar{Q}]^k$ is the laminate stiffness of the k^{th} ply in global coordinates

t_k is the thickness of the k^{th} ply

The elastic laminate strains $\{\varepsilon\}^e$ and the force resultants $\{N\}$ may then be related as,

$$\{N\}_{xy} = [A]\{\varepsilon\}^e_{xy} \tag{2.8}$$

or

$$\{\varepsilon\}^e_{xy} = [A]^{-1}\{N\}_{xy}$$

To calculate the ply stresses in the k^{th} ply,

$$\{\sigma\}^k_{12} = [Q]^k\{\{\varepsilon\}^t_{12} - \{\varepsilon\}^r_{12}\} = [Q]^k\{\varepsilon\}^e_{12} \tag{2.9}$$

where $\{\varepsilon\}^t_{12}$ - total laminate strain in 1-2 coordinate system of ply k

$\{\varepsilon\}^r_{12}$ - residual laminate strain in 1-2 system

where the residual strains are any non-elastic strains such as thermal strains, hygroscopic strains, creep strains, etc.

Linear Viscoelasticity

For linear elastic materials, the constitutive equation is given by,

$$\varepsilon_{ij} = S_{ijk\ell}\,\sigma_{k\ell} \qquad i,j,k,\ell = 1,2,3$$

For linear viscoelastic materials under creep loading, the compliance can be generalized to a function of time

$$\varepsilon_{ij}(t) = S_{ijk\ell}(t)\,\hat{\sigma}_{k\ell} \tag{2.10}$$

where

$$\sigma_{k\ell}(t) = \hat{\sigma}_{k\ell}\,H(t) \tag{2.11}$$

and H(t) is the Heaviside function.

For more general loading states, one may express:

$$\varepsilon_{ij}(t) = S_{ijk\ell}(t)\,\sigma_{k\ell_0}\,H(t) + S_{ijk\ell}(t - t_1)\,\sigma_{k\ell_1}\,H(t - t_1) + \ldots$$

which may be generalized to the following Duhammel integral:

$$\varepsilon_{ij}(t) = \int_{-\infty}^{t} S_{ijk\ell}(t - \tau)\,\frac{d\sigma_{k\ell}(\tau)}{d\tau}\,d\tau \tag{2.12}$$

This expression is often referred to as the Boltzman Superposition Principle and is a consequence of and is only valid for a linear material [20].

As with the linear elastic case, the viscoelastic compliance tensor is symmetric. Schapery [66] has verified this analytically as long as each of the constituent phases is symmetric. Morris, Yeow, and Brinson [55] have shown that this is borne out experimentally.

For plane stress analysis of an orthotropic material, the compliance matrix may be reduced to four independent functions of time [44]

$$\begin{Bmatrix} \varepsilon_1(t) \\ \varepsilon_2(t) \\ \gamma_{12}(t) \end{Bmatrix} = \begin{bmatrix} S_{11}(t) & S_{12}(t) & 0 \\ S_{12}(t) & S_{22}(t) & 0 \\ 0 & 0 & S_{66}(t) \end{bmatrix} \begin{Bmatrix} \hat{\sigma}_1 \\ \hat{\sigma}_2 \\ \hat{\tau}_{12} \end{Bmatrix} \tag{2.13}$$

For our project, all experimental compliance data were obtained from uniaxial tension tests. Compliance properties were assumed to be the same in compression as in tension. For a linear viscoelastic material, Eqn. 2.13 applies to any general plane stress state, although no biaxial tests were run for verification.

An analogous development may be used for the relaxation modulus

$$\sigma_{ij}(t) = C_{ijk\ell}(t)\ \hat{\varepsilon}_{k\ell} \tag{2.14}$$

where

$$\varepsilon_{k\ell}(t) = \hat{\varepsilon}_{k\ell}\ H(t) \tag{2.15}$$

The creep compliance has been used throughout the present analysis because of the difficulty in obtaining a pure relaxation test for the current material system.

Time Shift Superposition Principles

The underlying premise for an accelerated characterization of a material system is that one can in some way use short term experimental data to predict long term material response. The Time Temperature Superposition Principle (TTSP) has found wide use in polymeric studies since its introduction by Leaderman in 1943. The basic idea is that compliance curves at different temperatures are of the same basic

shape, but only shifted in time. Thus by taking short term compliance data at several temperatures and then shifting these curves horizontally in log time (some vertical shift may also be necessary, see Griffith [38]) one can obtain a smooth curve approximating the compliance over many decades of time.

The response of a single Kelvin element (a spring and dashpot in parallel) is

$$D(t) = E(1 - e^{-t/\tau}) \tag{2.16}$$

$$\tau = \eta/E$$

where D is the creep compliance, E is the modulus of the spring, τ is the retardation time, and η is the dashpot coefficient. If N Kelvin elements are connected in series, the overall creep compliance is given by the Prony series,

$$D(t) = \sum_{i=1}^{N} E_i(1 - e^{-t/\tau i}) \ . \tag{2.17}$$

Any monotonically increasing creep compliance function of a linear material may be approximated by a generalized Kelvin model composed of many individual Kelvin elements connected in series. As the number of Kelvin elements becomes infinite, the fit becomes exact. A finite number of elements would result in a discrete distribution of the retardation times whereas an infinite number of elements would yield a continuous retardation spectrum where the creep compliance may be given by,

$$D(T_o,t) = D_o(T_o) + \int_{-\infty}^{\infty} L(T_o,\ell n\ \tau)[1 - e^{-t/\tau}]d\ \ell n\ t + t/\eta_o(T_o) \tag{2.18}$$

where D is the creep compliance

T_o is a reference temperature

D_o is the initial compliance due to a free spring

L is the retardation spectrum

τ is the retardation time

and t/η_o represents the flow of a free dashpot, which was assumed to be zero for the current material

For Thermorheologically Simple Materials (TSM), the compliance at other temperatures is represented by,

$$D(T,t) = D_o(T_o) + \int_{-\infty}^{\infty} L(T_o,\ell n\ \tau)[1 - e^{-\xi/\tau}]d\ \ell n\ \tau \tag{2.19}$$

where ξ is the reduced time given by,

$$\xi = t/a_T \tag{2.20}$$

and a_T is the temperature shift factor. When the retardation spectrum and compliance are plotted vs a log time scale, the effect of a_T is merely to shift these curves to the right or left in time according to,

$$\log \xi = \log t - \log a_T \tag{2.21}$$

Unfortunately, most engineering materials do not fit into the TSM description, and are classified as thermorheologically complex materials (TCM). For this case, there will be a vertical shift in the

retardation spectrum and compliance, as well as a horizontal shift. The compliance at a temperature T is given by,

$$D(T,t) = D_0(T) + \int_{-\infty}^{\infty} L(T,\ell n\ \tau)[1 - e^{-\xi/\tau}]d\ \ell n\ \tau \qquad (2.22)$$

For many materials and temperature ranges, however, the temperature dependence of D_0 and L tends to be fairly small. The horizontal shift for various temperatures remains the fundamental concept. A more detailed discussion of these concepts may be found in Ferry [28]. To use the TTSP for either TSM or TCM, compliance data is taken for a number of different temperatures. The duration of these tests is normally quite short because of practical considerations. This short term data is then shifted to form a smooth and continuous "master curve" which is assumed to be valid over many decades of time at an arbitrary reference temperature. Various techniques have been used to determine the appropriate amount of horizontal and vertical shift. A good discussion of these aspects is found in Griffith [38]. To obtain the compliance at other temperatures, the master curve is shifted to coincide with the short term data at that temperature. Rosen [62] illustrates the application of the TTSP technique for the relaxation modulus of a TSM polymer, as is reproduced in Fig. 2.2.

The point of primary interest to the current paper is simply that these techniques have been successfully used to shift compliance data obtained at one temperature to predict the compliance at another temperature. Shifting procedures are rigorously justifiable only above the glass transition temperature, T_g, although they have been

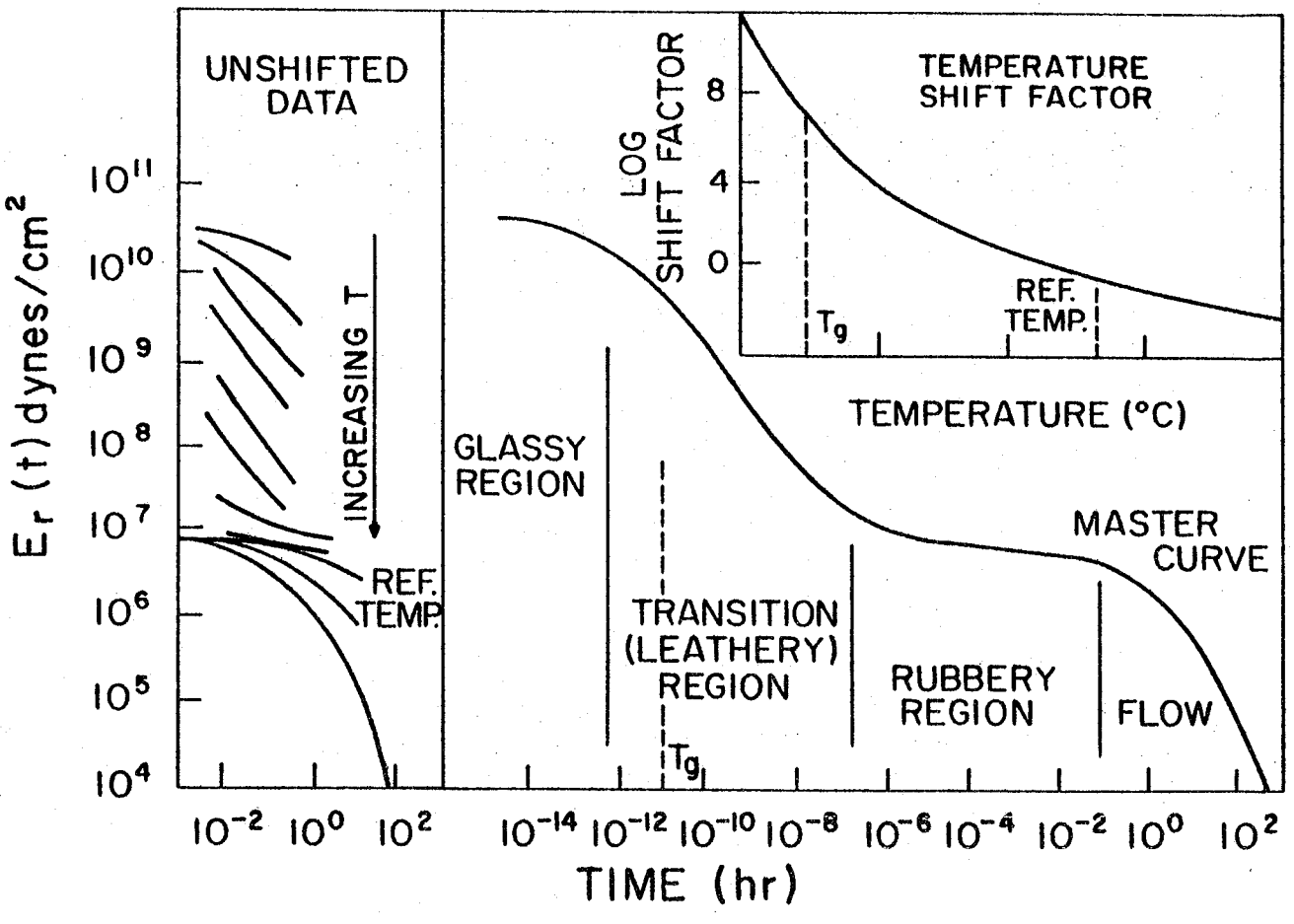

Fig. 2.2 TTSP formation process as given by Rosen [62].

successfully employed below the T_g as well. For small stresses and strains in the linear range, Yeow [82] found the TTSP to be applicable to the current material system.

Furthermore, others have proposed that delayed yield or failure master curves may be constructed in an analogous manner from short term data at various temperatures. Lohr [52] constructed yield stress master curves for constant strain rate testing of several polymers. Similar yield master curves for creep loading were also presented by Lohr, Wilson, and Hamaker [53]. No long term verification of their results was given. Nonetheless, there does seem to be some justification for this technique in the Tobolsky-Eyring Reaction Rate Equation.

Thus, although most of the current experimental work was conducted at 320°F, it is possible to utilize such data in predicting longer term response at lower temperatures. Once an understanding and predictive capability have been established at a given temperature, testing at other temperatures can be used to extrapolate this information to long term behavior.

In addition to temperature, there are also other accelerating factors such as moisture content, stress level, cyclic loading, and the absorption of jet fuel in wet wing designs. Similar superposition principles have been proposed for these factors individually and in combinations.

The effect of moisture on composite laminates is usually pronounced but is not being studied directly in the current work. Nearly constant moisture levels were maintained in the test specimens to minimize any influence on measurements. The acceleration due to stress

level is of current interest because epoxy behaves nonlinearly at moderate and high stress levels. While moisture effects and cyclic loads can be minimized for laboratory experimentation, the stress level nonlinearities cannot be avoided. Several nonlinear approaches have been proposed by a number of investigators as reviewed by Griffith [38].

Unfortunately both the Boltzman and TTSP techniques are referred to as superposition principles. Clearly, from all outward appearances, the two techniques are unrelated. The first deals with the strain resulting from a variable load history and is analogous to the superposition principles employed in linear elastic analysis. The latter implies that compliance data may be shifted in time and superimposed on similar data taken at a different temperature. The former is limited to linear viscoelastic materials, whereas the latter applies to a much more general response. Conceptually, the two types of superposition principles are completely different. It is interesting to note, however, that the Schapery procedure described in a following section incorporates elements of both techniques in a nonlinear expression for strain due to a general load history. Generalization of this concept to include temperature could provide a unified approach to account for the two different problems addressed by the individual techniques.

Nonlinear Viscoelasticity

A number of techniques have been used to account for nonlinear viscoelastic behavior. One such approach is the Time Stress Superposition Principle (TSSP) given by the basic equation

$$D(\sigma,T) = D_0(\sigma) + b_\sigma \Delta D(\xi) \tag{2.23}$$

where

b_σ is the vertical shift factor

ξ is the reduced time given by $\xi = t/a$

and a_σ is the horizontal shift factor due to the stress level.

The similarities between the TTSP and TSSP are apparent. The implication is that compliance data at various stresses rather than various temperatures may be shifted in log time to predict long term compliance based on short term testing. Darlington and Turner [25] note that while the TSSP rests on a less rigorous development, it has been used with some success. Griffith [38] has done considerable work in determining the appropriate horizontal and vertical shift functions for a combined Time Temperature Stress Superposition Principle (TTSSP) application to the current graphite/epoxy material system. Griffith's results, however, were not readily adaptable for implementation into a numerical scheme.

The Green-Rivlin Theory, or multiple integral approach has also been used to model nonlinear viscoelastic materials. For the one dimensional case, the creep strain due to a constant stress is assumed to be a polynomial in stress [20]:

$$\varepsilon(t) = D_1(t)\sigma_0 + D_3(t,t,t)\sigma_0^3 + D_5(t,t,t,t,t)\sigma_0^5 + \ldots \tag{2.24}$$

Even powers of σ_0 are omitted to avoid negative values of the stored energy. For general loading, the response is expressed in terms of multiple convoluted integrals:

$$\varepsilon(t) = \int_{-\infty}^{t} D_1(t - \tau) \frac{d\sigma(\tau)}{d\tau} d\tau$$

$$+ \int_{-\infty}^{t} \int_{-\infty}^{t} \int_{-\infty}^{t} D_3(t-\tau_1, t-\tau_2, t-\tau_3) \frac{d\sigma(\tau_1)}{d\tau_1} \frac{d\sigma(\tau_2)}{d\tau_2} \frac{d\sigma(\tau_3)}{d\tau_3} \cdot$$

$$d\tau_1 \, d\tau_2 \, d\tau_3 + \ldots \qquad (2.25)$$

Arridge [4] notes that the series may be truncated after the third order term for some materials, although such a simplification may not be accurate in general. He points out that few applications of the procedure have been made because of the difficulty in using the technique and the prohibitive amount of testing required for general characterization.

Schapery Approach to Nonlinear Viscoelasticity

Another nonlinear approach of interest is that proposed by Schapery [68]. His approach is derived from thermodynamic considerations and has been used successfully by several investigators [54, 68,14] to predict the behavior of polymers both with and without fiber reinforcement. The form of the constitutive equation for uniaxial stress is given by,

$$\varepsilon(t) = g_0 D_0 + g_1 \int_{-\infty}^{t} \Delta D(\psi - \psi') \frac{dg_2\sigma}{d\tau} d\tau \qquad (2.26)$$

where g_0, g_1, and g_2 are functions of the streys level, D_0 is the instantaneous compliance, ΔD is the transient compliance, ψ and ψ' are reduced time parameters as given by,

$$\psi = \psi(t) = \int_0^t \frac{dt'}{a_\sigma} \quad ; \quad \psi' = \psi'(\tau) = \int_0^\tau \frac{dt'}{a_\sigma} \tag{2.27}$$

where a_σ is the stress dependent time shift factor. As mentioned earlier, the basic form is very similar to the Boltzman superposition integral. In fact, in the linear range of the material when σ is small, $g_0 = g_1 = g_2 = a_\sigma = 1$ and the Boltzman integral is regained. Furthermore, the reduced time and shift factor concept is also employed. It seems reasonable to hypothesize extending this procedure to include the features of temperature superposition by perhaps letting

$$\varepsilon(t) = g_0(\sigma)\, D_0(T)\sigma + g_1(\sigma) \int_{-\infty}^t \Delta D(T, \psi-\psi') \frac{d(g_2(\sigma)\sigma)}{d\tau}\, d\tau \tag{2.28}$$

where ψ and ψ' are now reduced times with respect to both stress and temperature shift factors,

$$\psi = \psi(t) = \int_0^t \frac{dt'}{a_\sigma\, a_T} \quad ; \quad \psi' = \psi'(\tau) = \int_0^\tau \frac{dt'}{a_\sigma\, a_T} \tag{2.29}$$

While this approach was not pursued in the current study, the development of a unified technique to account for both temperature and nonlinear stress effects would be very advantageous.

The Schapery procedure is very appealing from the standpoint that it provides a unified approach to predicting the nonlinear viscoelastic response to an arbitrarily varying stress. The difficulties arise in the experimental determination of g_0, g_1, g_2, and a_σ. Because the approach is more general, it requires more information to

evaluate the functions of stress. In particular, Schapery uses creep and creep recovery data to determine the unknown functions. Creep data alone is insufficient to explicitly characterize the functions of stress; all one can obtain is the ratio $g_1 g_2 / a_\sigma$.

In the previous testing program for the current material system, only creep data but no creep recovery data was taken. This limited data prevented the utilization of the Schapery procedure at the present time. Obtaining sufficient data at various stress levels, temperatures, and fiber angles would have been beyond the current scope.

In discussions with colleagues the authors have been led to believe that because the Schapery procedure is so general, the determination of unique expressions for g_0, g_1, g_2 and a_σ is virtually impossible. Apparently, an admissible set of expressions obtained from creep-creep recovery, may not be valid for another load history such as a multiple step loading. If unique expressions cannot be obtained experimentally, the whole procedure will be of little practical use. A carefully controlled test program could substantiate these contentions, or validate the technique for the current material system.

For the materials he investigated, Schapery proposed that the transient compliance would be given by a simple power law which is not a function of stress.

$$\Delta D(\psi) = m \, \psi^n \tag{2.30}$$

By forcing the compliance to be independent of stress, the necessity for a stress shift factor is created. The concept of a stress shift factor is not required in other nonlinear procedures because the

compliance is expressed as a function of stress. For creep loading, it can be shown that the two approaches are equivalent.

Findley Approach to Nonlinear Viscoelasticity

A nonlinear viscoelastic characterization method extensively studied by Findley [30-34] was eventually used in the current analysis. The basic concept behind the Findley analysis is that for any given creep load, the specimen strain is given by,

$$\varepsilon(t) = \varepsilon_o + m\, t^n \tag{2.31}$$

where ε_o, m, and n are material properties. Further, the assumptions are made that

n = constant, independent of stress level

$$\varepsilon_o = \varepsilon_o' \sinh \sigma/\sigma_\varepsilon \tag{2.32}$$

$$m = m' \sinh \sigma/\sigma_m \tag{2.33}$$

where ε_o', σ_ε, m', and σ_m are material constants for any given temperature, moisture level, etc. The nonlinear effect of stress is accounted for by the hyperbolic sine terms. Apparently, the approach is essentially empirical, although there is some basis in the reaction rate equation [30,68]. Nonetheless, Findley's technique was found to provide an accurate means to express the current experimental results.

Time Independent Failure Criteria

Numerous failure criteria have been proposed and used with varying degrees of success to predict static strengths of general laminated composites. It is expected that an extension of these strength

criteria to include time dependent effects can be used to predict creep rupture in general laminates. While there are several basic approaches to predicting static strengths, the most widely used method independently compares the stress (or strain) state in each ply against a lamina failure criteria. If any ply has "failed", the properties of that ply are reduced to reflect the damage sustained due to failure. If there are intact plies remaining, the load may be increased and the process repeated until total laminate failure occurs.

Several of these failure criteria are described below:

Maximum Stress: The maximum stress failure criteria is a simple, straightforward approach involving comparison of the ply stresses in principal material directions against their respective critical values in tension and compression.

$$X_c < \sigma_1 < X_t$$

$$Y_c < \sigma_2 < Y_t$$

$$|\tau_{12}| < S$$

Maximum Strain: The maximum strain criteria is similar to the maximum stress theory except ply strains in principal material directions are compared against their respective failure strain value

$$\varepsilon_{1_c} < \varepsilon_1 < \varepsilon_{1_t}$$

$$\varepsilon_{2_c} < \varepsilon_2 < \varepsilon_{2_t}$$

$$|\gamma_{12}| < \gamma_{12_f}$$

While these two theories are easy to apply, they do predict cusps in the failure stress vs fiber angle which are not borne out by experimental data [77].

Tsai-Hill: Hill proposed an extension of the von Mises distortional energy yield criteria to anisotropic materials:

$$(G + H)\sigma_1^2 + (F + H)\sigma_2^2 + (F + G)\sigma_3^2 - 2H\,\sigma_1\sigma_2 - 2G\,\sigma_1\sigma_3$$

$$- 2F\,\sigma_2\sigma_3 + 2L\,\tau_{23}^2 + 2M\,\tau_{13}^2 + 2N\,\tau_{12}^2 = 1 \qquad (2.34)$$

For a plane-stress analysis, this may be reduced to

$$\left(\frac{\sigma_1}{X}\right)^2 - \frac{\sigma_1\sigma_2}{X^2} + \left(\frac{\sigma_2}{Y}\right)^2 + \left(\frac{\tau_{12}}{S}\right)^2 = 1 \qquad (2.35)$$

There is no distinction for compressive or tensile critical stress values, but investigators have used X_c when σ_1 is compressive, X_t for σ_1 tensile, etc.

Equation (2.35) is generally accepted to be a more accurate representation of experimental data than the previous theories. One drawback is that this method only predicts the occurrence of failure but does not predict the manner in which failure will occur.

Tsai - Wu: Another quadratic failure theory is the Tsai - Wu Tensor Polynomial criteria.

$$F_i\sigma_i + F_{ij}\sigma_i\sigma_j + \ldots = 1 \qquad i,j = 1,2,\ldots,6 \qquad (2.36)$$

where F_i and F_{ij} are second and fourth order strength tensors respectively. For plane-stress, this failure criteria may be expressed as:

$$F_1\sigma_1 + F_2\sigma_2 + F_6\tau_{12} + F_{11}\sigma_1^2 + F_{22}\sigma_2^2 + 2F_{12}\sigma_1\sigma_2 + F_{66}\tau_{12}^2 = 1 \tag{2.37}$$

Although quite similar to the Tsai-Hill approach, this method is more general in the sense that it can account for strength differences in tension and compression and provides for independent interactions between the normal stress components.

Note, however, that the independence of the $\sigma_1\sigma_2$ interaction effect does not permit the accurate determination of F_{12} from uniaxial tests. The inconvenience of running biaxial tests to determine F_{12} renders this greater generality more of a liability than an asset. Because of the increased number of parameters, however, this method does tend to be slightly more accurate than the Tsai-Hill formulation. The improved accuracy does not usually warrant the extra trouble, and Tsai-Hill finds wider use.

Sandhu Analysis: Another approach to failure criteria is that of Sandhu [65]:

$$f(\sigma,\varepsilon) = K_i \left[\int_{\hat{\varepsilon}_i} \sigma_i \, d\varepsilon_i\right]^{m_i} = 1 \qquad i = 1,2,6 \tag{2.38}$$

where

$$K_i = \left[\int_{\varepsilon_{i_u}} \sigma_i \, d\varepsilon_i\right]^{-m_i} \tag{2.39}$$

The appeal of Sandhu's procedure is that account is made for material nonlinearities and failures are based on total energy sustained by the material. This approach is somewhat inconsistent with other failure criteria in that it is based on total energy rather

than distortional energy but may have some merit.

Puppo-Evensen: While the previous techniques involve application of the particular failure criteria in a plywise fashion, the Puppo-Evenson approach [58] uses a failure criteria based on the laminate as a whole. Claim is made that the method incorporates interlaminar effects and does not require lamination theory or constitutive equations. Admittedly, interlaminar effects are neglected with lamination theory approaches; however, there is no rigorous correlation with actual interlaminar effects in the P-E theory either. The shortcoming of this theory is that it is valid only for predicting failure due to general loading on the one specific laminate being studied. Obviously, such a technique may be quite accurate, but of limited usefulness to the designer who has the option to vary the layup. Yeow [82] has used the P-E criteria in a plywise manner. In addition to being cumbersome to apply, this defeats the purpose of the tensorial approach required in the original development of the P-E theory [58].

Several basic types of static failure criteria have been mentioned. Other techniques exist, but most require large amounts of biaxial data or other properties which are difficult to obtain. An excellent review of static, orthotropic failure criteria may be found in Rowlands [64].

Time Dependent Failure Criteria

A number of time dependent failure criteria have been proposed to predict the time to failure of different materials. Most of these techniques are valid only for a uniaxial, constant stress state in

homogeneous materials. A relationship often credited to Zhurkov has been used quite successfully by Zhurkov [85] to predict the time to failure of a wide class of materials. This relationship is given by,

$$t_r = t_o \exp\left[\frac{U_o - \gamma\sigma}{KT}\right] \tag{2.40}$$

where

t_r = rupture time

t_o = a material constant supposedly based on atomic vibrations. Zhurkov contends that this term is the same for most materials.

U_o = activation energy (material constant)

γ = a constant

σ = applied uniaxial true stress

K = Boltzman's constant

T = absolute temperature

While the technique is highly acclaimed in the Russian literature, it is not as widely accepted among other investigators.

Slonimski et al [70] have modified the basic Zhurkov equation to,

$$t_r = t_o \exp\left[\frac{U_o}{KT} - \gamma\sigma\right] \tag{2.41}$$

This form, known as the modified rate equation, has been successfully used by Griffith [38] to fit the delayed failure data of 90°, 60°, and 45° off axis specimens at 290, 320, 350, and 380°F. Predictive capabilities of the procedure have not been verified, however.

A variety of other time dependent stress limit failure criteria have also been proposed. A discussion of several of these methods may be found in Griffith [38], and an excellent overview of a number of these techniques is presented by Grounes [43].

Of particular interest in the current analysis is an extension of the Tsai-Wu tensor polynomial for anisotropic materials to include time dependent strengths. Wu and Ruhmann [81] have proposed this technique and applied it to unidirectional glass/epoxy composites. They envision a Tsai-Wu static failure surface (t_o) in σ_1, σ_2, τ_{12} space. Other surfaces within $F(t_o)$ describe the time dependent strength for any arbitrary stress state vector and are given by,

$$F(t) = \int_{t_o}^{t} \frac{dF}{d\tau}\, d\tau + F(t_o)$$

The integral reflects the decreasing magnitude of the strength vector with time. Wu and Ruhman have suggested that this could be an exponential decay following Zhurkov. This is a classic paper containing statistical analysis of data obtained from room temperature creep rupture in an air and a hostile benzene environment.

Chapter 3

CONSTITUTIVE BEHAVIOR MODEL

There are a wide variety of approaches that could be used to model the constitutive properties of an orthotropic viscoelastic material. The criteria used to select the model subsequently developed was for the approach to be nonlinear and to provide a good fit for the existing unidirectional compliance data. Also, an important consideration was for the model to be a fairly simple approach which could easily be adapted to the numerical scheme developed in Chapter 5. There are several difficulties in extending existing theories to the case of a variable, biaxial stress state for a nonlinear viscoelastic orthotropic material. These problems and the approach eventually used will be discussed in this chapter.

Constant Uniaxial Stress for Isotropic Materials

In order to analyze the compliance of the current material system, a necessary consideration was to understand how to characterize the creep compliance for the simplest case--creep of an isotropic material under a constant uniaxial stress. Hundreds of studies have been conducted for creep of different materials, different conditioning (e.g., aging), different temperatures, and ways to predict the response, the temperature effect, and the nonlinear stress effect. Nearly all have only dealt with this simplest situation. It is only fitting that the study of a variable biaxial stress state in an orthotropic material should begin here.

Fessler and Hyde [29] have suggested that much of the work in the area of predicting creep has been the characterization of the following type expressions for the initial component of strain

$$\varepsilon_i = \sigma/E + f_1(\sigma)\, f_3(T) \tag{3.1}$$

and the creep strain

$$\varepsilon_c = f_1(\sigma)\, f_2(t)\, f_3(T) \tag{3.2}$$

The assumption of separation of variables seems to be one of convenience rather than physical reasoning.

Common types of stress dependence are:

$$f_1(\sigma) = A\sigma^m \tag{3.3a}$$

$$f_1(\sigma) = A \sinh (\sigma/\sigma_o) \tag{3.3b}$$

or $$f_1(\sigma) = A \exp (\sigma/\sigma_o) \tag{3.3c}$$

The hyperbolic sine expression will subsequently be used in the current investigation. It should be noted that this form falls between the other two expressions, tending towards $A\sigma^m$ for small σ, and towards $A \exp (\sigma/\sigma_o)$ for large values of σ.

Expressions for the time dependence are very numerous. The most common is the power law:

$$f_2(t) = t^n \, . \tag{3.4}$$

Conway [22] discusses a wide variety of other expressions which have been used with varying degrees of success for many materials. These range from logarithmic forms to polynomials in time:

$$f_2(t) = at^{1/2} + bt + ct^{3/2}$$

to the famous Andrade one-third creep law:

$$f_2(t) = (1 - \beta t^{1/3})\, e^{kt} - 1$$

Fessler and Hyde [29] point out that the temperature dependence is almost invariably assumed to be

$$f_3(T) = \exp(-U/KT) \tag{3.5}$$

where

U = activation energy

K = Boltzman's constant

T = absolute temperature.

Supposedly, this expression is fundamental to all rate processes.

The Power Law for Creep

A power law representation for transient strain is independent of stress or temperature dependence assumptions provided the uncoupled form of Eqs. 3.1 and 3.2 is appropriate. Conway [22] points out that the power law is by far the most widely used form, and is applicable to a wide variety of materials.

Consider the power law in the form

$$\varepsilon(t) = \varepsilon_o + mt^n \tag{3.6}$$

$$\dot{\varepsilon}(t) = nmt^{n-1} \tag{3.7}$$

where ε_o, m, and n are material parameters valid at a certain stress, temperature, etc. In Eqn. 3.6, ε_o is referred to as the initial or instantaneous component, and the second term represents the transient or creep component of the strain. Note that while ε_o is often

considered to be the initial or instantaneous strain, it is actually a curve fitting parameter. As such, ε_0 may not necessarily correspond to an actual instantaneous strain even if this value can be physically measured. In fact, often the assumption of $\varepsilon_0 = 0$ is made in cases where the instantaneous response is small in comparison to the total strain. For these cases, the predicted total strain may provide a good fit for the data over a considerable time range, but not be valid at very short times [54].

Several techniques can be used to determine the material constants for the power law from experimental data. Remembering that a power law plots a straight line on log-log paper, an obvious procedure is to use a trial and error approach for determining ε_0. The correct value of ε_0 would result in the best fit to a straight line on log-log paper of the transient component of strain. The slope of the line gives the value of the exponent n, and the t = 1 intercept is the value of m. This method, although probably the most accurate, is also very tedious.

Another approach is to record the strains ε_1, ε_2, and ε_3 at times t_1, t_2, and t_3, where

$$t_2 = \sqrt{t_1 t_3} \ .$$

The power law parameters may be easily determined from the following equations as found in Boller [7]:

$$n = \frac{\log[(\varepsilon_3 - \varepsilon_2)/(\varepsilon_2 - \varepsilon_1)]}{\log\ (t_2/t_1)} \tag{3.9}$$

$$\varepsilon_o = \frac{\varepsilon_1 \varepsilon_3 - \varepsilon_2^2}{\varepsilon_1 - 2\varepsilon_2 + \varepsilon_3} \tag{3.10}$$

$$m = \frac{\varepsilon_1 - \varepsilon_o}{t_1^n} \tag{3.11}$$

This approach, while much simpler, is probably not as accurate as the preceding method because the fit is based on only 3 data points rather than a larger number as might be used in a graphical trial and error approach. Obviously greater care must be exercised in using this simpler method.

Conway [22] discusses another method to determine the power law parameters which is based on creating a point to point difference table from the experimental data. Values of m and ε_o are then calculated for each step. The average value of m and ε_o are assumed to be the best values for these parameters. This technique is worthy of note although the procedure was not used in the current analysis.

Eqns. 3.9, 3.10, and 3.11 were used in the current study to avoid the tedious process of plotting data for various guesses of ε_o until a satisfactory value had been obtained. The time values t_1 and t_3 were chosen to span the time range for the experimental data.

Perhaps part of the reason the power law has found such wide usage is its great versatility to represent a variety of material responses. Depending on the value of the exponent n, the power law may be used to describe several viscoelastic material types as is shown in Fig. 3.1.

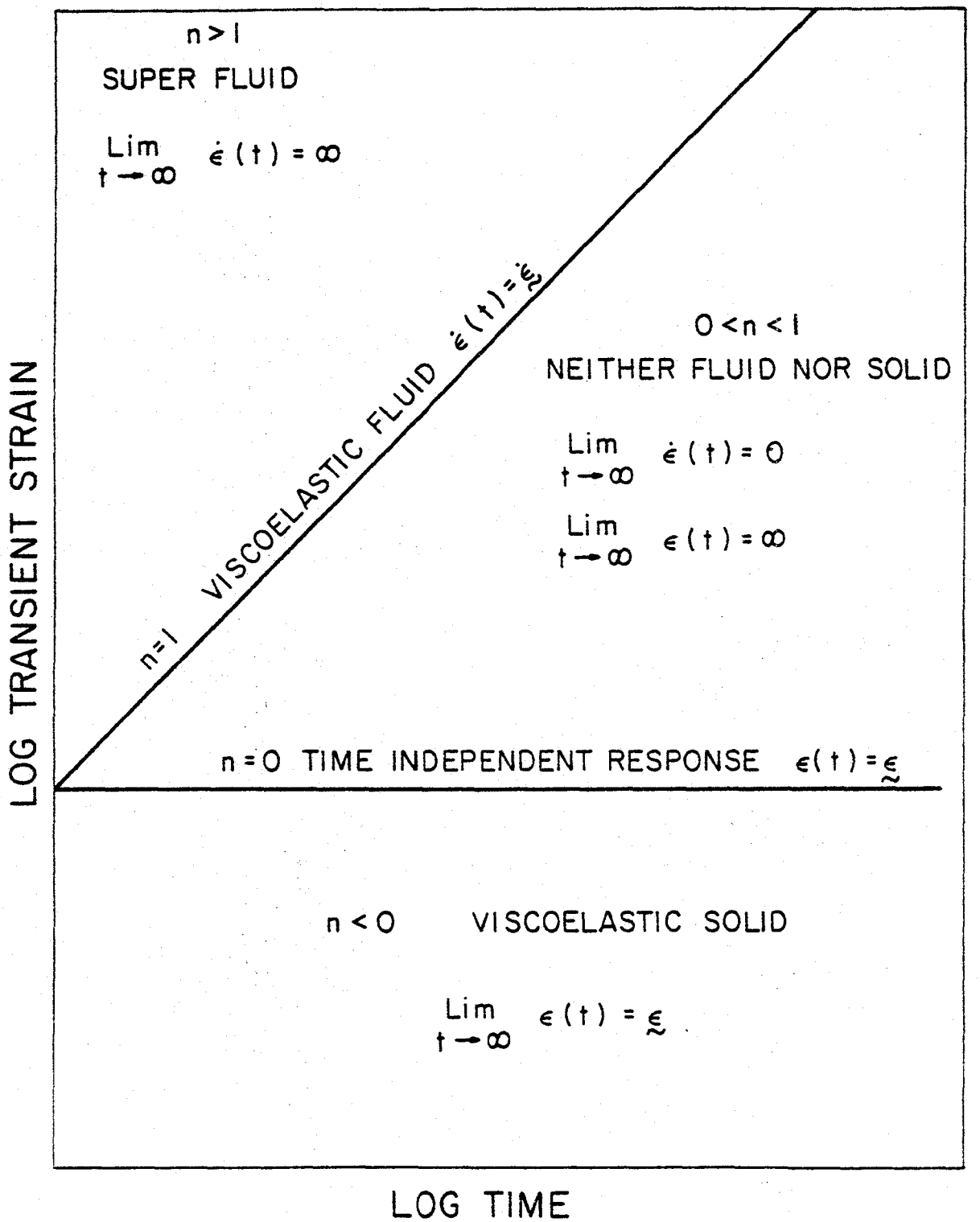

Fig. 3.1 Versatility of the power law in predicting a variety of material responses.

Both $\varepsilon(t)$ and $\dot{\varepsilon}(t)$ approach infinity as t increases without bound for $n > 1$. This region has been labeled as a super fluid in Fig. 3.1 because the strain rate at a constant creep load increases with time. While not relevant to the present materials, this region could be used to characterize fluids with a decreasing viscosity such as perhaps an engine oil deteriorating with usage. Such response is known as shear thinning or pseudoplastic [51].

For the case of $n = 1$, the response is that of a viscoelastic fluid. Specifically, this represents a Maxwell element which may consist of a nonlinear spring and/or dashpot. Despite this generality, the strain rate is always a constant, $\dot{\underset{\sim}{\varepsilon}}$, at any given stress, thereby limiting the usefulness of this equation for real fluids.

The region of $0 < n < 1$ accounts for most practical applications of the power law. As n approaches a value of unity, the response is fluid-like; as n approaches zero, the behavior is solid-like. For intermediate values, however, the behavior is neither that of a true solid, because the strain increases without bound, nor of a true fluid, because the strain rate approaches zero. Actually, this is the accommodating feature of the power law because most engineering materials are neither true fluids nor true solids, but somewhere in between.

For $n = 0$, the obvious conclusion is that the response is not time dependent. However, as will be discussed later, Eqns. 3.9, 3.10, and 3.11 can predict singular values of ε_0 and m when $n = 0$. Singular values of ε_0 and m may suggest a time dependent response for this case but bounded values yield time independent response.

While most power law studies require that m and n be positive quantities, interestingly the case of $n < 0$ actually describes a true viscoelastic solid. This condition simply implies that the strain is a bounded quantity and requires that $\varepsilon_o > \varepsilon(t)$ and $m < 0$.

One drawback is that the power law does not have a simple mechanical analog as does the generalized Kelvin element, for instance. The lack of a mechanical analogue poses no problem mathematically but one may miss the physically meaningful features of a system of linear springs and dashpots. Lockett [51] contends that the power law represents a simpler approach than the use of several exponential terms associated with a generalized Kelvin element, and is often just as accurate. His reasoning is quite understandable when one considers that the effect of a discrete retardation time for a simple Kelvin element is significantly felt over only a decade of time. The power law provides a continuous distribution of retardation times for the retardation spectrum.

In using the power law for current creep data, the author was quite concerned about the extreme sensitivity of the technique to small deviations in the strain values. Upon further investigation, the power law was found to have a singularity in the vicinity of the current data. The acknowledgement of a singularity is quite disconcerting when, from all appearances, the power law is quite well behaved. Fig. 3.2 illustrates a typical representation of the variety of forms that the power law may assume. In this case, the functions are constrained to pass thru (0,0) and (1,1). Fig. 3.3 illustrates a different representation of the power law wherein the strains are

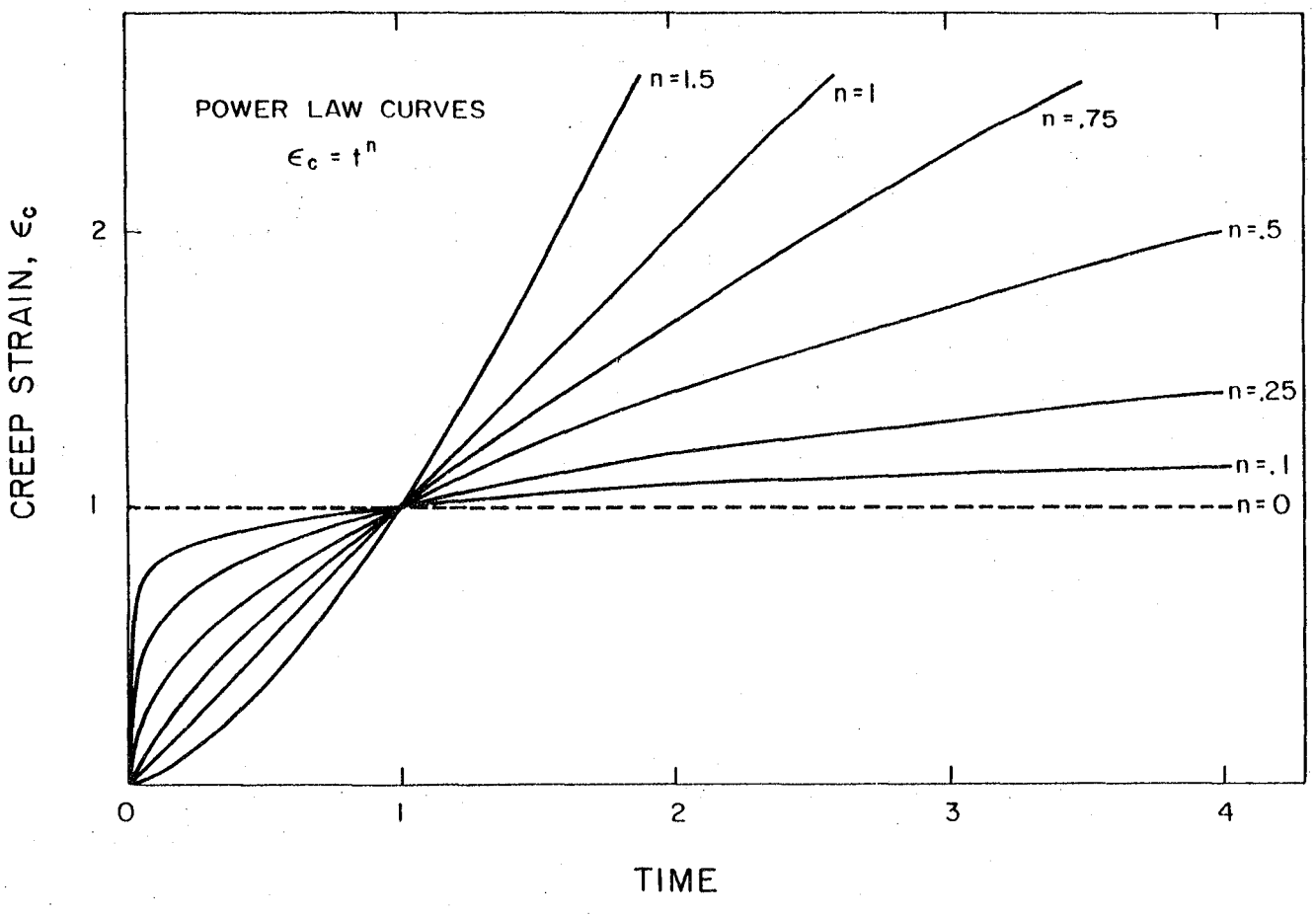

Fig. 3.2 Power Law Curves Constrained To Go Through the Origin and (1,1).

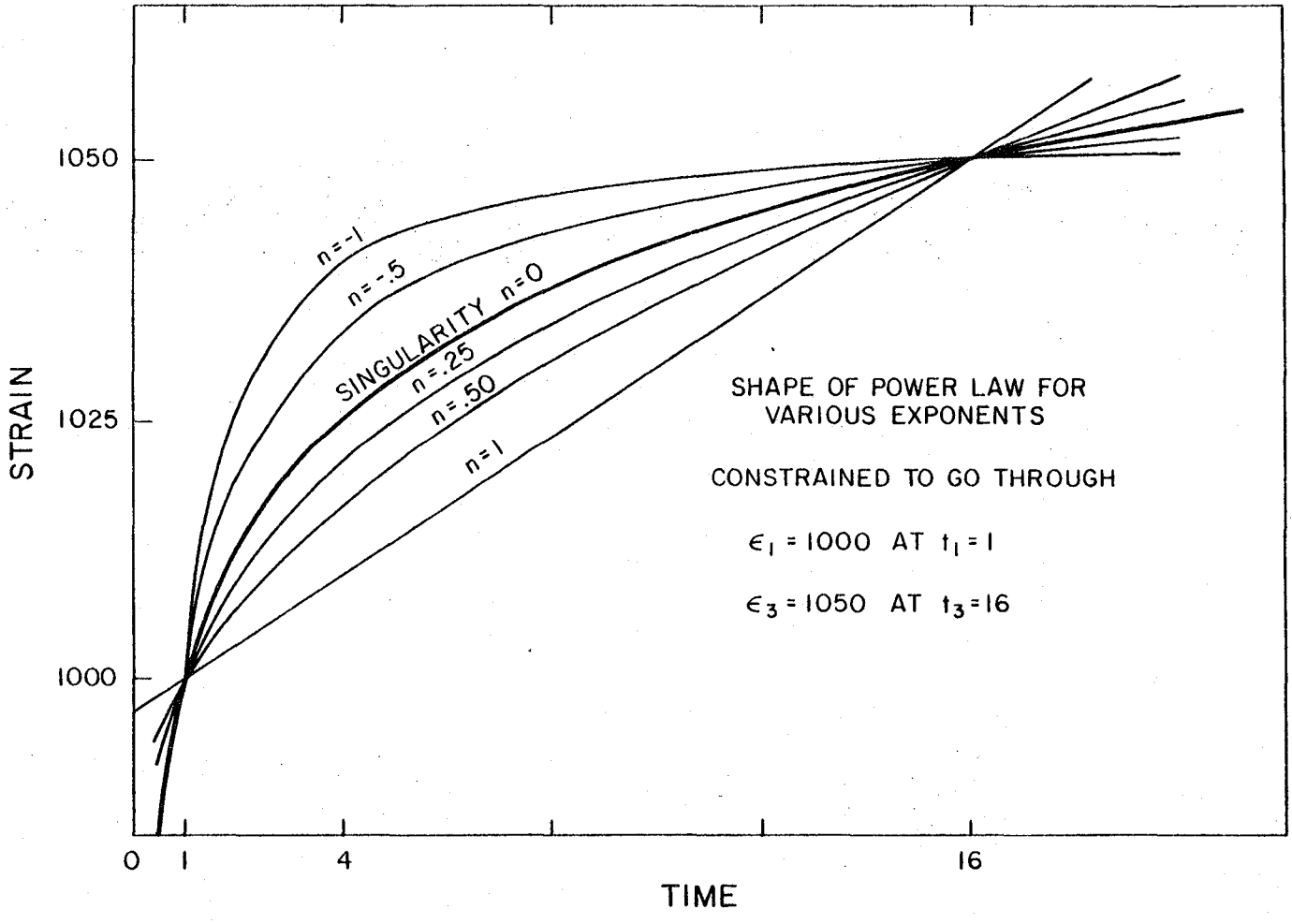

Fig. 3.3 Power Law Curves Constrained To Go Through Given Strains at Two Non-zero Times.

required to pass thru certain values at $t_1 = 1$ and $t_3 = 16$. These times are typical of the time interval span for our experimental creep data. A totally different character is now associated with the power law. Unlike the representation in Fig. 3.2, the resulting response for the case $n = 0$ is no longer time independent. In fact, this case could accurately represent actual creep response over a particular time range.

Equation 3.9 reveals that $n = 0$ results from $\varepsilon_2 = (\varepsilon_1 + \varepsilon_3)/2$. For these values of strain, Eqn. 3.10 indicates that ε_0 is singular, as is m calculated by Eqn. 3.11. Because the experimental data falls near the singularity, evaluations of the power law parameters are very sensitive to small variations in the experimental data. This is particularly true when the creep strains are small compared to the total strains.

Figs. 3.4 and 3.5 illustrate the behavior of the power law parameters in the neighborhood of the singularity. The figures are based on $t_1 = 1$, $t_2 = 6$, $t_3 = 36$, $\varepsilon_1 = 1000$, and $\varepsilon_3 = 1050$. These are typical values from the current experimental data. At the singularity, $\varepsilon_2 = 1025$, the value of n passes thru zero and the values of m and ε_0 diverge without bound. A value of $n = .25$ was typical for the current data. This requires $\varepsilon_2 = 1019.5$. The cross-hatched regions indicate the errors in computing ε_0, n, and m based on reading ε_2 within $\pm$ 1/2% accuracy. Because of the disasterous effects associated with small errors, precise measurements are imperative to the procedure. Nonetheless, the technique is believed to be quite useful. As the relative difference between ε_1 and ε_3 increases, the

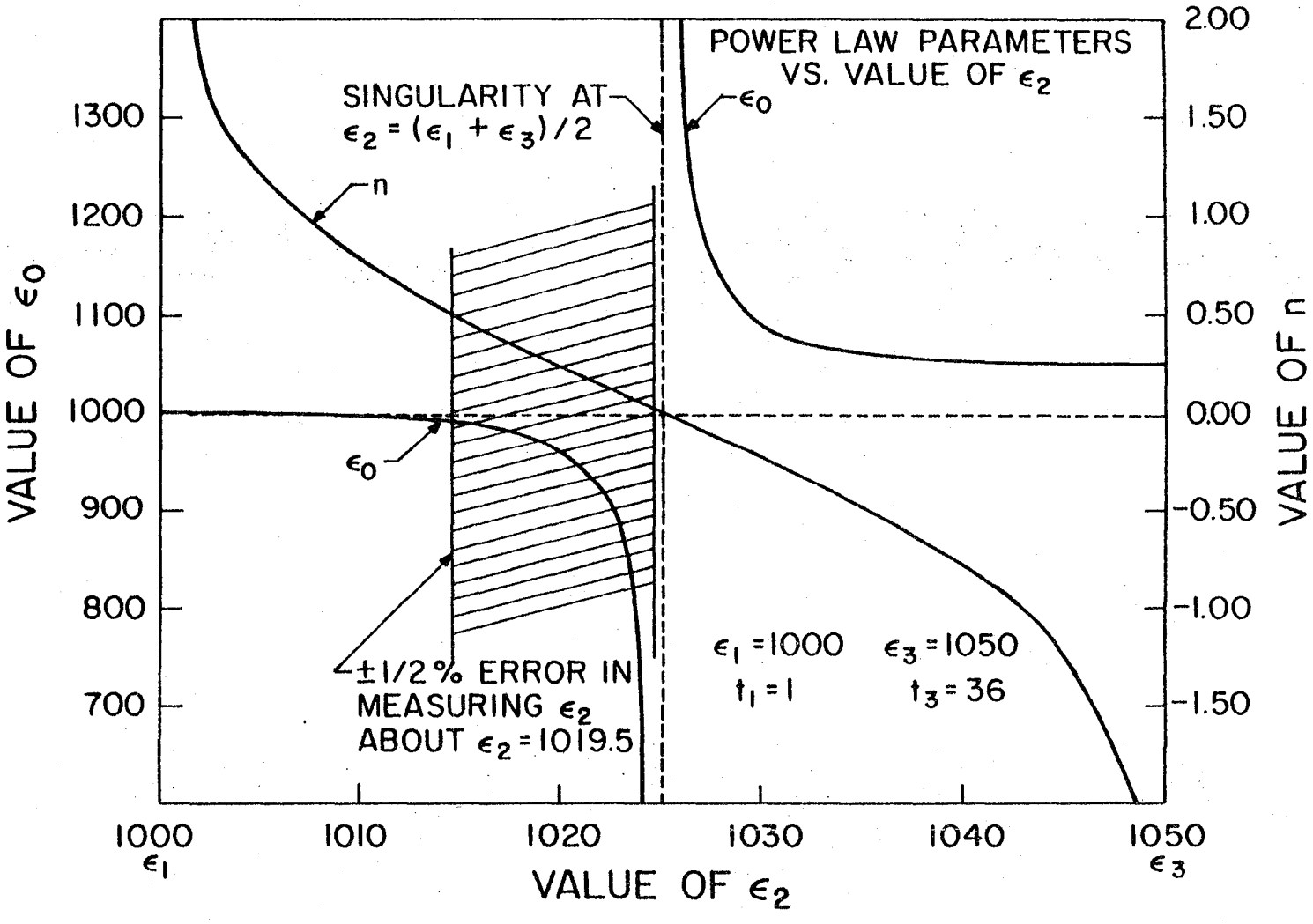

Fig. 3.4 Dependence of power law parameters ε_0 and n on ε_2, for given values of ε_1 and ε_3.

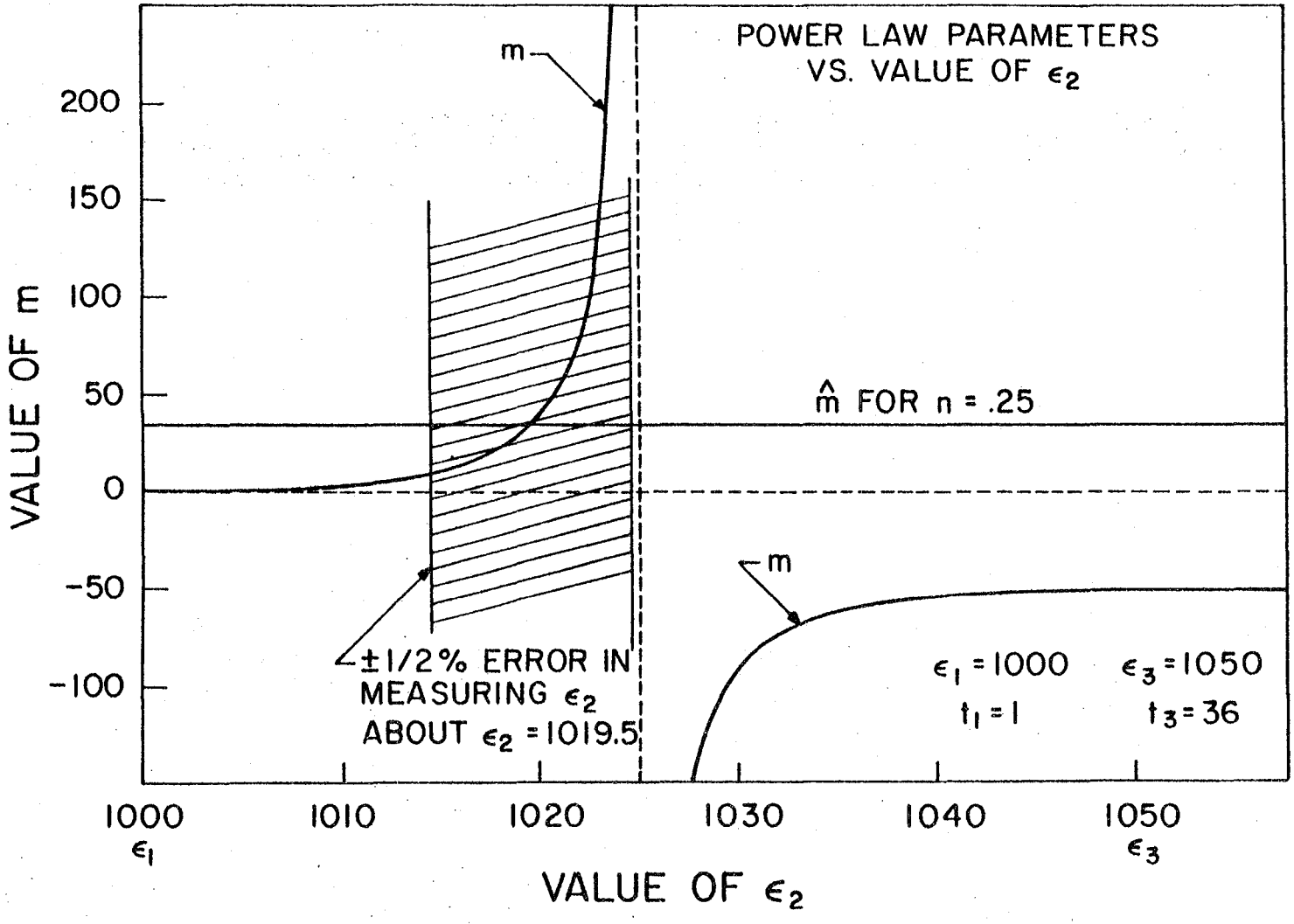

Fig. 3.5 Dependence of power law parameter m on ϵ_2, for given values of ϵ_1 and ϵ_3.

approach becomes less sensitive to small errors. For specimens exhibiting larger amounts of creep, the computed values of the parameters were quite consistent. The difficulties arise primarily with specimens having a very small transient response.

The singularity problems do not arise exclusively with the use of Eqns. 3.9 - 3.11. Although this approach does contribute to the sensitivity, the basic problem is rooted in the nature of the power law and how it is employed to fit experimental creep data. The power law is not the governing equation for the creep process, but rather an empirical technique which has been found to accurately approximate the measured creep behavior over a specific time span. The experimental data does not suggest any singularities. It is merely that the coefficients of the power law equation may become singular when attempting to model a specific set of data. The power law singularity coincides with the transition between a true viscoelastic solid and the region labeled as "neither fluid nor solid" in Fig. 3.1. If one assumes that a true viscoelastic solid (i.e., infinite creep time results in a finite creep strain) exists, it seems obvious that a material could also exist with the properties of the transition. Clearly then, the singularity is not a result of the technique used to determine the power law parameters but is an intrinsic quality of the power law in attempting to fit the response characteristics of transition type materials.

No implication is intended that the current epoxy matrix is such a transition material. One should realize, however, that the power parameters being calculated may be in a steep region of the ε_o

and m curves in Figs. 3.4 and 3.5. Small errors in reading the experimental data may result in large errors in the determined values of the power law parameters. The power law singularity is significant primarily because it explains the sensitivity encountered in determining the power law parameters.

In evaluating the creep data of a specimen subject to several stress levels, the values of n, m, and ε_0 may be quite inconsistent with each other. Realizing, however, that the goal is to express this data in the form:

$$\varepsilon(t) = f_1(\sigma) + \hat{f}_1(\sigma)\, t^{\bar{n}} \quad , \tag{3.12}$$

steps can be taken to improve the results. The computed values of m may be stabilized by modifying Eqn. 3.11 to remove the dependence on the erratic values of ε_0. Knowing that the power law exponent will be taken as some constant value $\bar{n}$ for all stress levels, one may write

$$\hat{m} = \frac{\varepsilon_3 - \varepsilon_1}{t_3^{\bar{n}} - t_1^{\bar{n}}} \tag{3.13}$$

This produces consistent values of m.

One final comment on the power law is that while it is commonly assumed that the value of n is a constant independent of stress, there is some evidence that better fits could be obtained by making n a function of stress. Fessler and Hyde [29] have found that the creep strain of a lead alloy could be expressed up to 14 MN/m^2 by:

$$\varepsilon_c = 5.56 \times 10^{-6} \sinh(\sigma/2.27)\, t^{(.0700 + .0689\sigma - .00312\sigma^2)}$$

One set of Griffith's [41] creep data for a 90° specimen indicated a linear increase in n with stress. Most of our data, however, was too inconsistent to determine functional relationships between n and applied stress. There did seem to be a gradual increase in n with increasing σ, however.

Principal Orthotropic Properties

As was noted earlier, the plane stress constitutive properties of a linear orthotropic material is completely characterized by four independent properties. For the current development, the four independent compliances used are: S_{11}, $S_{12} = S_{21}$, S_{22}, and S_{66}. Expressing these as functions of time permits the calculation of any viscoelastic response.

Because the material is nonlinear, however, the response is no longer governed by:

$$\varepsilon_{ij}(t,\theta) = S_{ijk\ell}\,(t,\theta)\,\hat{\sigma}_{k\ell} \tag{3.14}$$

for the creep load

$$\sigma_{k\ell}(t) = \hat{\sigma}_{k\ell}\,H(t) \tag{3.15}$$

where θ represents the environmental state such as temperature and/or moisture content. For nonlinear elastic materials, the expression for strain is often expanded into an odd power series in stress. Similarly, for a nonlinear viscoelastic material, one can write

$$\varepsilon_{ij}(t,\Xi) = S_{ijk\ell}(t,\Xi)\,\hat{\sigma}_{k\ell} + S_{ijk\ell mnop}(t,\Xi)\,\hat{\sigma}_{k\ell}\,\hat{\sigma}_{mn}\,\hat{\sigma}_{op} + \ldots \tag{3.16}$$

To analyze such a material, the simplest approach is a piecewise linearization of the compliances about the current stress state, Σ. This simplifies the equation to

$$\varepsilon_{ij}(t, \ ) = S_{ijk\ell}(t, \ ,\Sigma)\ \hat{\sigma}_{k\ell} \tag{3.17}$$

where the compliance tensor has been expressed as a function of the stress state. For an orthotropic material under plane stress conditions, one obtains:

$$\begin{Bmatrix} \varepsilon_1(t) \\ \varepsilon_2(t) \\ \gamma_{12}(t) \end{Bmatrix} = \begin{bmatrix} S_{11}(t,\Sigma) & S_{12}(t,\Sigma) & 0 \\ S_{21}(t,\Sigma) & S_{22}(t,\Sigma) & 0 \\ 0 & 0 & S_{66}(t,\Sigma) \end{bmatrix} \begin{Bmatrix} \hat{\sigma}_1 \\ \hat{\sigma}_2 \\ \hat{\tau}_{12} \end{Bmatrix} \tag{3.18}$$

At this point, it should be noted that Yeow [82] and Griffith [38] have indicated that the fiber dominated compliances, S_{11} and S_{12}, of the T300/934 material system are neither functions of time nor stress, but are linear elastic properties.

Interestingly, even if the fibers are elastic, as they are believed to be, there should be some slight time dependent response for S_{11} (and S_{12}) in a composite material. Sturgeon [73] points out that such time dependence of the creep compliance is not due to creep of either component, but to relaxation of the matrix in an essentially fixed grip configuration. The additional load transferred to the fibers results in a small additional strain, which to all outward appearances is creep. An important difference between "relaxation creep" (as Sturgeon calls it) and creep of the matrix dominated compliances is that the former is ultimately limited by the fiber response, whereas the latter is dependent on the matrix response and

is not limited by the fiber properties.

While this is an interesting digression, experimental creep strains in the fiber direction comprise an imperceptible portion of the total strains and may be considered negligible. The elastic values of S_{11} and S_{12} as obtained by Griffith [38] are used throughout the current analysis. Thus it is assumed that only S_{22} and S_{66} will be functions of time or stress state.

The question now becomes what the interaction of stresses will be. S_{22}, for instance, is clearly a function of σ_2 but whether it is also a function of σ_1 or τ_{12} is not apparent. These problems do not arise when one considers a uniaxial load state in an isotropic material. For combined loadings, or with an orthotropic material, however, interaction effects are an important consideration. Griffith [38] assumed there was no interaction effect for the compliances. Thus the compliances were expressed as

$$S_{22} = S_{22}(t, \sigma_2)$$

$$S_{66} = S_{66}(t, \tau_{12})$$

If one likens creep of nonlinear viscoelastic materials to the nonlinear phenomenon of yielding in metals, it would seem appropriate to consider interaction effects. In this light, the non-interactive expressions of compliance correspond to a maximum stress type yield theory. In plasticity theory, the octahedral shear stress, as given by,

$$\tau_{oct} = \frac{1}{3}[(\sigma_{11} - \sigma_{22})^2 + (\sigma_{22} - \sigma_{33})^2 + (\sigma_{11} - \sigma_{33})^2 + 6(\tau_{23}^2 + \tau_{13}^2 + \tau_{12}^2)]^{1/2} \quad (3.19)$$

is commonly assumed to be an accurate simple indicator of the onset of yielding. This, of course, is the famous von Mises or Distortional Energy Theory of yielding. Thus, in plasticity theory, the octahedral shear stress could be considered as the nonlinearizing parameter because it controls the onset of the plastic flow.

The amount of deformation due to the plastic flow is often assumed to be governed by the Prandtl-Reuss Flow Rule

$$d\varepsilon_{ij}^{p} = \sigma_{ij}' \, d\lambda \quad (3.20)$$

where $d\varepsilon_{ij}^{p}$ are the incremental components of the plastic strain tensor

σ_{ij}' are the components of the deviatoric stress tensor given by

$$\sigma_{ij}' = \sigma_{ij} - \frac{1}{3}\delta_{ij}\sigma_{kk}$$

and $d\lambda$ is an instantaneous proportionality constant.

Fessler and Hyde [29] note that Johnson, Henderson, and Khan have evidence to support an expression of the creep strain as

$$\varepsilon_{ij}^{c} = \frac{3}{2} f_1(\tau_{oct}) \frac{\sigma_{ij}'}{\tau_{oct}} f_2(t) \exp(-U/KT) \quad (3.21)$$

This expression is consistent with the Prandtl-Reuss Flow Rule and may be expressed as

$$d\varepsilon_{ij}^{c} = \sigma_{ij}' \, d\lambda \quad (3.22)$$

This form is consistent with the incompressibility of creep strains, although this assumption is not universally accepted. A recent review of creep under combined stresses may be found in Findley, Cho, and

Ding [34]. They have noted a paper by Mark and Findley in which it was shown that the creep vectors are normal to the Mises ellipse, substantiating Eqn. 3.21.

Lou and Schapery [54] have considered the combined matrix stress state induced by uniaxial tests on unidirectional, off-axis specimens of glass/epoxy. They have used the matrix octahedral shear stress as the nonlinearizing parameter for applying the Schapery integral to determine a nonlinear characterization for their material. In their work, strain has been expressed as,

$$\begin{Bmatrix} \varepsilon_1(t) \\ \varepsilon_2(t) \\ \gamma_{12}(t) \end{Bmatrix} = \begin{bmatrix} S_{11} & 0 & 0 \\ S_{12} & S_{22}(t,\tau_{oct}) & 0 \\ 0 & 0 & S_{66}(t,\tau_{oct}) \end{bmatrix} \begin{Bmatrix} \hat{\sigma}_1 \\ \hat{\sigma}_2 \\ \hat{\tau}_{12} \end{Bmatrix} \qquad (3.23)$$

Creep in the fiber direction is negligible because the elastic fibers are much stiffer than the resin. As a result Eqn. 3.21 is not directly applicable to fiber reinforced materials. Furthermore, creep in shear [38,54] has been shown to be much larger than that perpendicular to the fiber direction. Eqn. 3.23 has been used in the current analysis.

Matrix Octahedral Shear Stress

To be a meaningful parameter in predicting the nonlinear aspect of the creep of the matrix material, the octahedral shear stress should be based on the actual matrix stress. The implication is simply that the creep of the matrix should not be dependent on the stresses in the fibers. Several approaches have been used to evaluate the matrix stresses from the ply stresses. These approaches involve aspects from the micro-geometry of the material as well as the individual properties

of the matrix and fibers as could be determined from independent testing of the two components.

The simplest approach, known as the mechanics of materials approach, models the composite as parallel alternating strips of fiber and matrix. This approach results in the rule of mixtures approximations for E_{11} and ν_{12}:

$$E_{11} = E_f v_f + E_m(1 - v_f) \tag{3.24}$$

$$\nu_{12} = \nu_f v_f + \nu_m(1 - v_f) \tag{3.25}$$

E_{22} and G_{12} are given by

$$E_{22} = \frac{E_f E_m}{E_f(1 - v_f) + E_m v_f} \tag{3.26}$$

$$G_{12} = \frac{G_f G_m}{G_f(1 - v_f) + G_m v_f} \tag{3.27}$$

where

v_f = fiber volume fraction

and f and m subscripts denote fiber and matrix properties respectively. The matrix stresses based on this model are given by

$$\begin{Bmatrix} \sigma_1^m \\ \sigma_2^m \\ \tau_{12}^m \end{Bmatrix} = \begin{bmatrix} \frac{E_m}{E_{11}} & \left(\nu_m - \frac{E_m}{E_{11}}\nu_{12}\right) & 0 \\ 0 & 1 & 0 \\ 0 & 0 & 1 \end{bmatrix} \begin{Bmatrix} \sigma_1 \\ \sigma_2 \\ \tau_{12} \end{Bmatrix}$$

or (3.28)

$$\{\sigma^m\} = [B]\{\sigma\}$$

More exact expressions for averaged values of the matrix stresses can be derived, based on more complex modeling of the matrix and fiber inclusion. Beckwith [6] has used the Halpin-Tsai equations in studying a viscoelastic matrix. Pindera and Herakovitch [57] have included residual stress effects and solved for accurate expressions for the components of the [B] matrix, based on the use of Hill's [47] elasticity approach to reinforced materials. Numerous finite element solutions for various fiber shapes and spacings have also been proposed (e.g., Foye [36]).

These techniques all provide improvements over the mechanics of materials approach in determining average values of the matrix stresses. The major limitation to these techniques is that they are based on linear material behavior. For our nonlinear material, the appropriateness of averaged values of the ply stresses is questionable. The variations of the matrix stresses between the fiber inclusions could be quite complex. Indeed, more rigorous expressions for averaged values are not necessarily any better for obtaining effective values of the matrix stresses in a nonlinear material.

Besides linear averaging, other averaging schemes can also be used. Lou and Schapery [54] have applied a root mean square averaging procedure to results from a finite element model. They found this approach yielded values of octahedral shear stress which were nearly proportional to linearly averaged results for the case of unidirectional off axis specimens. They also found these values to be in fair agreement with the mechanics of materials approach, which was subsequently used in their investigations.

Independent properties for the matrix and fiber were not available. Properties supplied by the manufacturer were inconsistent. By assuming a few properties and working backwards from Eqns. 3.24 - 3.27, the following values were determined and used in the analysis

$E_m = .487 \times 10^6$ psi

$E_f = 34.0 \times 10^6$ psi

$\nu_m = .35$

$v_f = 63.4\%$

$E_{11} = 21.7 \times 10^6$ psi

$\nu_{12} = .33$

While the matrix moduli do decrease with time, they were assumed constant in calculating the matrix stresses.

Once one has obtained the effective matrix stresses, the octahedral shear stress in the matrix for a plane stress situation can be computed by

$$\tau_{oct} = \frac{1}{3}\left[(\sigma_1^m - \sigma_2^m)^2 + (\sigma_1^m)^2 + (\sigma_2^m)^2 + 6(\tau_{12}^m)^2\right]^{1/2} \quad (3.29)$$

Fig. 3.6 illustrates the values of the ply stresses for a unidirectional off-axis laminate as a function of fiber angle. Along with the typical representations of σ_1, σ_2, and τ_{12}, the values of σ_1^m and τ_{oct} have also been presented. As in Eqn. 3.28, it is noted that $\sigma_2^m = \sigma_2$ and $\tau_{12}^m = \tau_{12}$.

Adaptations of the Findley Procedure

The Findley approach to nonlinear viscoelasticity was chosen because of ease of application and the available data was sufficient to

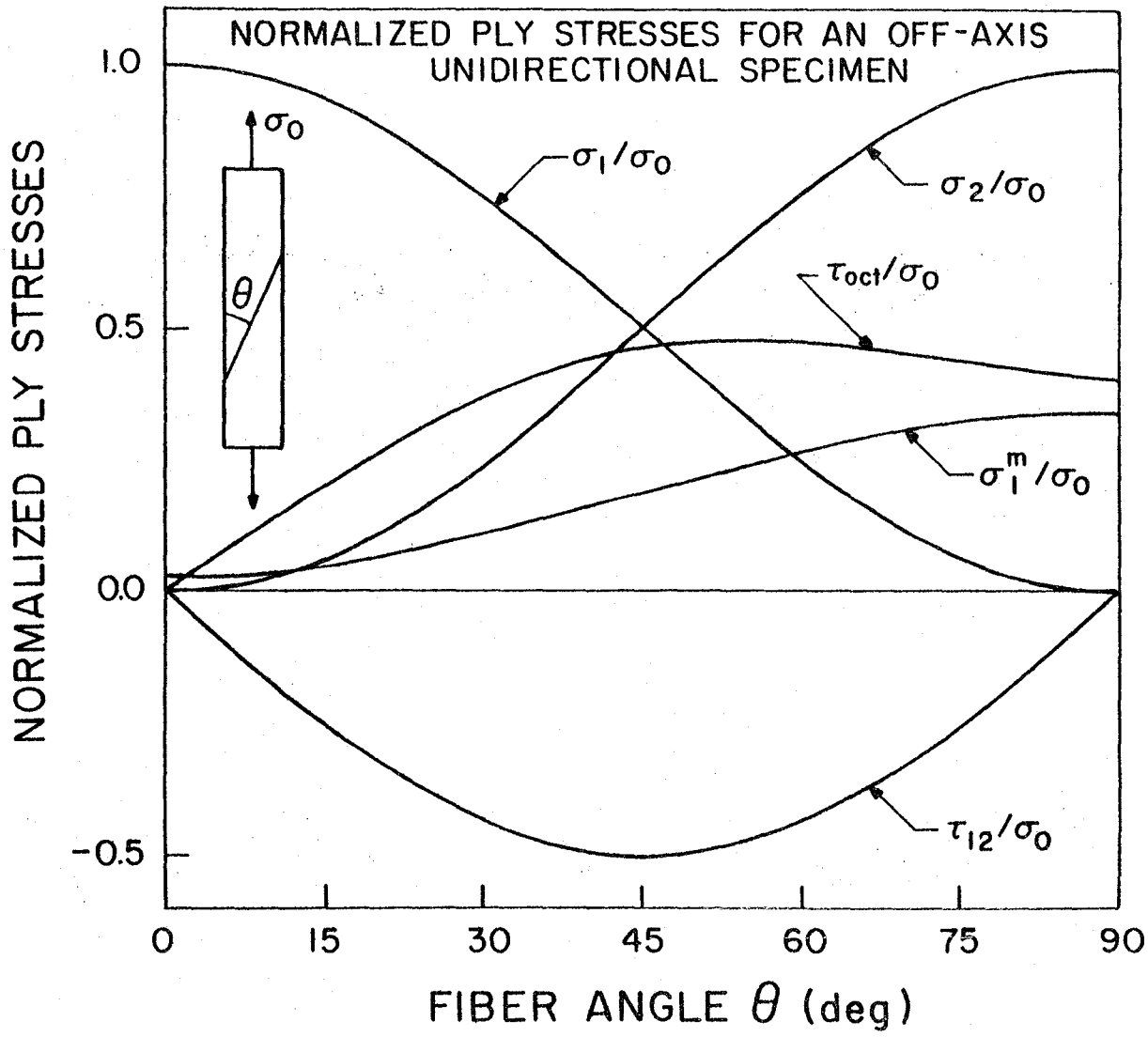

Fig. 3.6 Normalized ply stresses for an off-axis unidirectional specimen at various fiber angles.

determine the unknown parameters and seemed to match the data well. To evaluate the Findley parameters ε_o', σ_ε, m', and σ_m, creep compliance data is obtained for a given specimen configuration at several stress levels. The power law parameters ε_o, m, and n are then determined for each set of data.

Findley and his co-workers [31,32,33], and others (e.g., Boller [7]) have assumed that the value of n is independent of stress level. Their published data indicates wide scatter in the value of n. They usually take the average value of n to be the constant for the Findley equation. Apparently, this approach is based on the inability to determine a functional dependence of n on stress because of the data scatter. In the present study, the values of n were also widely scattered, due in part to the singularity discussed earlier. This was a particular problem for short term data where the creep strains were small. The values of n were felt to be more stable for specimens exhibiting larger creep strains.

The available data for the unidirectional material, as well as the current compliance data for the general laminates, were composed of short term (16 or 36 minute) data for several stress levels and week long data at some particular stress. Because the long term data exhibited larger creep strains, determination of the associated Findley parameters was less sensitive to errors than the short term data. It was also felt that by using the value of n from the long term data, the model would best predict the overall response of the material. Thus the short term data at various stress levels was used to evaluate the hyperbolic sine parameters, but the long term data at

a single stress level was used to evaluate the exponent n.

Once a set of ε_o and m as functions of the applied stress level has been obtained, the hyperbolic sine parameters may be obtained. A least squares fit program for a hyperbolic sine function was written to provide an accurate and efficient means to obtain ε_o', σ_ε, m', and σ_m. This procedure is described in Appendix A.

The end result is an equation for strain in terms of the applied stress. Knowing the values of the octahedral shear stress at a particular load case, one can modify this expression of strain to an expression of compliance

$$S(t,\tau_{oct}) = \frac{1}{\tau_{oct}} [\varepsilon_o' \sinh (\tau_{oct}/\sigma_\varepsilon) + m' \sinh (\tau_{oct}/\sigma_m) t^n] \quad (3.30)$$

In this manner, the uniaxial compliance fitting the experimental data at any fiber angle may be determined.

Determination of Actual Compliance Properties

Creep compliance data for 90° and 10° specimens at 320°F has been obtained by Griffith [41]. This data was used to determine expressions for the required S_{22} and S_{66} compliances. Fig. 3.7 presents the experimental short term compliance for a 90° specimen at several creep stress levels. Also included in the figure are the results from a week long compliance test at σ = 2750 psi.

The jump in the long term data at t ≈ 100 min was required to provide a good fit for the data points. Our original interpretation was that there had been a jump in the balance calibration. Consequently, this strain jump was subtracted from all strain values after

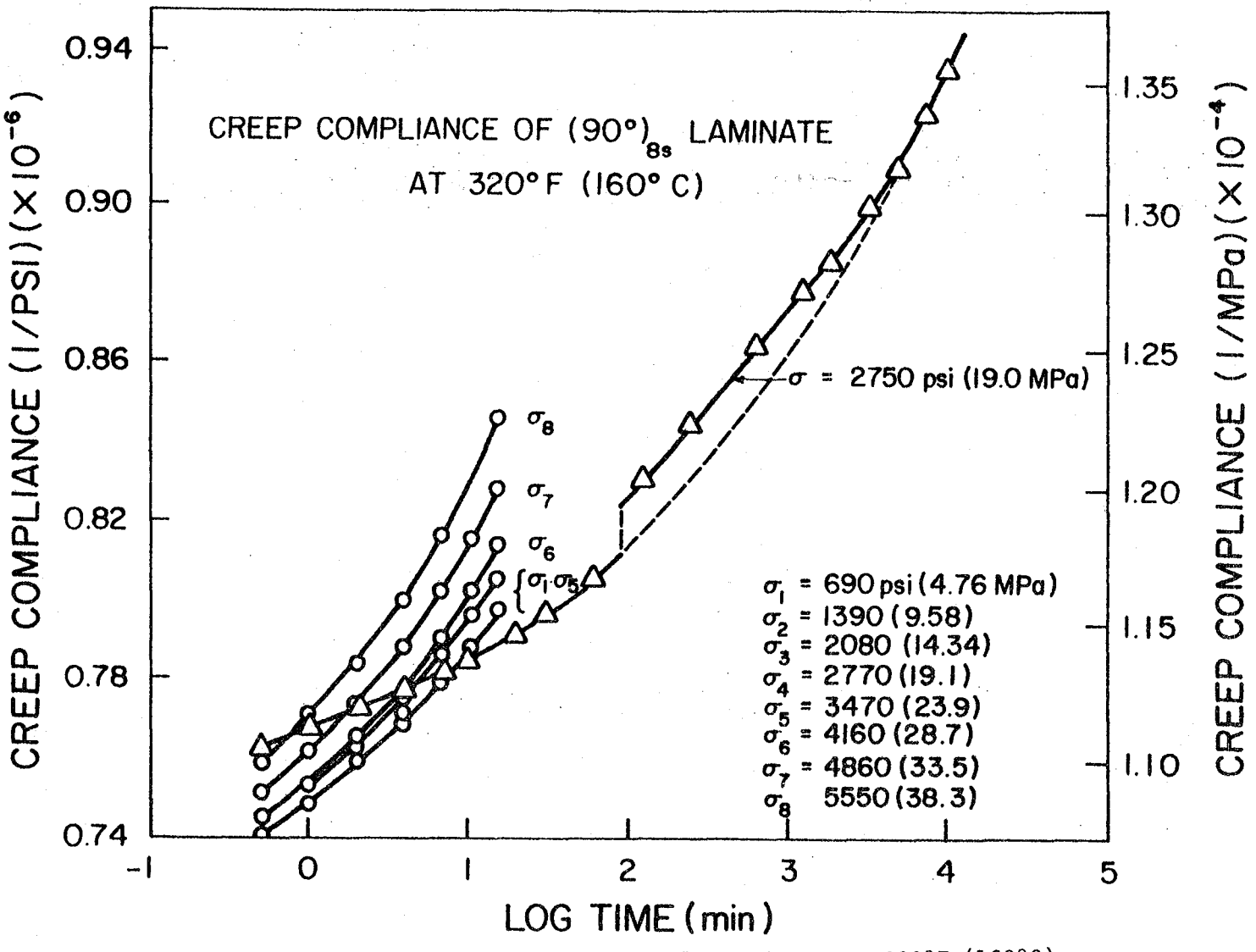

Fig. 3.7 Creep compliance for 90° unidirectional specimens at 320°F (160°C).

t = 100 min. This interpretation has been used to determine the power law exponent for the 90° specimen. In light of electrical problems encountered in our acquisition of creep strain data, however, it was recently decided that poor voltage regulation of the main power supply may have caused this discrepancy.

For most long term creep data from other laminates, the representation of log transient strain vs log time was found to be a fairly straight line. This, of course, is in accordance with the power law prediction. As seen in Fig. 3.8, however, there is a marked deviation from the power law prediction over the time range of 100 to 3000 minutes. The dashed line in Fig. 3.7 is currently believed to represent the best interpretation of the experimental data. The value of n predicted from this assumption is 0.22, as opposed to a value of 0.183 as determined from the strain jump approach.

Also of concern is that the short time creep rate for the long term test is less than half as much as the creep rate for the short term data at a comparable stress level. This aspect was not noticed until the data were superimposed in the final compilation. The only proposed explanation for this disturbing result is that perhaps one of the specimens had been postcured and the other had not. An additional test or two would be required to correct this anomaly. There is a slight difference in the t = 1/2 min compliancesfor the long term data and the short term data at a comparable load. This is believed to be due to small errors in determining the cross-sectional area of the specimen, etc., and is not considered significant.

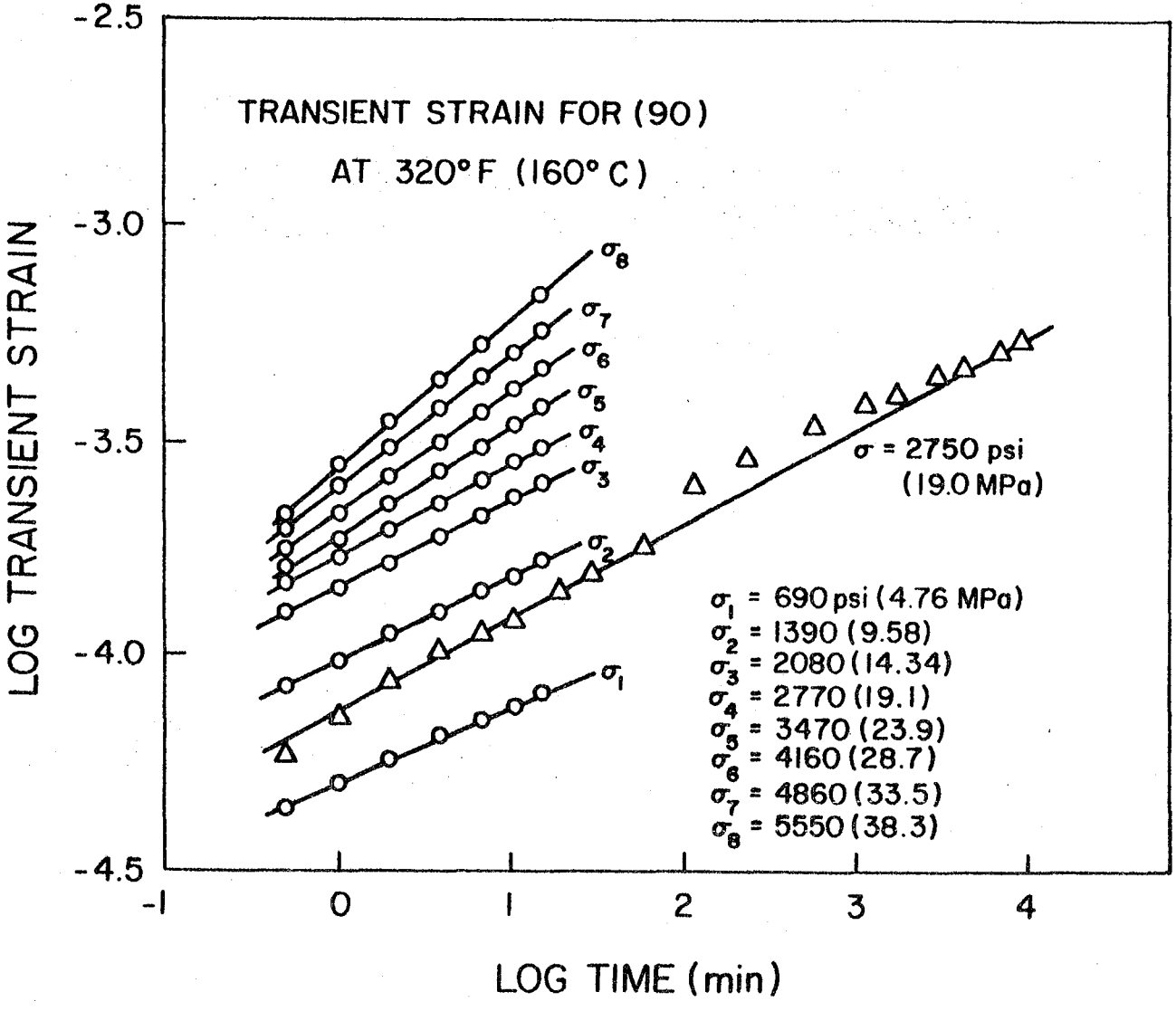

Fig. 3.8 Transient strain for 90° specimens at 320°F (160°C).

As mentioned earlier, the short term data at various stress levels was used to evaluate the stress dependence, while the long term results were used to calculate the power law exponent. Figure 3.8 indicates that the data may indeed be plotted along a straight line as predicted by the power law. Note that the slope, and hence n, tends to increase with increasing stress. Figure 3.9 illustrates a tendency to a linear increase in n with increased stress but as mentioned before, a constant value was used. Also provided in this figure, are plots of ε_o and m vs applied stress level. The curves represent the least squares fits for hyperbolic sine functions thru the data. The fit provided by the Findley approach is considered excellent. It should be noted that the transient response is considerably more nonlinear than the initial response.

Figures 3.10, 3.11, and 3.12 represent similar results for the 10° off-axis data from Griffith [41]. Fig. 3.10 shows that the long term compliance is quite similar to that obtained from the short term test at a similar stress level. Figure 3.11 indicates that the exponent again tends to increase slightly with increasing stress and Fig. 3.12 shows that the fit of the Findley approach is again very good. The widely scattered values of n are typical of those obtained in this study. Published literature indicates a similar degree of scatter as may be found in [31,32,33,7].

It should be noted that the slopes in Fig. 3.11 vary in a slow, regular manner, while the corresponding values of n in Fig. 3.12 are very erratic. The explanation is that the values of n plotted in Fig. 3.12 are those obtained from Eqn. 3.9. The values of ε_o used to

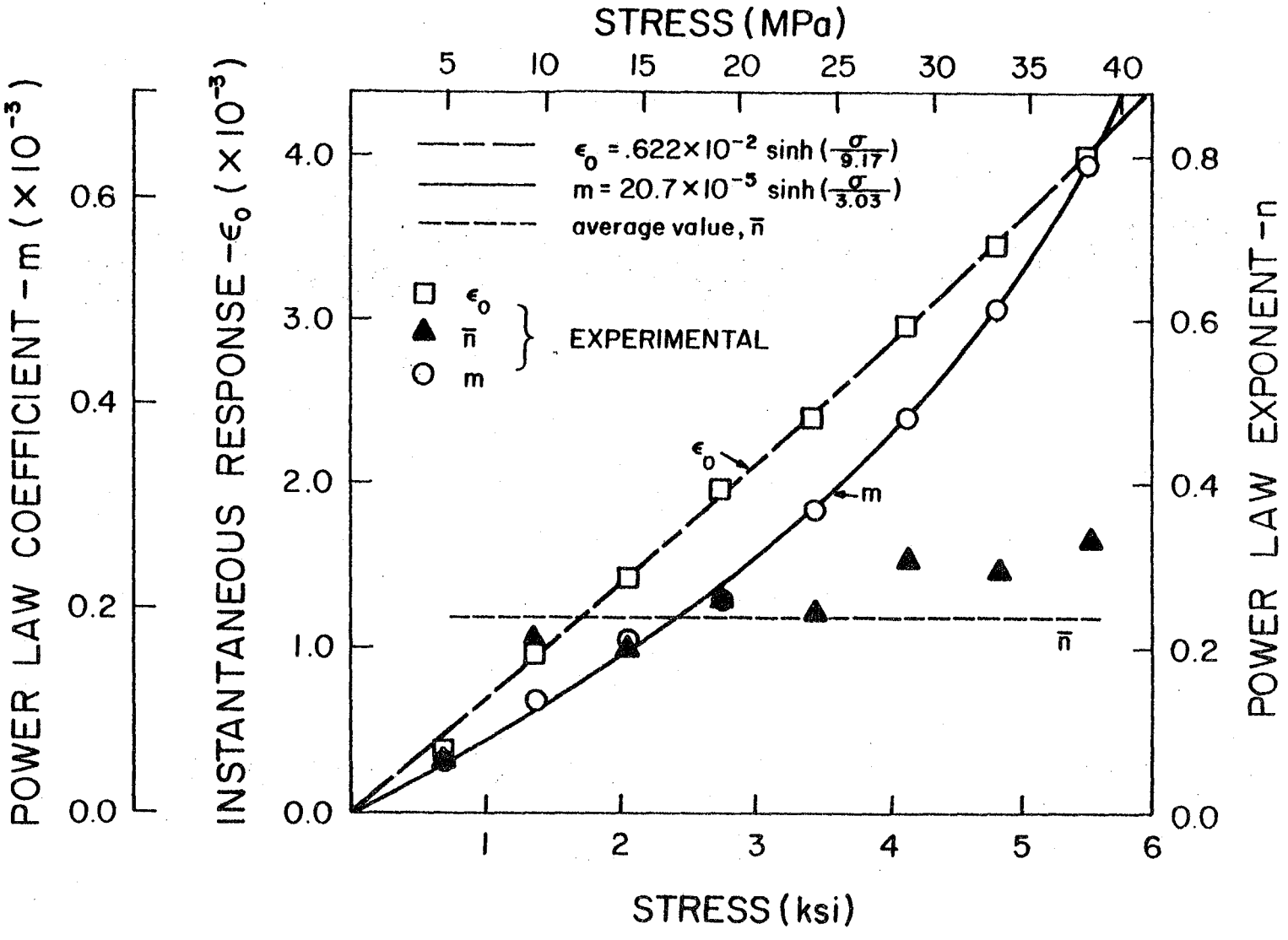

Fig. 3.9 Power law parameters for $[90]_{8s}$ specimen at 320°F (160°C).

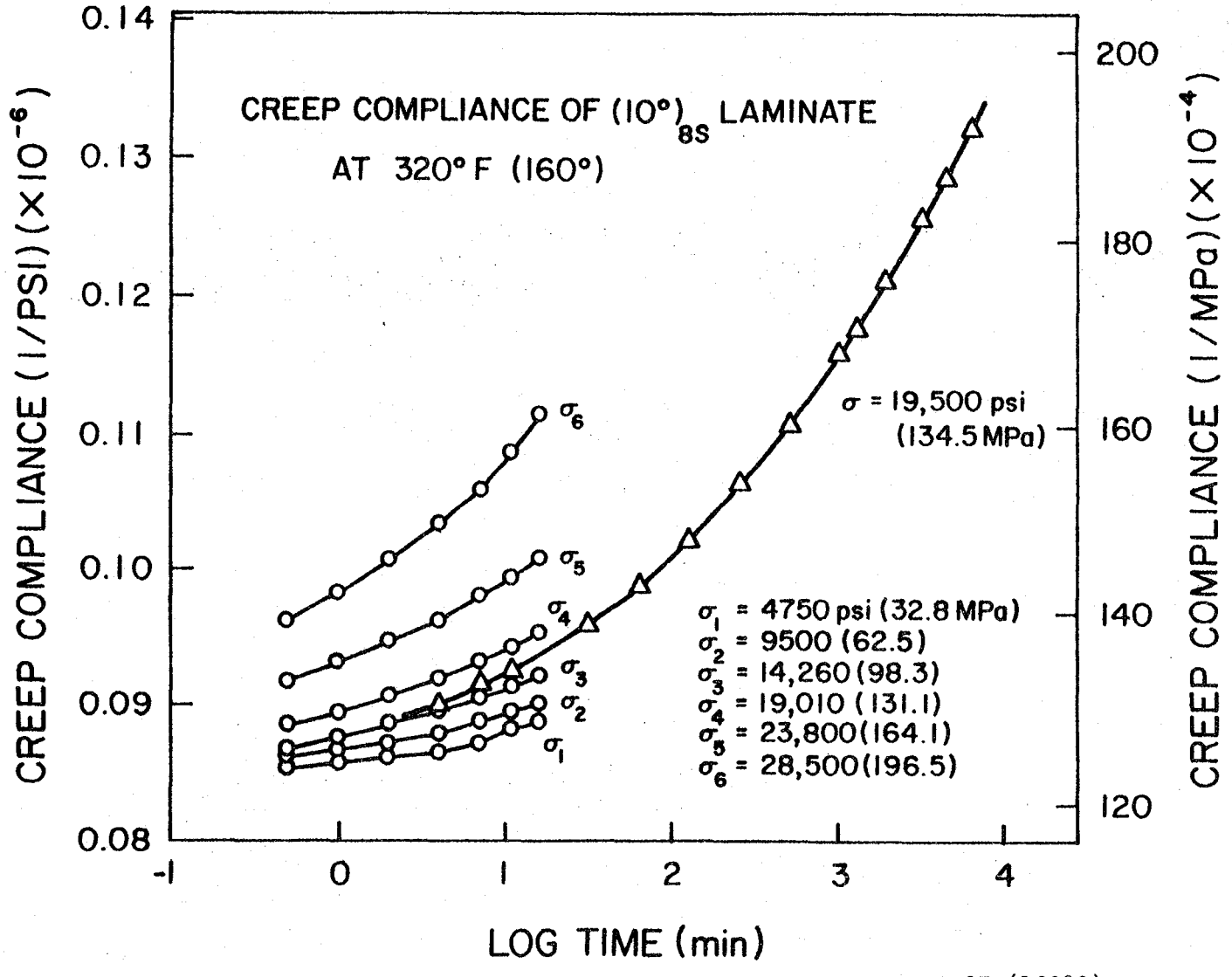

Fig. 3.10 Creep compliance for 10° unidirectional specimens at 320°F (160°C).

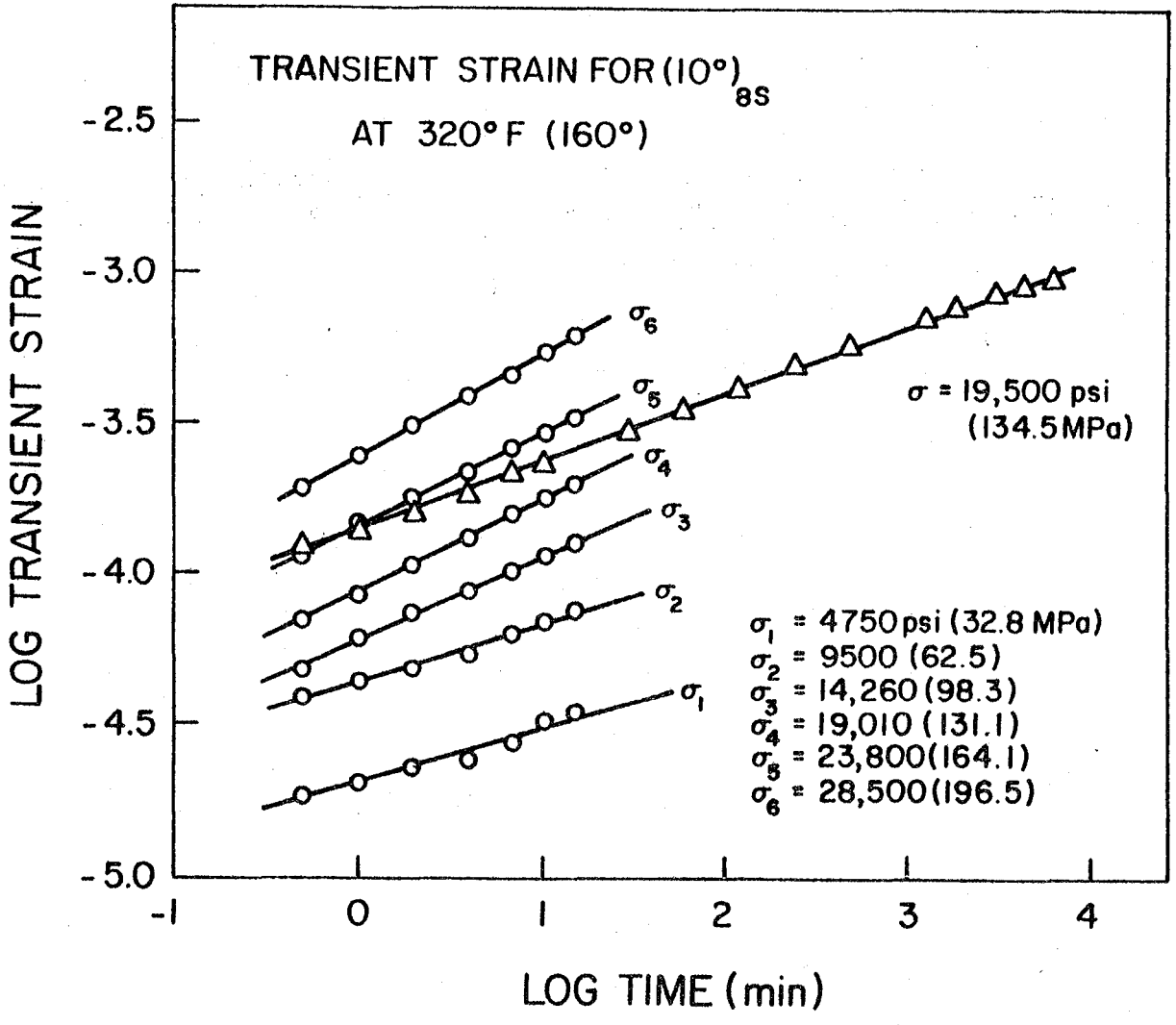

Fig. 3.11 Transient strain for 10° specimens at 320°F (160°C).

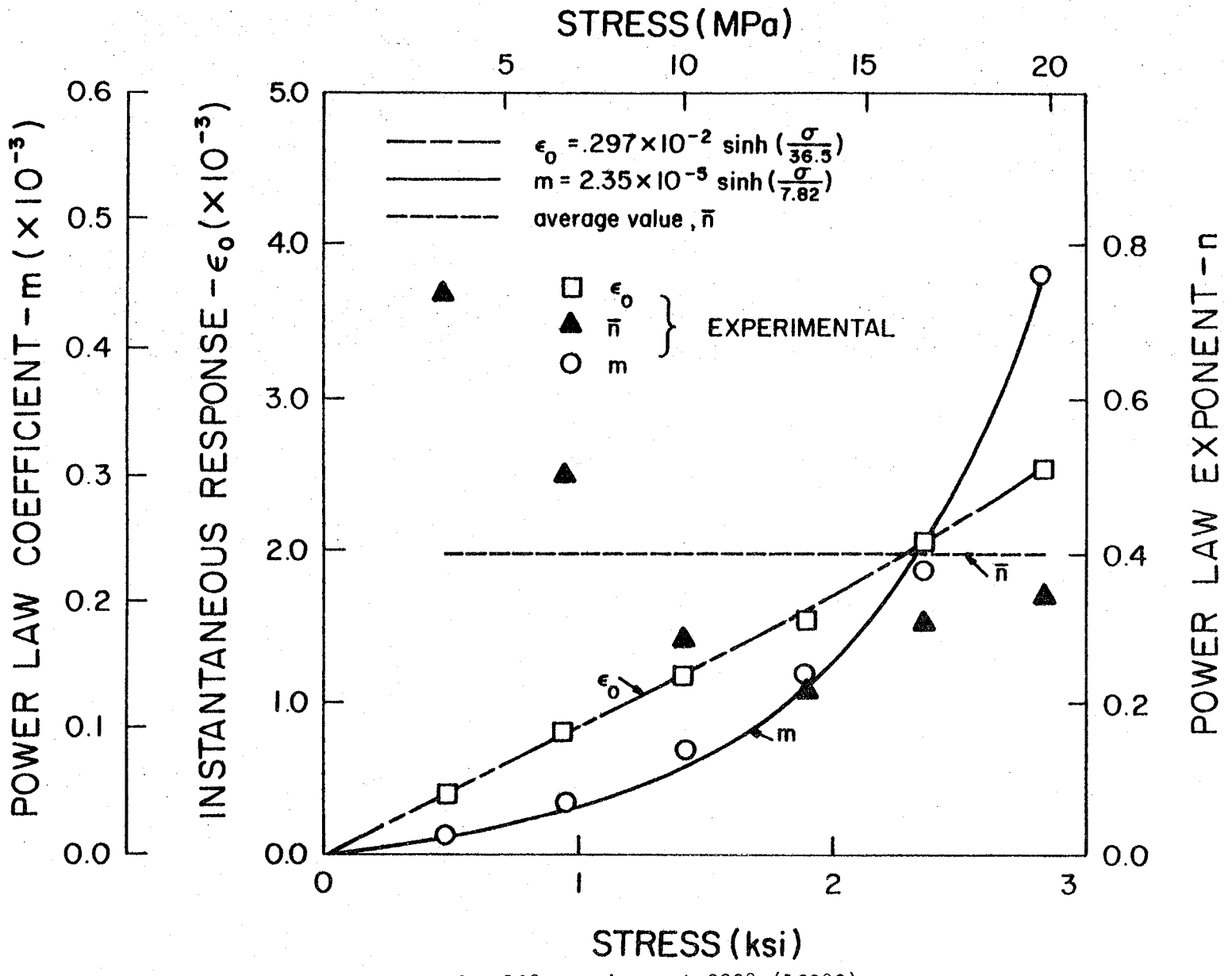

Fig. 3.12 Power law parameters for 10° specimen at 320° (160°C).

determine the transient strains plotted in Fig. 3.11 were the values predicted by the hyperbolic sine function which represents the actual values of ε_o. Had the actual values of ε_o, as determined from Eqn. 3.10 been used, the slopes of the lines in Fig. 3.11 would have been the same as the erratic calculated values of n. The use of the predicted values of ε_o rather than the raw values, results in a moderating effect which minimizes the erratic behavior introduced by the singularity.

The S_{66} compliance data obtained using the previously discussed transformation equations together with the Findley predictions for the 90° and 10° data is shown in Fig. 3.13. Because the input data is in the hyperbolic sine form, the application of the Findley approach to the calculated S_{66} also gives excellent results as shown in Fig. 3.14.

Based on the long term compliance data, the corrected value of n for the 90° data and the value of n for the 10° data were both equal to 0.22. While the agreement for the 10° and 90° exponents is excellent, the exponents calculated from Griffith's [38] long term 30° and 60° compliance data were significantly larger, 0.35 and 0.32 respectively. If S_{22} and S_{66} are based on the 90° and 10° results, the predicted 30° and 60° response will not be in good agreement with the experimental results. The reasons for the discrepancies in exponent value have not been investigated. Lou and Schapery [54] have indicated that the value of the power law exponent should be independent of the fiber angle. It is possible that additional damage such as matrix microcracking could have occurred in the 30° and 60°

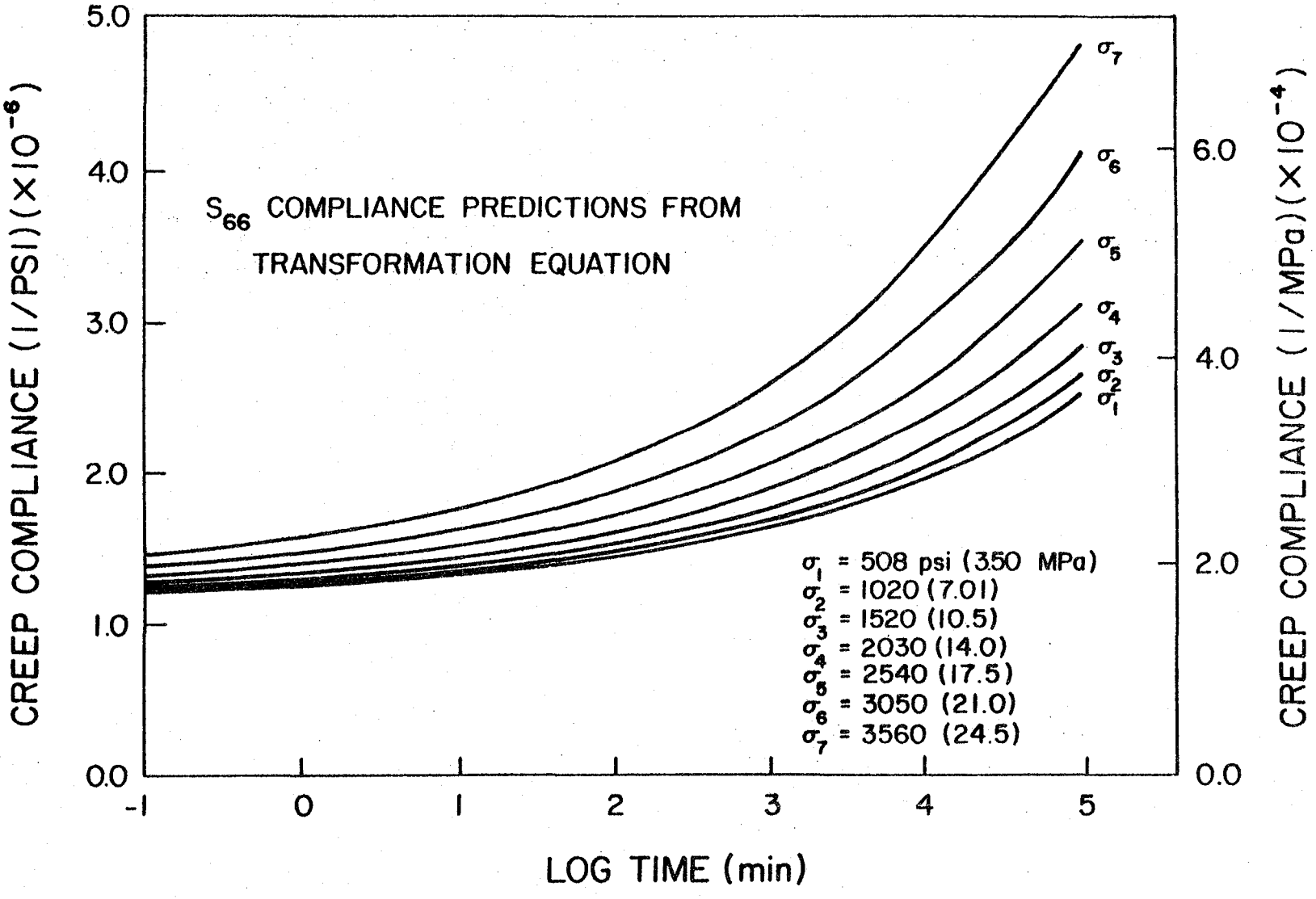

Fig. 3.13 S_{66} compliance predictions based on transformation equation.

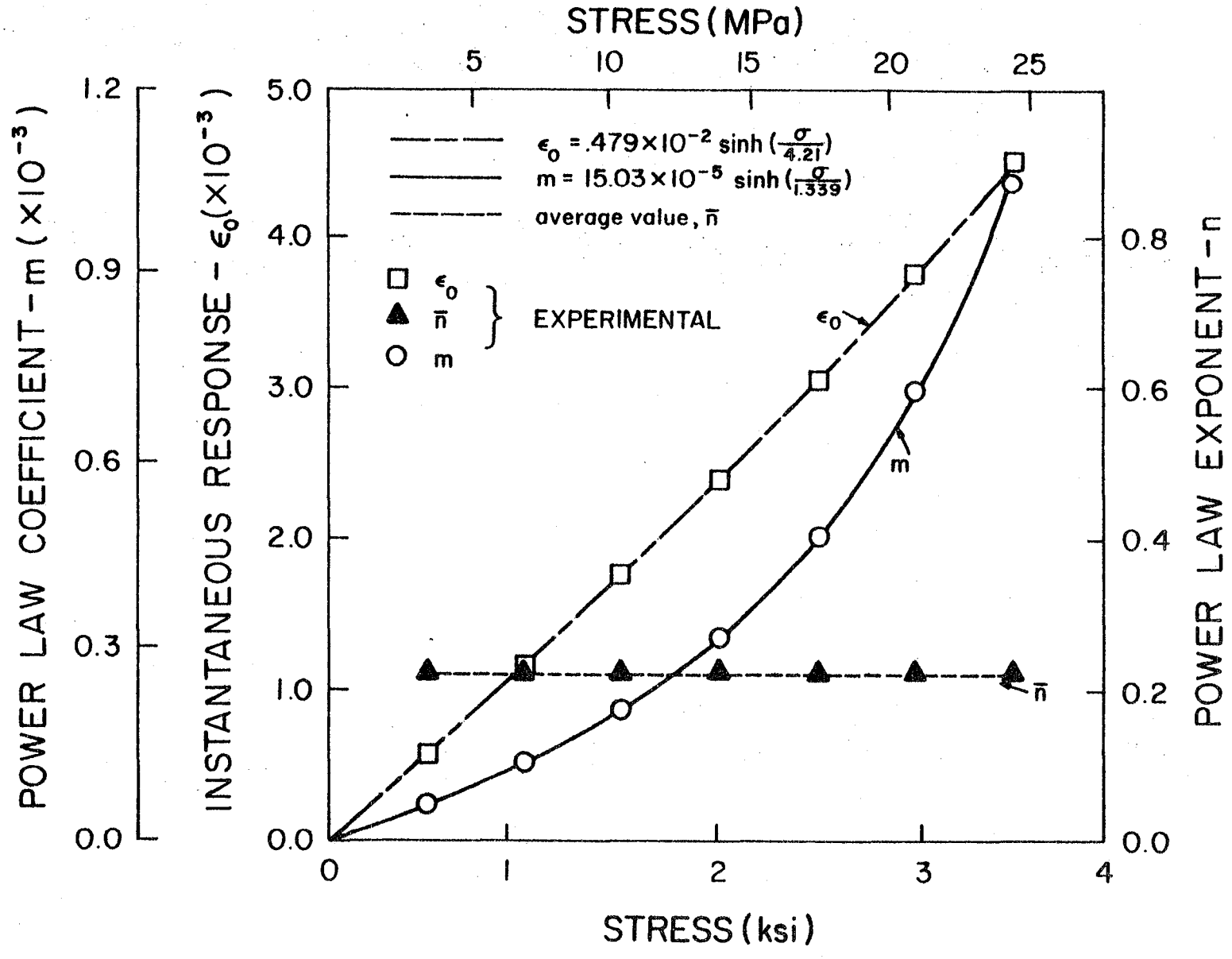

Fig. 3.14 Power law parameters for generated S_{66} data at 320°F (160°C).

specimens to result in the larger values for n.

The compliance properties for T300/934 Gr/Ep at 320°F as developed in this section may be summarized as,

$$S_{11} = 4.587 \times 10^{-8} \text{ in}^2/\text{lb}$$

$$S_{12} = -1.514 \times 10^{-8} \text{ in}^2/\text{lb}$$

$$S_{22} = (1/\hat{\tau})[.006728 \sinh (\hat{\tau}/9330) + .00009246 \sinh (\hat{\tau}/3030)\ t^{.1826}] \text{ in}^2/\text{lb}$$

$$S_{66} = (1/\hat{\tau})[.009431 \sinh (\hat{\tau}/8324) + .0002957 \sinh (\hat{\tau}/2648)\ t^{.2162}] \text{ in}^2/\text{lb}$$

These values have been expressed in terms of the normalized octahedral shear stress as given by

$$\hat{\tau} = 2.410\ \tau_{oct}$$

This constant is different from that used in plasticity theory because $\sigma_1^m \neq 0$. This normalized octahedral shear stress is equal to the applied stress for a 90° specimen, and is used as a convenience.

Variable Stress State

The ply stresses are constantly changing with time due to the differential creep rates among the plies and possible failure of an individual ply. Some type of superposition principle is required to account for the strain produced by a variable stress state. The Boltzman superposition integral is valid for linear viscoelastic materials but not for a nonlinear material. Being an extension of the Boltzman integral form to nonlinear materials, the Schapery integral expression should directly account for a variable stress history. As mentioned earlier, however, this approach was not used because there

was insufficient data to evaluate the g_0, g_1, g_2, and a_σ functions. The Green-Rivlin approach could be used but, again, is very difficult. Furthermore, while these forms do represent a variable stress history, their ability to predict strains for varying stresses has not been established.

A variety of simpler approaches have been proposed to account for variable stresses applied to nonlinear materials. Most have been limited to a uniaxial stress state. Also, they have been used and experimentally verified for only one or, in a few cases, several load steps. Many of these approaches are graphical in nature so that they can account for a general, nonlinear response without requiring a characterization of the response. Fessler and Hyde [29] have summarized several of these basic approaches.

Fig. 3.15 illustrates the predictions of several graphical procedures for a simple step loading given by,

$$\sigma(t) = \sigma_0 H(t) + (\sigma_1 - \sigma_0) H(t - t_1) \tag{3.31}$$

Their application requires knowledge of the independent responses,

$$\varepsilon(t,\sigma_0) \qquad \text{for} \qquad \sigma(t) = \sigma_0 H(t)$$

and

$$\varepsilon(t,\sigma_1) \qquad \text{for} \qquad \sigma(t) = \sigma_1 H(t)$$

A linear case has been used for illustrative purposes in Fig. 3.15 even though the graphical procedures are applicable to any general nonlinear response. This permits comparisons with the Boltzman superposition integral which is only applicable to linear materials. A linear case is schematically represented by letting the σ_0 response be a constant

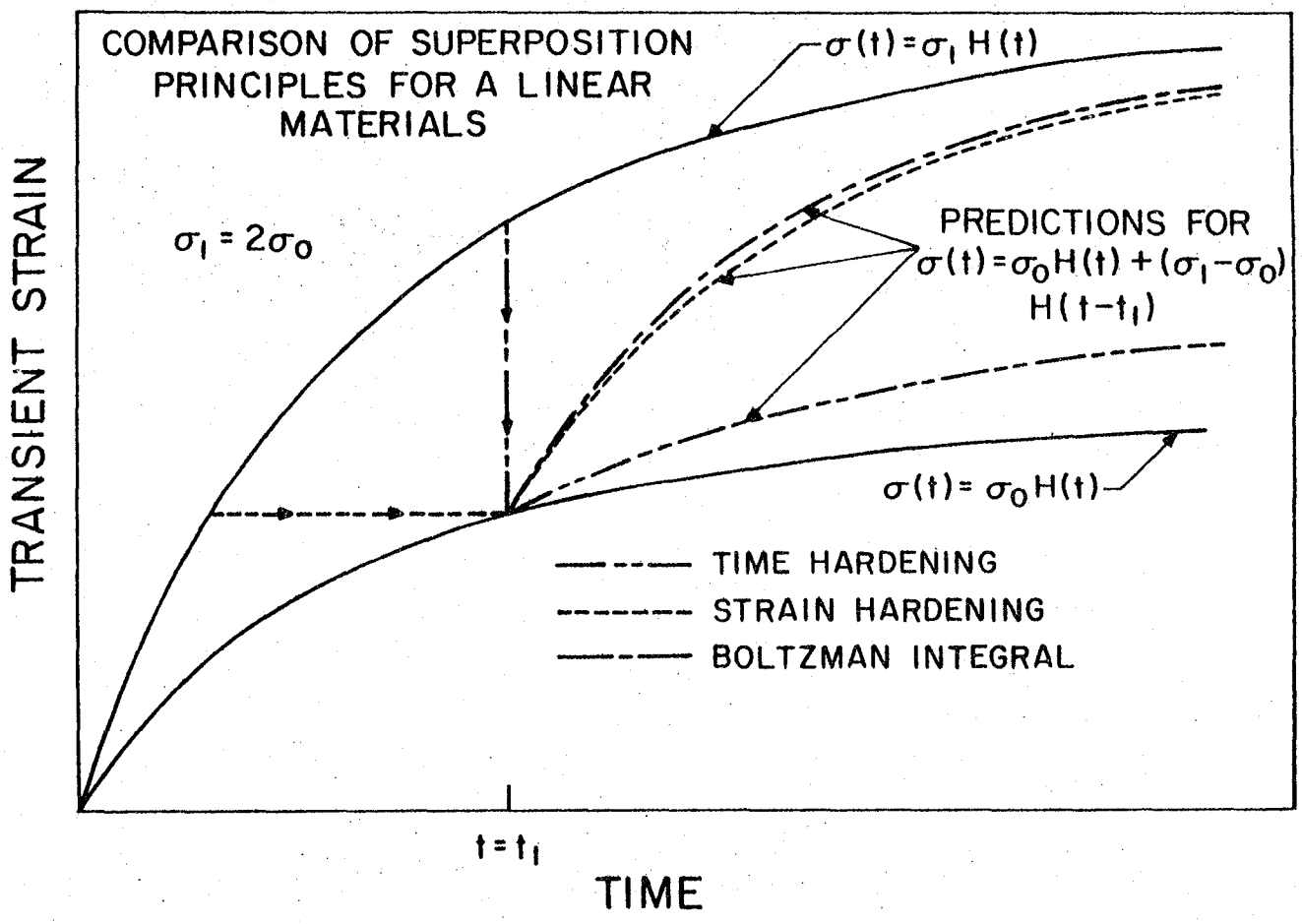

Fig. 3.15 Comparison of superposition principles for the case of a linear material.

proportion (1/2 in this case) of the σ_1 response.

The time hardening hypothesis requires a vertical (strain) shift of $\varepsilon(t,\sigma_1)$ to coincide with $\varepsilon(t,\sigma_0)$ at $t = t_1$. The strain hardening hypothesis requires a horizontal (time) shift for the same situation. The work hardening hypothesis in general involves a diagonal shift to equate the works done in creep. This approach, which is advocated by Fessler and Hyde [29], is similar to the strain hardening approach. In fact, for a linear material, these two approaches are the same. It is interesting to note that none of these graphical techniques simplify to the Boltzman integral for a linear viscoelastic material.

Another approach which has been used for variable stress state with nonlinear materials is basically a modification of the Boltzman superposition integral. Findley and Khosla [31] have proposed the use of a modified superposition principle of the form,

$$\begin{aligned}\varepsilon(t) = {} & \varepsilon_0(\sigma_0) + m(\sigma_0)\, t^n \\ & + \varepsilon_0(\sigma_1 - \sigma_0) + m(\sigma_1 - \sigma_0)(t - t_1)^n \\ & + \ldots \\ & + \varepsilon_0(\sigma_i - \sigma_{i-1}) + m(\sigma_i - \sigma_{i-1})(t - t_i)^n \end{aligned} \tag{3.32}$$

for the stress history

$$\begin{aligned}\sigma(t) = {} & \sigma_0 H(t) + (\sigma_1 - \sigma_0)\, H(t - t_1) + \ldots \\ & + (\sigma_i - \sigma_{i-1})\, H(t - t_i) \end{aligned} \tag{3.33}$$

While good agreement with experimental data was claimed, it should be noted that this approach is not consistent. A counterexample is found in a simple creep test with

$$\varepsilon(t) = \varepsilon_o(\hat{\sigma}) + m(\hat{\sigma})\, t^n \qquad (3.34)$$

for $\sigma(t) = \hat{\sigma}\, H(t)$

Now consider a load history of the form

$$\sigma(t) = (\hat{\sigma}/2)\, H(t) + (\hat{\sigma}/2)\, H(t - \Delta t) \qquad (3.35)$$

As $\Delta t \to 0$, the load history approaches that of a simple creep test, but the response

$$\begin{aligned}\varepsilon(t) &= \varepsilon_o(\hat{\sigma}/2) + m(\hat{\sigma}/2)\, t^n \\ &\quad + \varepsilon_o(\hat{\sigma}/2) + m(\hat{\sigma}/2)(t - \Delta t)^n \\ &= 2[\varepsilon_o(\hat{\sigma}/2) + m(\hat{\sigma}/2)\, t^n] \end{aligned} \qquad (3.36)$$

approaches that of a linear material. Obviously this scheme should not be used for a nonlinear system.

In a later paper, Findley and Lai [33] have proposed an alternative modified superposition equation of the form

$$\begin{aligned}\varepsilon(t) &= [\varepsilon_o(\sigma_o) + m(\sigma_o)\, t^n] \\ &\quad + [\varepsilon_o(\sigma_1) + m(\sigma_1)(t - t_1)^n - \varepsilon_o(\sigma_o) - m(\sigma_o)(t - t_1)^n] \\ &\quad + \ldots \\ &\quad + [\varepsilon_o(\sigma_i) + m(\sigma_i)(t - t_i)^n - \varepsilon_o(\sigma_{i-1}) \\ &\quad - m(\sigma_{i-1})(t - t_i)^n] \end{aligned} \qquad (3.37)$$

While this form does not have the drawback of the previous form, its validity for complex stress histories has not been established. Nonetheless, the approach is quite straightforward and easily adaptable to a numerical scheme. The method should be used with caution as there

are no additional parameters with this approach as exists in the Schapery procedure to modify the response for a varying stress level. The procedure is a straight superposition of the material response to simple creep loading. As such, it requires fewer tests than the Schapery integral, but is also less general.

The author's feeling is that the latter modified superposition principle is a simple attempt at predicting the response to a variable stress state but its accuracy for complex histories is doubtful. Nonetheless, the approach was used in the current investigation. Because the variation in ply stresses for creep loading is quite small and regular, any valid superposition principle should give reasonable results for creep loading.

Chapter 4

DELAYED FAILURE MODEL

Prediction of ply failure within a laminate requires the development of a delayed failure model. Because the state of stress for a ply in a laminate is more general than can be modeled by a uniaxial specimen, the failure model must account for any arbitrary stress state. The approach taken was to generalize an existing orthotropic static failure criteria to account for time dependent strengths as predicted by existing uniaxial creep strength theories. This combination should provide accurate static or very short time failures for general loading states, as well as accurate predictions of long term failures for a few specific load states. It is then assumed that the predictions for long term failures of arbitrary loading will also be accurate.

Most creep rupture criteria for homogeneous isotropic materials are based on a linearly decreasing logarithm of the time to rupture with increasing stress. This form, as exemplified by the Zhurkov, Larson and Miller, and Dorn methods, is given by

$$\log t_r = A - B\sigma \tag{4.1}$$

where t_r is the time to rupture for a constant creep load of σ. A and B are material constants for a given temperature [23]. Landel and Fedors [50] have noted that in some circles, the form,

$$\log t_r = A - B \log \sigma \tag{4.2}$$

is viewed more favorably. Because the form of Eqn. 4.2 is a power law,

its use would be more consistent with a constitutive relation based on the creep power law. Furthermore, the relation does not suffer from the limitation that a finite rupture time is predicted at zero stress. Because of the data scatter and the small range of stresses involved with our creep rupture data, however, the preference for one form over another becomes academic. Equation 4.1 provides an adequate representation for the current data and has been used throughout the present analysis.

Experimentally, the creep stress level is the independent variable and the time to rupture at that stress level is the dependent variable. For the analysis, however, it is convenient to rearrange Eqn. 4.1 to express the creep rupture strength, R, as a function of the time to rupture.

$$R(t_r) = (A - \log t_r)/B \tag{4.3}$$

The interpretation is that to obtain a failure at time $\hat{t}_r$, one would apply a creep stress level as given by

$$\sigma = R(\hat{t}_r)$$

Of the several orthotropic static failure theories discussed in Chapter 2, the Tsai-Hill criteria was chosen for the current analysis. While the Tsai-Wu Tensor Theory is often considered slightly more accurate because of its more general form, the requirements of compression and biaxial failure data to correctly evaluate the parameters prevents wider usage of this technique. While some investigators have assumed values for the interaction terms and assumed that tensile and compressive strengths are the same, this yields a criteria very

similar to the Tsai-Hill approach. Such assumptions do not take advantage of the more general nature of the tensor approach and thus minimize any advantages over the Tsai-Hill method.

If the Tsai-Hill criteria is extended to account for time dependent creep rupture strengths, the following form results,

$$\frac{\sigma_1^2}{[X(t_r)]^2} - \frac{\sigma_1\sigma_2}{[X(t_r)]^2} + \frac{\sigma_2^2}{[Y(t_r)]^2} + \frac{\tau_{12}^2}{[S(t_r)]^2} = 1 \qquad (4.4)$$

Here, the time independent strengths have been replaced by the creep rupture strengths which result in failure at $t = t_r$. $X(t_r)$ represents the creep rupture strength for a uniaxial creep load parallel to the fiber direction. For the current material the assumption was made that delayed failures do not occur for 0° specimens and that $X(t_r) = X$. $Y(t_r)$ represents the functional relation with time of the creep rupture strength for a uniaxial creep load perpendicular to the fiber direction. $S(t_r)$ is a similar functional relation for the shear creep rupture strength. Theoretically, $S(t_r)$ can be determined from uniaxial creep rupture of off-axis specimens and prior knowledge of X and $Y(t_r)$.

Thus, experimental creep rupture data for unidirectional laminates is used to determine functional expressions for the creep rupture strengths. For creep loading of any arbitrary biaxial stress state $[\sigma_1,\sigma_2,\tau_{12}]^T$, one can compute the associated rupture time by solving Eqn. 4.4.

Griffith [41] has obtained creep rupture data for 90°, 60°, and 45° off-axis specimens at several temperatures. This data has been

replotted with the results for the three orientations at a specific temperature on a single graph, and best fit lines have been drawn through the data points. The results are given in Figs. 4.1, 4.2, 4.3, and 4.4. This data was originally presented [38] to show the temperature dependence of creep rupture for the various fiber angles. The modified rate equation was shown [38] to provide the best analytical representation of the data.

The current interest is in the 320°F data as presented in Fig. 4.2. The points denoted as "Postcured 60° off-axis" were obtained during the present work to determine the effect of postcuring on creep rupture. While the magnitude remained about the same, there did seem to be a smaller decrease in the creep rupture strength with increasing rupture time. Because of the considerable data scatter, however, it is not known if this observation is justified. These postcured data points were not used for the best fit lines.

Assuming that the creep rupture strengths may be represented by Eqn. 4.3, determination of the slope and intercept for each best fit line in Fig. 4.2 allows the determination of the constants A and B. Thus one may determine the functional relationship as identified by, $R_{90}(t_r) = Y(t_r)$, $R_{60}(t_r)$ and $R_{45}(t)$. Using the 90° creep rupture strength and one of the off-axis creep rupture strengths, $R_\theta(t_r)$, one should be able to substitute these into Eqn. 4.4 to solve for $S(t_r)$. This is accomplished by letting

$$\sigma_1 = \cos^2 \theta \, R_\theta(t_r)$$

$$\sigma_2 = \sin^2 \theta \, R_\theta(t_r)$$

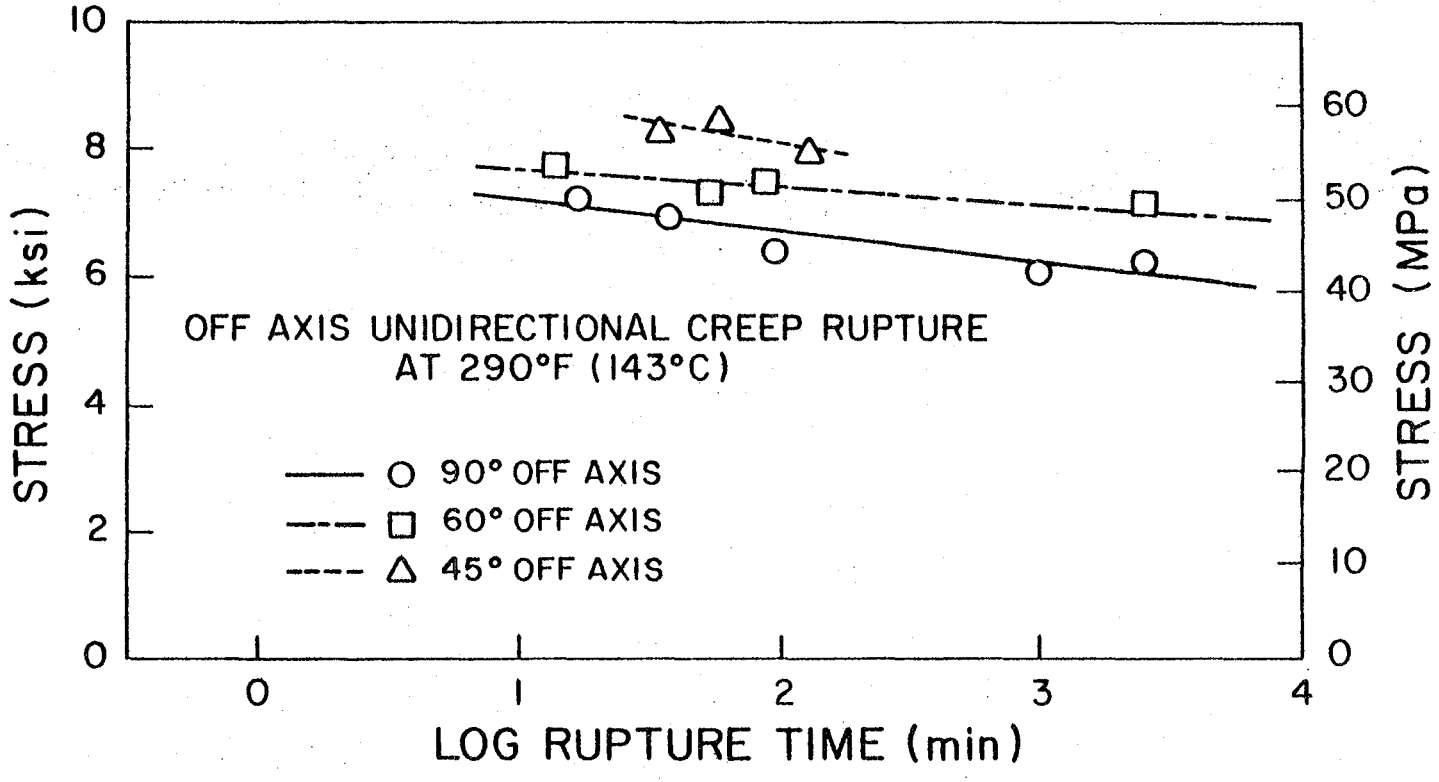

Fig. 4.1 Creep Rupture of Off-Axis Unidirectional Specimens at 290°F (143°C).

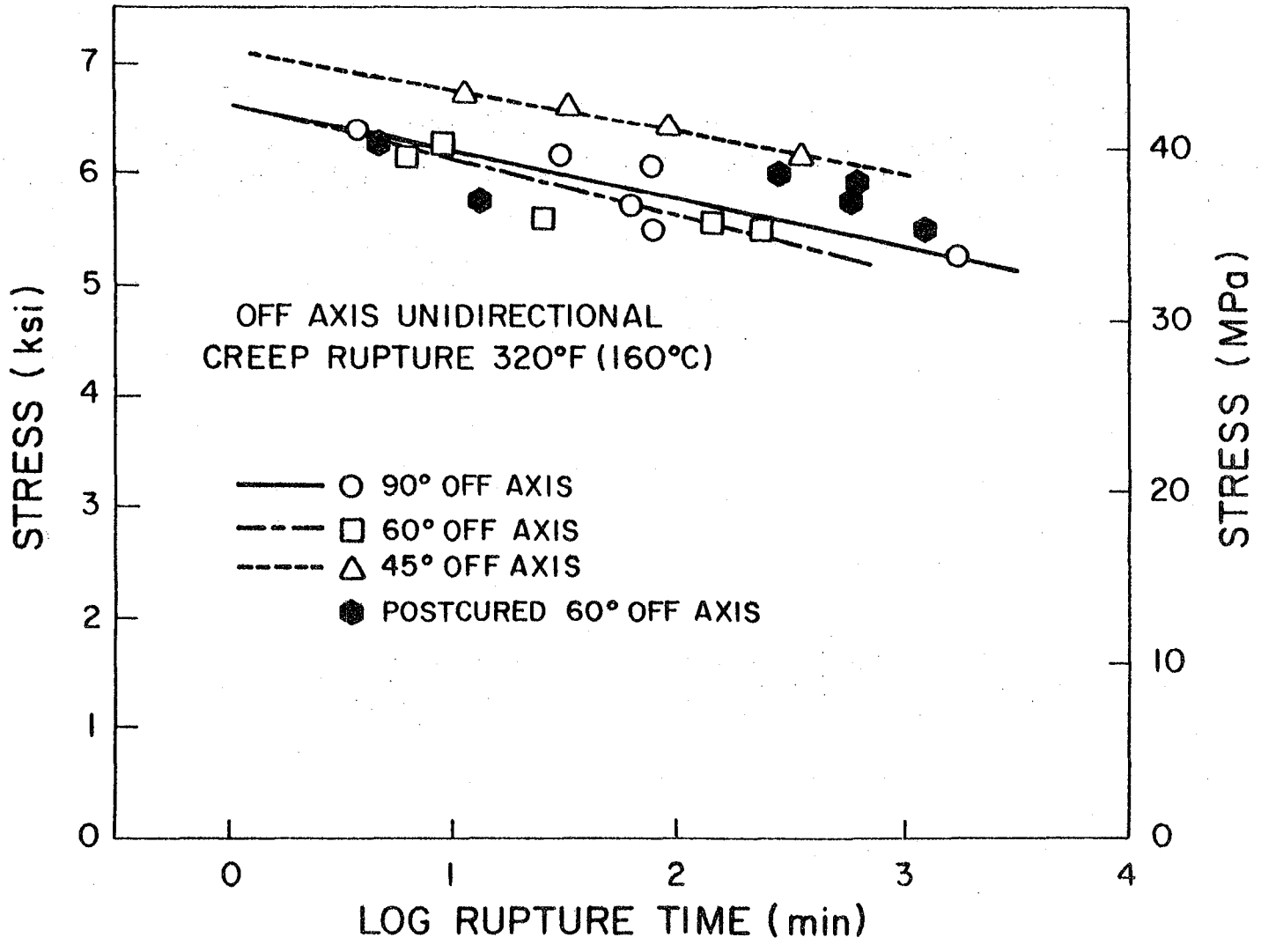

Fig. 4.2 Creep rupture of off-axis unidirectional specimens at 320°F (160°C).

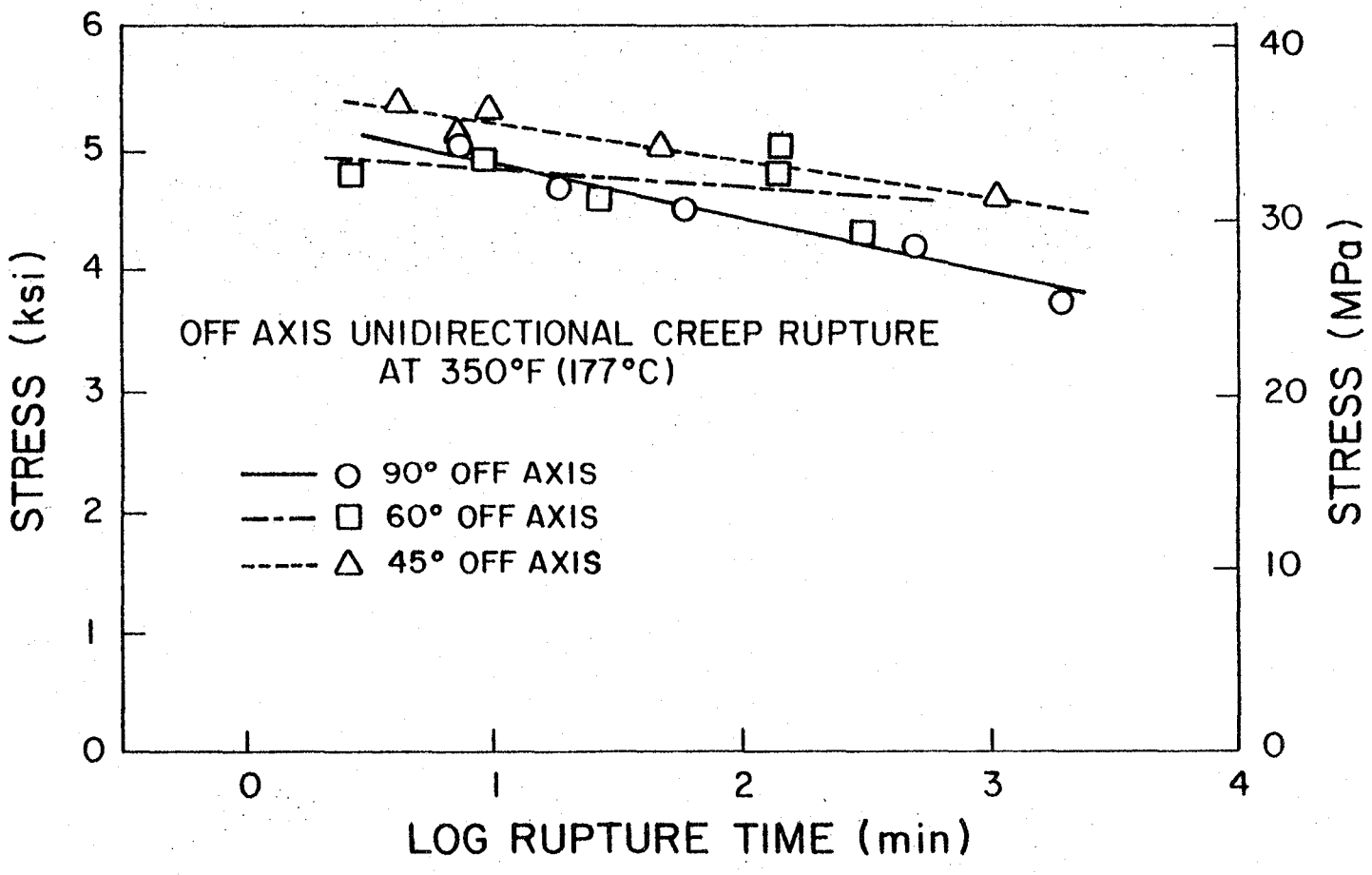

Fig. 4.3 Creep rupture of off-axis unidirectional specimens at 350°F (177°C).

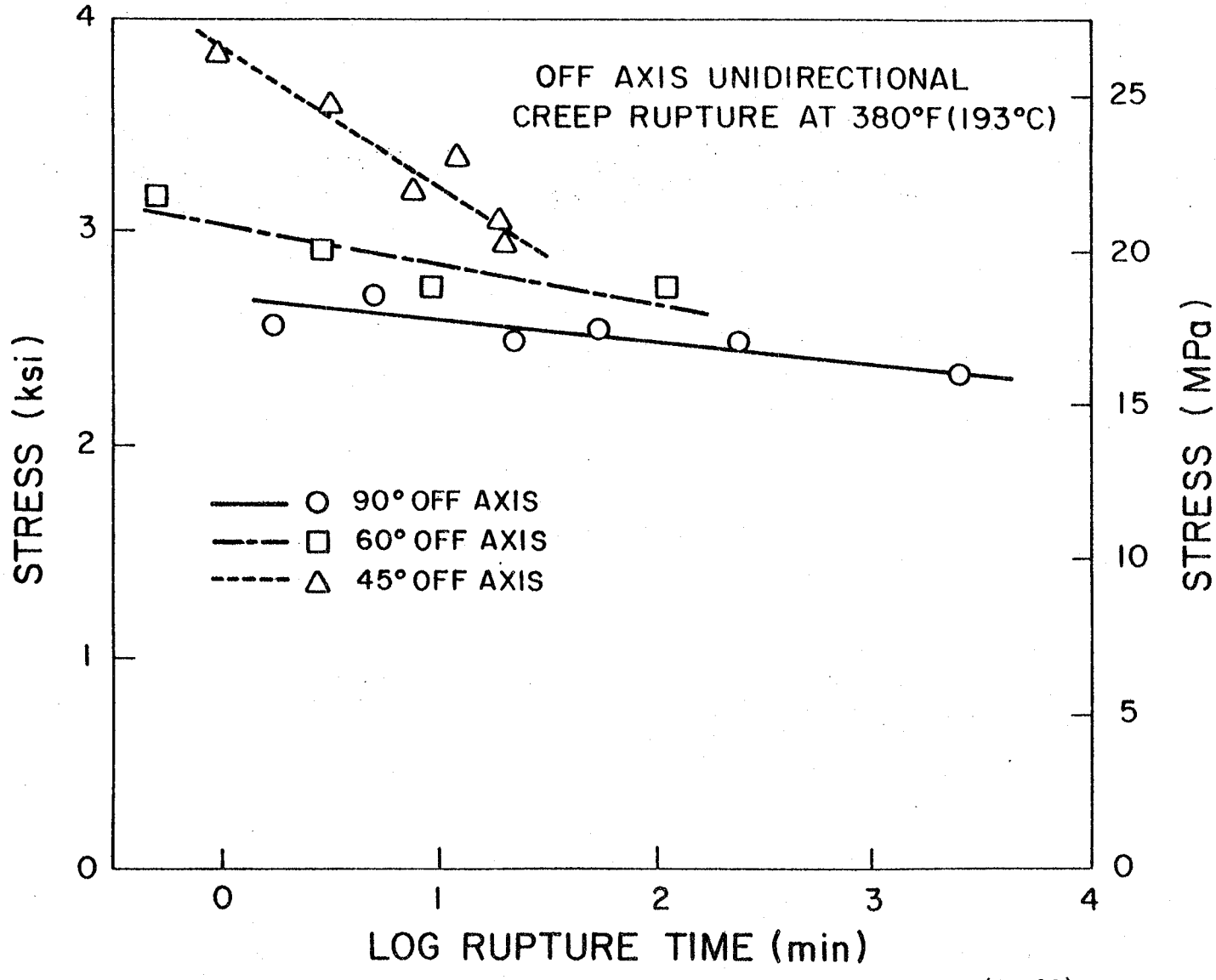

Fig. 4.4 Creep rupture of off-axis unidirectional specimens at 380°F (193°C).

$$\tau_{12} = \sin\theta \cos\theta \, R_\theta(t_r)$$

After rearranging the resulting equation, one obtains an expression for the shear creep rupture strength, $S(t_r)$, which is not necessarily of the form given in Eqn. 4.3.

This procedure, though straightforward, proved unsatisfactory for the available data. Because of considerable scatter in the limited amount of creep rupture data available, accurate determination of functional expressions for the experimental data are impossible. Slight changes in the functions for the 90° and off-axis strengths resulted in large variations in the function for the shear strength. In fact, if the best fit lines are used for the 60° and 90° data at 320°F, the predicted shear creep rupture strength increases with increasing rupture times. Furthermore, the shear strength predicted using the 60° data is inconsistent with that obtained using the 45° data. Obviously, there are inherent problems in determining an independent shear strength relationship by transformations without an extensive amount of data.

To alleviate this situation, the shear creep rupture strength was assumed to be of the form

$$S(t_r) = \alpha \, Y(t_r) \qquad (4.5)$$

Thus, all that must be determined from the data is the value of the proportionality constant, α, as the functional form of $S(t_r)$ has been established a priori. There is no rigorous justification to assume that the shear strength is proportional to the 90° strength, but such appears to be quite reasonable from an intuitive standpoint.

Primarily, this procedure reduces the degrees of freedom to a more manageable level.

To determine the appropriate value of α, the unidirectional creep rupture data was again employed. A specific rupture time, $\hat{t}$, was selected within the range of the available data. Values of the creep rupture strengths for this particular rupture time were taken as the intercept values of the $t_r = \hat{t}$ line and the best fit lines. These represent the values of creep stress, for the 90°, 60°, and 45° specimens, which would result in rupture at time $\hat{t}$. The 60° and 45° creep rupture strengths may be normalized with respect to the 90° value at that particular rupture time and temperature.

These normalized creep rupture strengths have been plotted in Fig. 4.5 for several times and temperatures. Superimposed upon this data are normalized parametric curves representing the Tsai-Hill predictions given by Eqn. 2.35 for various values of α. It should be noted that these curves will shift slightly depending on the ratio of the 90° strength to the 0° strength. For our material, this ratio is always very small, and this effect is completely negligible. Based on the modified rate equation predictions [38] rather than the best fit lines for the creep rupture data, similar results have been presented in Fig. 4.6. The octahedral prediction curve in each figure is based on failure occurring at a constant value of the octahedral shear stress as obtained using equation 3.29.

These figures are particularly useful in indicating several aspects of the failure data. Aside from the parametric curves, the points indicate the change in the normalized strengths at a particular

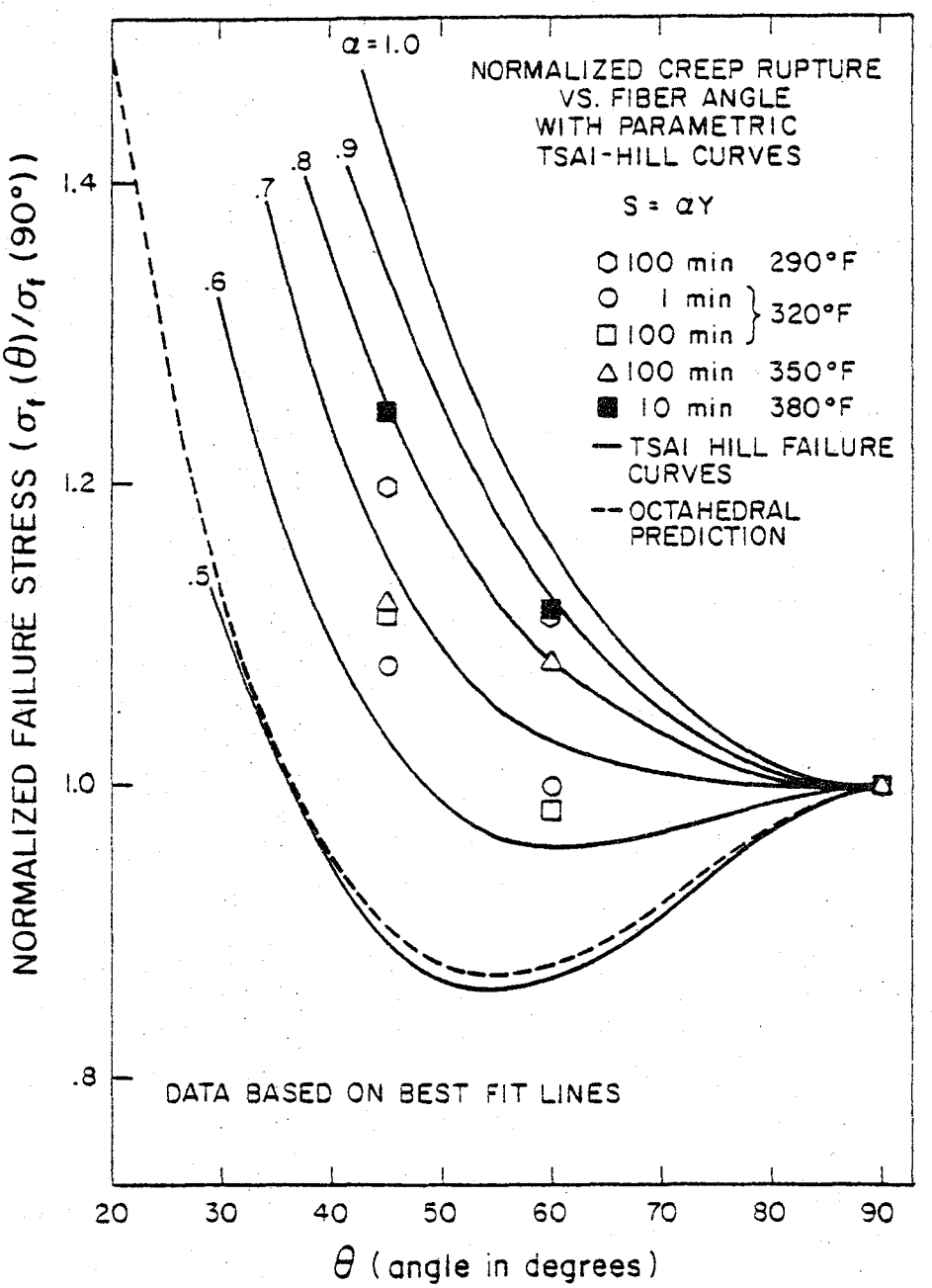

Fig. 4.5 Normalized creep rupture vs. fiber angle with parametric Tsai-Hill curves, S = αY.

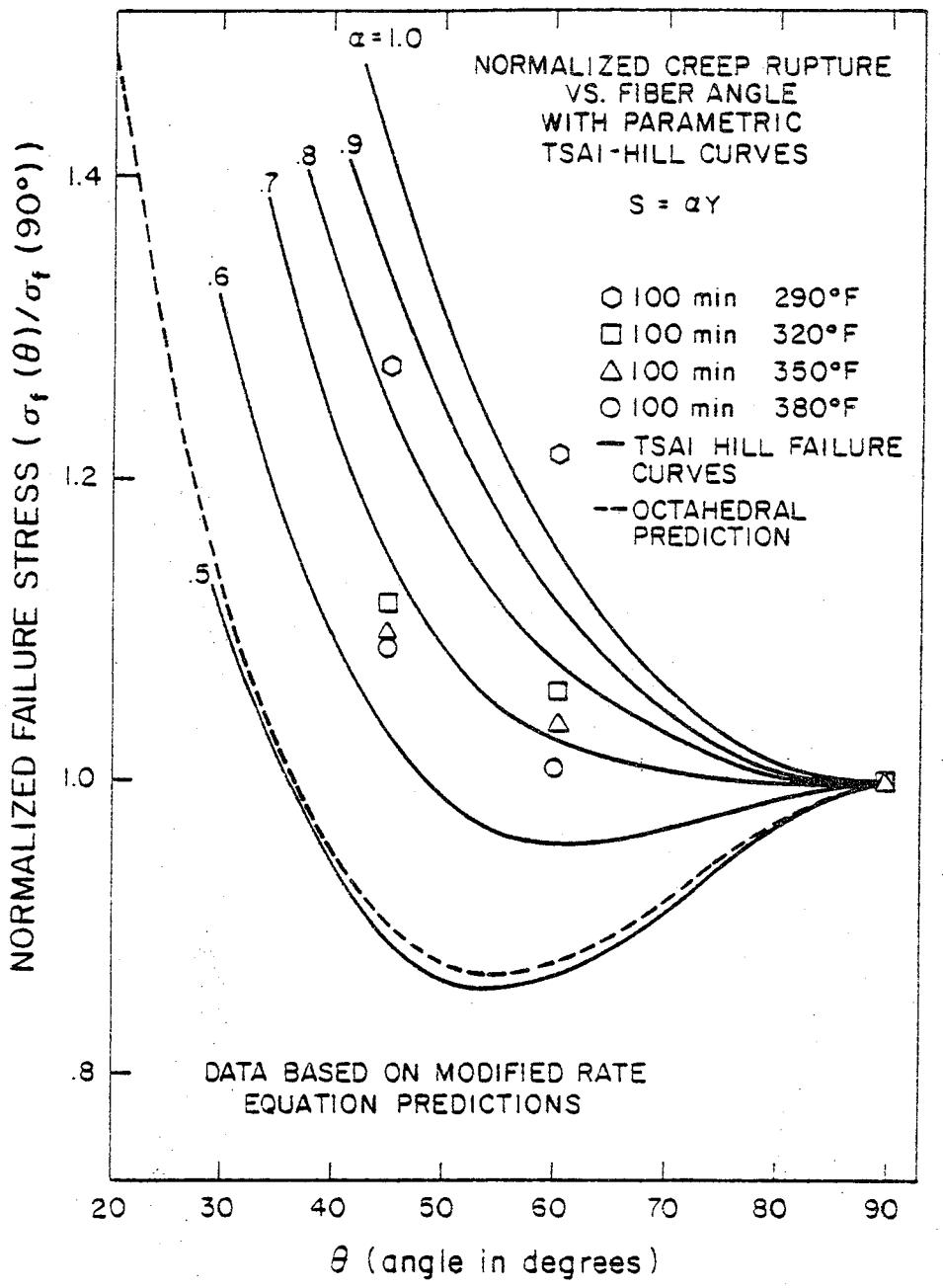

Fig. 4.6 Normalized creep rupture vs. fiber angle with parametric Tsai-Hill curves, S = αY.

orientation with respect to temperature. The tendency of the strengths at a particular time and temperature to fall along a line of constant

indicates the appropriateness of the Tsai-Hill criteria. A tendency for the points at different rupture times to fall along the same curve indicates the accuracy of the assumption that the time dependent shear strength is a constant proportion of the 90° strength. Presentation of information in this form provides a concise yet complete interpretation of the data.

Figs. 4.5 and 4.6 indicate a considerable variation in the $R_\theta(t_r)/R_{90}(t_r)$ ratio at the given values of time and temperature. Fig. 4.6 illustrates a correlation between increasing α and decreasing temperature for the modified rate equation predictions. Furthermore, on both figures there appears to be a direct correlation between the values of α for R_{45} and R_{60} at a given time and temperature. It is of interest to note that the values of α associated with R_{60} tend to be higher than those for R_{45}. This represents a deviation from the Tsai-Hill equation, which requires the same value of α for all fiber angles. Nonetheless, the results for the case of interest, 320°F, indicate that the 45° and 60° creep rupture strengths for t_r = 1 and t_r = 100 minutes are closely clustered around an α = .65 curve. This tends to verify that at 320°F the modified Tsai-Hill criteria and the assumption that $S(t_r)$ = .65 $Y(t_r)$ are appropriate. Such a formulation has been used for the failure model.

It should be noted that the results plotted in Fig. 4.5 (and 4.6, as well) are still based on drawing a line through only a few scattered creep rupture data points. As such, these values are

highly subject to error. Verification of the assumed model with any degree of confidence would require a more extensive data base and is felt to be a priority item for future work in the area.

The failure properties for T300/934 Gr/Ep at 320°F found from the foregoing analysis were as follows:

$$X = 195{,}600 \text{ psi} \tag{4.6a}$$

$$Y(t_r) = (6800 - 544 \log t_r) \text{ psi} \tag{4.6b}$$

$$S(t_r) = \alpha\, Y(t_r) \tag{4.6c}$$

$$\alpha = .65 \tag{4.6d}$$

Modification of Failed Ply Stiffness

The first ply failure does not necessarily result in total laminate failure. When failure of one ply has been predicted by the failure criteria, the stiffness properties of the ply must be reduced to indicate the effect of the failure. Basically, there are two modes of failure for parallel fiber reinforced materials. The fibers themselves may break, or the matrix may split along the fiber direction. As noted earlier, the Tsai-Hill failure criteria predicts the occurrence of failure, but does not predict the failure mode. An additional criteria was used to determine the manner in which failure occurred. If the failure criteria predicted a failure but the stress in the fiber direction did not exceed the 0° strength, a matrix failure was assumed to have occurred, but no fibers had broken. The matrix compliances, S_{22} and S_{66}, were increased by a factor β, which was an input parameter in the program. Fiber failure was assumed if the stress in the fiber direction exceeds the 0° strength. Because so much

energy is released in fiber failure, the matrix will generally break up and total lamina failure results. Thus for a total lamina failure, all compliances for that ply were increased by the factor β. The results of the numerical analysis to be presented in Chapter 7 are based on β being a large number so that failure effectively eliminates the scaled stiffness contributions of the failed ply. Smaller values of β could be used to allow a failed ply to remain partially effective.

Cumulative Damage

Just as a variable stress state causes problems with the non-linear constitutive equations, so it complicates the failure analysis. While the basic interest at present is to be able to predict creep ruptures under a constant load, an important future consideration will predict the behavior due to a varying load state. There has been much work done for fatigue of composites, but the author was more interested in slowly varying loads with only slight variation, as might occur, for instance, in a relaxation test. While these predictions for a laminate were not intended for the current investigation, they are necessary for the ply by ply analysis because of differential creep rates and because when a ply fails, the loads are increased in all remaining plies.

A great deal of study has been done in the area of creep rupture but nearly all has been based on a constant stress level. The forms of the prediction equations do not lend themselves to adaptation for a varying stress level. One possibility is the use of some type of cumulative damage approach where one takes into account the effect of

all the various stress levels acting over their respective interval of time. Such approaches have been widely used in fatigue in which it is often assumed that failure will occur when

$$\Sigma\left[\frac{n_i}{n_{r_i}}\right]^m = 1$$

where n_i is the number of cycles at stress level σ_i and n_{r_i} is the number of cycles required for a constant amplitude fatigue failure. When the parameter m is taken as unity, the familiar Miner's rule for fatigue is obtained. Robinson [61] has proposed a similar form for damage accumulation in creep, known as Robinson's Life Fraction Rule,

$$\Sigma \frac{t_i}{t_{r_i}} = 1 \tag{4.7}$$

where t_i is the time at creep load σ_i and t_{r_i} is the time to creep rupture at σ_i. Gerhards [37] has proposed the use of this approach for computing residual lifetime in wood. Woo, et al [79] have used the approach in predicting cracking in boiler tubes. Davis and Coleman [26] have discussed the general conditions under which damage may be additive. Kargin and Slonimsky [49] have generalized the linear cumulative damage concept to an integral form with temperature effect,

$$\int_0^t \frac{dt}{t_r[\sigma(t),T(t)]} = 1 \tag{4.8}$$

It is of interest to note that Woo, et al [79] have alluded to a combined fatigue and creep cumulative damage law of the form

$$\Sigma \frac{n_i}{n_{r_i}} + \Sigma \frac{t_i}{t_{r_i}} = 1 \tag{4.9}$$

Because creep and fatigue damage seem quite different in nature, one wonders about the additive nature of the two phenomena.

Miner's rule for fatigue, as is commonly known, may be grossly in error for some applications. The accuracy of a linear cumulative damage law for creep is not well established. Preliminary results from creep to yield tests on polycarbonate specimens at 75°C indicate that this approach may be grossly in error for creep also. There is some indication that this is also the case for graphite/epoxy. Primarily, the lifetime at a high stress level tends to be increased rather than decreased by a previously applied lower load. This is in direct contradiction of a cumulative damage theory. This phenomenon is believed to be due to some beneficial aging or structural modification process. Nonetheless, the linear cumulative damage law for creep has been incorporated into the failure model.

In addition to the cumulative damage law discussed above, a number of other approaches have also been proposed. Roberts, Ellis, and Bynum [59] have noted several of these approaches, among them:

Lieberman Strain Fraction Rule

$$\Sigma \frac{\varepsilon_i}{\varepsilon_{r_i}} = 1 \tag{4.10}$$

Freeman and Voorhees Mixed Rule

$$\Sigma \left(\frac{t_i}{t_{r_i}} \cdot \frac{\varepsilon_i}{\varepsilon_{r_i}} \right)^{1/2} = 1 \tag{4.11}$$

and

Abo El Ata and Finnie Mixed Rule

$$K \Sigma \frac{t_i}{t_{r_i}} + (1 - K) \Sigma \frac{\varepsilon_i}{\varepsilon_{r_i}} = 1 \qquad (4.12)$$

where ε_i is the strain accumulated at σ_i, ε_{r_i} is the rupture strain at σ_i, and K is a weighting constant. Judging from these methods, apparently the incorporation of the strain fraction is an important addition to the cumulative damage law. While the latter approaches are considered more accurate than Robinson's Life Fraction Rule, they are also more difficult to use because they require strain data. Use of these techniques was not possible as sufficient strain data to rupture was not available for the current material. More recent developments in damage accumulation are discussed by Bui-Quoc [13] and Woodford [80].

Chapter 5

THE NUMERICAL PROCEDURE

Predictions of time dependent deformations and failures for a general laminate require the knowledge of the combined stiffnesses of the plies as well as the variation in the ply stresses due to differential creep rates. While the linear elastic properties of a general laminate may be obtained quite easily from lamina properties by the use of simple lamination theory, there are no simple algebraic equations to incorporate viscoelastic behavior. Schapery [66,67] has reviewed the use of Alfrey's Correspondence Principle and Laplace Transforms to solve boundary value problems for linear viscoelastic anisotropic materials. The applicability of this approach to a general laminate is based on knowing the time dependent laminate compliance tensor. Determination of these functions from compliance properties of the individual plies is not trivial. A closed form solution along these lines would be very unwieldy to use even if one could be developed.

DeRuntz and Crossman [27] have developed a numerical procedure based on the linear viscoelastic properties of a generalized Maxwell element and lamination theory. Crossman and Flaggs [24] have used the procedure to analyze time dependent warping of nonsymmetric laminates for hygrothermally induced strains. Using the finite element method, Foye [36] has modeled the fiber inclusion for linear viscoelastic materials. He has averaged the micromechanical response to determine the time dependent behavior of a lamina. Using lamination theory, this information is incorporated to predict general laminate

response. The approach is interesting but the approximation appears to have inconsistent accuracies of the approximations at various stages.

For the nonlinear model used in the present analysis, the conclusion was made that a numerical scheme incremental in time was necessary to predict general laminate response from lamina properties. Approaches based on the finite element method and lamination theory were considered for this application.

A finite element approach would have involved discretization of each ply into a large number of 3-dimensional elements in order to describe the geometry of the test specimen, etc. The advantage of the finite element approach would be a complete solution that could predict edge effects due to the interlaminar stresses, a 3-dimensional stress state distribution throughout the model, and the effects of the end constraints. The disadvantages of this powerful approach would be the difficulty in developing and using the technique, and the cost of solution. To be effective, the grid should be fine enough to reflect the variation of the stresses normal to the plane. A refined grid would be required all along the free edges and in the vicinity of the constrained end. For viscoelastic analysis, a large number of storage locations would be required for each element in order to reflect the hereditary integral constitutive relations. Use of a grid fine enough to show the effect of free edges and constrained ends would require such a large amount of storage and computing time, that it was undesirable for use at this time. Furthermore, note that the stiffness matrix continuously changes with time, which poses a real cost problem for the repetitive solution of a large number of

simultaneous equations.

The finite element approach should provide more accurate predictions than a lamination theory approach but would represent an expensive overkill at the present stage of development. The data scatter inherent in creep rupture in general and laminated composite materials in particular tends to mask the added accuracy of the FEM. Thus while still looking at basic phenomena and trends, the lamination theory approach was identified as the most efficient formulation to study delayed failures in laminated composites for the present effort.

The Lamination Theory Program

Classical lamination theory provides a simple means to combine the individualized ply stiffnesses to form a unified laminate. As mentioned earlier, the fundamental assumption for lamination theory is that normals remain straight and normal for any deformation which, in effect, causes interlaminar stresses to be neglected. This assumption is strictly valid only for interior regions of panels. Without resorting to other techniques, basic lamination theory results do not lend themselves to the analysis around cut-outs or the effect of end constraints. In essence, lamination theory provides a technique to determine the overall stiffness properties of a laminate based on the properties of the constituent laminae.

A computer program based on lamination theory has been developed in the current study. The primary feature of the program is the analysis of a general laminate composed of several nonlinear viscoelastic

laminae. While the current application has been for constant uniaxial creep loads, the procedure was written to handle time-varying biaxial loadings as well. Nonlinear viscoelastic laminae properties are input internally. The power law has been used in the present work but other forms, such as a generalized Kelvin element representation, are completely admissible. Compliance interaction effects may be neglected or may be assumed to depend on the matrix octahedral shear stress. The modified Findley superposition principle (Eqn. 3.37) has been used to account for the variable ply stresses caused by differential creep rates and in the event of a lamina failure. The modified Tsai-Hill failure criteria (Eqn. 4.4) has been used as the ply-wise failure theory. The linear damage accumulation rule (Eqn. 4.7) has been used to account for the variable ply stresses. All of these procedures are subroutines which could easily be modified for other approaches. If the initial response is nonlinear in stress, an iterative procedure is used to converge on the actual solutions. If a ply "fails", the ply properties are modified to reflect the damage state.

The basic concept behind the incremental lamination theory approach is quite straightforward. The solution scheme is based on obtaining successive stress, strain, and accumulated damage solutions as time is incremented. The strain state is determined at time $t + \Delta t$, based on the assumption that the stress state at time t is constant for the time step Δt. New ply stresses are determined at $t + \Delta t$ based on the current creep strains and the applied mechanical load. Accumulated damage in each ply is monitored until ply failure is predicted. This procedure is continued until total laminate failure

occurs.

While the actual laminates tested were composed of 16 plies, the numerical model need only contain as many plies as the number of different fiber orientations. This simplification would not be possible if one were considering a finite element model or an out-of-plane response.

Numerical Details

The flow chart in Fig. 5.1 summarizes the numerical procedures used in the current approach. The equations for each step can be found by reference to Chapter 2. The equations representing the compliance and failure models are more involved and have not been stated explicitly in the figure. The reader is referred to Chapters 3 and 4, respectively, for these formulations. The program proceeds as follows: Initially, the program reads in the laminae properties, the stacking sequence of the laminate, and the control parameters. The laminae and laminate creep strains are initialized to zero. The instantaneous (hereafter referred to as elastic) laminae compliance matrix is determined, based on the current properties and stress state. Using lamination theory, the laminae compliance matrices are inverted, transformed, and combined to form the laminate stiffness matrix. Based on the current applied load, the elastic laminate strains are determined. The ply stresses are determined based on the total laminate strain and the creep component of the laminae strains. If the ply stresses are significantly different than those computed at the previous time, a nonlinear iterator is invoked to converge to the

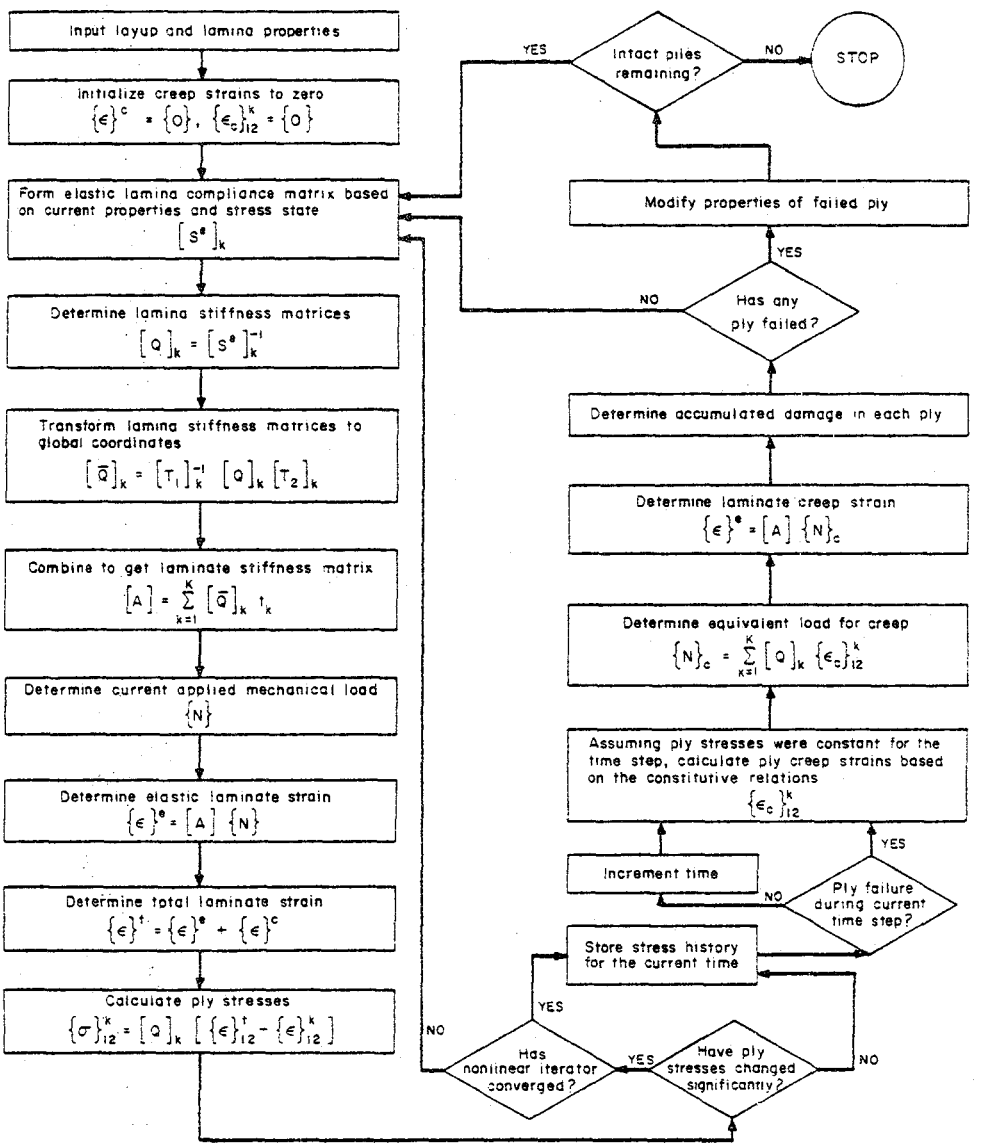

Fig. 5.1 Flow chart for viscoelastic laminated composite analysis.

actual solution. The current stresses are stored in a stress history matrix and time is incremented. Assuming ply stresses remained constant for the time step, the current ply creep strains are computed based on the compliance model discussed in Chapter 3. Determination of the total laminate strain requires obtaining the effective laminate creep strain. This is determined by first computing the equivalent mechanical load necessary to produce the same elastic laminate strain. The accumulated damage is evaluated in each ply and compared with the failure criteria model developed in Chapter 4. If any ply has "failed", the time of failure is calculated and the ply properties are modified. This procedure is repeated until all plies have failed.

Hereditary Integral Evaluation

Previous efforts in developing numerical procedures for creep analysis have primarily been limited to linear systems. For linear analysis, the Boltzman hereditary integral

$$\varepsilon(t) = \int_{-\infty}^{t} D(t - \tau) \frac{d\sigma(\tau)}{d\tau} d\tau \tag{5.1}$$

has been approximated by a finite series based on discrete time steps

$$\varepsilon(t) = \sigma_0 D(t) + (\sigma_1 - \sigma_0) D(t - t_1) + \ldots + (\sigma_i - \sigma_{i-1}) D(t - t_i) \tag{5.2}$$

This represents an exact solution for a discrete load history given by

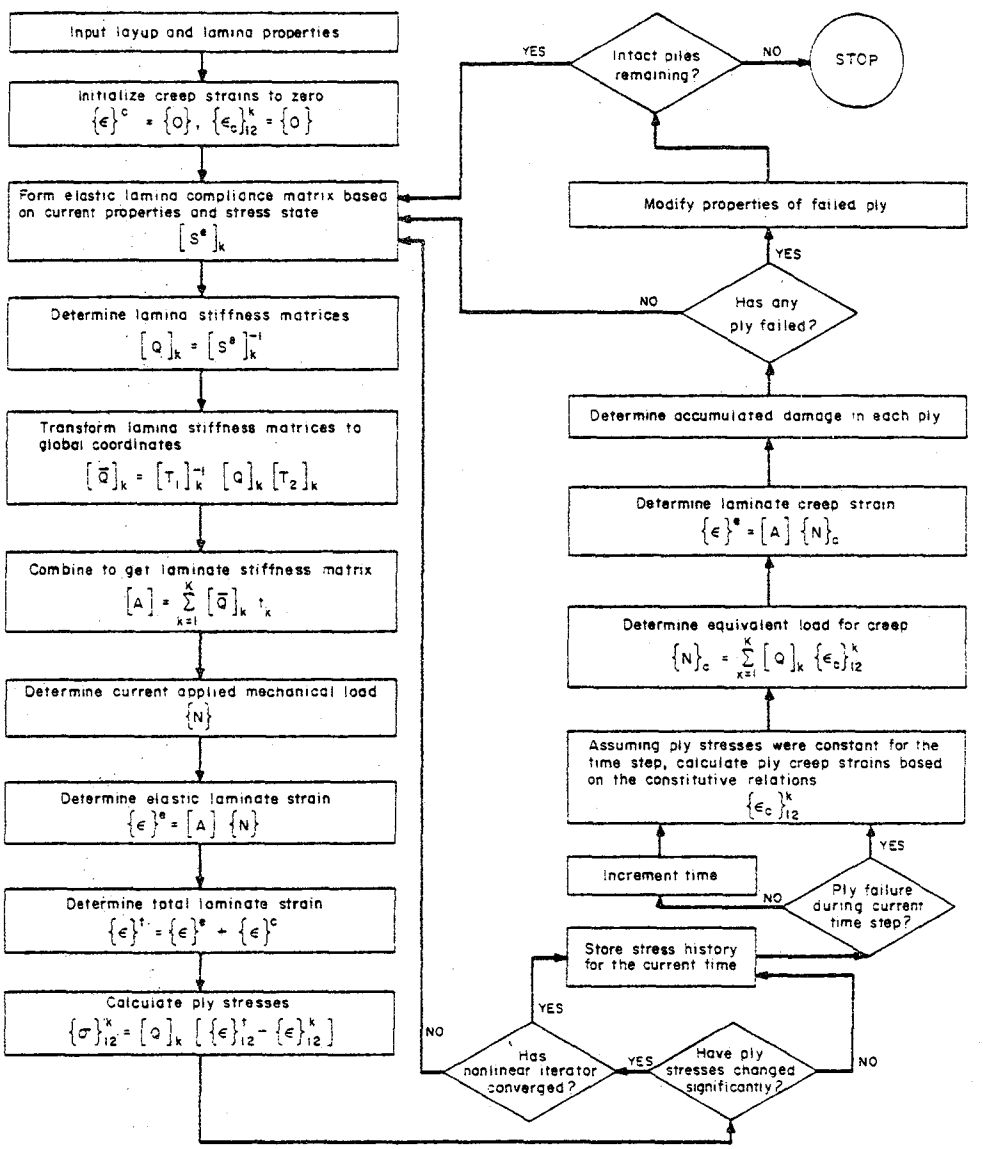

Fig. 5.1 Flow chart for viscoelastic laminated composite analysis.

actual solution. The current stresses are stored in a stress history matrix and time is incremented. Assuming ply stresses remained constant for the time step, the current ply creep strains are computed based on the compliance model discussed in Chapter 3. Determination of the total laminate strain requires obtaining the effective laminate creep strain. This is determined by first computing the equivalent mechanical load necessary to produce the same elastic laminate strain. The accumulated damage is evaluated in each ply and compared with the failure criteria model developed in Chapter 4. If any ply has "failed", the time of failure is calculated and the ply properties are modified. This procedure is repeated until all plies have failed.

Hereditary Integral Evaluation

Previous efforts in developing numerical procedures for creep analysis have primarily been limited to linear systems. For linear analysis, the Boltzman hereditary integral

$$\varepsilon(t) = \int_{-\infty}^{t} D(t - \tau) \frac{d\sigma(\tau)}{d\tau} d\tau \tag{5.1}$$

has been approximated by a finite series based on discrete time steps

$$\varepsilon(t) = \sigma_0 D(t) + (\sigma_1 - \sigma_0) D(t - t_1) + \ldots + (\sigma_i - \sigma_{i-1}) D(t - t_i) \tag{5.2}$$

This represents an exact solution for a discrete load history given by

$$\sigma(t) = \sigma_0 H(t) + (\sigma_1 - \sigma_0)\, H(t - t_1) + \ldots$$
$$+ (\sigma_i - \sigma_{i-1})\, H(t - t_i) \qquad (5.3)$$

As indicated in Chapter 3, the procedure used in the present approach is based on the modified Findley superposition principle of the form

$$\varepsilon(t) = \sigma_0\, D(t,\sigma_0)$$
$$+ \sigma_1\, D(t - t_1,\sigma_1) - \sigma_0 D(t - t_1,\sigma_0)$$
$$+ \ldots$$
$$+ \sigma_i D(t - t_i,\sigma_i) - \sigma_{i-1}\, D(t - t_i,\sigma_{i-1}) \qquad (5.4)$$

Equation (5.4), while not expressed as a convolution integral, is considered to be a discretization of a modified hereditary integral. Thus, subsequent solution techniques are referred to as a numerical evaluation of a convolution or hereditary integral.

Convolution integral evaluations require large amounts of storage locations to keep track of the time history effects. For linear materials, Zienkiewicz [86,87] has proposed the use of a generalized Kelvin model for the viscoelastic behavior. One may express the creep strain increments in terms of the current stress and the individual creep strains for each Kelvin element

$$\Delta\varepsilon_c = \left\{\left(\sum_{i=1}^{N} \frac{1}{\eta_i}\right)\sigma - \sum_{i=1}^{N} \frac{E_i}{\eta_i}\, \varepsilon_c{}^i\right\} \Delta t \qquad (5.5)$$

where $\Delta\varepsilon_c$ is the increment of creep strain

E_i - spring modulus of i^{th} Kelvin element

η_i - dashpot coefficient of i^{th} Kelvin element

σ - applied stress

ε_c^i - creep strain in i^{th} Kelvin element

and N - number of Kelvin elements.

This procedure is more computationally efficient than a direct integration of the convolution integral. Taylor, et al [76] have extended this approach to account for changes in the material properties due to temperature, etc. One problem with the technique is that of fitting a material with a generalized Kelvin model. To express an increasing compliance over many decades of time requires a large number of Kelvin elements to provide a good fit. Crossman and Flaggs [24] have shown a very wavy representation for the compliance of an epoxy matrix using 10 Kelvin elements over a 20 decade time span. If 10 to 20 Kelvin elements for several compliance terms of each ply are necessary, a large amount of storage is required as well. This approach was originally used in the current investigation but the bookkeeping became difficult. Keeping track of all the individual Kelvin element properties and creep strains was cumbersome. The main limitation of this approach, however, was that it is only valid for a linear material. Therefore, this procedure was eventually abandoned because it could not model the nonlinear behavior of the epoxy matrix.

The approach actually used, then, was a direct numerical integration of the modified convolution integral (if it could actually be expressed) by the finite sum given in Eqn. 5.4. By using logarithmic increments in time, the number of stress history storage locations required was quite reasonable.

Iterative Scheme for Nonlinear Instantaneous Response

If ε_o is not linear in σ, the material system exhibits nonlinear instantaneous response. As such, an iterative scheme must be used to determine the ply stresses based on the applied load. At first application of the load, ply stresses are calculated based on an arbitrary value of $\hat{\tau}$. Based on the ply stresses predicted from this first computation, revised values of $\hat{\tau}$ are calculated and the procedure is repeated until convergence is achieved. Convergence is checked by a square norm

$$\varepsilon = \sum_{k=1}^{K} \left[\left(\sigma_{1,i}^{k} - \sigma_{1,i-1}^{k} \right)^2 + \left(\sigma_{2,i}^{k} - \sigma_{2,i-1}^{k} \right)^2 + \left(\tau_{12,i}^{k} - \tau_{12,i-1}^{k} \right)^2 \right] \tag{5.6}$$

Because the material is only slightly nonlinear in the instantaneous response, convergence is achieved quickly and easily by this scheme. A more sophisticated scheme is required for highly nonlinear materials. This iterative convergence scheme is also required if the applied load changes, or if a redistribution of ply stresses occurs because of a ply failure.

Log Increments in Time

Because of the nature of creep response, the creep rate decreases significantly as time increases. Logarithmic rather than real time increments are used. Based on the rate of activity, this applies a more consistent amount of attention to the time regions. Thus, by running ten iterations per decade of time, for example, a more

consistent base is used for the time increments. This permits close scrutiny near the initial loading and minimizes computational efforts when analyzing the long time regions where the creep rate is extremely slow.

When a ply fails, the creep rates immediately following may be quite high as the stresses in each remaining ply adjust to carry the applied load. Thus, when a ply fails, the time step is reduced to carefully follow the action after failure of a ply. The logarithmic incrementation scheme is again employed, but with a constant time added to it equal to the time of ply failure.

Fiber Rotation Due to Large Deformations

Some specimen configurations may exhibit considerable deformations and corresponding fiber rotations. As the specimen elongates in the axial direction and contracts in the transverse direction due to the Poisson effect, fiber angles tend to become smaller, shifting more of the load to the fibers, effectively making the specimen stiffer. To account for this effect, one can calculate the amount of fiber rotation and use the new fiber direction in subsequent calculations. Assuming a general deformation of an element containing fibers at an arbitrary angle θ to the x axis, it can be shown that the new fiber angle θ' is given by:

$$\theta' = \tan^{-1}\left[\frac{(\tan\theta)(1+\varepsilon_y)}{1+\varepsilon_x+\gamma_{xy}\tan\theta}\right] \tag{5.7}$$

This procedure is applied to all plies at each time step. Assuming that the old fiber angle can be replaced by the new angle

represents a first order approximation of the actual effect. It should be noted that θ in Eqn. 5.7 must always be taken as the ply angle of the original layup. Use of the updated values would produce incorrect results.

Residual Thermal Stresses

Because of the considerable difference in the thermal expansion coefficients in the fiber and matrix directions, significant residual thermal stresses in general laminates may be induced by the cool-down process of the cure cycle. In fact, linear elastic analysis of this aspect may predict ply failure during cool-down and prior to the application of mechanical loads. Consideration of residual thermal stresses is often felt to be important in laminate strength predictions but have not been considered in the current numerical scheme. As discussed in the development, thermal stresses may be included by adding the independent thermal strains to the creep strains in Eqn. 2.9. All of the current work was done at elevated temperatures, and most were done at 50°F (28°C) below the glass transition temperature. At these high temperatures, the residual stresses should be quite small. Furthermore, Weitsman [78] has shown that a viscoelastic analysis yields residual stresses about 20% smaller than those predicted by linear elastic analysis. The soak at elevated test temperatures prior to testing should lead to even further relaxation of the residual stresses. Thus the thermal stresses have been assumed to be negligible for the current work, but they may need to be considered for work at lower temperatures.

Numerical Stability

As with many iterative numerical schemes, instability problems were encountered with the program. A minor problem arose from numerical oscillations produced by the sudden application of the initial mechanical load. Typical disturbances of the ply stresses were on the order of 10% and were damped out within about 8 iterations. This problem was improved by using a technique somewhat analogous to the central difference method. The octahedral shear stress in each ply was moderated by

$$\tau_{oct}^{k} = [\psi(\tau_{oct}^{k})_{old} + (\tau_{oct}^{k})_{new}]/(1 + \psi) \qquad (5.8)$$

Letting $\psi = 1$ results in a straight average of the previous and the current octahedral shear stress values. The "old" value comes from the previous iteration and the "new" value represents the value based on the current ply stresses. The result from Eqn. 5.9 is an averaged value which improves stability considerably.

The major instability problem occurred only when analyzing the two fiber orientation laminates. Theoretically, the procedure should be stable as long as the time steps are sufficiently small. The computed values of the octahedral shear stress in the two ply laminates are larger than those encountered in the three or more ply laminates. The nonlinear dependence is based on a hyperbolic sine function involving τ_{oct}. As τ_{oct} becomes larger, relatively small changes in τ_{oct} result in huge variations in the hyperbolic function. This provides the driving force for the instability. As seen in Figs. 3.7 and 3.10, the compliance turns up sharply at longer times when plotted

against log time. Thus with the use of logarithmic time increments, the compliance curve becomes harder to follow accurately at long times. This results in the initial perturbation of the solution.

Increasing ψ in Eqn. 5.9 to values on the order of 100 produces stable results but leads to a very sluggish response. However, when proper time increments are chosen, stable results are obtained over long time spans for most laminates.

Chapter 6

EXPERIMENTAL PROCEDURES

Several phases of experimental work were conducted so that the phenomena of creep and creep rupture in laminated composite materials would be better understood. The main emphasis was on obtaining creep rupture data for several different layups which heightened our understanding of creep rupture of general laminates and helped identify the significance of time dependent behavior for practical applications of laminated composites. Data was also furnished for comparison with the program predictions. Short and long term creep compliance data was taken at several stress levels for several specimens. This provided information on the nonlinear tendencies of general laminates, as well as a check on the program results.

The Material and Specimens

The material used for the current experimental work was Union Carbide T-300 graphite fibers preimpregnated with Fiberite 934 epoxy resin. The 16 ply panels were manufactured by Lockheed Corporation and had a nominal thickness of .086". Most of the material was procured in 1979 and will be referred to as "new" material. One panel was procured in 1978 and will be referred to as the "old" material. This is consistent with the notation used by Griffith [38]. Unless otherwise noted, the material is assumed to be from the new batch.

The specimens used for creep compliance and creep rupture testing were sawed from the panels with a diamond abrasive disk. Nominal

specimen dimensions were 10" x 1/2" which resulted in a gage length of 6-1/2" outside the grips. This produced an aspect ratio of 13 which is normally considered adequate for testing orthotropic materials. Alignment holes (1/8") were drilled in each end of the specimens.

A variety of specimen layups was desired to provide a wide base of experimental data. Because of the expense and time lag in obtaining additional graphite/epoxy panels, the specimens were cut at several off-axis angles from the panels on hand. While this permits many specimen configurations, the off-axis specimens are in general unbalanced about the test direction. The problems associated with this aspect are discussed in the following chapter.

Specimen Configurations

All specimens used in the current work were cut at various angles from one of the four available parent panels:

Panel #1	$[0/30/-30/0]_{2s}$	"old" material
Panel #2	$[0]_{8s}$	"new" material
Panel #3	$[0/45/-45/0]_{2s}$	"new" material
Panel #4	$[0/90]_{4s}$	"new" material

While panel #4 has been referred to throughout this paper as $[0/90]_{4s}$, it was recently found that the actual layup is $[0/90/0/90/90/0/90/0]_{s}$. The different specimen configurations were each assigned a designating letter as follows:

A - $[90/60/-60/90]_{2s}$

These specimens were cut at 90° from panel #1. These specimens are differentiated from the C specimens noted below

because the scrim cloth was not removed prior to the post-cure. The post-cure deteriorated the scrim cloth on each side of the specimen to a point where it would not peel off. It could only be removed by tediously flaking off small pieces. It was decided to leave the deteriorated scrim cloth on the specimens rather than risk damaging the specimen surface. The results from these specimens were considered equivalent to the C specimens.

B - $[60]_{8s}$ cut at 60° from panel #2.

C - $[90/60/-60/90]_{2s}$ cut at 90° from panel #1.

D - $[75/45/-75/75]_{2s}$ cut at 75° from panel #1.

E - $[10/55/-35/10]_{2s}$ cut at 10° from panel #3.

F - $[20/65/-25/20]_{2s}$ cut at 20° from panel #3.

G - $[90/45/-45/90]_{2s}$ cut at 90° from panel #3.

H - $[75/30/-60/75]_{2s}$ cut at 75° from panel #3.

I - $[60/15/-75/60]_{2s}$ cut at 60° from panel #3.

J - $[15/-75]_{4s}$ cut at 15° from panel #4.

K - $[30/-60]_{4s}$ cut at 30° from panel #4.

Panel #3 is similar to the layups used in current applications of graphite/epoxy to military aircraft wing skins, etc. Specimens E and F represent the situation of the principal stress being slightly off axis to the principal axes of the material. Such loading is particularly pertinent to the stress distributions around cutouts and pylons, and near leading and trailing edge fittings.

Post-Cure

In studying the "old" material, Yeow [82] found no dependence of the material response on the thermal conditioning, or aging, of the specimens by holding them at an elevated temperature for given periods of time. Griffith [38] however, found that for his specimens cut from the "new" material, there was significant dependence of the material compliance on the amount of time the specimen was held in the test oven before testing. He concluded that there was a significant post-curing effect occurring in the "new" material. It was also discovered that the "old" batch of material had been subjected to a post-cure process, but that this extra step had been eliminated from the manufacturing process for the "new" batch of material.

In an effort to reduce this aging effect of the specimens while under creep loading in the oven and to insure that previous conditioning of all specimens was similar, all specimens used in the current work were subjected to a thermal conditioning cycle shortly after being cut from their parent panel. The post-cure cycle was chosen to give a gradual heat-up period from room temperature to 380°F at a rate of 50°F/hour, followed by a 36 hour hold at 380°F, and then a very slow cool-down to room temperature at a rate of 5°F/hr. This very gradual cool-down helped minimize the lock-in of excess free volume and reduced the residual stresses.

A cam was cut for the Blue M oven to provide the required temperature for the cycle. The specimens, with end holes already drilled, were hung vertically on wire hangers in the oven. The hangers were made in such a way to space the specimens apart to prevent

them from colliding because of the forced convection currents of the oven. Many of the specimens became bowed as a result of the post-cure cycle. This warping was limited to specimens cut with matrix dominated test directions. Specimens of a given configuration all warped in the same direction and about the same amount. Fiberite indicated that this warping may result when the plies are not nested. Apparently, a ply is not symmetric about its midplane, but has a preferred side and if all the plies of a panel are stacked with the same side towards the tool, the panel will also not be symmetric about its midplane and could result in warping in the post-cure process. While the warping was not considered particularly detrimental for the specimens, it is thought that this effect can be eliminated by properly nesting the plies in the layup process. Nesting implies alternately placing the backing side of the plies toward and away from the layup tool.

Moisture Content

Moisture content is known to have a significant effect on the strength and stiffness of the epoxy resin. Absorption of moisture is believed to have an effect similar to lowering the glass transition temperature [45]. Thus, in light of the Time Temperature Superposition Theory, moisture content is seen to be an accelerating parameter for the creep process. Obviously, therefore, moisture content could be a factor in creep studies but was not studied directly in the current investigation. To minimize the effect of moisture, efforts were taken to maintain consistent moisture levels in the

specimens. The specimens were placed in a desiccator upon removal from the post-cure oven and stored there until tested. The moisture content of the air within the desiccator was maintained at 13-18% relative humidity.

The moisture content of several specimens was monitored over a 6 month period. The specimens lost about 1% of their total weight during the post-cure cycle, presumably moisture. There seemed to be a very slight decrease in weight (.05%) over the first few days in the desiccator. The only explanation for this phenomena is that the long cool-down period for the post-cure cycle permitted humid room air to enter the oven and provide moisture for the specimens to absorb. The desiccator air was drier and removed some of the moisture. The weight of the specimens then remained essentially constant throughout the 6 month period. Thus, moisture content of all specimens was felt to be quite consistent.

Equipment

Three lever arm creep machines were used for creep loading of the specimens: a 6000# Budd machine, a homemade frame similar to the Budd, and a 20,000#, Series 2330, ATS machine with automatic releveler. Each machine was equipped with an ATS Series 2912 oven and Series 230 temperature controller. These control units were very temperamental but when working, maintained oven temperatures within ± 2°F (± 1°C) of the desired temperature. Temperatures were determined with a Doric Model 412A Trendicator. Hewlett Packard 7100B Strip Chart Recorders were used to record the strain data for the creep compliance

testing. A 2100 Vishay System was used to condition the strain gage output. Shunt resistors were used for calibration of the strain gages.

Fluctuations in line voltage plagued the collection of creep compliance data. The Vishay conditioning unit could not provide adequate compensation for the erratic line voltage. The 110V line in the lab surged in the evenings and on weekends as if from reduced power consumption during off hours. To minimize this problem, a SOLA Constant Voltage Transformer was connected to the 220V line. The off hour power surges were eliminated with this arrangement, but large voltage spikes at one minute intervals would sometimes occur on this circuit. These spikes were very annoying, but did not disturb the data as much as the power surges. This phenomena was apparently due to the operation of some piece of equipment which was operational primarily on Friday through Monday. Several other experimenters in the building indicated that they have experienced similar phenomena. While the source of the problems could not be located, it is recommended that the situation be remedied before further creep testing is undertaken.

Creep Rupture Data

Before testing, the specimens were measured to determine the cross-sectional area used to compute the stress level. Failure was assumed to occur at the location of minimum cross-sectional area within the specimen length. The minimum cross-sectional area may not correspond with either the minimum width or thickness when both vary

over the length of the specimen. Because this evaluation of the minimum cross-sectional area would be very tedious, it was assumed that one could scan the length of the specimen for the minimum thickness (width), measure the width (thickness) at that location, and use these values to compute the minimum cross-sectional area.

The measured specimen was mounted in clamping grips and placed in the test frame. At least one half hour was allowed before the test was begun so the specimen could reach thermal equilibrium at the test temperature. Full application of the load was spread over several seconds so that the dynamic effects were minimized. The ATS machine at the 20:1 lever arm ratio tended to jerk the specimen at loading and during lever arm releveling. This caused oscillation of the load train system. This was of some concern, but was found to be negligible if care was used in loading the specimen. See Appendix B.

Previous efforts indicated that end tabs bonded on unidirectional and $[90/60/-60/90]_{2s}$ specimens precipitated creep rupture at the end tab. Based on these findings, end tabs were not used on most creep rupture specimens. However, without end tabs, the two strongest configurations (specimens E and F), however, failed through the hole within the grips. To prevent such failures, cross ply glass/epoxy end tabs were bonded to these specimens with Epoxylite 5403 (M-Bond GA-61). This adhesive requires a high temperature cure cycle. To prevent cool down anomalies, the post cure cycle was repeated but with a 3 hr hold at 380°F. The tabs were successful in preventing grip failures in most cases.

Specimen Measurement Difficulties

Probably the most difficult part of creep rupture experiments is the measurement of the cross-sectional dimensions of the specimens. The problem is to measure the specimen at the precise location before loading where fracture will occur after loading. Once the failure has occurred, the specimen cannot be reliably measured because the delaminations and splintering may extend for a considerable distance beyond the actual separation. Thickness measurements within these debonded regions would be meaningless. If one goes far enough away from these zones to obtain an accurate thickness measurement, the thickness at the new location may be considerably different than that at the fracture point.

Part of the problem lies in the existence of thin spots occurring in many of our specimens. These regions were, in some cases, 1/2" long over which the thickness tapered so as to be .003"-.005" thinner than the nominal thickness. Such thin spots were believed to correspond to splice locations where the edges of two plies were not quite brought together. During the cure process, resin flowed in to fill the void. If all the splices on several ply levels occurred at the same locations, as in mortar joints in a brick wall, the resin flow could result in a significant thin spot. For some specimens, the thin spots were noticeable enough to be located merely by passing the fingers over the specimen. When splice lines were far enough apart, it was sometimes possible to cut the specimens in such a manner that the thin spots did not occur within the test length of the specimen. If, however, one is trying to get as many specimens as

possible out of a panel at some angle to the splice direction, that is not always an option. The best solution to these problems in the future would be to persuade the manufacturers to stagger their splices, in spite of possible claims of increased waste.

Often in composite work, the specimen strength is thought to be somewhat insensitive to the thickness. In fact, in some circles, the thickness is often assumed to be some nominal value for all specimens. The concept is based on the assumption that a thick or thin spot indicates only the amount of matrix present while the fiber content remains fairly constant. This is probably a good assumption for specimens with fiber dominated strengths, but not for matrix dominated specimens.

Specimens do not always fail at the thin spots, because the actual load situation is considerably different than the idealized creep test of a uniform homogeneous material under a uniform uniaxial stress state. As stated previously, for a specimen of varying width and thickness, the smallest corss-sectional area does not necessarily occur at the location of either the minimum width or thickness. Further, the specimen contains flaws and defects which may render the specimen weakest at still some other location, than the one for minimum area. Also, particularly in the unbalanced specimens, the stress state is neither uniform nor uniaxial. Furthermore, especially for specimens with small fiber angles, it is possible for a failure initiating at one location to result in a final separation some distance away. These reasons indicate that the strength of laminated specimens may not be as sensitive to cross-sectional area as a

homogeneous, isotropic material might be. This could result in greater data scatter for composite specimens than is observed for metals or polymers.

Crooked Fibers

An interesting anomaly was noticed in many of the specimens cut from the "old" $[0/30/-30/0]_{2s}$ panel. Many specimens contained fibers with a large degree of curvature in certain regions of certain plies. These plies exhibited deviations from the desired fiber angle by as much as 30°. These sharp bends occurred over a very local region, but could indeed have had a significant effect on the strength of a specimen. Typical photographs of some of these specimens are shown in Plates 6.1 and 6.2. An examination of all the specimens from this panel which were creep ruptured showed that those specimens exhibiting crooked fibers at the fracture zone had often failed at shorter than predicted time to rupture. While the correlation was not perfect, it was very significant. Obviously, the stress state induced near these knees could be considerably worse than the nominal stress. Also, if the fiber angle increased, the laminate would lose part of its load-carrying capacity. It should be noted that some of the specimens which broke prematurely did not externally exhibit significantly crooked fibers. However, only a few plies are actually visible at the failure zone. Possibly, therefore, some of the internal plies were crooked and precipitated the failure mechanism.

There was little that could be done to account for the effects of crooked fibers. What portion of the manufacturing process of the

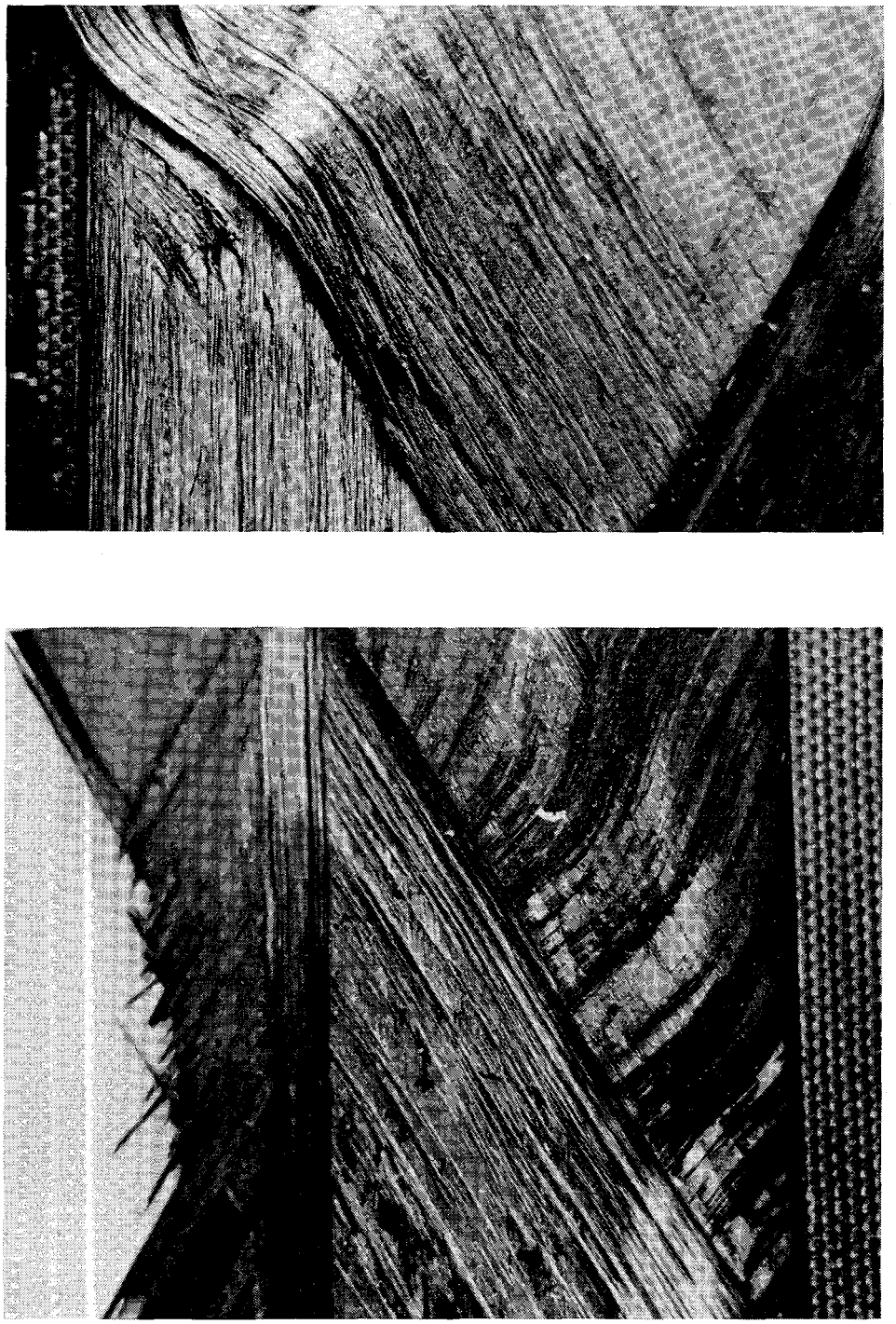

Plate 6.1 Crooked Fibers.

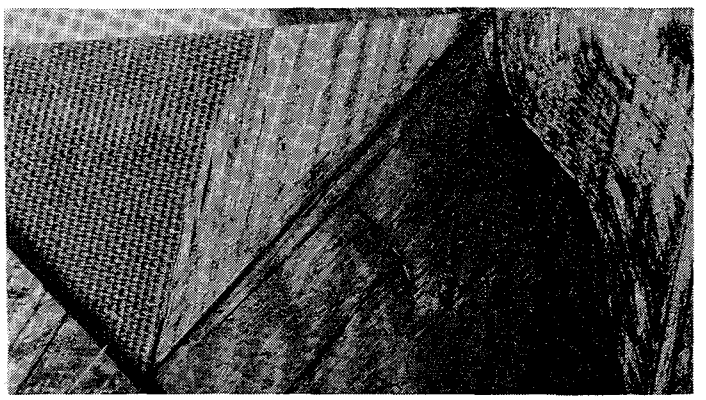

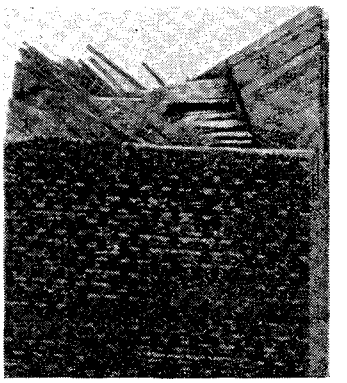

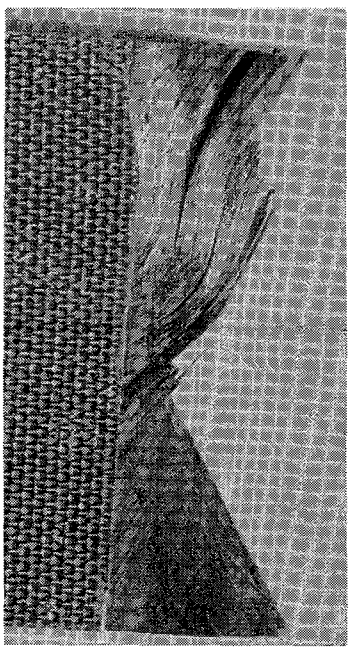

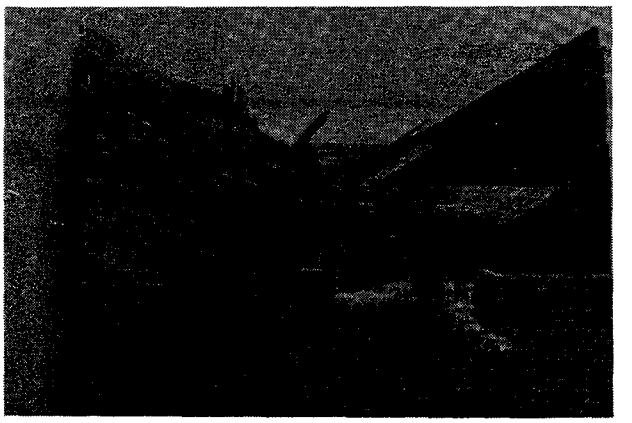

Plate 6.2 Crooked Fibers.

$[0/30/-30/0]_{2s}$ panels which caused this phenomena is not understood. Crooked fibers were not noticed in other panels. Our recommendation is for more careful processing of all composite panels. If commercial producers cannot provide better products, it may be desirable to obtain the equipment to produce panels in the department under more careful supervision. One would still wonder about the quality of products used in practical applications, however.

Baseline Data for Creep Rupture

Baseline strength data is needed prior to taking actual creep data in order to minimize the trial and error procedure necessary to determine the stress range for which delayed failures will occur in a reasonable amount of time. Baseline static strengths were determined from constant crosshead tests on an Instron Test Machine. Fig. 6.1 illustrates the baseline data for a $[90/60/-60/90]_{2s}$ laminate taken at several temperatures. Note that the strength declined as the temperature increased.

Creep Yield of Polycarbonate

Because Gr/Ep is expensive, difficult to obtain, and hard to machine, finding other materials which can be used to investigate basic rate processes in general is desirable. Polycarbonate is inexpensive, readily obtained, and easily machined and had been previously studied in our laboratory by Brinson [8]. While brittle, fiber reinforced epoxy seems quite different than ductile, isotropic polycarbonate, there are several similarities in their time dependent response. Therefore, polycarbonate dogbone specimens have been tested

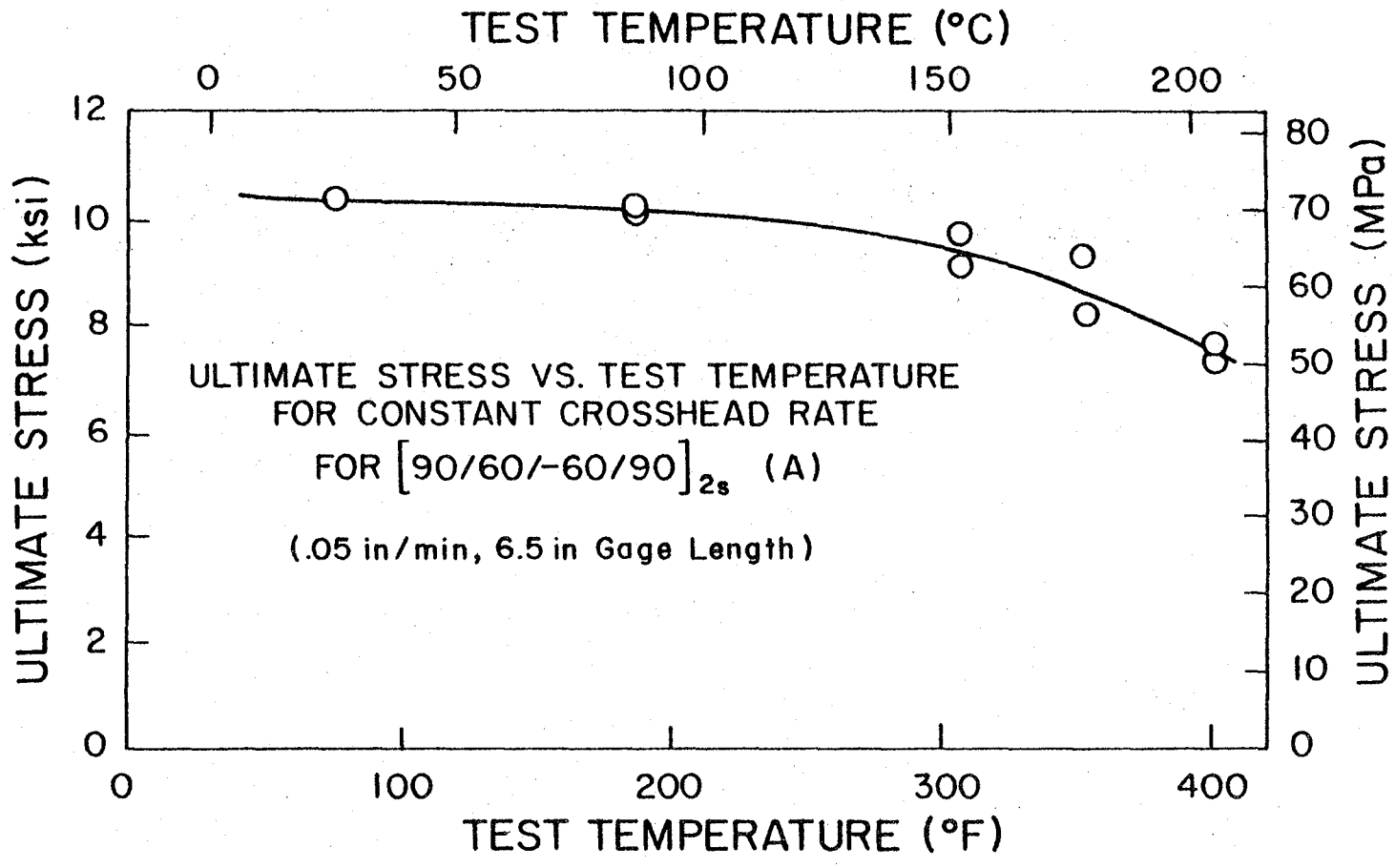

Fig. 6.1 Ultimate stresses for laminate A at constant crosshead rate for various test temperatures.

to obtain creep yield failure data. Yield was defined as large scale yielding or Lüder's band formation as measured by an extensometer and strip chart. The results from this work along with the repercussions for Gr/Ep are discussed in the next chapter.

Strain Measurements

Griffith [38] investigated several methods of preparing Gr/Ep specimens for mounting strain gages to be used for determining creep compliance and the procedure he described was used to mount the strain gages for our compliance testing. Two 350Ω gages were mounted on opposite sides of each specimen and wired in series. This produced an effective 700Ω configuration which minimized gage heating and eliminated specimen bending effects. Because only one specimen from each laminate was strain gaged, a specimen from the same laminate but not the same fiber orientation was used for thermal compensation. The errors introduced by this aspect were completely negligible for the ± 2°F temperature variation maintained during the compliance testing.

Chapter 7

RESULTS AND COMPARISONS

This chapter contains the experimental and numerical results of the current investigation. The creep rupture data is reported first to permit an independent assessment of the delayed failure results. Creep compliance data--both experimental and as predicted by the lamination program--are presented and compared. Predicted creep rupture strengths are then presented and compared with the experimental data. Photographs of typical delayed failure zones are shown along with photomicrographs of edgeviews of several specimens. The polycarbonate results are indicated and similarities in the rate processes and physical aging effects of polycarbonate and Gr/Ep are noted. Comments about the accuracy of predictions are then given. Finally, a discussion of the grip constraint stresses in the unbalanced laminates is presented.

Creep Rupture Data

Obtaining creep rupture data for several laminates was a primary thrust of the experimental phase of this work. One hundred-ninety specimens from nine different laminates were prepared and tested to obtain creep rupture data. Much of the data shows considerable scatter, as is typical of creep rupture data in general. Nonetheless, delayed failures were produced in all of the nine different laminates tested, substantiating the claim that creep and delayed failures are of real engineering concern.

The creep rupture data for each laminate is presented in Figs. 7.1 - 7.12. The figure legends indicate the type of failure that occurred. "Good failure" indicates that the separation was located well within the test region. "Failed near grip" signifies that the fracture occurred within the test region of the specimen, but was very near the grip. While most of these data points are believed to be valid, it should be noted that the stress state near the grips may be more complex. This is particularly true for the unbalanced laminates in which the stress state induced by the grip constraints may be considerably different than the desired uniaxial stress state. "Failed in grip" denotes a failure within the grip. These data points are not viewed as being representative creep ruptures. The "+" symbol denotes an A specimen tested with the scrim cloth intact. These points are comparable with the C specimen results and they have been plotted together.

All pertinent data points have been depicted in the figures. A least squares fit (LSF) straight line has been drawn through the data points which are believed to be valid. Those points not considered as representative creep ruptures have not been used in the least squares fit and have been darkened in on the figures. Such points include:

1) failure within a very short time of loading (20 sec.)
2) failure within the grip
3) specimens with obvious crooked fibers (laminates A and C only)
4) specimens which did not fail
5) specimens with loading anomalies.

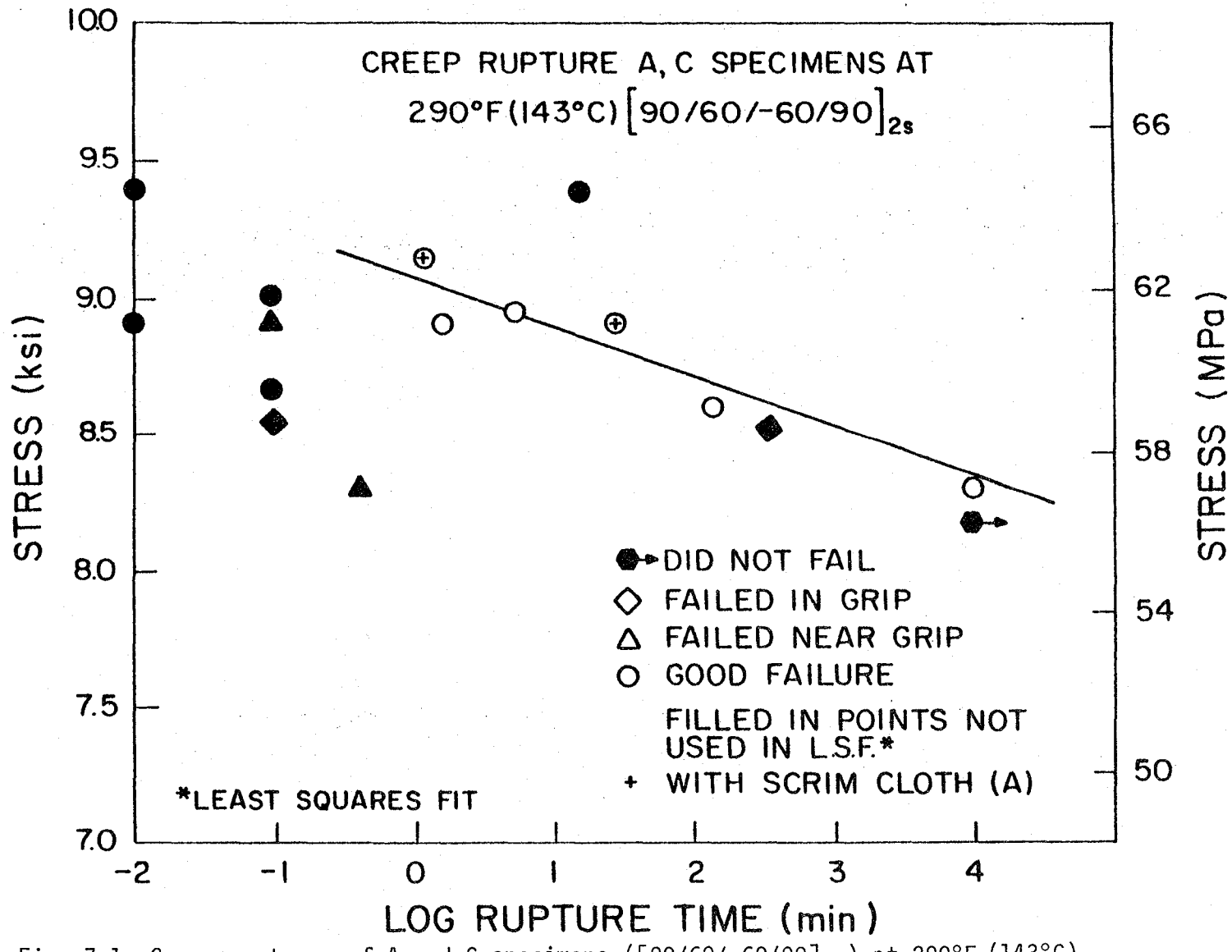

Fig. 7.1 Creep ruptures of A and C specimens ($[90/60/-60/90]_{2s}$) at 290°F (143°C).

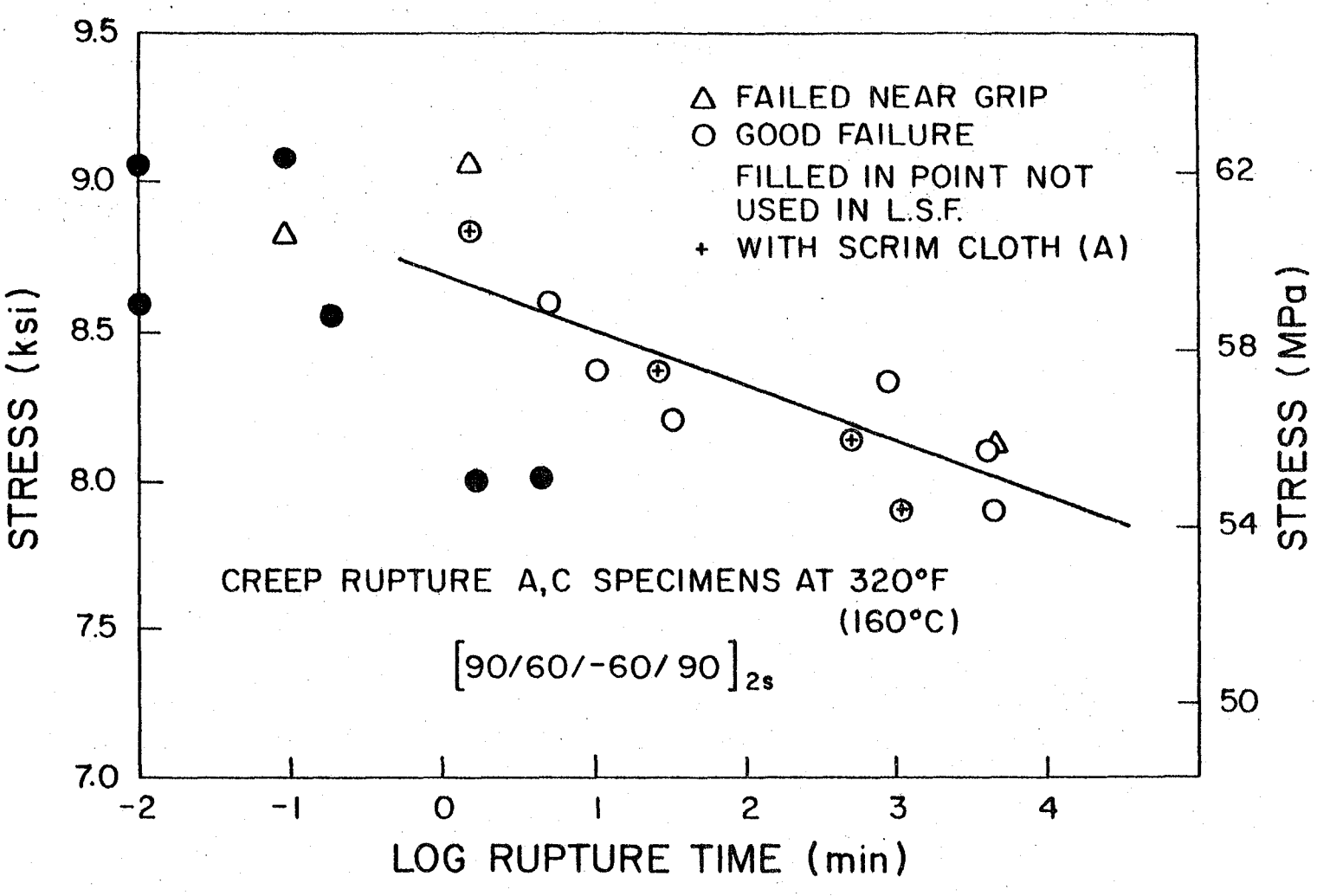

Fig. 7.2 Creep ruptures of A and C specimens ($[90/60/-60/90]_{2s}$) at 320°F (160°C).

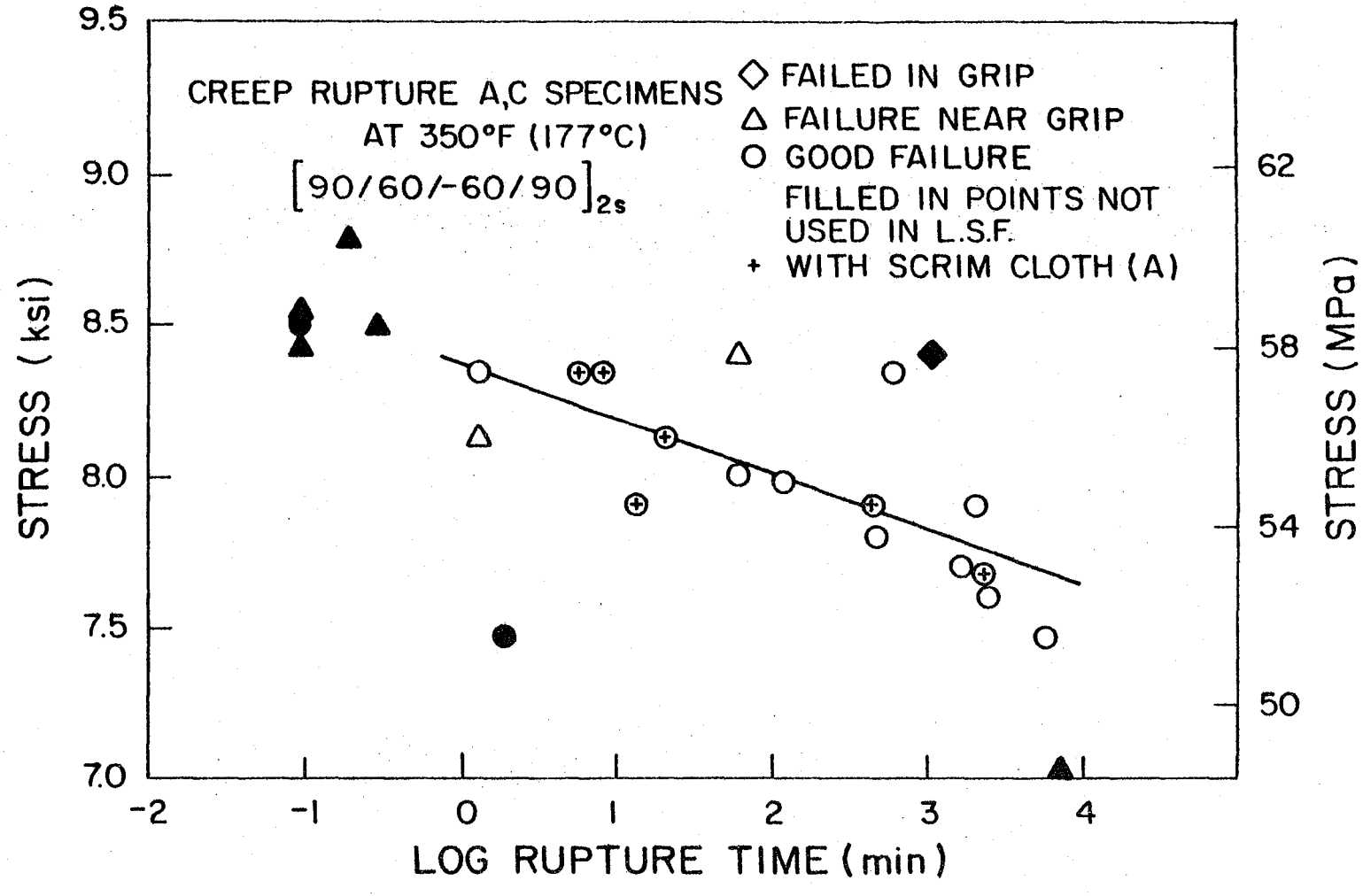

Fig. 7.3 Creep ruptures of A and C specimens ($[90/60/-60/90]_{2s}$) at 350°F (177°C).

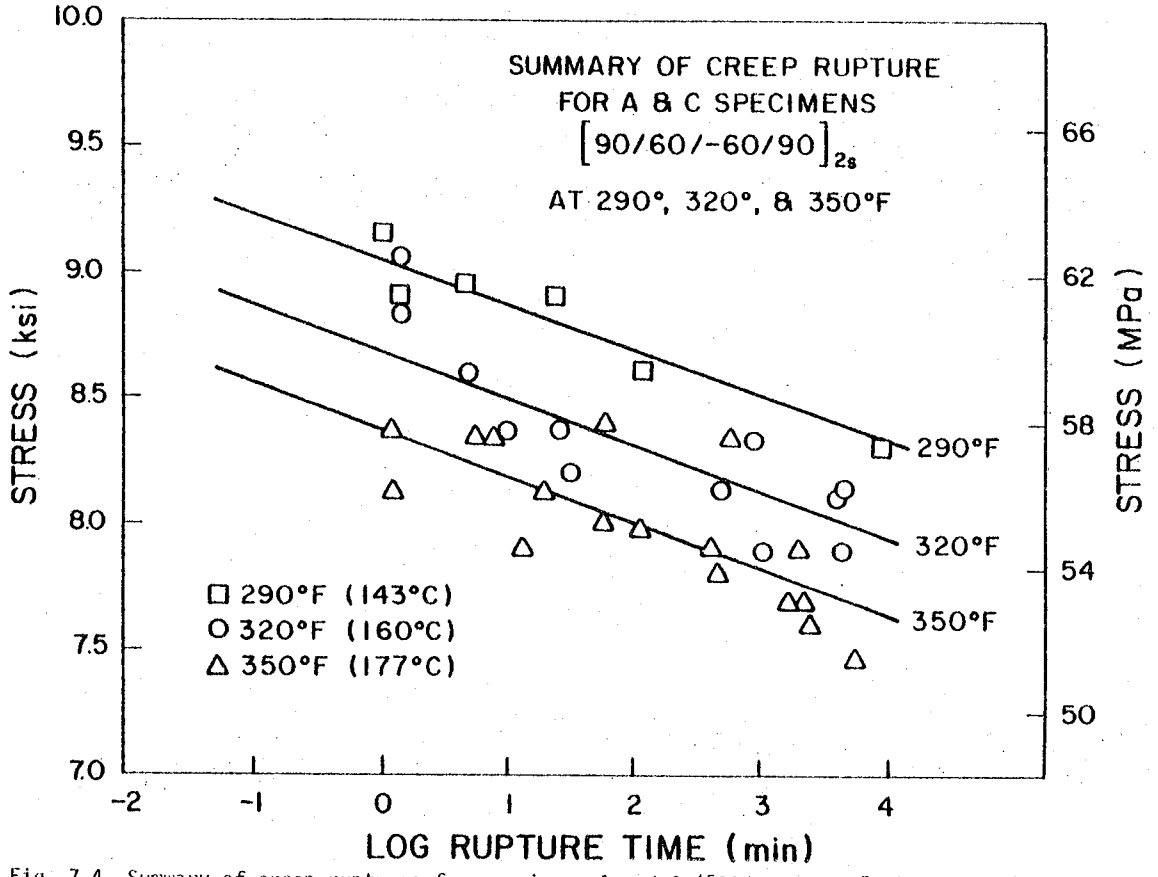

Fig. 7.4 Summary of creep ruptures for specimens A and C ($[90/60/-60/90]_{2s}$) at 290° (143°C), 320° (160°C), and 350°F (177°C).

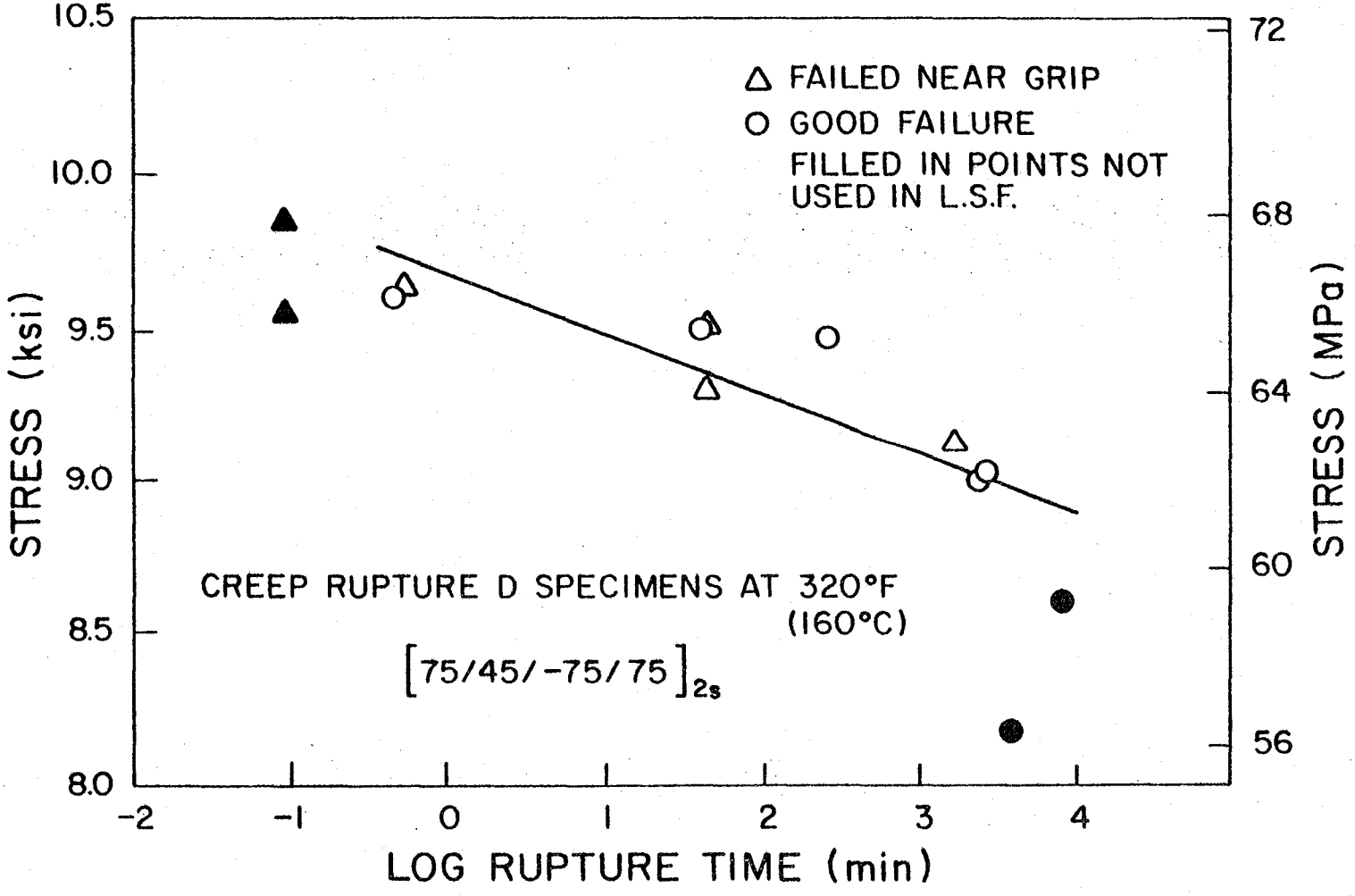

Fig. 7.5 Creep ruptures of D specimens ($[75/45/-75/75]_{2s}$) at 320°F (160°C).

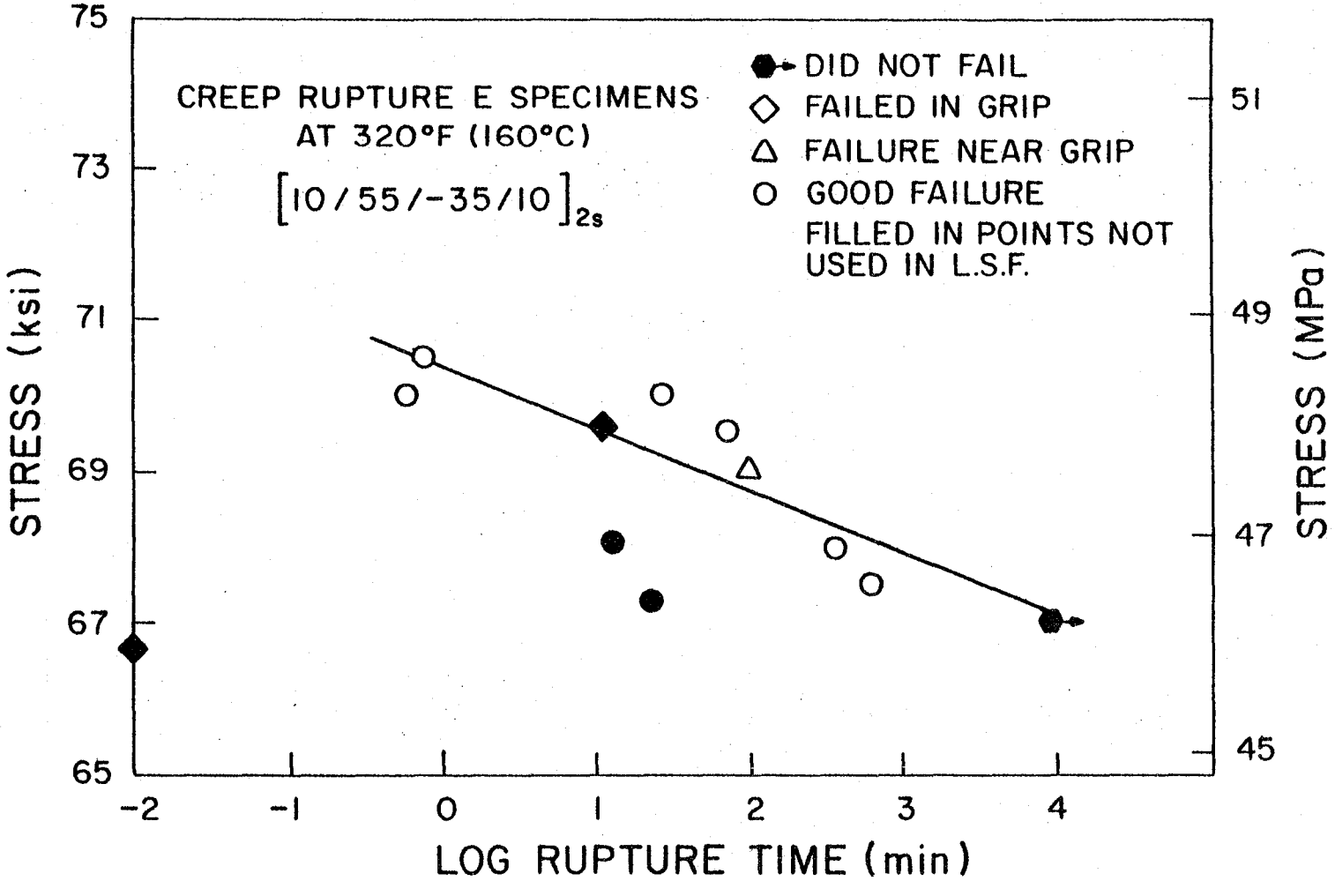

Fig. 7.6 Creep ruptures of E specimens ($[10/55/-35/10]_{2s}$) at 320°F (160°C).

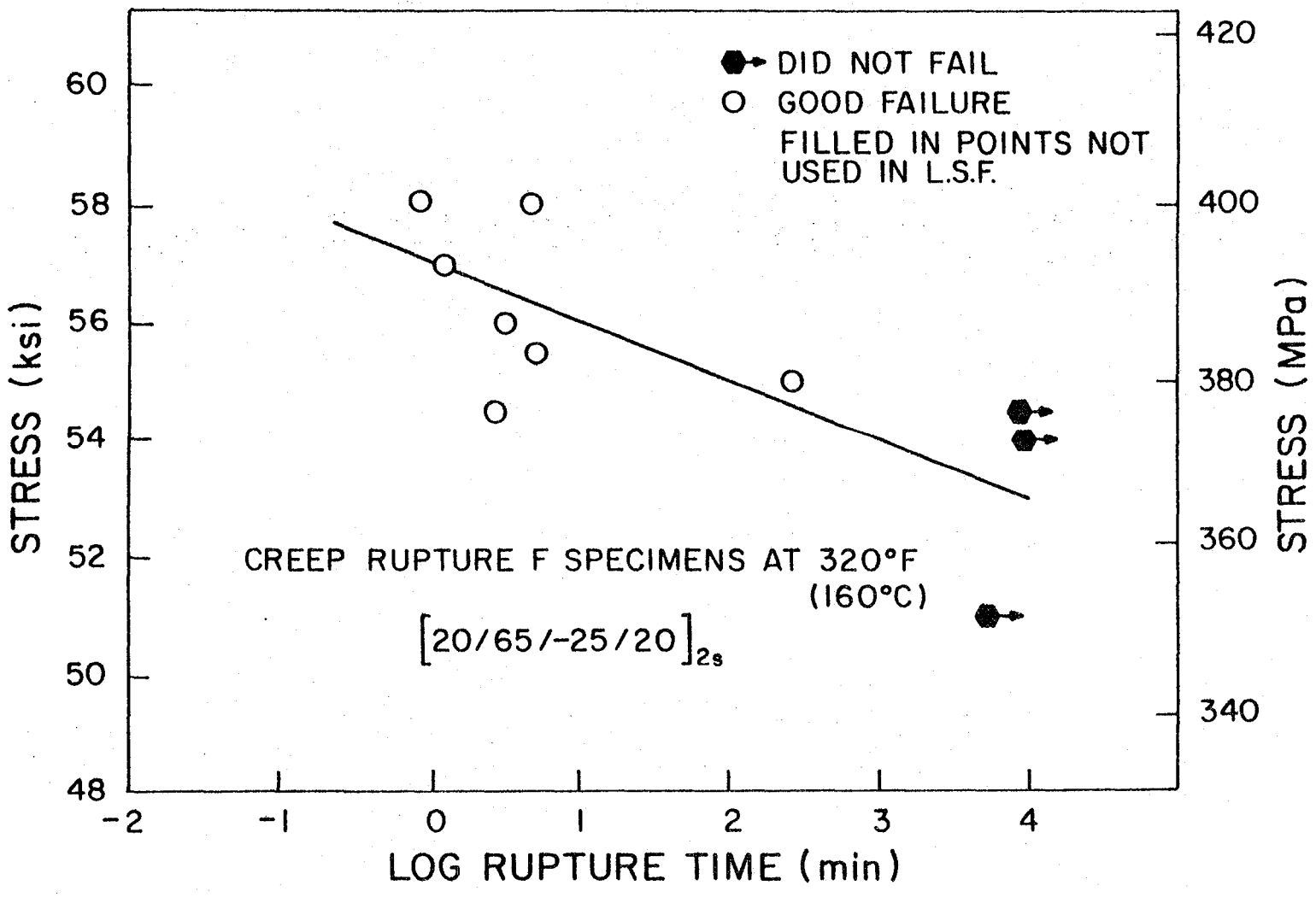

Fig. 7.7 Creep ruptures of F specimens ($[20/65/-25/20]_{2s}$) at 320°F (160°C).

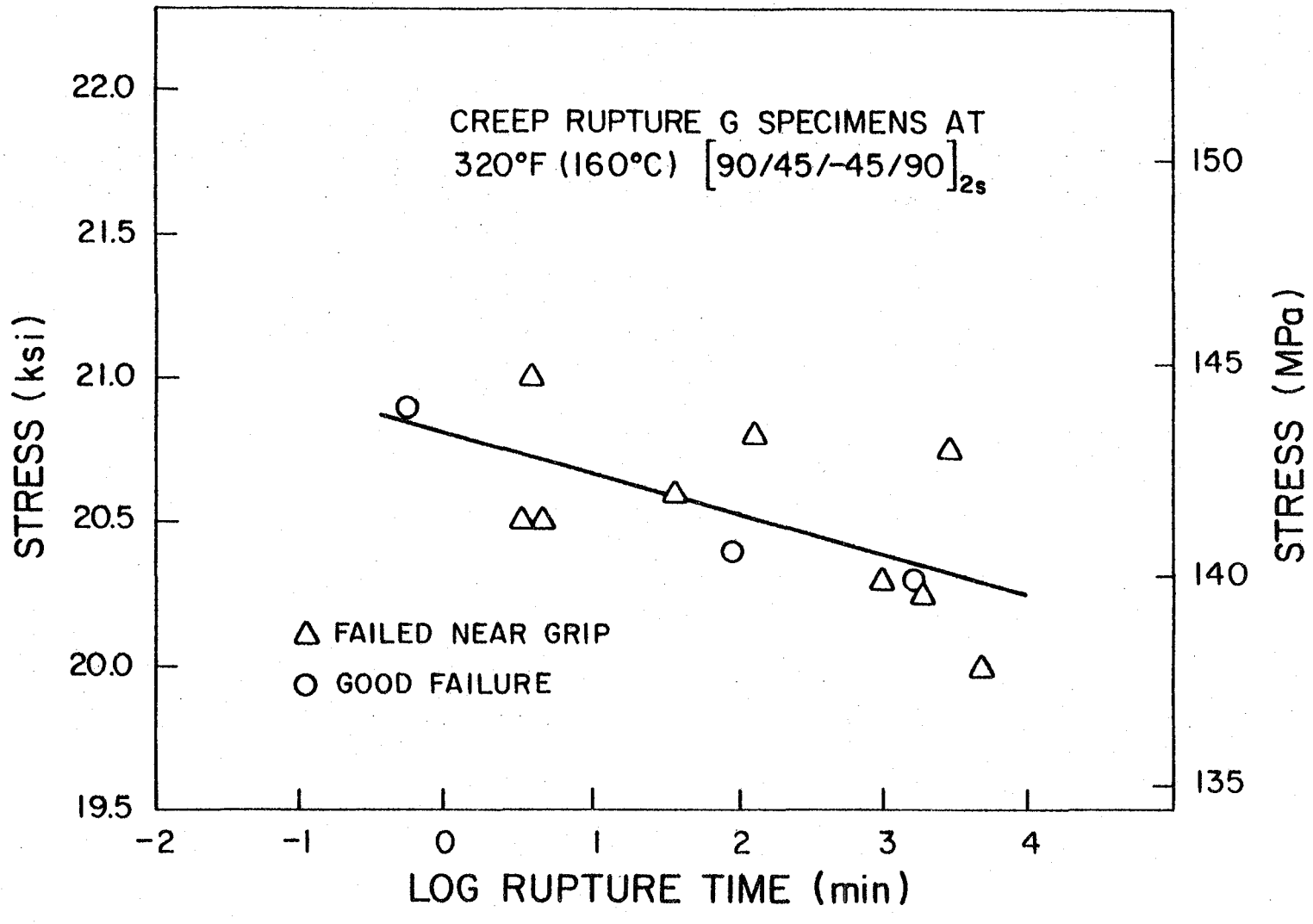

Fig. 7.8 Creep ruptures of G specimens ($[90/45/45/90]_{2s}$) at 320°F (160°C).

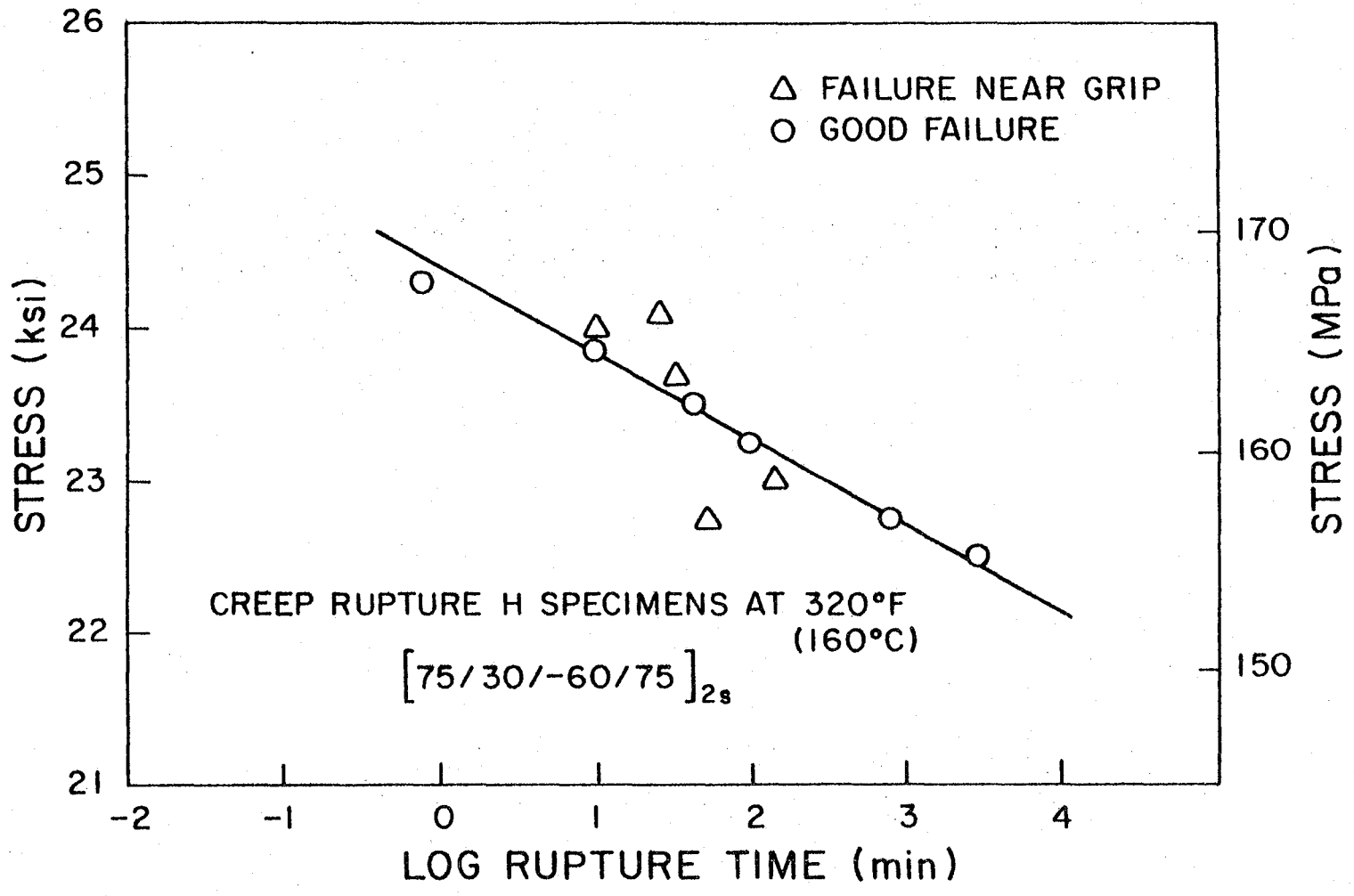

Fig. 7.9 Creep ruptures of H specimens ($[75/30/-60/75]_{2s}$) at 320°F (160°C).

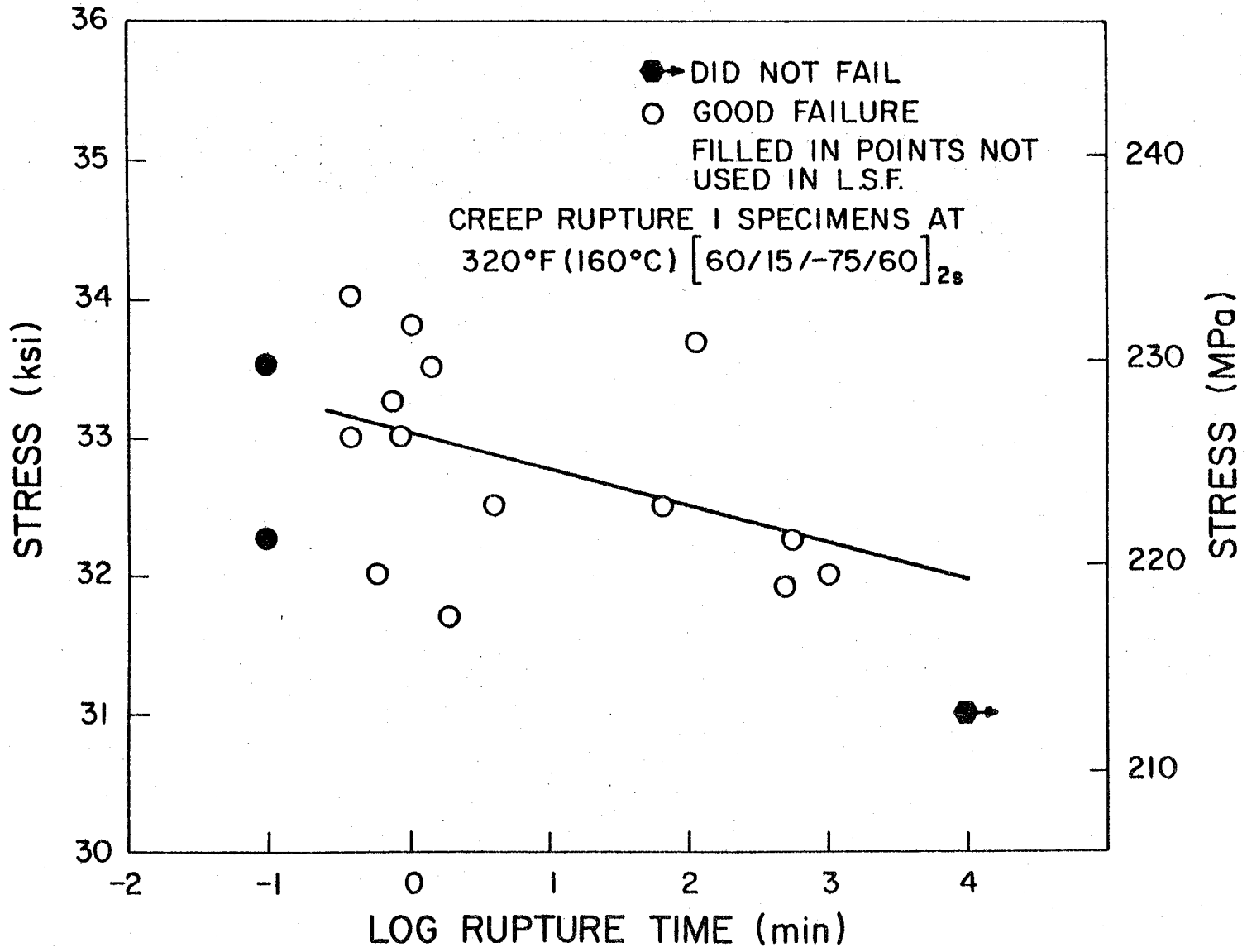

Fig. 7.10 Creep ruptures of I specimens ($[60/15/-75/60]_{2s}$) at 320°F (160°C).

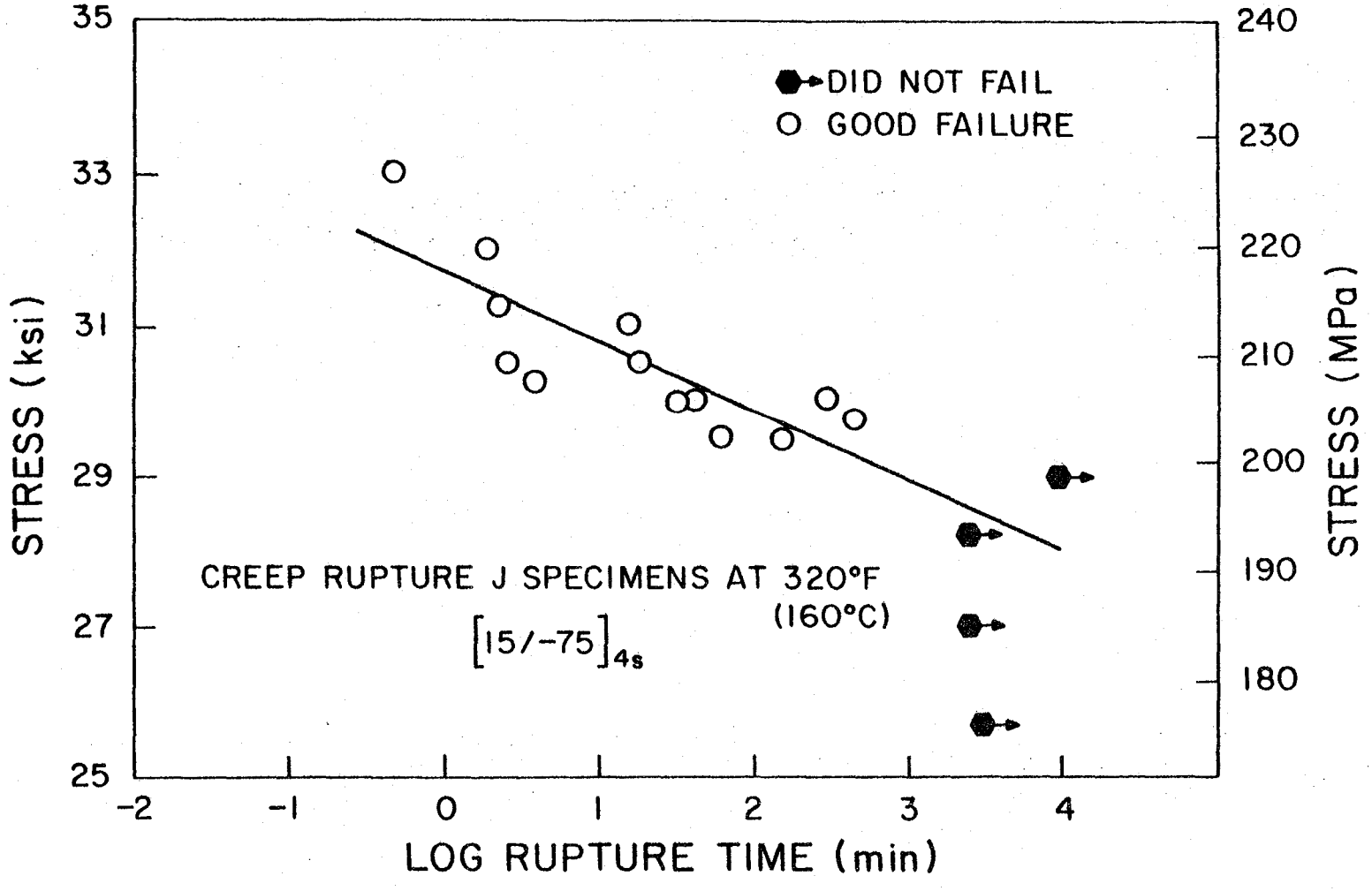

Fig. 7.11 Creep ruptures of J specimens ($[-15/75]_{4s}$) at 320°F (160°C).

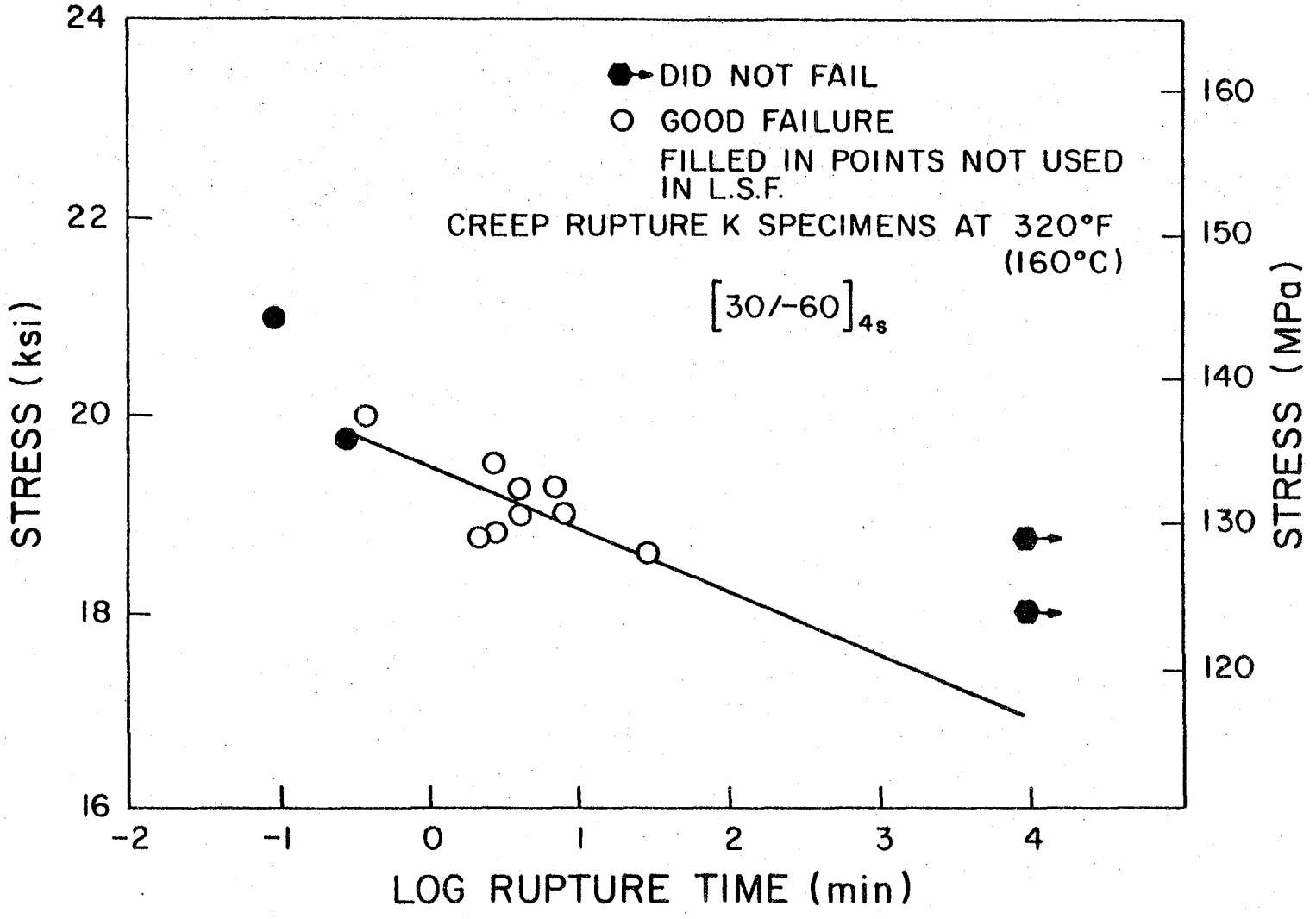

Fig. 7.12 Creep ruptures of K specimens ($[-30/60]_{4s}$) at 320°F (160°C).

The cross-sectional areas for specimen configurations A, B, and C were based on the dimensions at the narrowest width. It was later realized that this was probably the wrong measurement method for these matrix dominated laminates. Because of the large fiber angles, the damage zone was quite short and the dimensions near the fracture could be obtained. Creep rupture data based on these failure dimensions was plotted in addition to data based on pre-test dimensions. While individual data points were slightly shifted, the best fit line and degree of data scatter were found to be similar for the two measurement techniques. Only the data based on the original dimensions is presented herein.

The cross-sectional areas for specimen configurations D, E, F, G, H, I, J, and K were based on the dimensions at the smallest thickness within the test length. A dial indicator with .0001" sensitivity was used to facilitate scanning the lengths of these specimens for the thinnest location. Watching the dial while passing each specimen under the indicator stylus provided an efficient means to locate the minimum thickness.

Creep rupture data based on a nominal thickness was also plotted for each specimen. This was, in general, found to be less satisfactory than the creep rupture data based on either the initial dimensions or the failure dimensions. For a general laminate, the effective thickness is probably somewhere between the actual thickness and some nominal value, as was discussed in Chapter 6.

A and C specimens were tested at three different test temperatures. Figs. 7.1 - 7.3 illustrate creep rupture of the A and C

specimens at 290°, 320°, and 350°F, respectively. In Fig. 7.4, the valid creep rupture data points from the three previous figures have been superimposed along with their best fit lines. It is observed that the lines are parallel and nearly equally spaced. The modified rate equation (Eqn. 2.41) was applied to these lines and very good agreement was obtained as expected when the three parameter equation is used.

All subsequent creep rupture data was taken at 320°F. This temperature provides a good compromise for staying well below the glass transition temperature yet above the temperatures at which the creep compliance and creep rupture curves flatten out. Fig. 7.5 illustrates the creep rupture of the D specimens. Data for the E laminate is found in Fig. 7.6. As noted earlier, the latter specimen represents a principal stress 10° off axis from the primary fiber orientation of a practical laminate. Delayed failures were obtained and indicate a noticeable decrease in strength with time for creep loading. The results from the F specimens are presented in Fig. 7.7. These were the first specimens for which the 20:1 lever arm ratio were used. Part of the data scatter is related to becoming accustomed to using the machine at this ratio. The results from G, H, and I laminates are indicated in Figs. 7.8, 7.9, and 7.10. It is not known why the data is more consistent for the H specimens than for the other two. All three represent quite similar laminates. The data for the J specimens is presented in Fig. 7.11 and is seen to be quite consistent. At first it was somewhat difficult to obtain good creep ruptures for the K specimens. This data is shown in Fig. 7.12.

The J and K laminates were composed of only two fiber orientations and underwent considerable creep elongation.

The creep rupture results have been summarized in Table 7.1. Based on the best fit lines drawn through the data points, the creep rupture strengths for each laminate at 1 minute and at 10,000 minutes have been indicated. The percentage decrease in the creep rupture strengths over this 10,000 minute time span have also been given. While all cases indicate a reduced creep rupture strength at long times, the reduction is quite small for several laminates. Interestingly the smallest decreases occurred in two laminates with very large amounts of scatter, G and I. Strength reductions would possibly have been more consistent with the other laminates had less data scatter been present. The most important aspect is simply that delayed failures have occurred in all the laminates tested. Considering the fact that laminates have a design lifetime of many years, the likelihood for delayed failures for small loads over a long time is quite obvious.

Creep Compliance

Creep compliance data was taken at several stress levels for most laminates. Based on the experimental creep rupture strengths, a stress value, σ_5, was chosen for each laminate which would permit compliance testing near the failure strength but would not result in failure during the compliance test. Four intermediate, equally spaced stress levels, σ_1 through σ_4, were also determined. Starting with the lowest stress level, short term (36 minute) compliance data

TABLE 7.1. Comparison of 1 and 10,000 minute creep rupture strengths for the laminates tested.

LAMINATE		R(1 MIN)	R(10,000 MIN)	% DECREASE IN R
A,C	$[90/60/-60/90]_{2s}$	8.86 ksi	7.94 ksi	8.5
D	$[75/45/-75/75]_{2s}$	9.665	8.88	8.1
E	$[10/55/-35/10]_{2s}$	70.35	67.1	4.6
F	$[20/65/-25/20]_{2s}$	57.0	52.95	7.1
G	$[90/45/-45/90]_{2s}$	20.81	20.25	2.7
H	$[75/30/-60/75]_{2s}$	24.4	22.21	9.0
I	$[60/15/-75/60]_{2s}$	33.03	31.98	3.2
J	$[15/-75]_{4s}$	31.71	28.97	8.6
K	$[30/-60]_{4s}$	19.45	16.9	13.1

was taken at 320°F. After an 80 minute or more recovery period, the specimen was reloaded at the next highest stress level. At the σ_5 stress level, the test was continued to obtain week long compliance data. This testing procedure provided nonlinear behavior information based on the short term results, as well as long term compliance data. These results have been presented in the subsequent figures, along with the compliance predictions for each stress level from the lamination program. Because the strain gages on several specimens were rendered inoperable before or during the compliance testing, the experimental results are incomplete or not present in several figures. Compliance testing was begun at σ_2 rather than σ_1 for a few laminates because the creep frames could not apply a small enough load.

Specimens cut at various angles from the $[0/30/-30/0]_{2s}$ panels exhibit much less transient strain than specimens cut from the $[0/90]_{4s}$ panel. For example, the 10,000 minute transient strain of the J specimen was nearly two orders of magnitude greater than that of the E specimen. For specimens containing three or more fiber orientations, a vast network of triangular trusses is formed by the fibers. Lamination theory assumes that normals remain straight and normal which implies that the trusses are effectively "pin connected." These triangular structural elements can support the load with the matrix material supporting any σ_2 or τ_{12} stresses. Compliance predictions based on the use of lamination theory will predict an upper bound on the compliance for such laminates. This limiting value may be determined by allowing the matrix properties to go to zero.

On the other hand, laminates with fewer than three fiber orientations do not contain the triangular skeleton and do not possess a limiting compliance. These laminates rely on the shear panel support of the matrix to carry a substantial portion of the load. For these reasons, the time dependent compliance of laminates composed of three or more fiber orientations is expected to be much smaller than that of laminates composed of less than three fiber directions. It should be further noted that for the lamination theory model, an applied creep load on the truss-like laminates will result in a "relaxation creep" loading for the in-plane matrix stresses within each ply.

While lamination theory assumes rigid "pin connected" fiber trusses, actual laminates undergo interlaminar shear deformations. Because these displacements are controlled by the matrix, real specimens undergo a time dependent relieving of the "pin connection" constraint. Thus, experimental compliances are not bounded by the compliance asymtote which limits the program predictions. For laminates with matrix dominated compliances, the program predictions may be quite good. For laminates whose compliance is approaching the asymtote, however, the experimental compliances may be significantly higher than the predictions. Calculated and actual compliances have been schematically illustrated in Fig. 7.13. The use of lamination theory places a severe limitation on the prediction of time dependent compliances of general laminates. Fiber truss compliances have been indicated in the following figures to show how near the predicted compliances approach their limiting value.

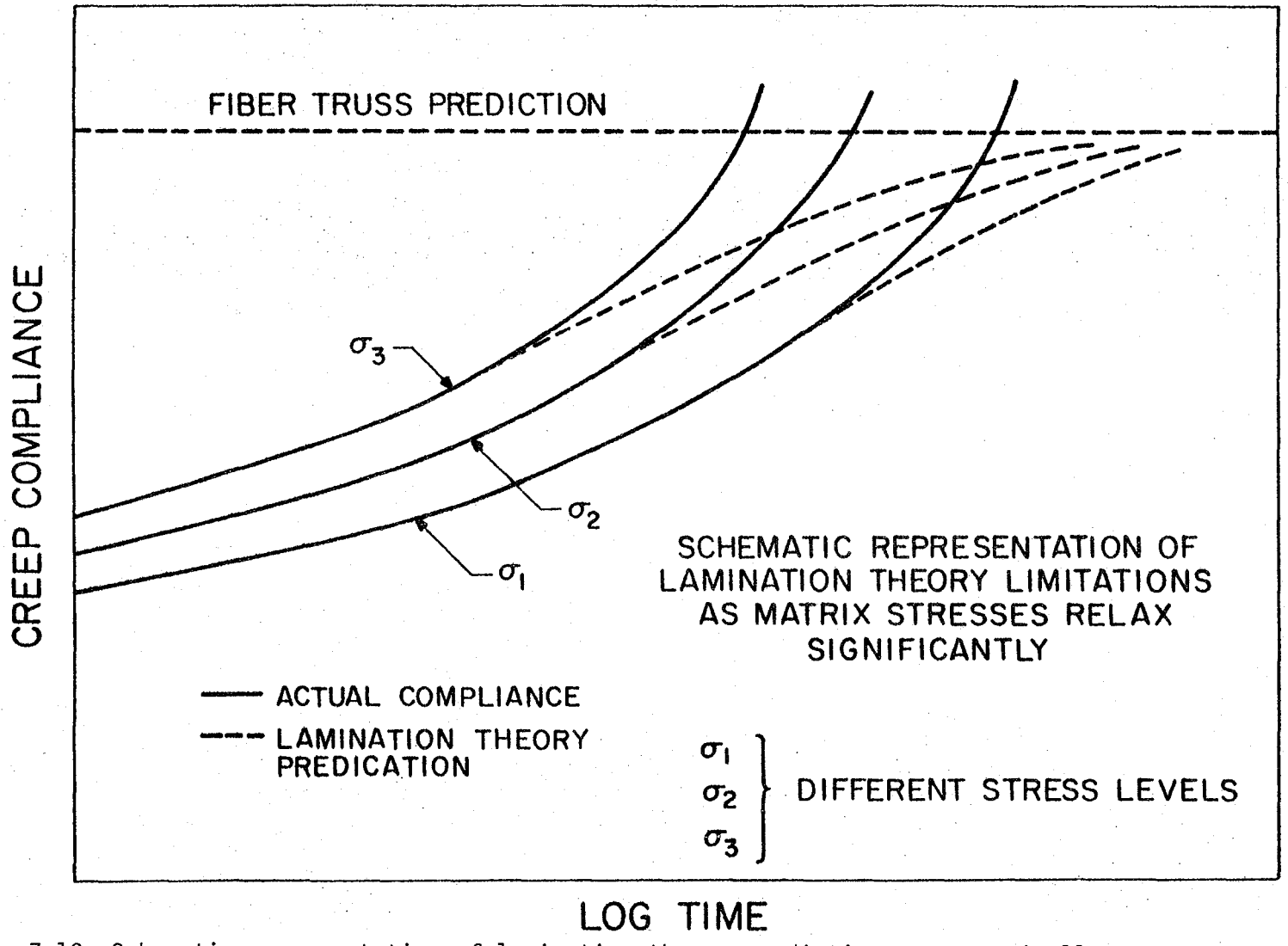

Fig. 7.13 Schematic representation of lamination theory predictions asymptotically approaching the limiting compliance value whereas actual compliances are unbounded.

Figs. 7.14 and 7.15 show the creep compliance results for the C and D laminates. These specimens are from the "old" batch of material, while the program predictions were based on the properties of the "new" material. Nonetheless, as may be observed, the agreement is quite good. The comparisons indicate that the experimental values are not as nonlinear in stress as the program predicts. These compliances are well below the fiber truss limiting value and the predicted compliances fan out appropriately.

The results for laminate E are presented in Fig. 7.16 with the fiber truss asymptote indicated near the top of the figure. The compliance predictions are seen to be converging as they approach the limiting value. While the magnitudes of the compliances agree quite well, the experimental short time compliance at the lowest stress level is greater than that at the highest stress level. This behavior is not consistent with the nonlinear compliance models considered and raises some concern. This anomaly was also observed for the F specimen orientations, but not in any other laminate. This behavior was noted during testing and the test was restarted to verify this aspect. Calibration errors associated with changing scales could only account for a small amount of such behavior. Our feeling is that this phenomena is real and is not simply due to experimental error. Lou and Schapery [54] have noted a decreasing compliance after unidirectional Gr/Ep specimens have been loaded and unloaded several times. They have recommended repeated load application to mechanically condition specimens prior to creep compliance testing. Future efforts in this area should consider and investigate the possibility of mechanical

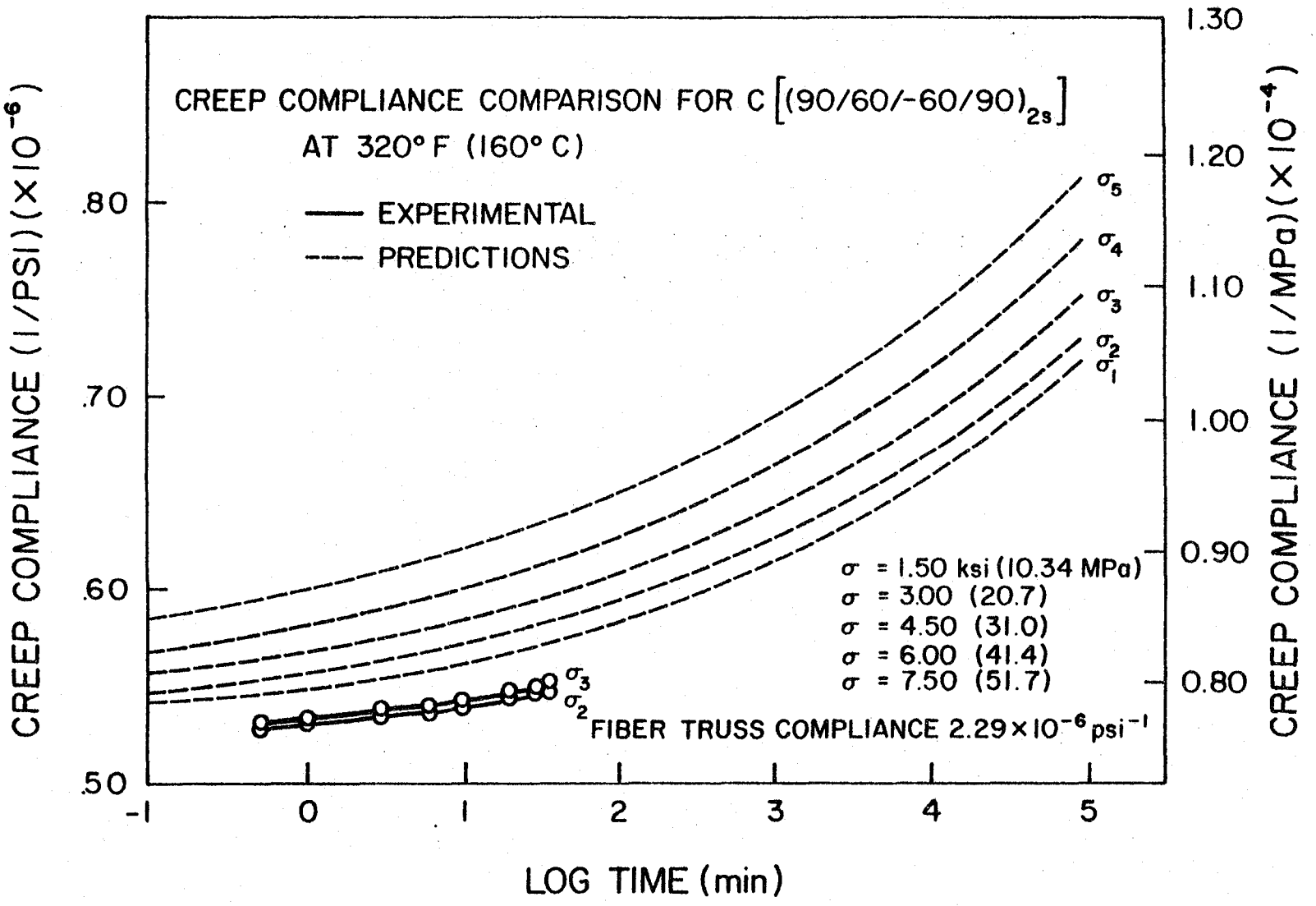

Fig. 7.14 Comparison of predicted and experimental creep compliance for laminate C ($[75/45/-45/75]_{2s}$) at 320°F (160°C).

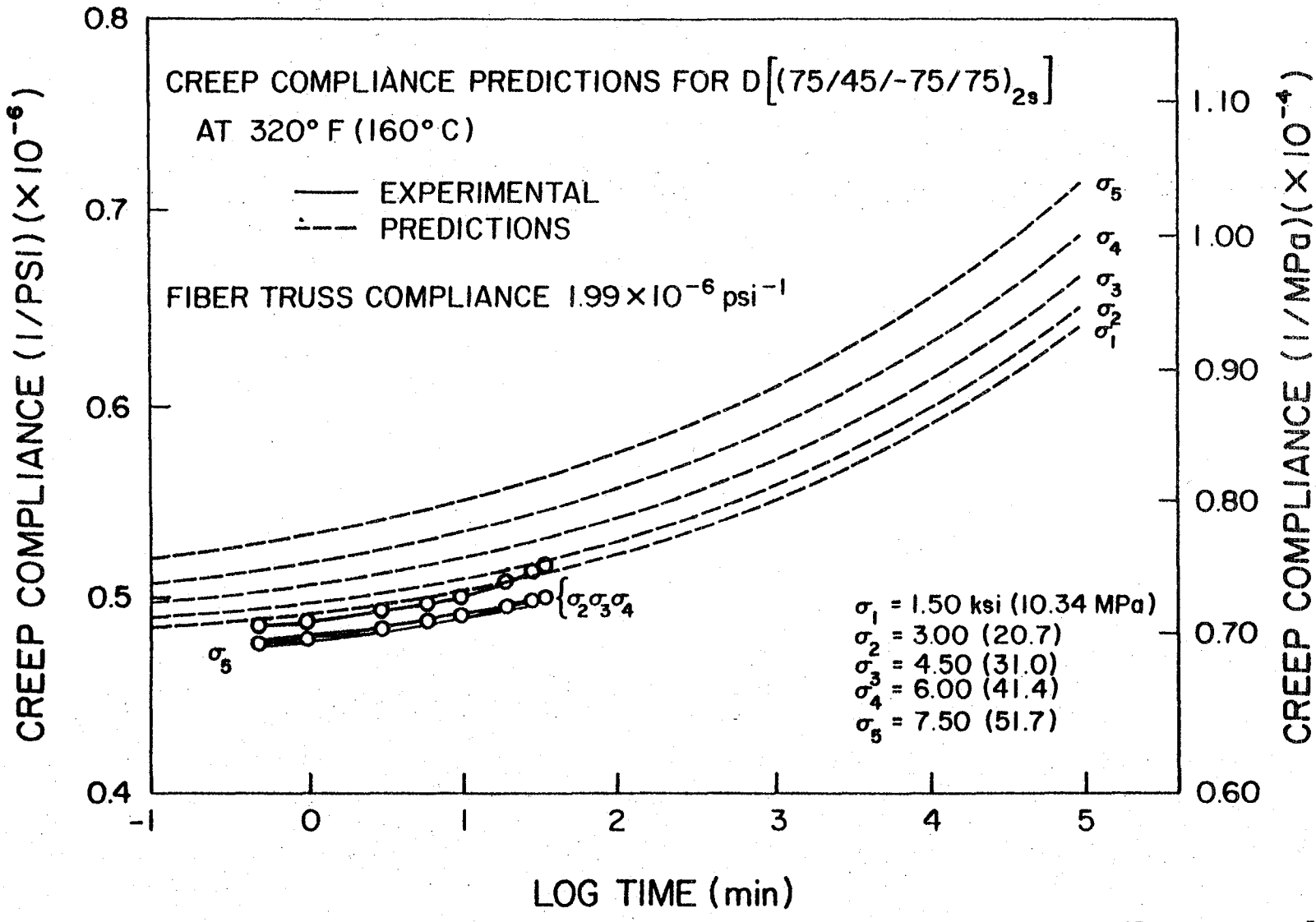

Fig. 7.15 Comparison of predicted and experimental creep compliance for laminate D ($[75/45/-75/75]_{2s}$) at 320°F (160°C).

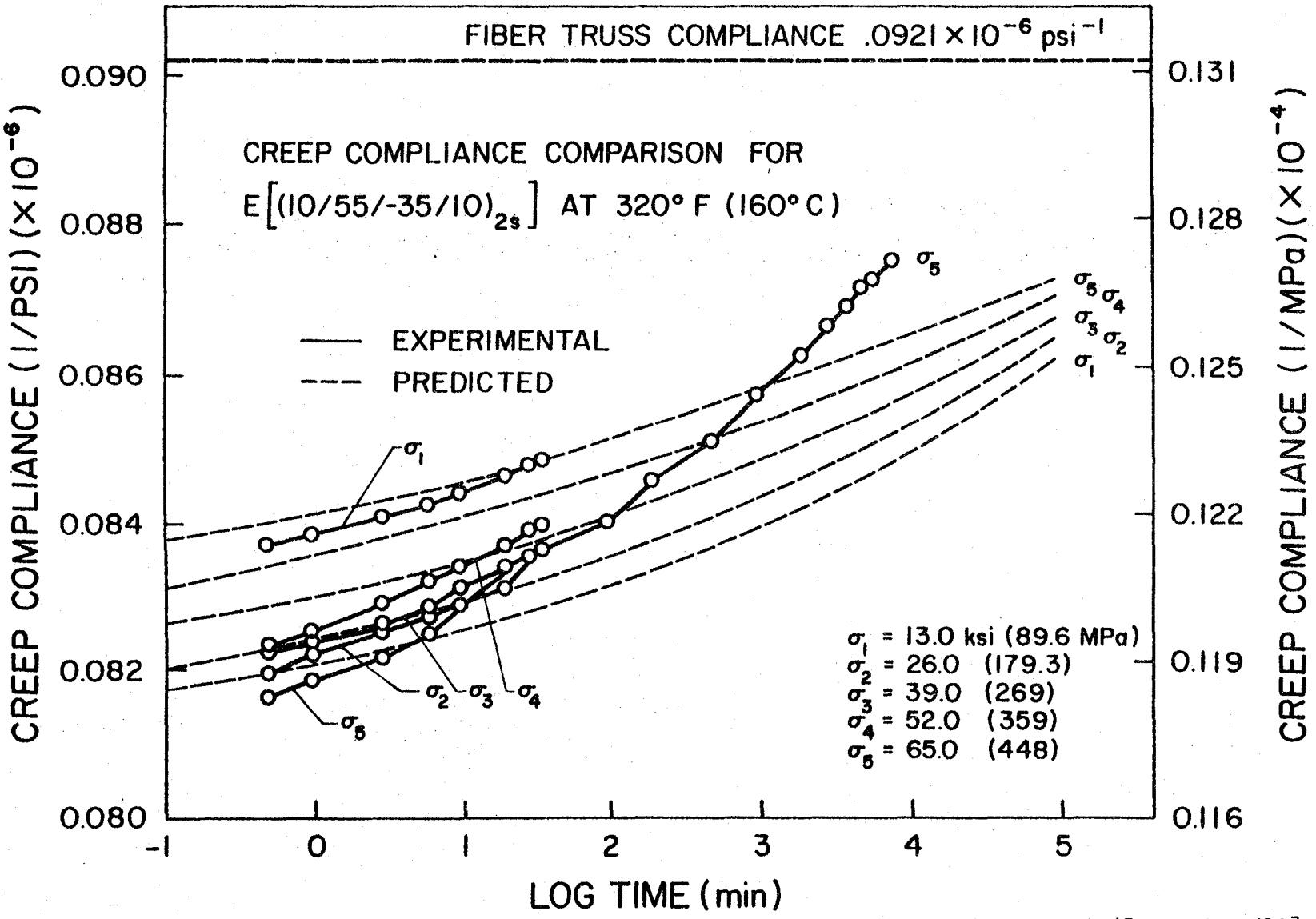

Fig. 7.16 Comparison of predicted and experimental creep compliance for laminate E ($[10/55/-35/10]_{2s}$) at 320°F (160°C).

conditioning. Possibly repeated loading at increasingly higher stress levels could have some effect on the measured compliances. It is felt, however, that the use of successively higher stress levels should minimize any repeated loading effects.

A log-log plot of experimental transient strain vs time is shown in Fig. 7.17. The long term data points fall short of the line determined from the short term data. Note, however, that these points can be made to fall on a straight line by choosing an appropriate value of ε_0 based on the long term data. Figure 7.18 indicates the degree of fit for the same data using the Findley approach. ε_0 appears to be a linear relationship, while the values of m are seen to describe the characteristic hyperbolic sine function.

The experimental and predicted compliance results for laminate F are shown in Fig. 7.19. Again the anomaly of decreasing compliance with increasing stress level should be noted. Because the creep strains for both the E and F laminates were quite small, there is some deviation of the plotted experimental compliance points from a smooth curve. Note that the experimental compliance for σ_5 has passed through the fiber truss bound on compliance predictions.

Faulty gages on the G and H laminates prevented obtaining experimental compliance data. However, Figs. 7.20 and 7.21 show the predicted compliances. As shown in Fig. 7.22, the results for the I laminate agree quite well at the low stress levels, although the experimental compliance is much larger than predictions at the highest stress level. The belief is held that the large measured compliance for σ_4 and σ_5 resulted from matrix cracking in some of the plies.

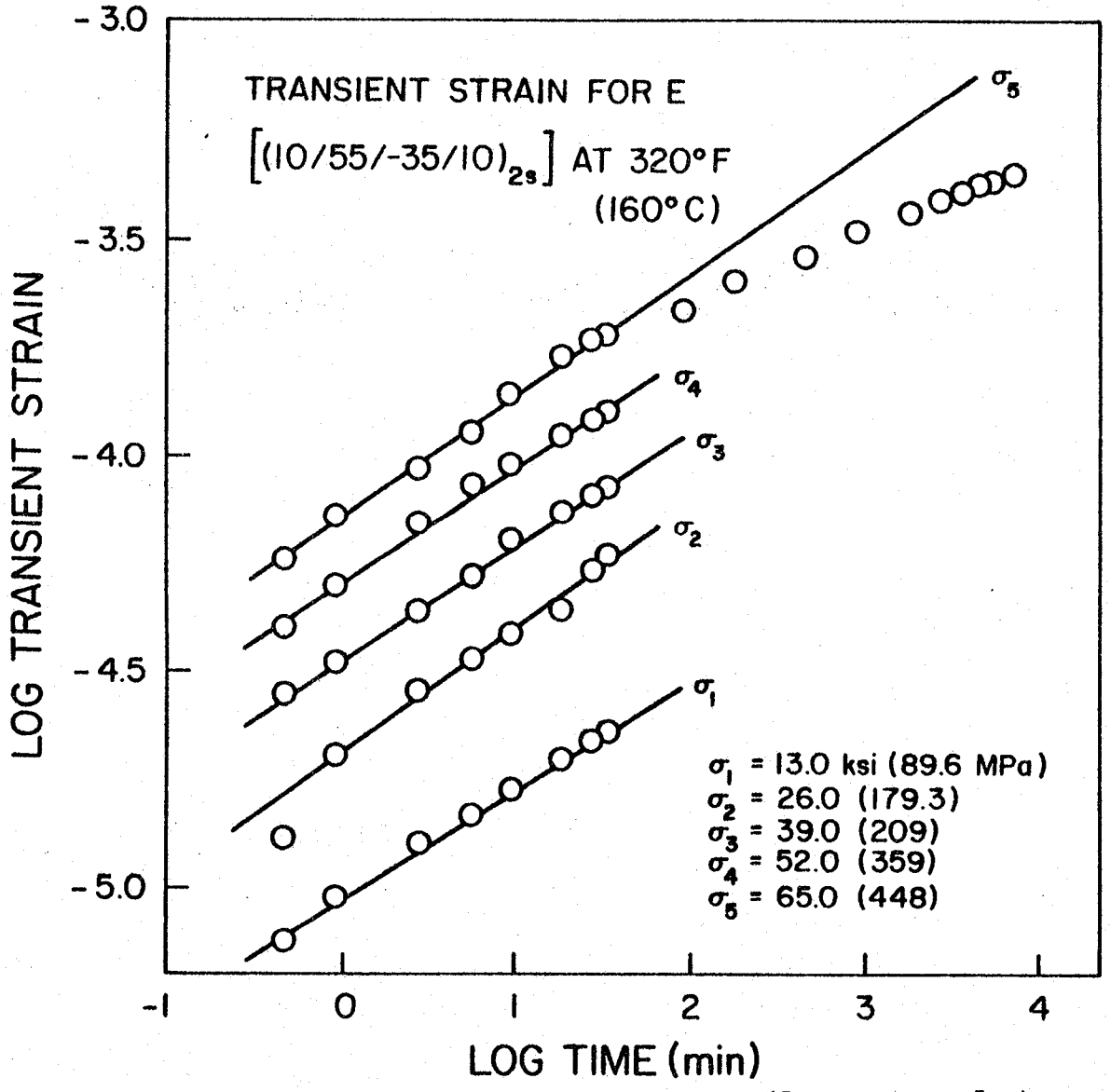

Fig. 7.17 Log-log plot of transient strain for laminate E ($[10/-35/55/10]_{2s}$) at 320°F (160°C).

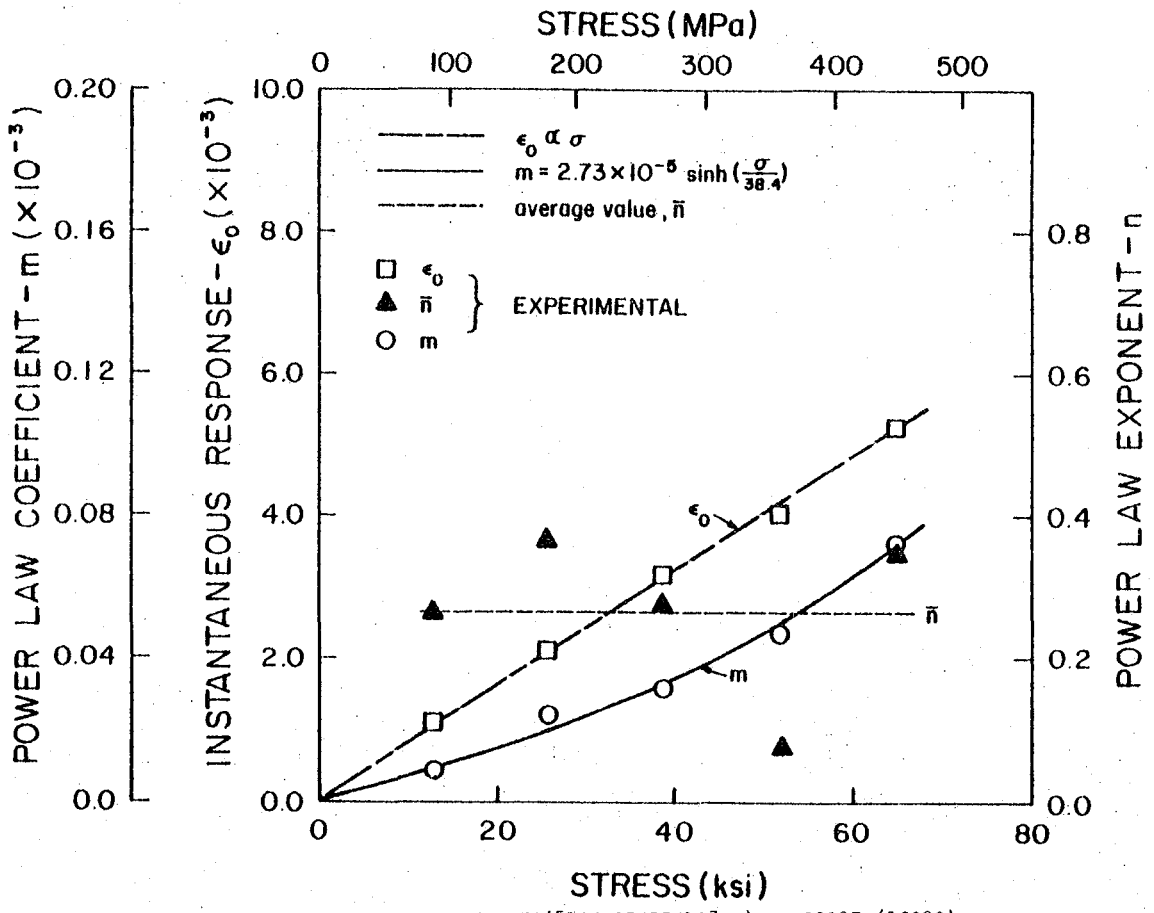

Fig. 7.18 Power law parameters for E ($[10/-35/55/10]_{2s}$) at 320°F (160°C).

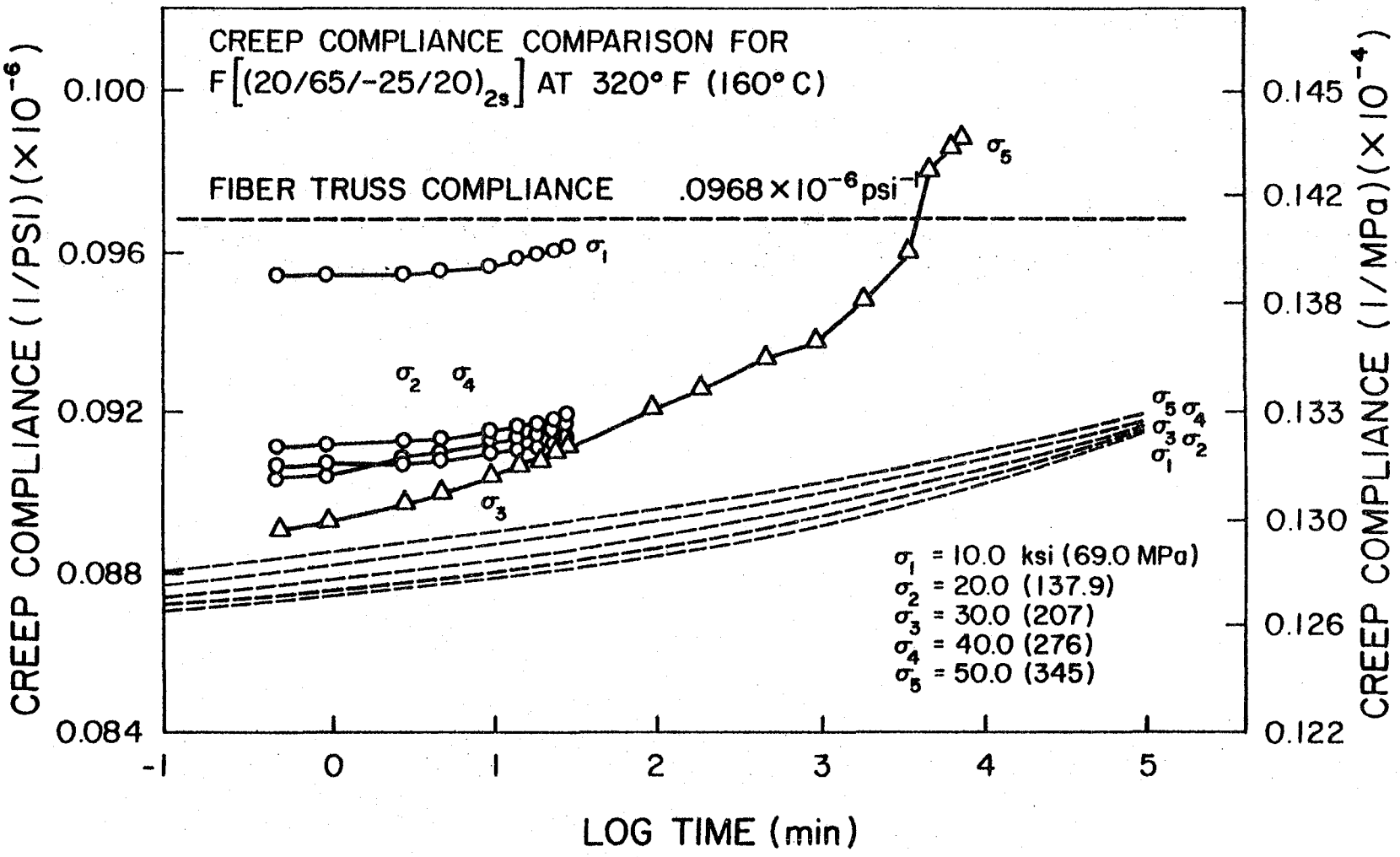

Fig. 7.19 Comparison of predicted and experimental creep compliance for laminate F ($[20/65/-25/20]_{2s}$) at 320°F (160°C).

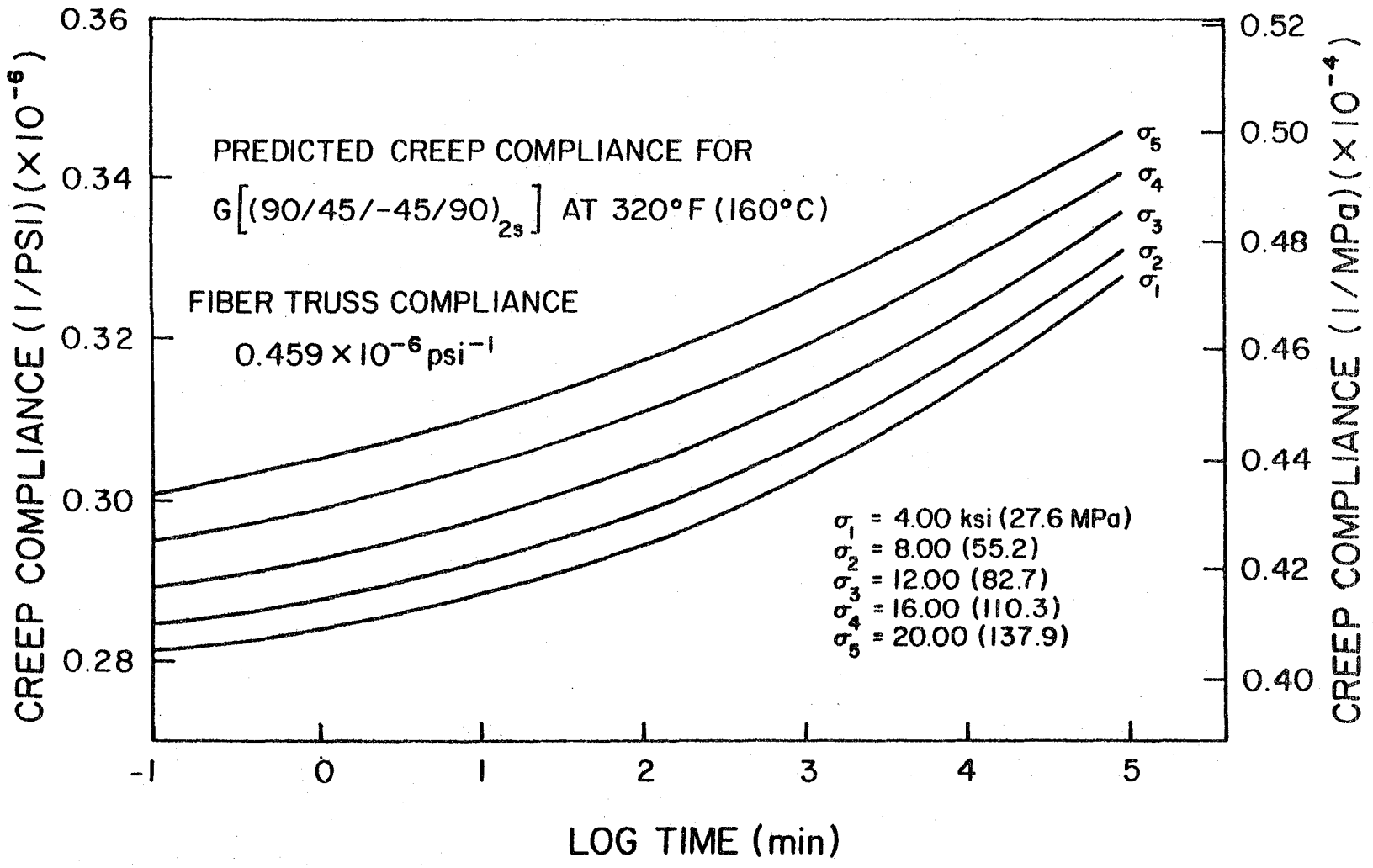

Fig. 7.20 Predicted creep compliance for laminate G $[90/45/-45/90]_{2s}$ at 320°F (160°C).

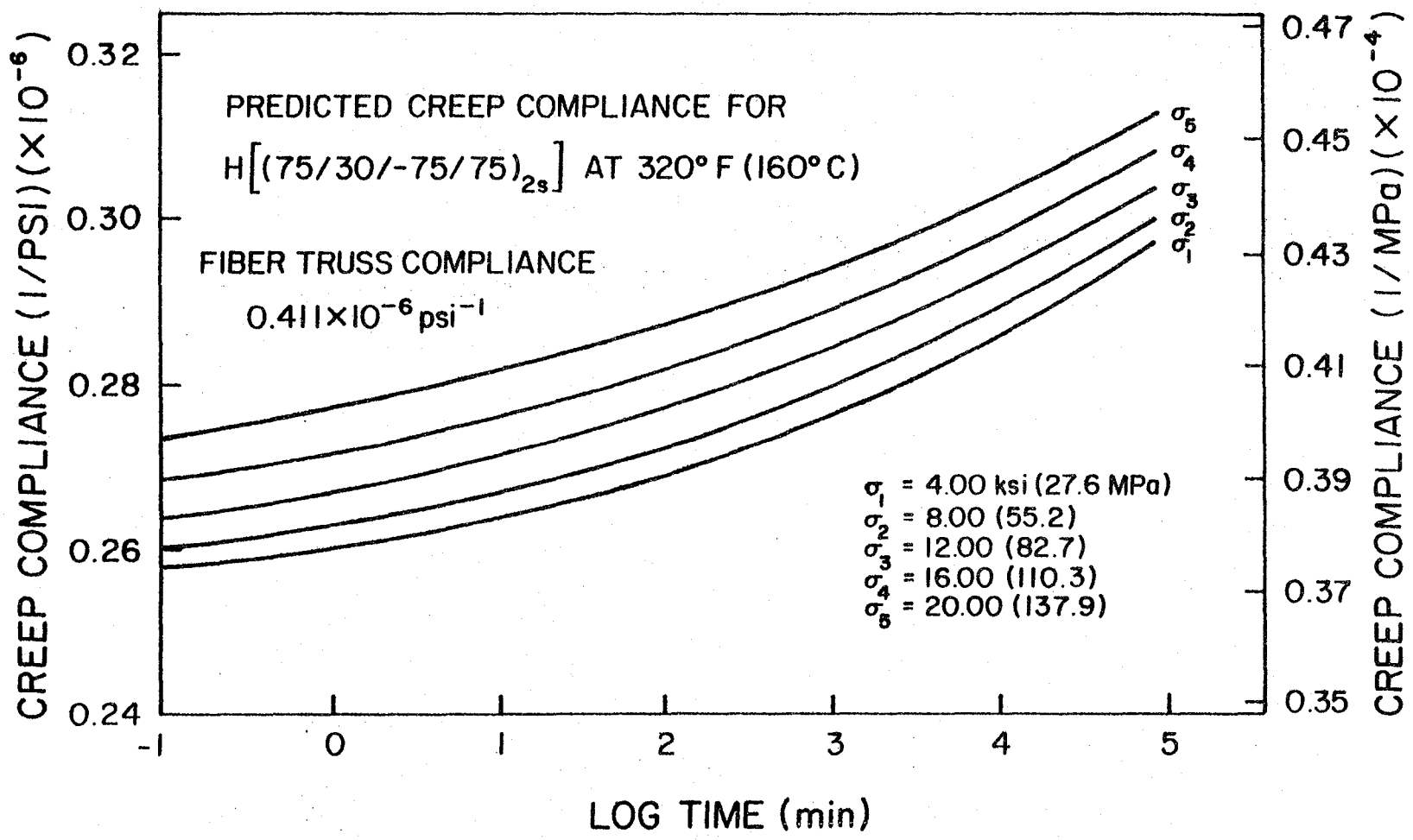

Fig. 7.21 Predicted creep compliance for laminate H ($[75/30/-75/75]_{2s}$) at 320°F (160°C).

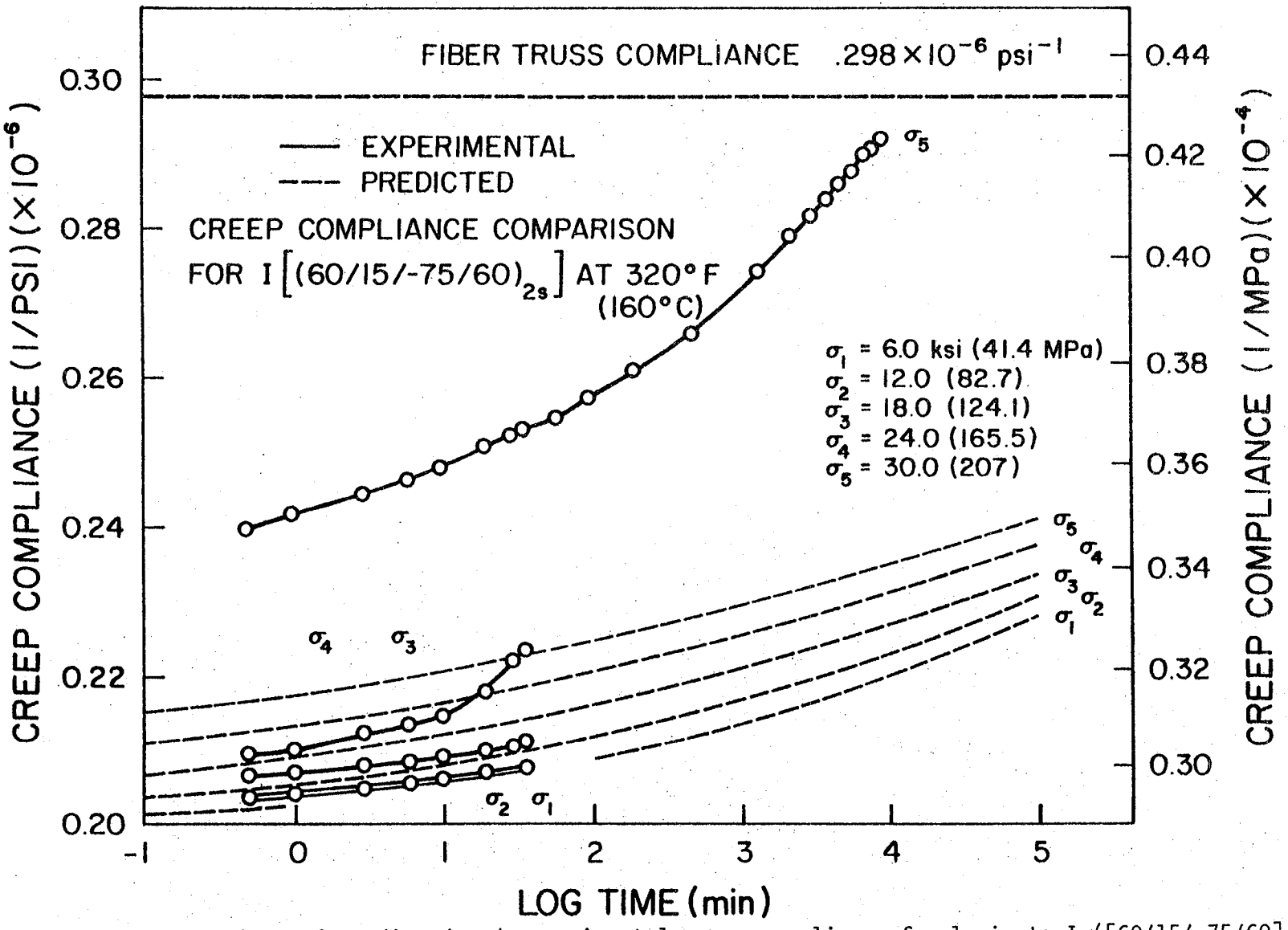

Fig. 7.22 Comparison of predicted and experimental creep compliance for laminate I ($[60/15/-75/60]_{2s}$) at 320°F (160°C).

The rapid upturn of the experimental compliance at σ_4 was due to a series of jumps in the strain output. A schematic drawing in Fig. 7.23 details the nature of these strain steps. The shape of the steps tends to indicate that they resulted from localized matrix cracking of plies within the region under the strain gages. As some plies crack, the remaining laminate became more compliant. The experimental transient strains are indicated in Fig. 7.24.

The compliance results for the J laminate are indicated in Fig. 7.25. The agreement with the experimental data is considered to be very good. The experimental transient strains are shown in Fig. 7.26. The results from the application of the Findley procedure to this data are shown in Fig. 7.27. The degree of fit is considered to be excellent.

Fig. 7.28 presents the K results. Because the J and K laminates each contain only two fiber orientations, there is no fiber truss limiting compliance. Experimentally, these laminates are characterized by very large transient deformations. Also plotted in this figure are the predicted compliances for several stress levels based on neglecting the fiber rotations. This laminate underwent the largest deformations and fiber rotations. As may be observed, predictions are considerably more compliant if significant fiber rotations are not accounted for. Unfortunately, the K specimen broke prematurely and long term data was not obtained. The transient strain data is presented in Fig. 7.29. The Findley results are given in Fig. 7.30 and are considered to be very good.

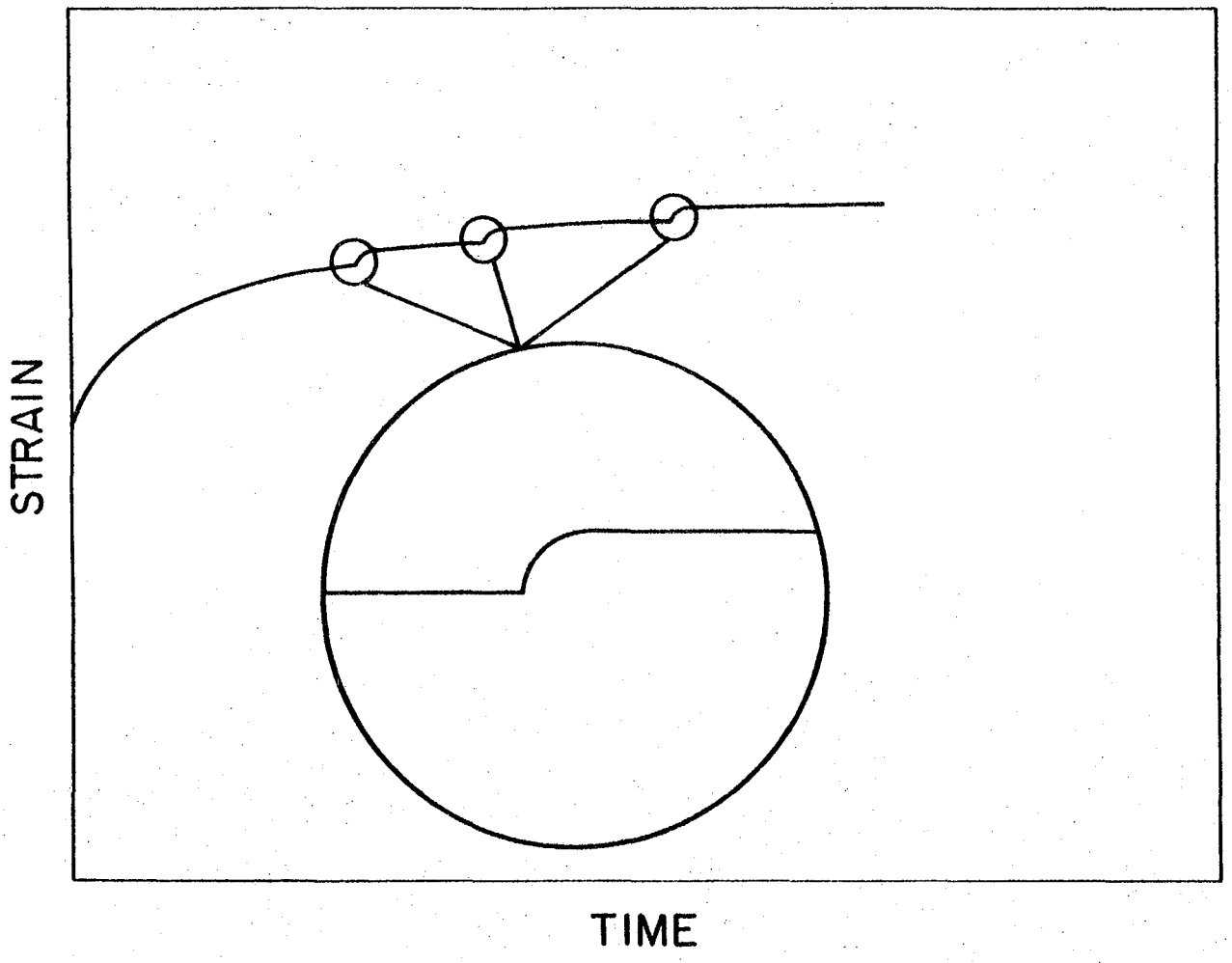

Fig. 7.23 Schematic representation of strain jumps for creep loading.

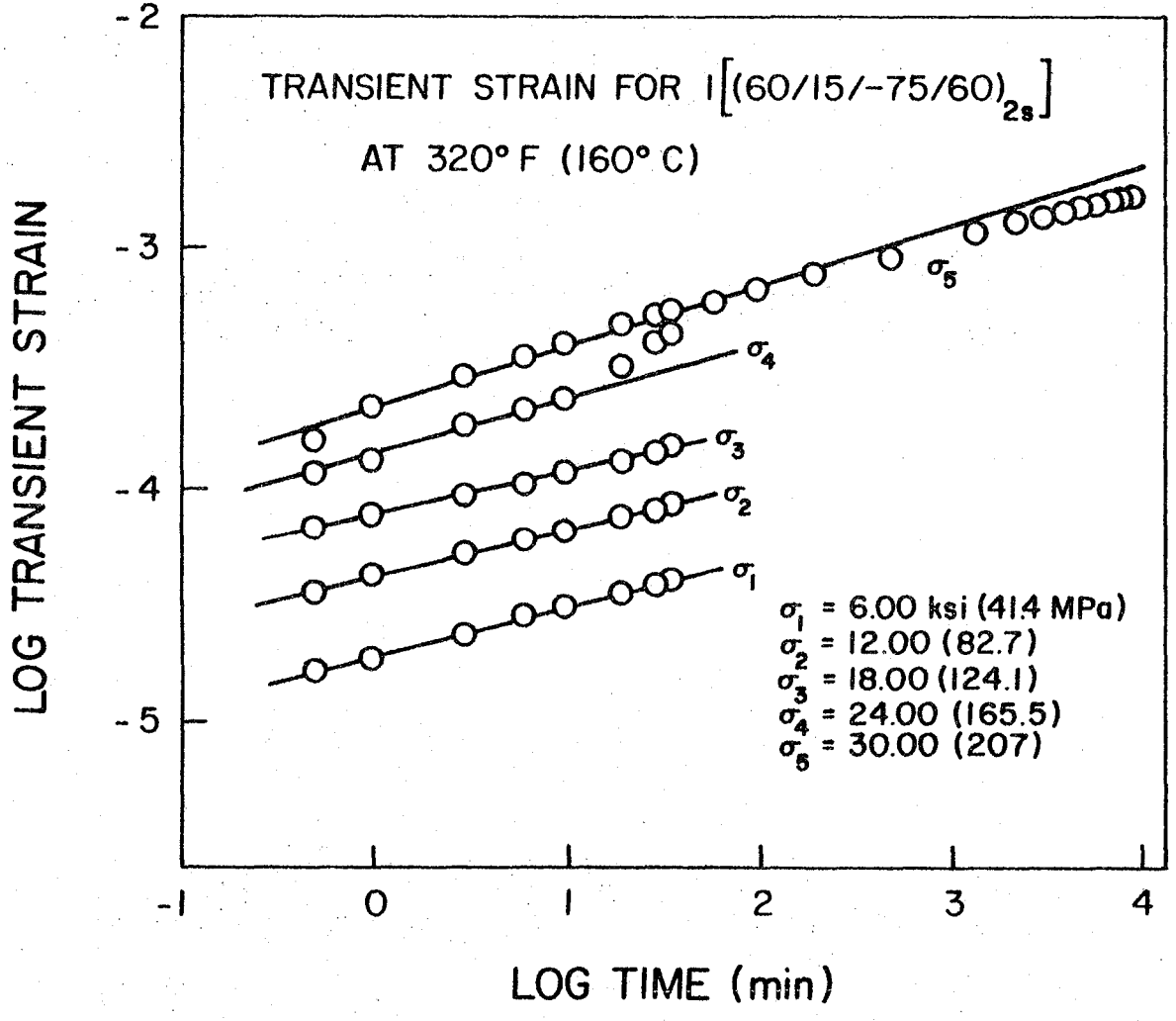

Fig. 7.24 Log-log plot of transient strain for Laminate I ($[60/15/-75/60]_{2s}$) at 320°F (160°C).

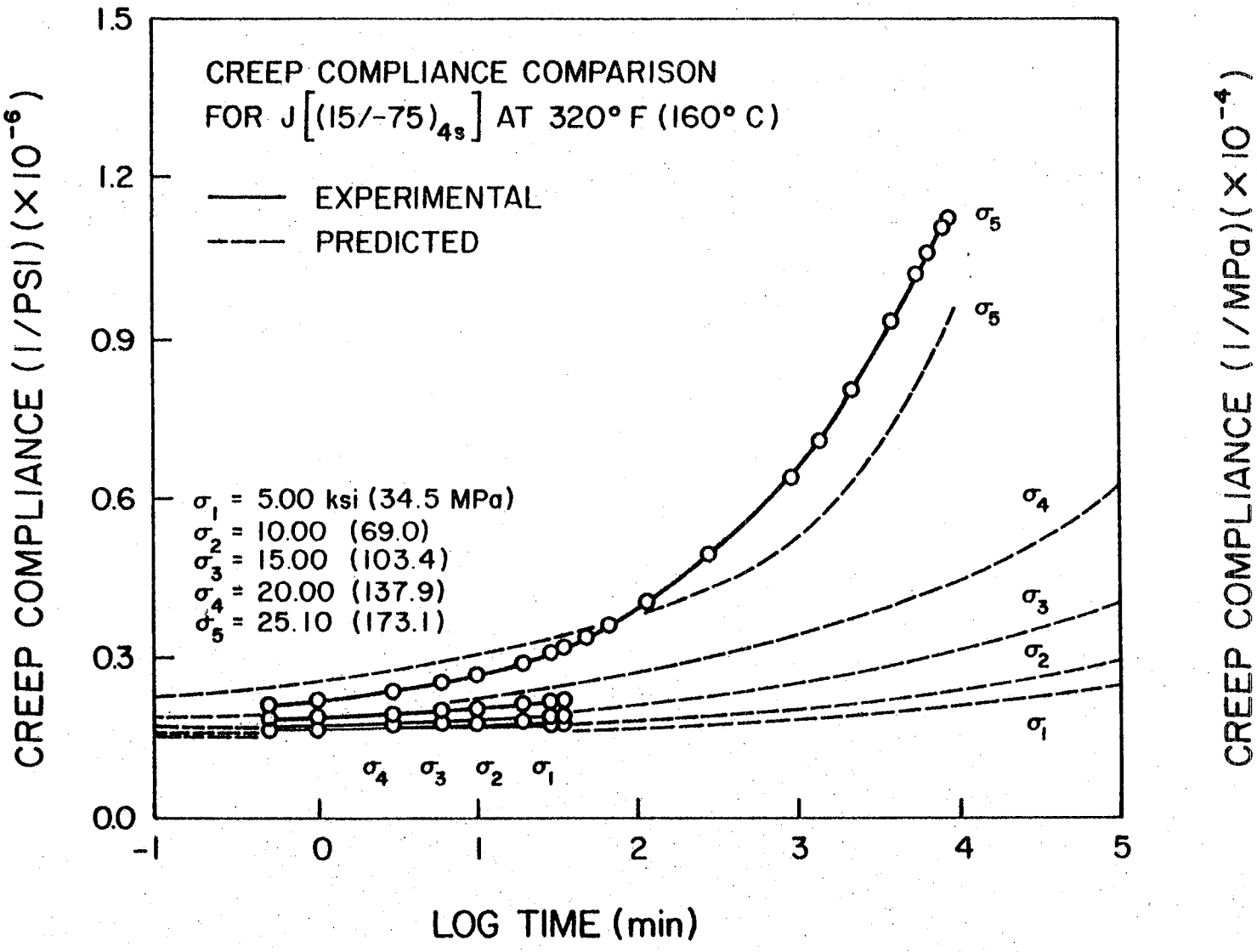

Fig. 7.25 Comparison of predicted and experimental creep compliance for laminate J ($[15/-75]_{4s}$) at 320°F (160°C).

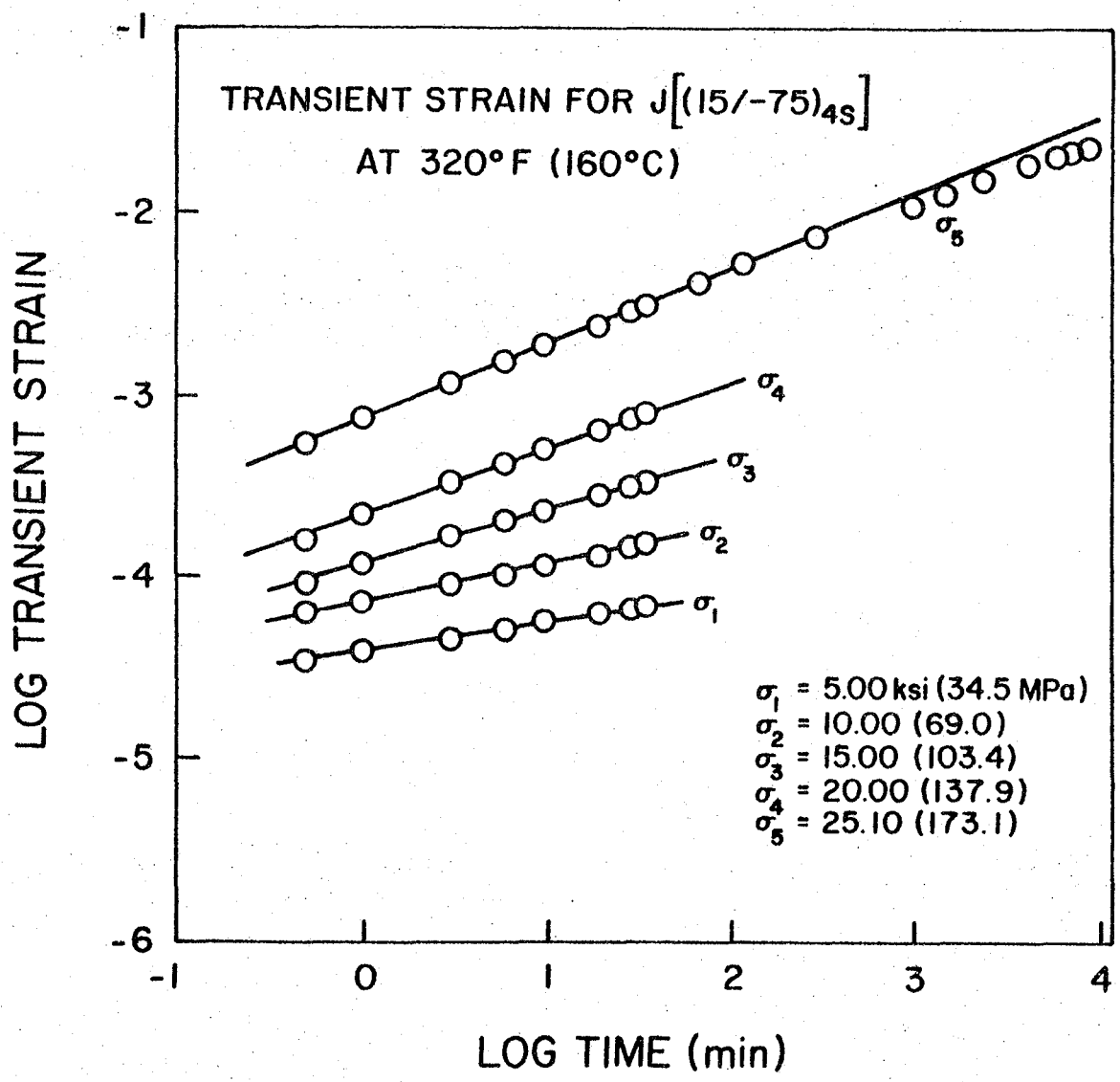

Fig. 7.26 Log-log plot of transient strain for laminate J ($[15/75]_{4s}$) at 320°F (160°C).

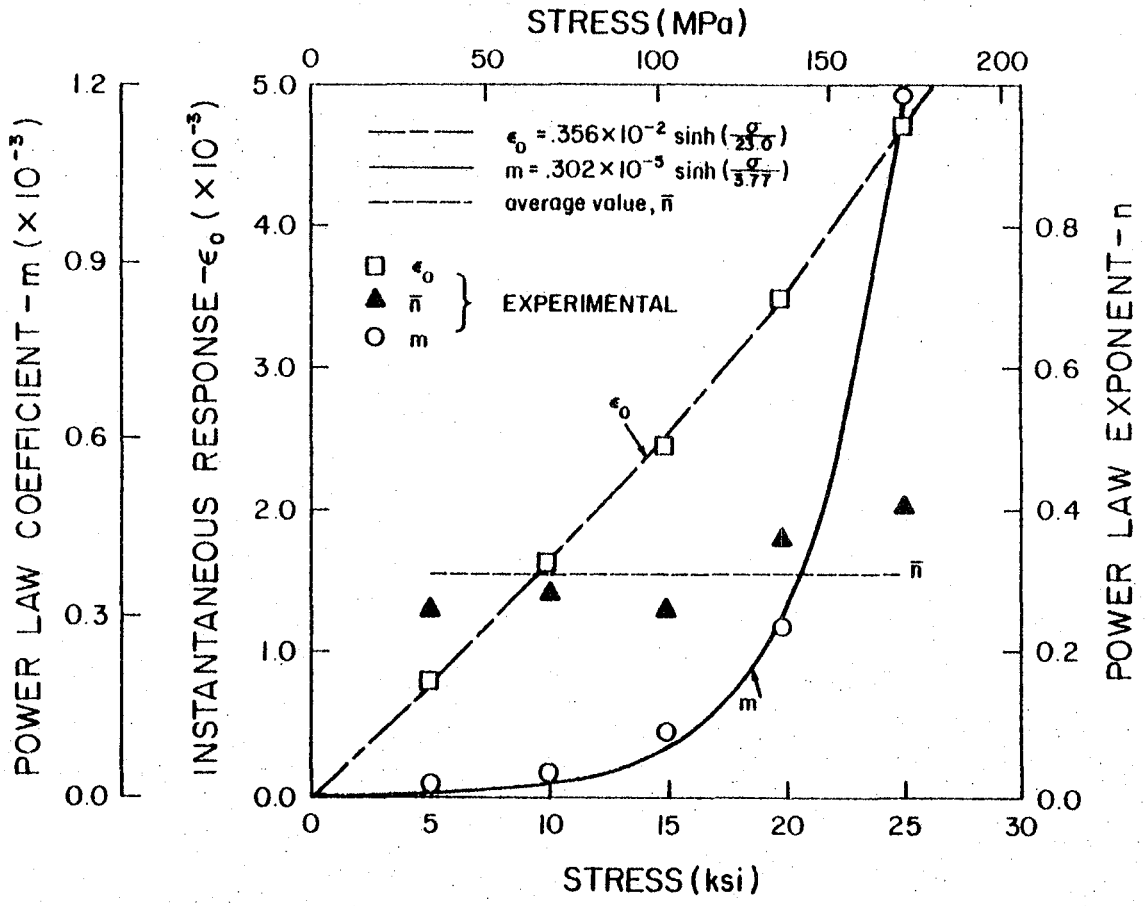

Fig. 7.27 Power law parameters for J ($[15/-75]_{4s}$) at 320°F (160°C).

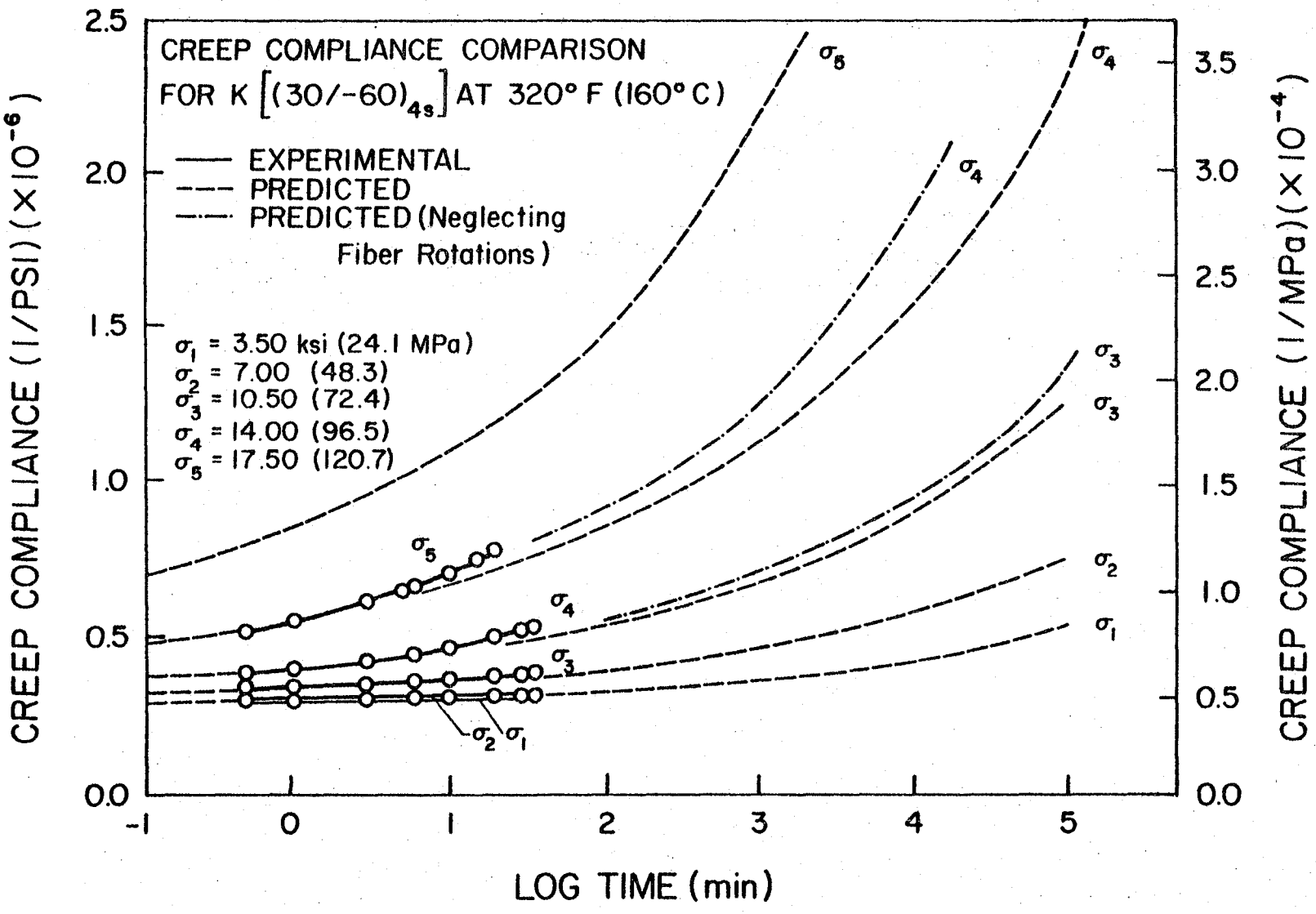

Fig. 7.28 Comparison of predicted and experimental creep compliance for laminate K ($[30/-60]_{4s}$) at 320°F (160°C).

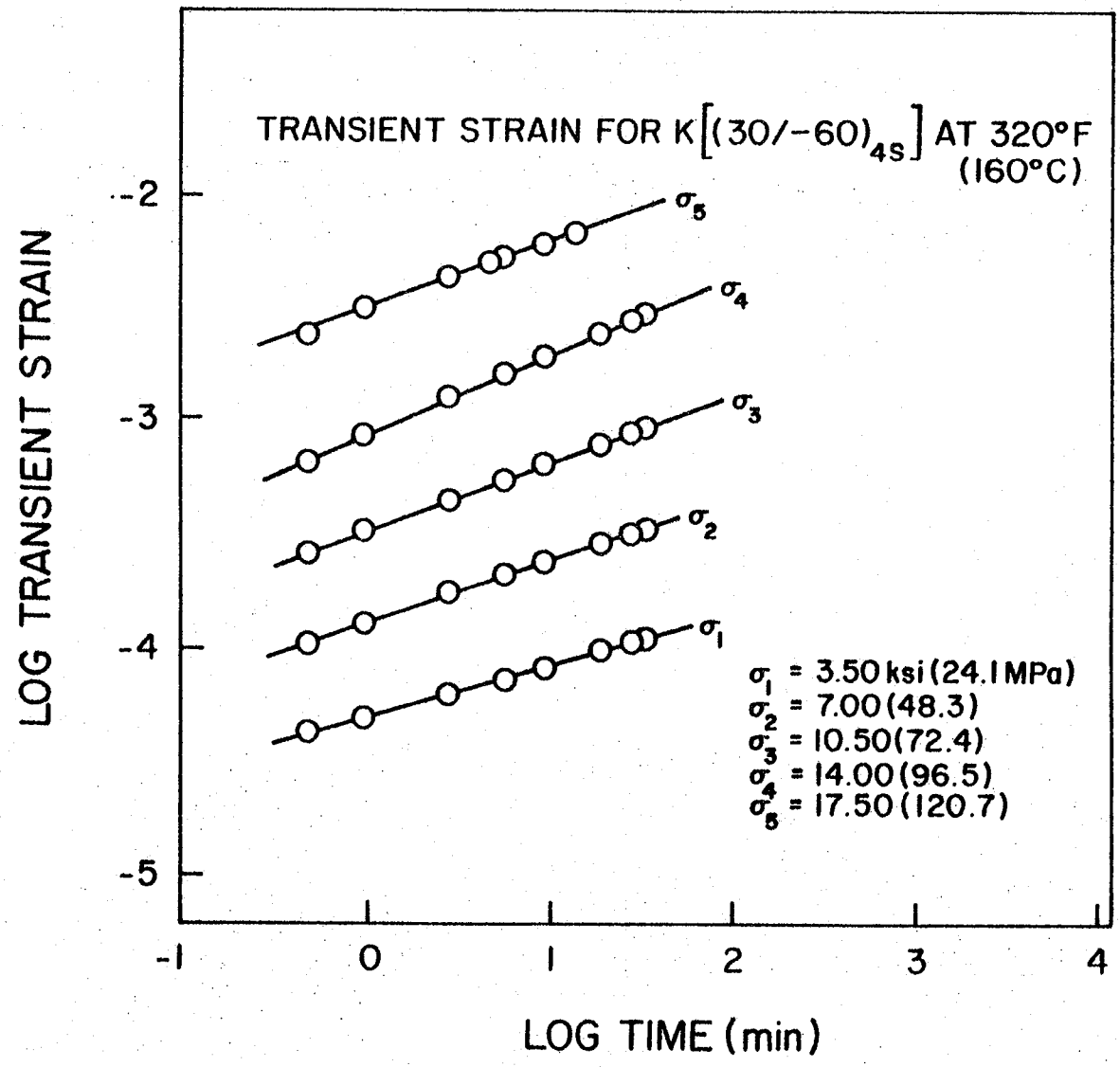

Fig. 7.29 Log-log plot of transient strain for laminate K ($[30/-60]_{4s}$) at 320°F (160°C).

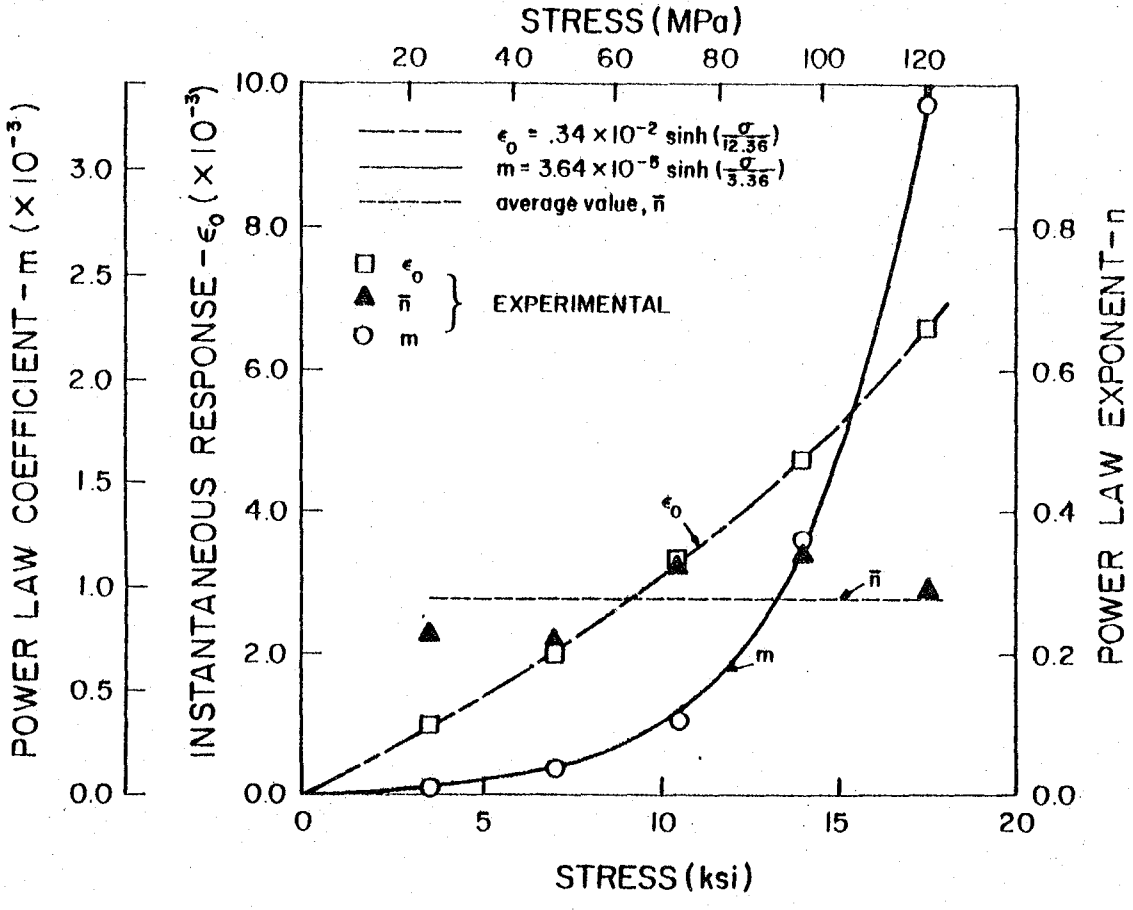

Fig. 7.30 Power law parameters for laminate K ($[30/-60]_{4s}$) at 320°F (160°C).

Although the Findley procedure was developed for homogeneous, isotropic materials, the present endeavor has been to apply this approach to the 90° and shear compliances for a unidirectional lamina. While this appears to be an appropriate use of the technique, the Findley procedure cannot be indiscriminately applied to any arbitrary black box material. For example, the predicted compliances of the E and F laminates are significantly affected by the limiting fiber truss compliance. If the Findley procedure is applied to this model, the hyperbolic sine relations are found to be totally inappropriate.

The implications of applying the Findley approach to the experimental compliance data of a general laminate have not been fully assessed. The procedure, however, was found to be quite appropriate in describing the material response, as indicated in the previous figures. The power law was also considered to be quite applicable to the general laminate response. The results presented herein tend to suggest that one could generate carpet plots of the Findley parameters for a family of general laminates and such information could be used to predict the nonlinear response of arbitrary laminates of the same general family.

Creep Rupture Predictions

The valid creep rupture data points from Figs. 7.2, 7.5 - 7.12 are replotted in Figs. 7.31 - 7.39 along with the incremental lamination program predictions of the creep rupture strengths. Program predictions based on both $\alpha = 0.65$ and $\alpha = 0.80$ are presented. Program predictions and experimental data are compared with creep

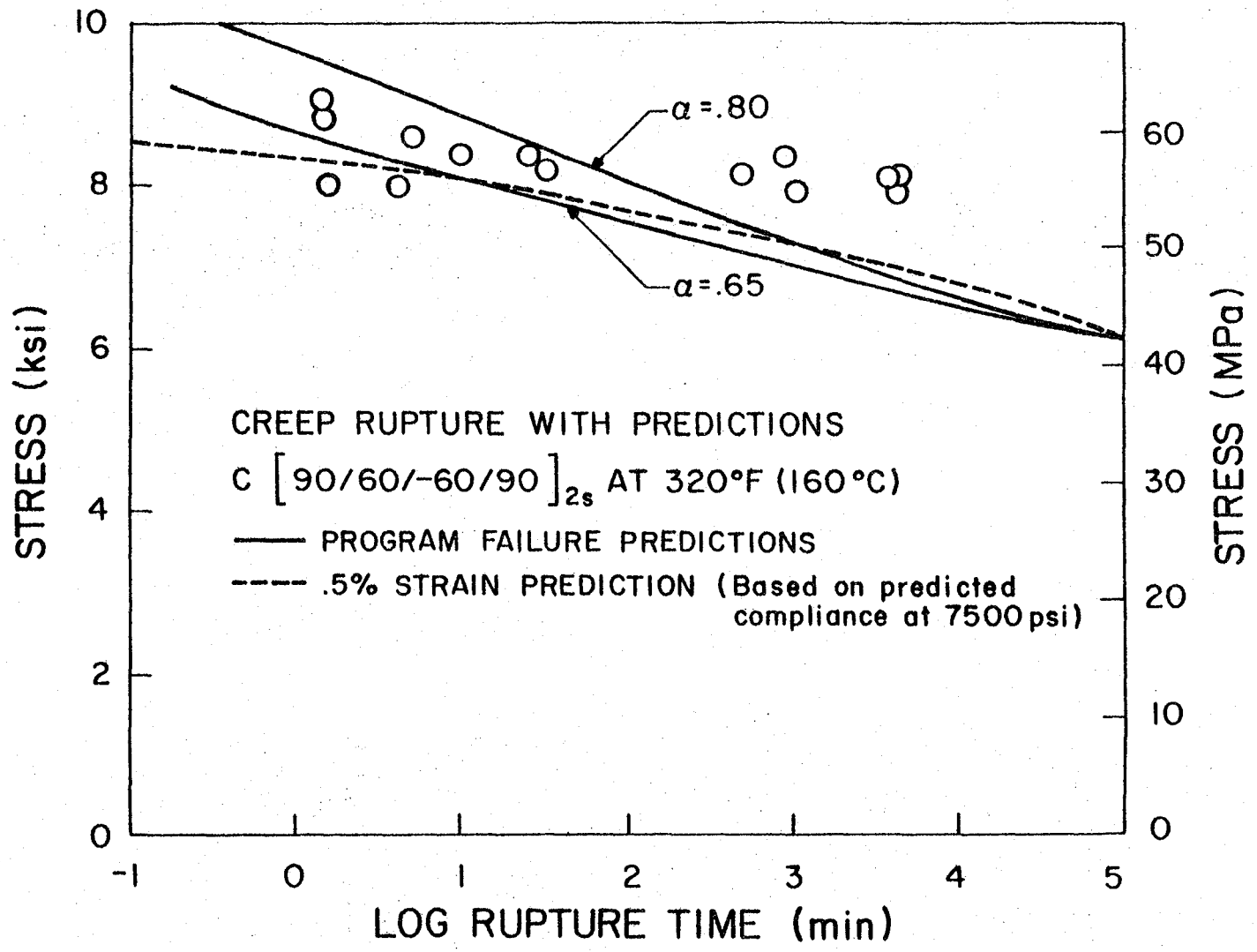

Fig. 7.31 Creep rupture data with predictions for laminate C $[90/60/-60/90]_{2s}$ at 320°F (160°C).

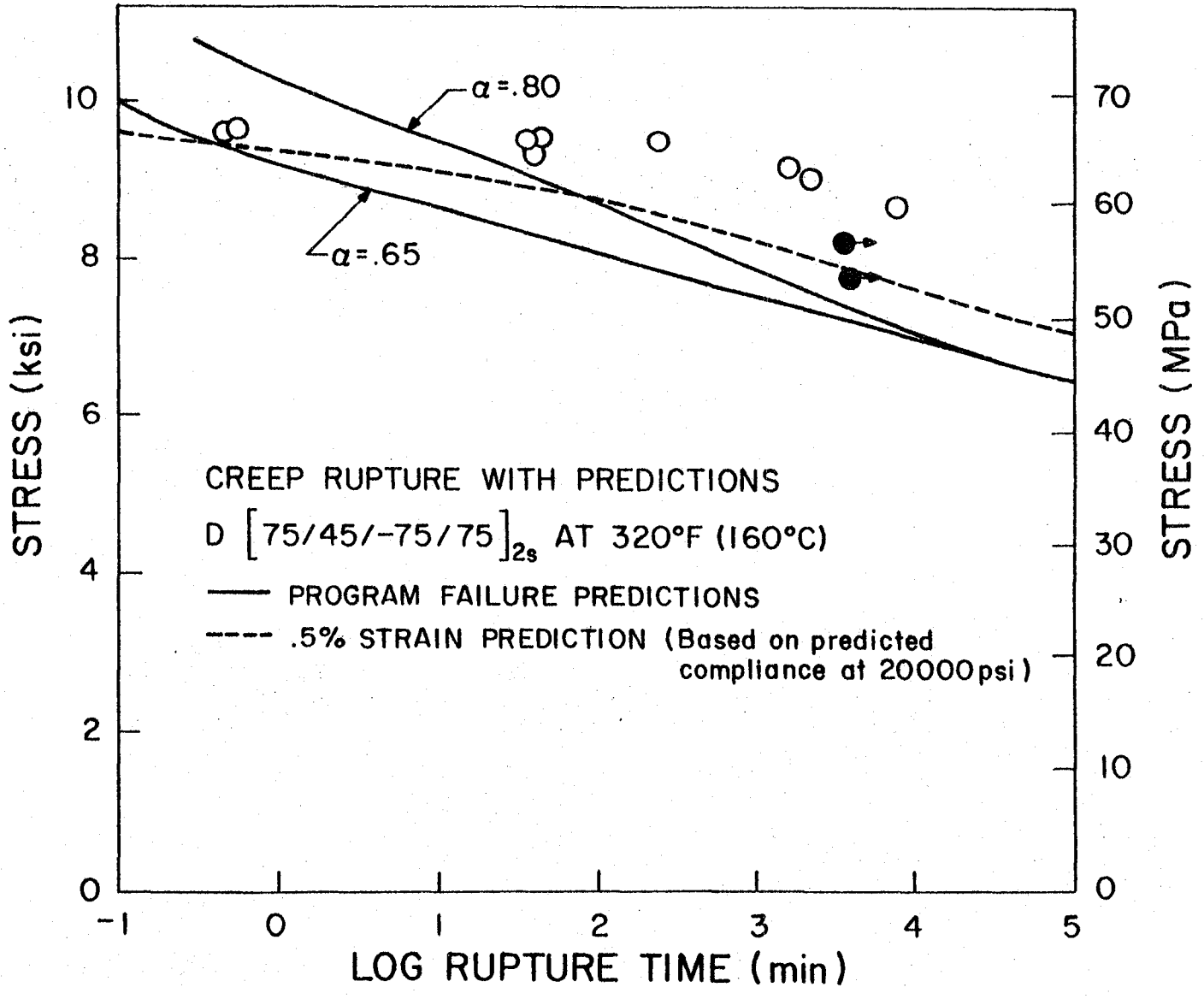

Fig. 7.32 Creep rupture data with predictions for laminate D $[75/45/-75/75]_{2s}$ at 320°F (160°C).

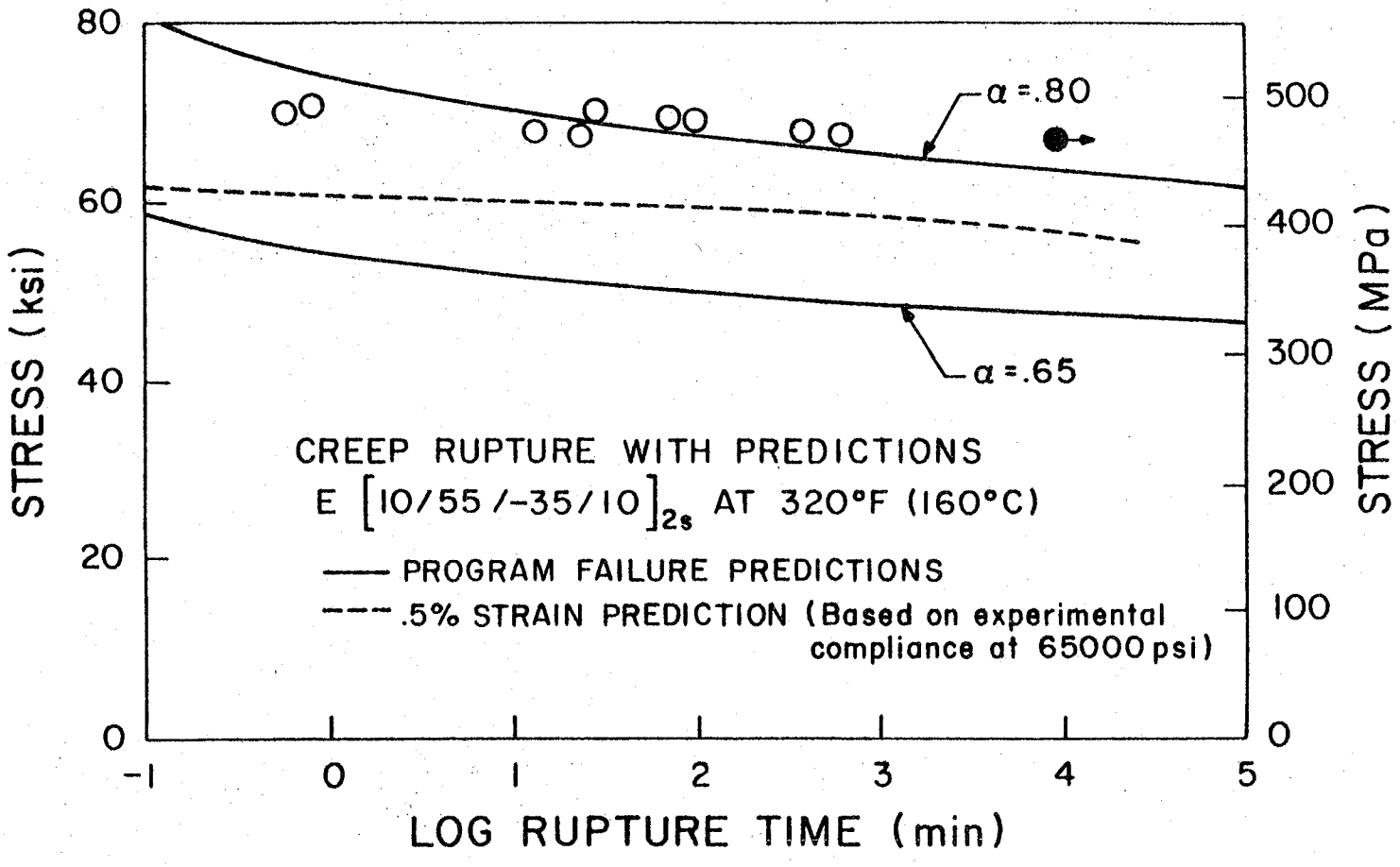

Fig. 7.33 Creep rupture data with predictions for laminate E $[10/55/-35/10]_{2s}$ at 320°F (160°C).

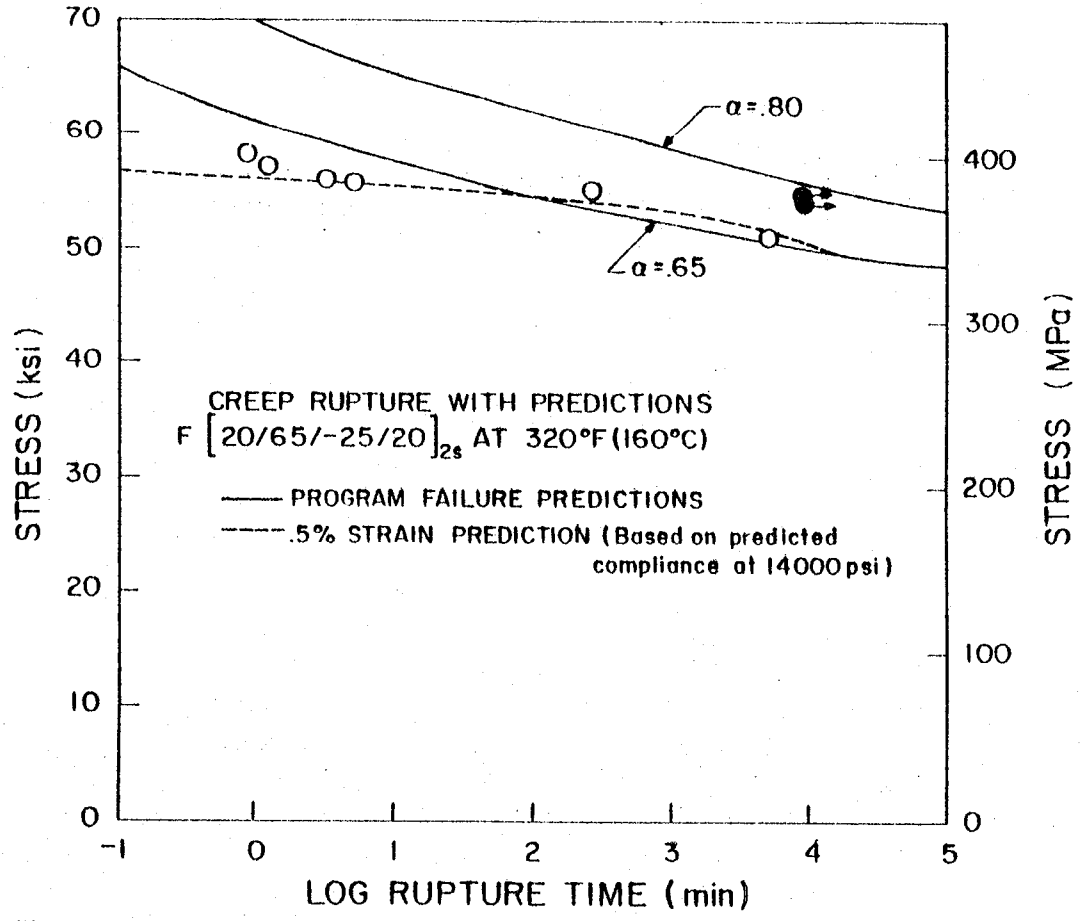

Fig. 7.34 Creep rupture data with predictions for laminate F $[20/65/-25/20]_{2s}$ at 320°F (160°C).

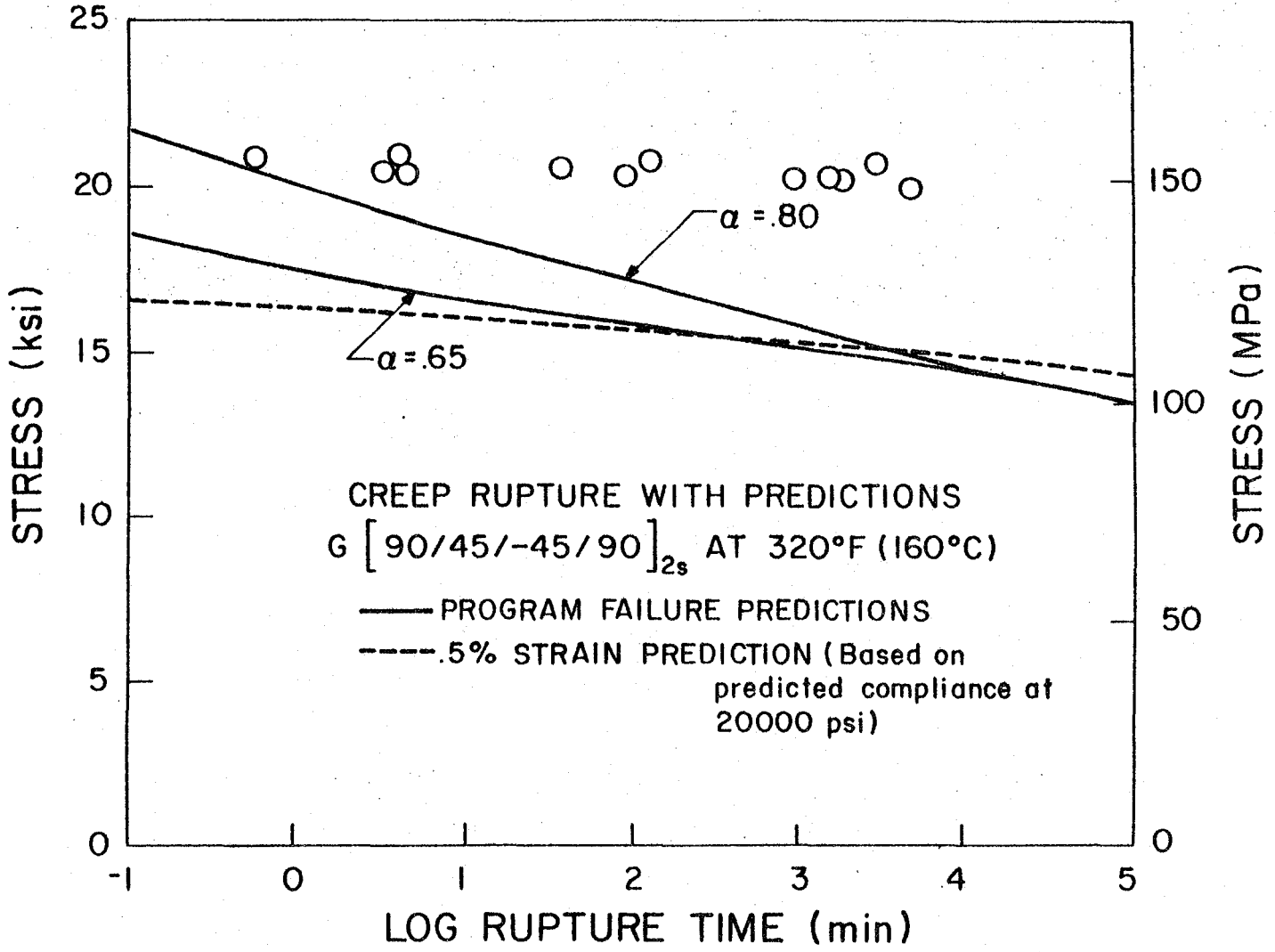

Fig. 7.35 Creep rupture data with predictions for laminate G $[90/45/-45/90]_{2s}$ at 320°F (160°C).

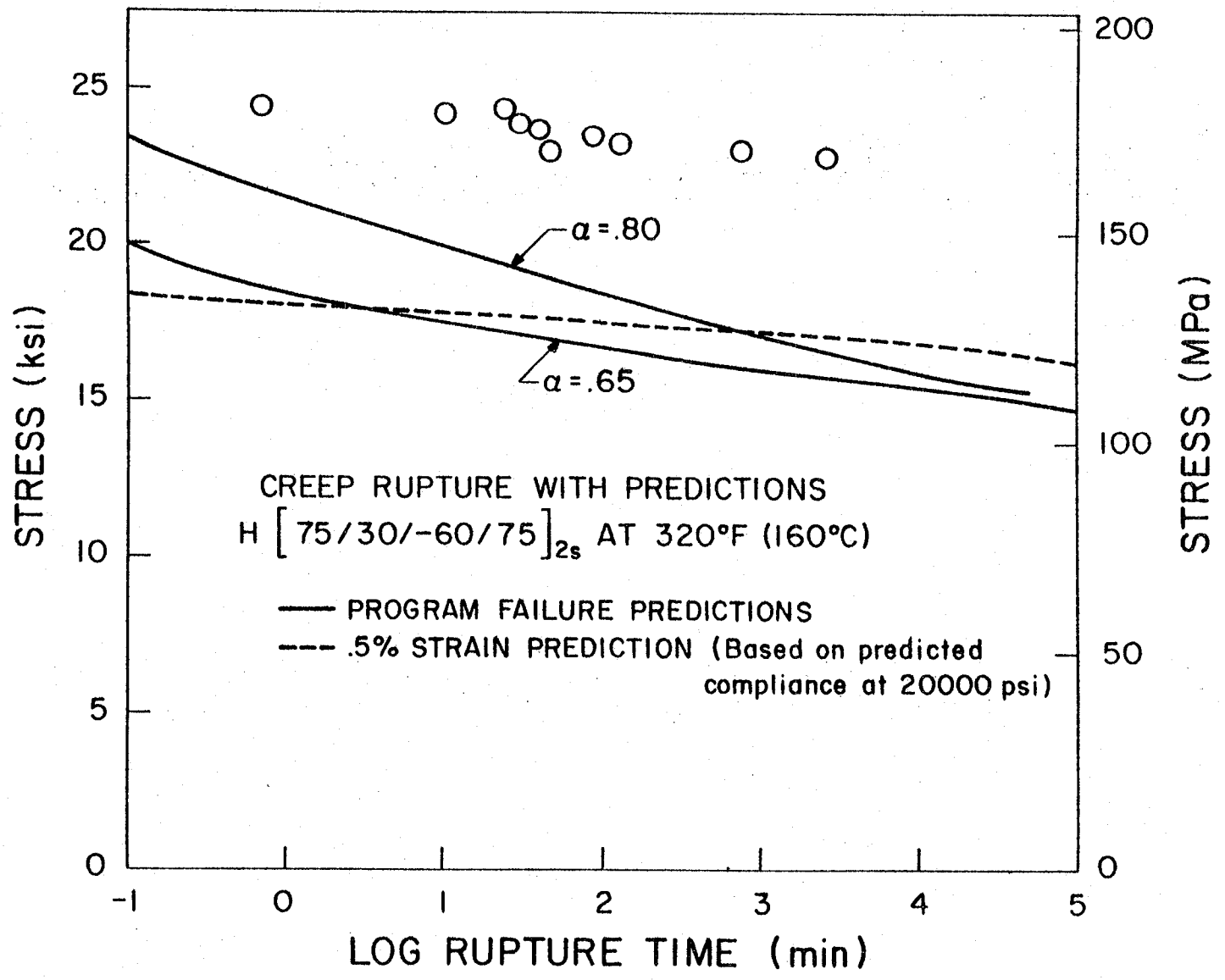

Fig. 7.36 Creep rupture data with predictions for laminate H $[75/30/-60/75]_{2s}$ at 320°F (160°C).

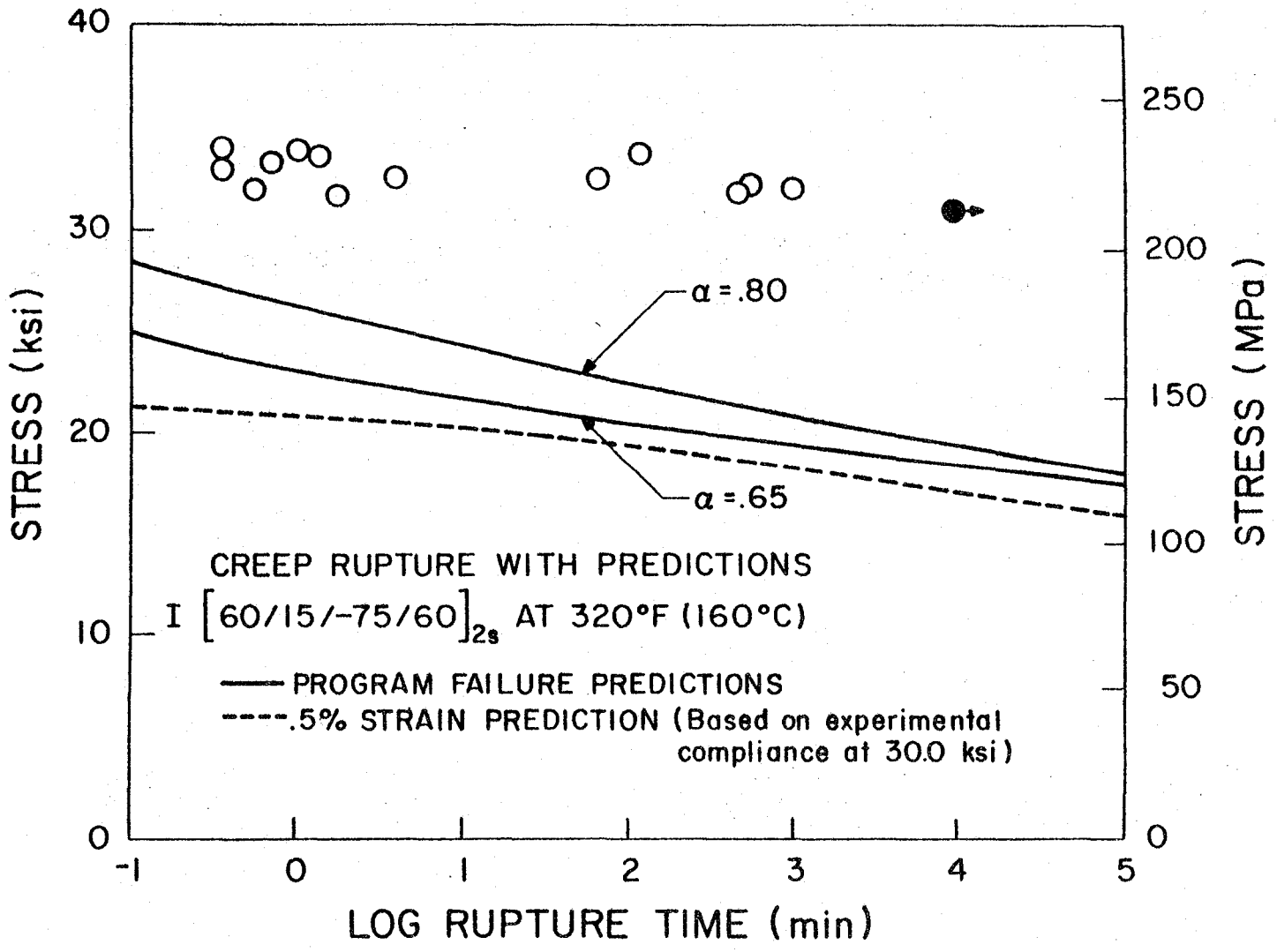

Fig. 7.37 Creep rupture data with predictions for laminate I $[60/15/-75/60]_{2s}$ at 320°F (160°C).

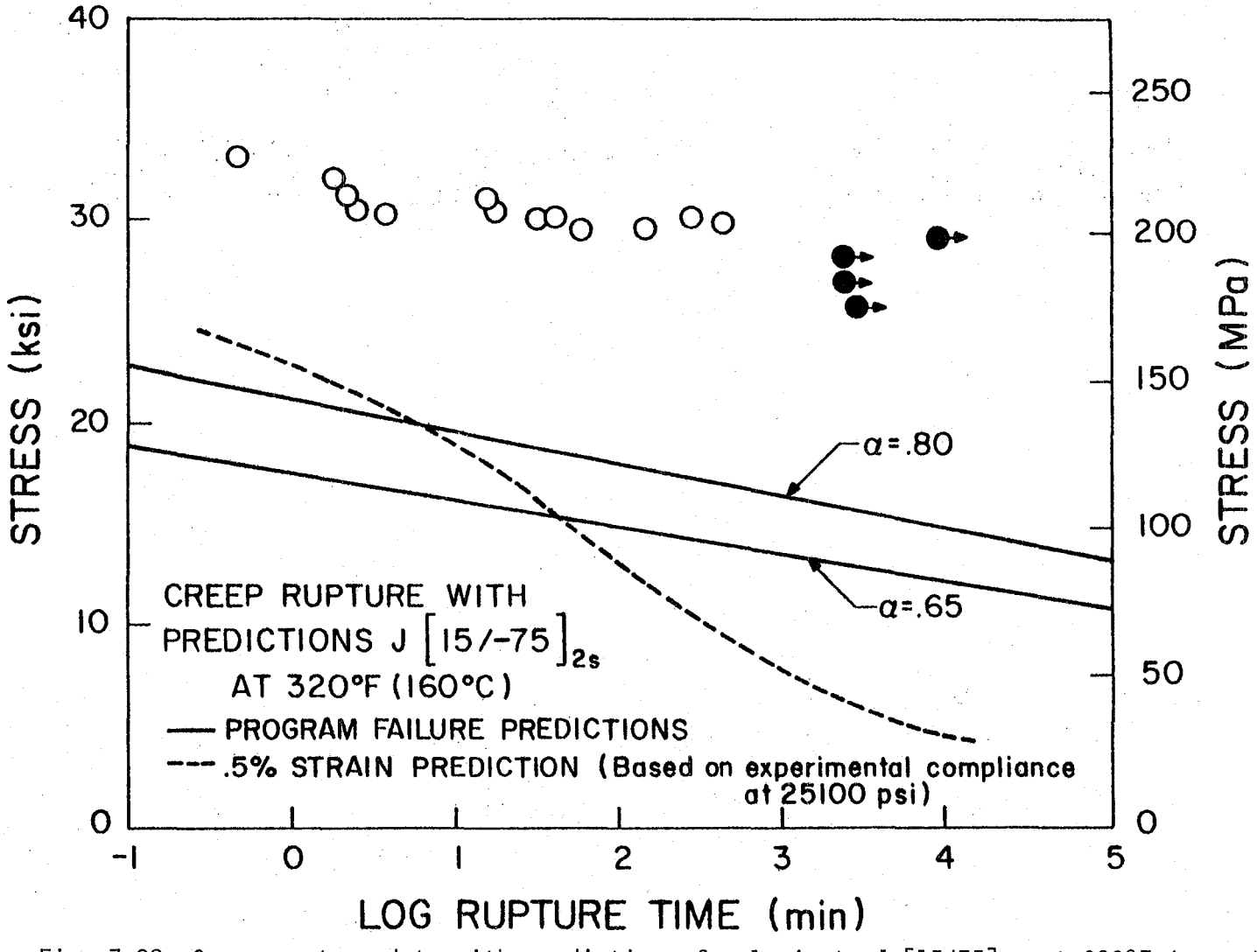

Fig. 7.38 Creep rupture data with predictions for laminate J $[15/75]_{4s}$ at 320°F (160°C).

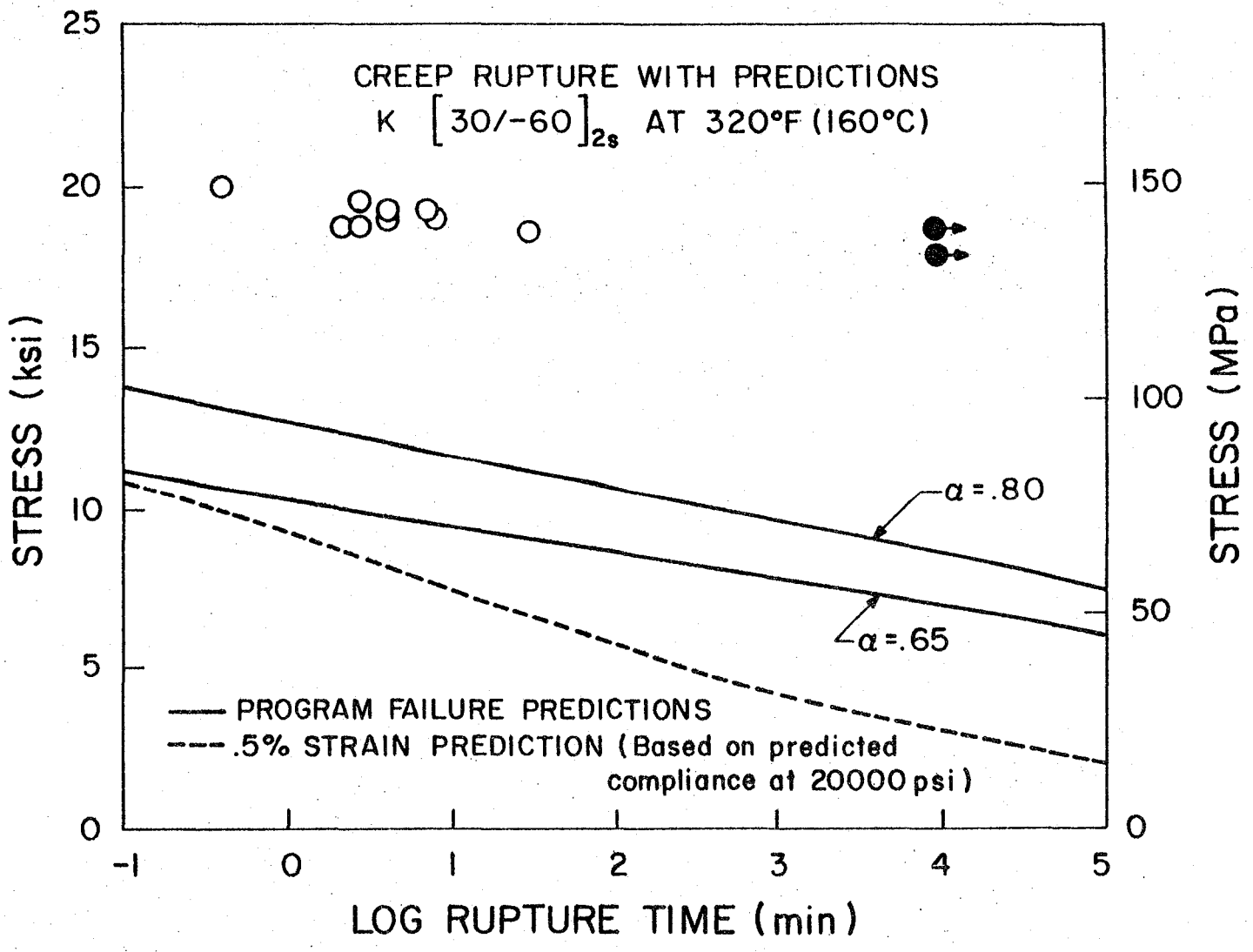

Fig. 7.39 Creep rupture data with predictions for laminate K $[30/-60]_{2s}$ at 320°F (160°C).

rupture strength predicted by a deformational failure approach which assumed that laminate failure would occur when the axial laminate strain reached an arbitrarily chosen strain value of 0.5%. Deformational failure predictions were based on long term experimental compliance data when available. Compliance values predicted by the program were used when experimental data was not available. Compliance values are a function of stress level because the material was nonlinear. The stress values used for the compliances were near the creep rupture strengths and are indicated in the figures.

The results previously given in Fig. 4.5 indicated that $\alpha = 0.65$ was an appropriate value for expressing the shear creep rupture strength in terms of the 90° strength. In Figs. 7.31 - 7.39, however, lamination program predictions based on $\alpha = 0.65$ fall consistently below the experimental data. Also, the results shown in Fig. 4.5, indicated that the value of α for the other temperatures tended to be greater than 0.65. Based on this evidence and because the program predictions all tended to be low, the value $\alpha = 0.80$ was used to obtain another set of program predictions. These values have also been indicated in Figs. 7.31 - 7.39.

The results for the C and D laminates are found in Figs. 7.31 and 7.32 and were obtained from specimens of the "old" material batch. Because input properties used in the program were for the "new" material, predictions for the "old" material specimens may not be appropriate. Interestingly, predictions based on the two values of α converge after a certain length of time and is due to a change in the order in which the plies fail. For example, at shorter times in

the C specimens, the ± 60° plies are predicted to fail first if $\alpha = 0.65$, but the 90° plies will fail first if $\alpha = 0.80$. For longer times, however, failure is predicted to originate in the 90° plies for either value of α, because matrix stresses in the 90° plies relax more slowly than in the ± 60° plies.

The results for E and F laminates are presented in Figs. 7.33 and 7.34. For the E laminate, $\alpha = 0.80$ predictions provide a better fit to the data than those based on $\alpha = .65$ but the same is not true for the similar F laminate. A possible explanation for this apparent discrepancy is that the F specimens encountered much larger bending stresses at the grips. Our belief is that end constraint stresses have substantially reduced the strength of the F specimens.

Results for the G, H, and I specimens are given in Figs. 7.35, 7.36, and 7.37 and, as may be observed, lamination program predictions fall consistently below the experimental data. Results for the J and K laminates with only two fiber orientations are given in Figs. 7.38 and 7.39. The $\alpha = 0.65$ predictions are seen to be low by nearly a factor of two, indicating an inability of the program to predict failures in the two fiber orientation laminates. A primary reason appears to be based on a great ability of these laminates to continue to sustain the creep load after all plies are cracked through the thickness. This is examined further in the next section.

Photographs of Delayed Failure Zones

The following photographs were taken to illustrate typical delayed failure zones in the laminates tested. These plates indicate

the manner in which failure occurred and the extent of the damage zone. Photomicrographs of typical specimen edges were taken near the separation zone and are also presented. The degree of matrix cracking in the individual plies should be noted in these plates. Typical C and D specimens have been shown in Plates 7.1 and 7.2 respectively. Note the very large amount of damage sustained by an E laminate in Plate 7.3a. The separation zone for an F specimen is illustrated in Plate 7.4a. Note in Plates 7.3b and 7.4b that neither E nor F laminates show any apparent matrix cracking away from the actual fracture zone. Similar photographs of G, H, and I laminates are presented in Plates 7.5, 7.6, and 7.7. The photographs of a J specimen in Plate 7.8 are very interesting. Note that all plies were cracked through but the laminate was still intact and capable of supporting the load.

The K specimens provided some very interesting details. Plates 7.9a, 7.9b, and 7.9c illustrate the failure zones for K specimens which ruptured at short, medium, and long times, respectively. Note the increasing degree of damage with the successively longer rupture times. Photomicrographs of these specimens reveals an increasing density of matrix cracks with longer rupture times. Several edge views of K specimens are illustrated in Plates 7.10 and 7.11. Note the more or less regular spacing of the matrix cracks. Stinchcomb, et al [71] have discussed such a saturation crack spacing. Although all individual plies may be shattered, the laminate remains intact and continues to support the load. To ascertain if the cracks actually extended across the specimen width, a K specimen was carefully

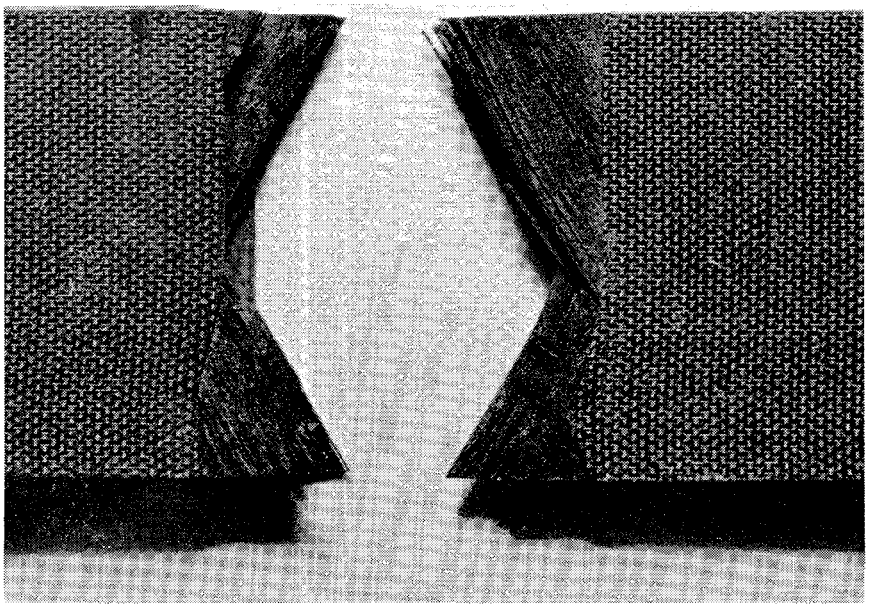

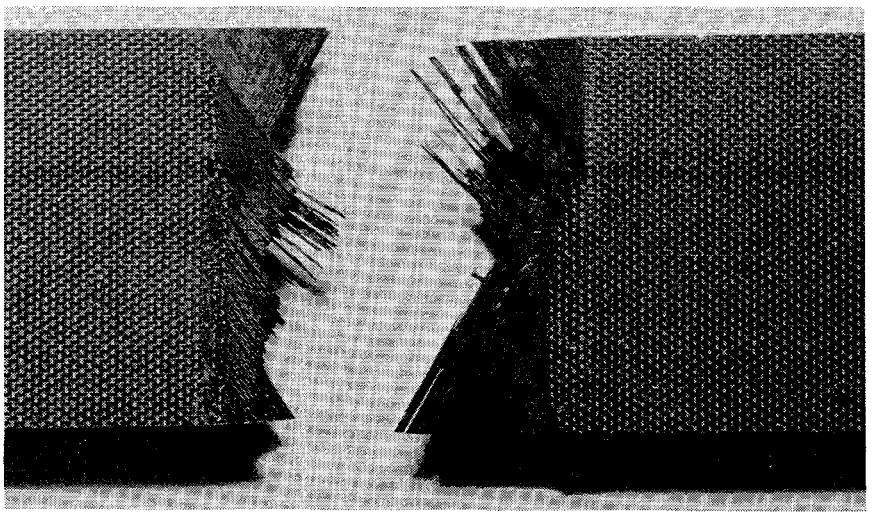

Plate 7.1 Typical Creep Rupture Zones for Laminate C $[90/60/-60/90]_{2s}$.

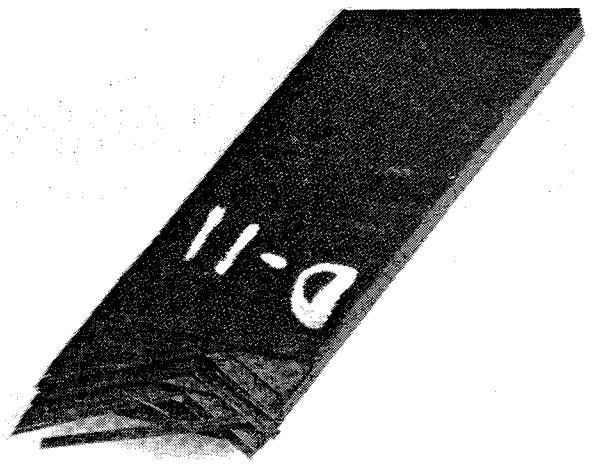

Plate 7.2a Failure Zone of Typical D Specimen $[75/45/-75/75]_{2s}$.

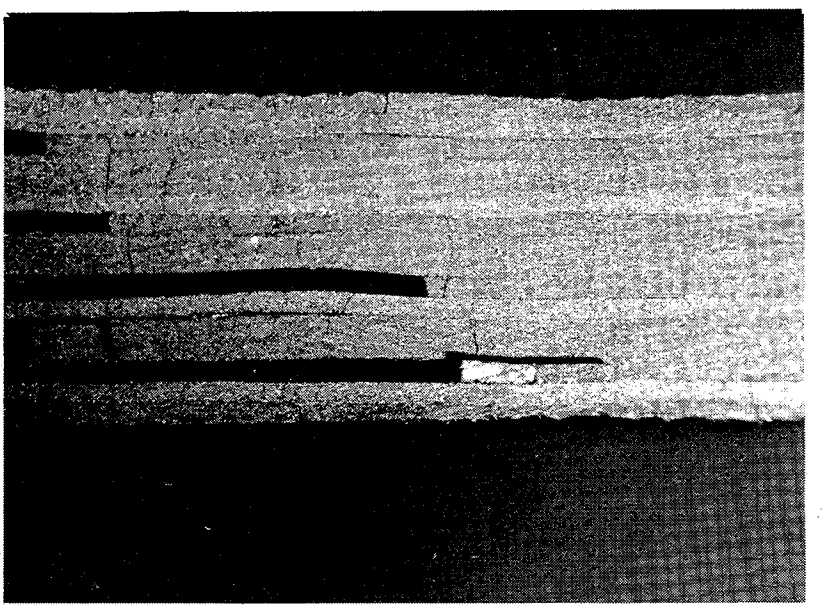

Plate 7.2b Edge Photomicrograph of Typical D Specimen $[75/45/-75/75]_{2s}$.

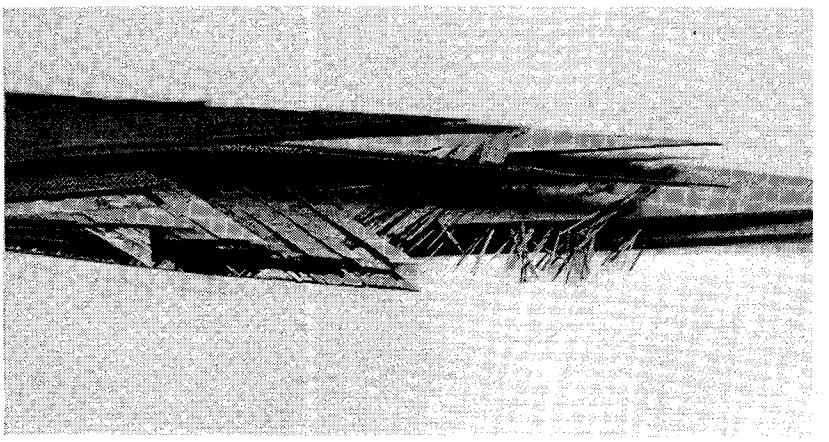

Plate 7.3a Typical Creep Rupture Zone for Laminate E $[10/55/-35/10]_{2s}$.

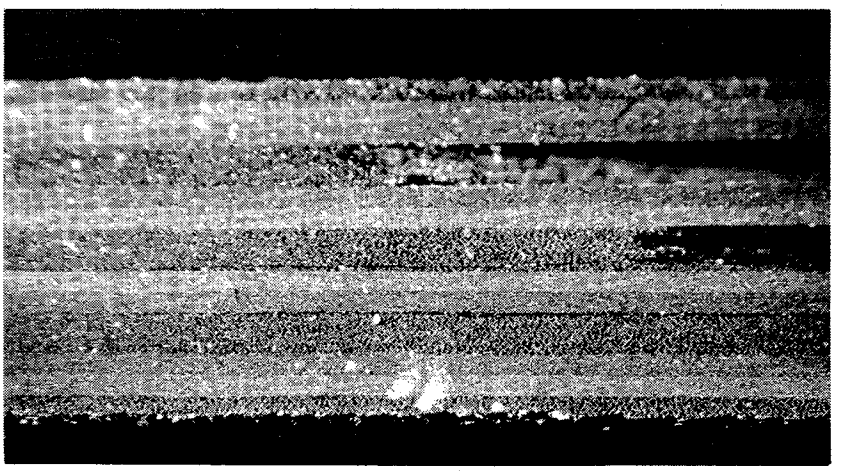

Plate 7.3b Edge Photomicrograph of Typical E Specimen $[10/55/-35/10]_{2s}$.

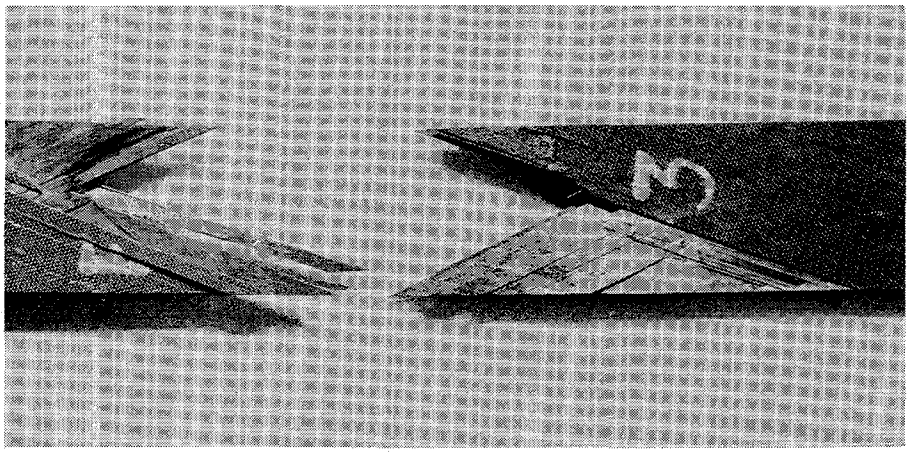

Plate 7.4a Typical Creep Rupture Zone for Laminate F $[20/25/-65/20]_{2s}$.

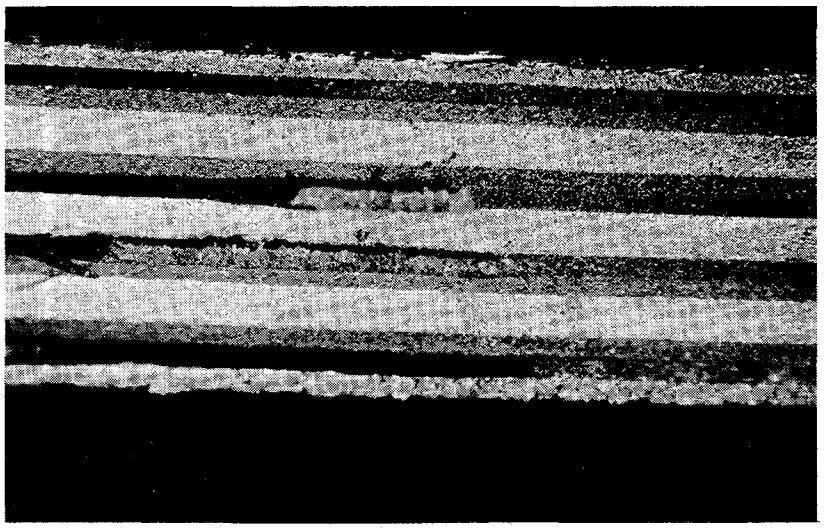

Plate 7.4b Edge Photomicrograph of Typical F Specimen $[20/25/-65/20]_{2s}$.

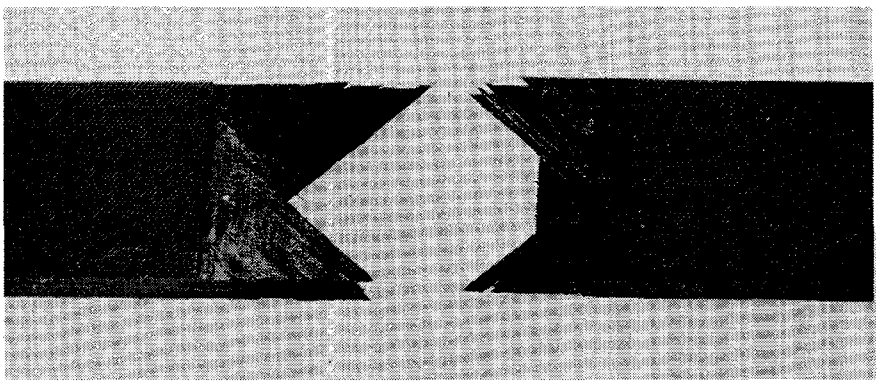

Plate 7.5a Typical Creep Rupture Zone for Laminate G $[90/45/-45/90]_{2s}$.

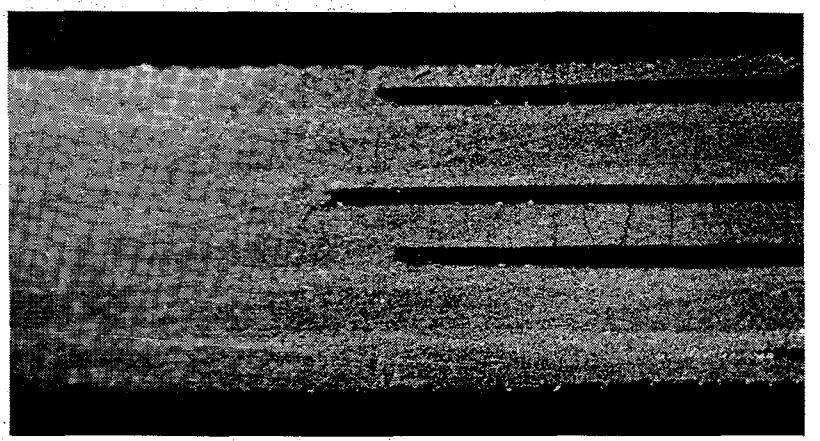

Plate 7.5b Edge Photomicrograph of Typical G Specimen $[90/45/-45/90]_{2s}$.

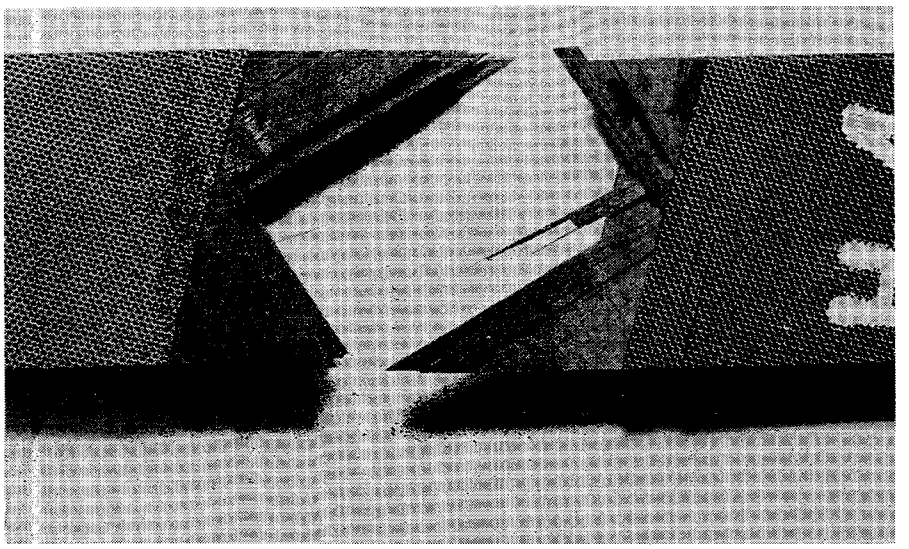

Plate 7.6a Typical Creep Rupture Zone for Laminate H $[75/30/-60/75]_{2s}$.

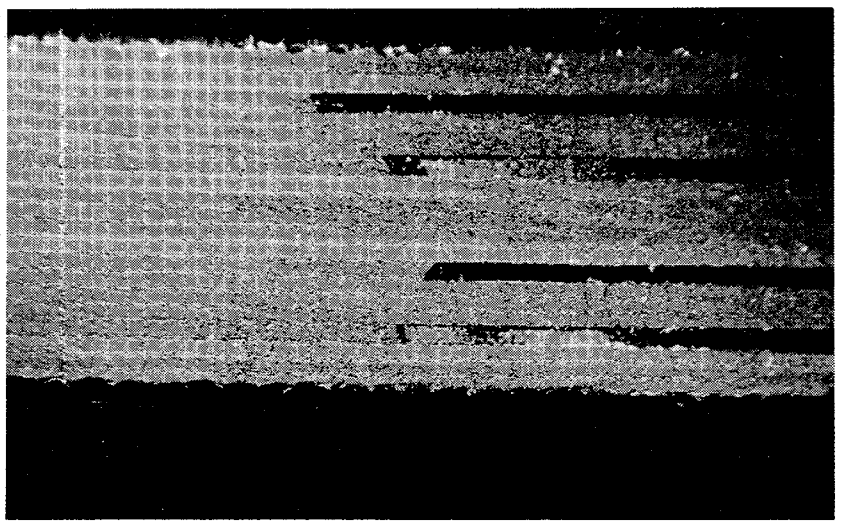

Plate 7.6b Edge Photomicrograph of Typical H Specimen $[75/30/-60/75]_{2s}$.

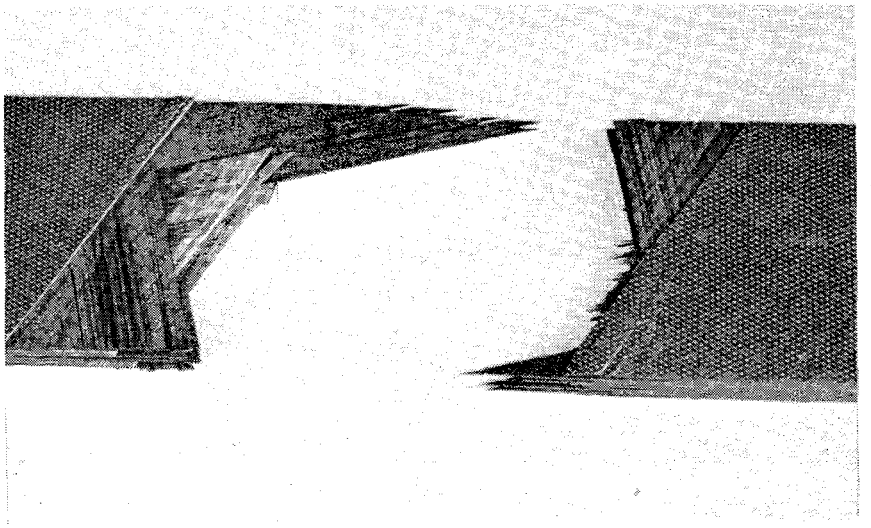

Plate 7.7a Typical Creep Rupture Zone for Laminate I $[60/15/-75/60]_{2s}$.

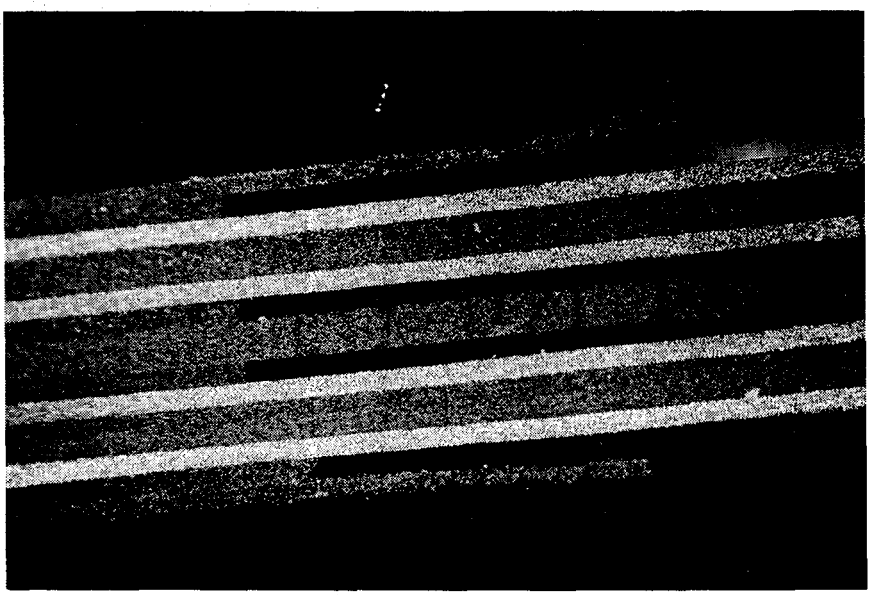

Plate 7.7b Edge Photomicrograph of Typical I Specimen $[60/15/-75/60]_{2s}$.

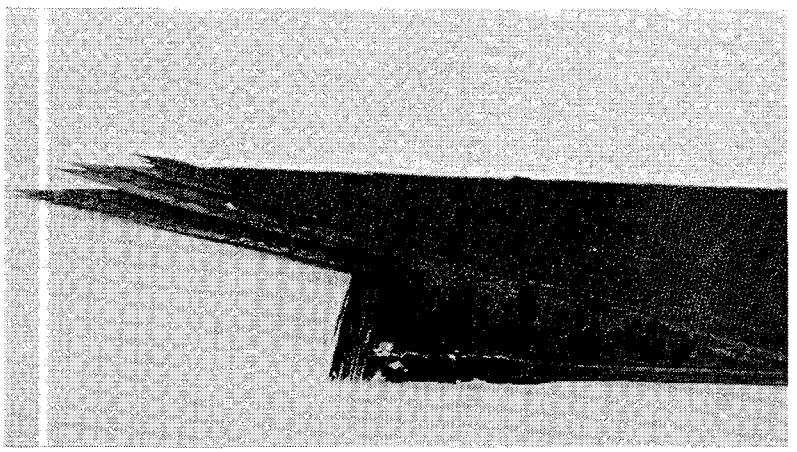

Plate 7.8a Typical Creep Rupture for Laminate J $[15/-75]_{4s}$.

Plate 7.8b Edge Photomicrograph of Typical J Specimen $[15/-75]_{4s}$.

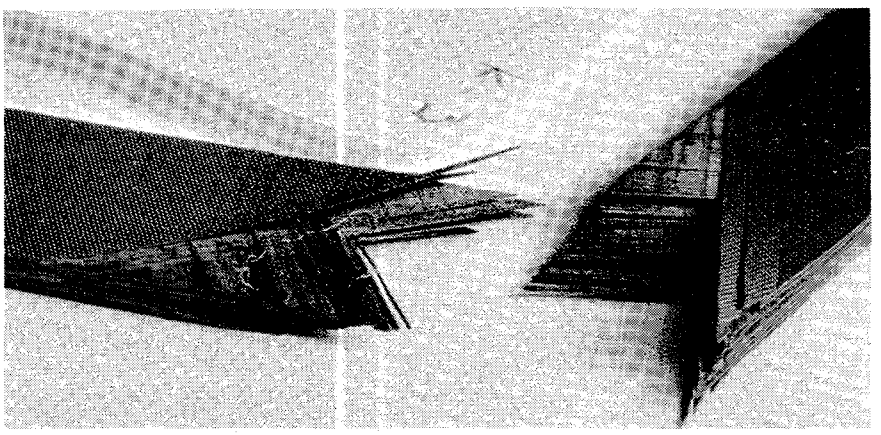

Plate 7.9a Creep Rupture Zone of Laminate K $[30/-60]_{4s}$ at 22.0 ksi, t_r = .1 min.

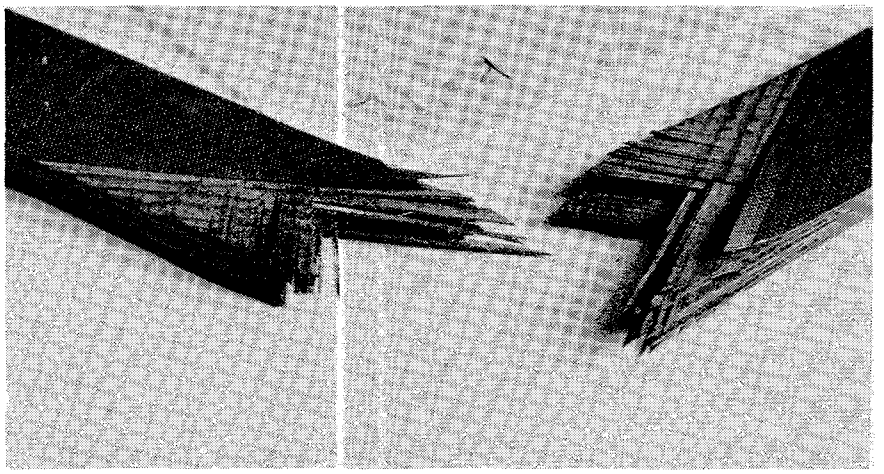

Plate 7.9b Creep Rupture Zone of Laminate K $[30/-60]_{4s}$ at 18.6 ksi, t_r = 30 min.

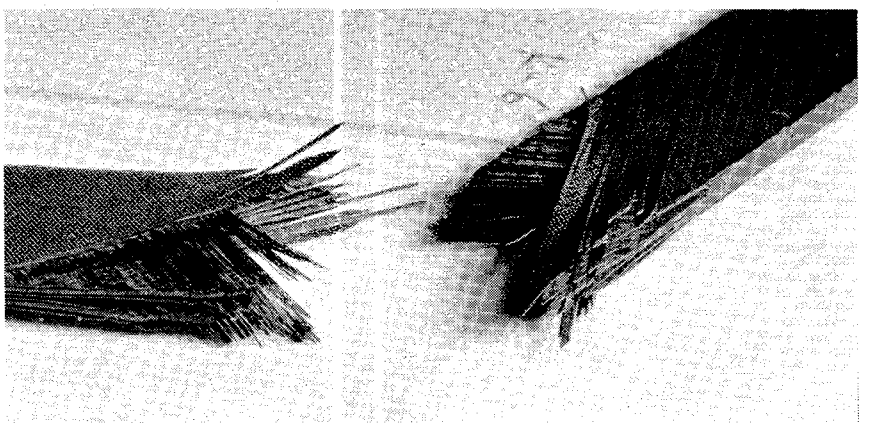

Plate 7.9c Creep Rupture Zone of Laminate K $[30/-60]_{4s}$ Manually Broken After 11,400 min at 18.0 ksi.

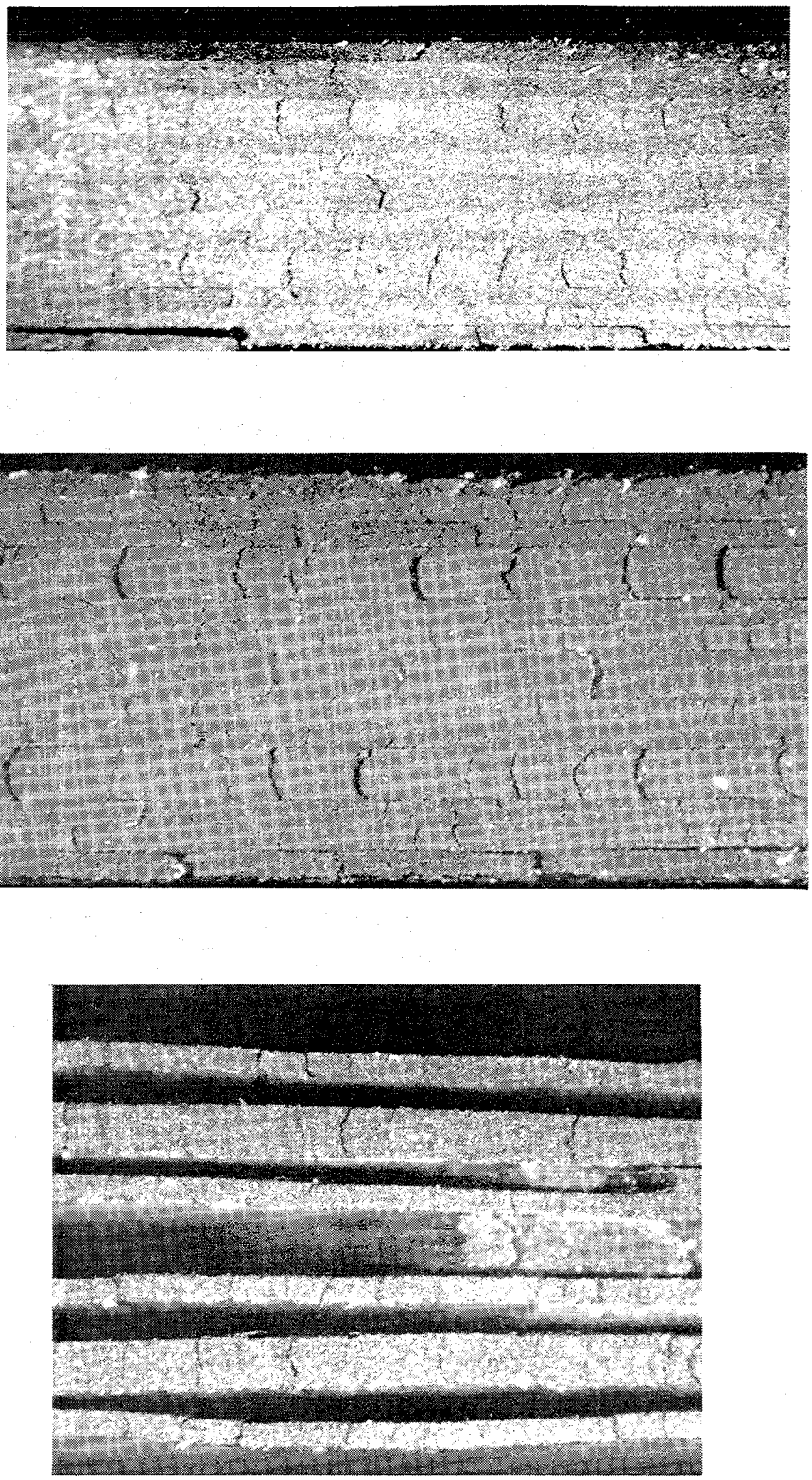

Plate 7.10 Edge Photomicrographs of Typical K Specimens $[30/-60]_{4s}$.

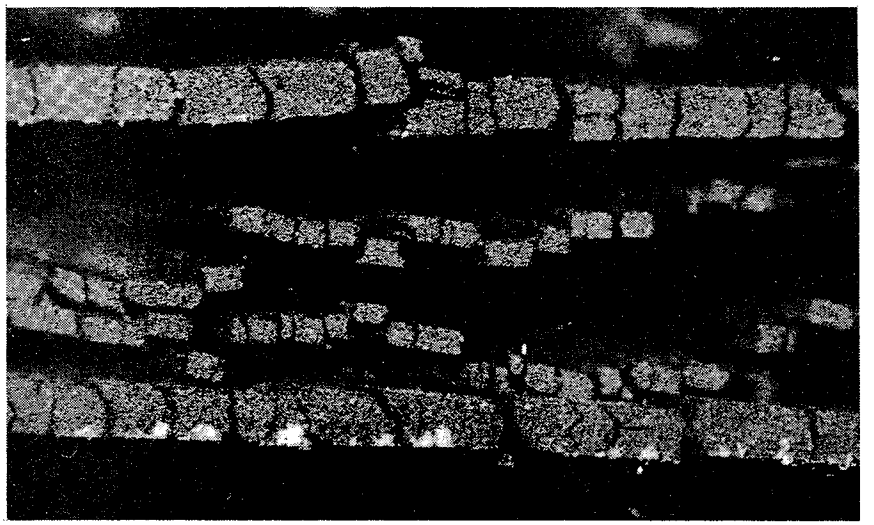

Plate 7.11 Edge Photomicrograph Within Creep Rupture Zone of Laminate K $[30/-60]_{4s}$.

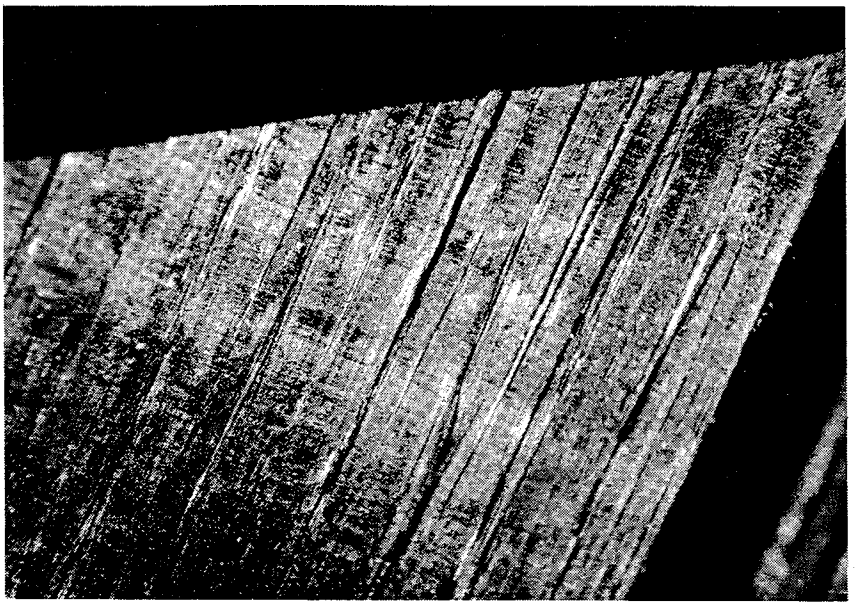

Plate 7.12 Normal View of an Interior -60° Ply of a K Specimen $[30/-60]_{4s}$ Indicating that Cracks Extend Across Specimen Width.

delaminated and a photomicrograph was taken looking down on an interior ply. As indicated in Plate 7.12, these cracks do extend across the width of the specimen.

Variation in Ply Stresses

The variation in ply stresses with time is often thought to be quite negligible. The computer predictions of ply stresses, however, indicates a considerable decrease in the σ_2 and τ_{12} stresses and a corresponding increase in σ_1. Figs. 7.40 and 7.41 indicate these results for a typical laminate. Fig. 7.40 illustrates the variation in σ_1, σ_2, and τ_{oct} for the 90° ply in a G specimen $[90/45/-45/90]_{2s}$ at 14,500 psi. For this ply, $\tau_{12} = 0$. Fig. 7.41 illustrates similar variation for the 45° ply (or -45° ply). The stresses have been normalized with respect to their respective values at t = .01 minute. Because the stresses at t = .01 minute were the first iteration in the analysis, convergence to correct values may not have been achieved. This explains why the normalized stress curves do not pass smoothly through a value of 1.00 at t = .01 min. The important concept is simply that the ply stresses can very significantly due simply to the differential creep rates of the various plies. For this laminate, the variation exceeded 40% for τ_{12} of the 45° ply before laminate failure occurred. Similar variations were found in the analysis of the other laminates.

Polycarbonate Results

As mentioned in the previous chapter, some creep yield studies were conducted on polycarbonate to investigate certain aspects of

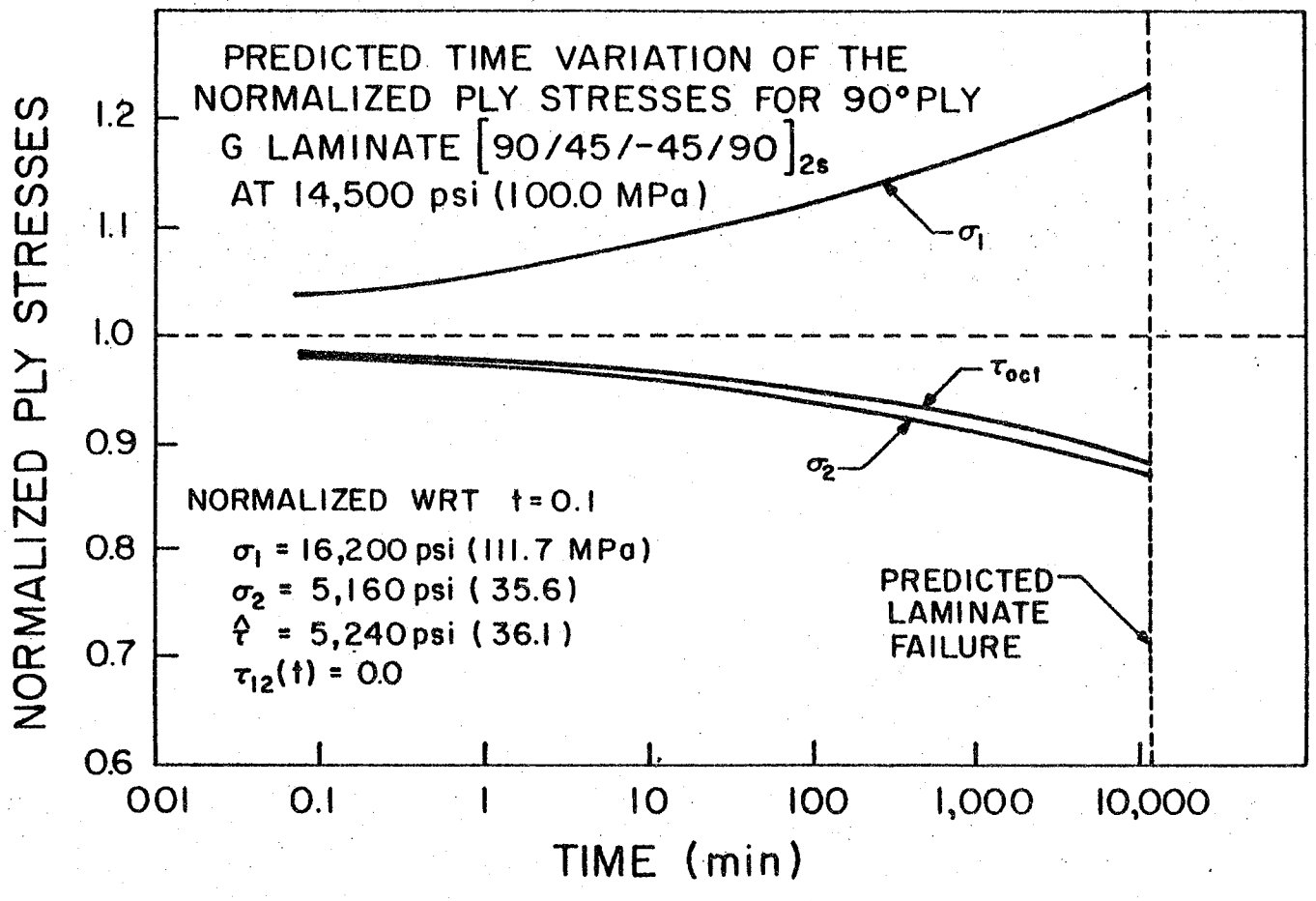

Fig. 7.40 Time variation of the normalized ply stresses for 90° ply laminate G $[90/45/-45/90]_{2s}$ at 14,500 psi.

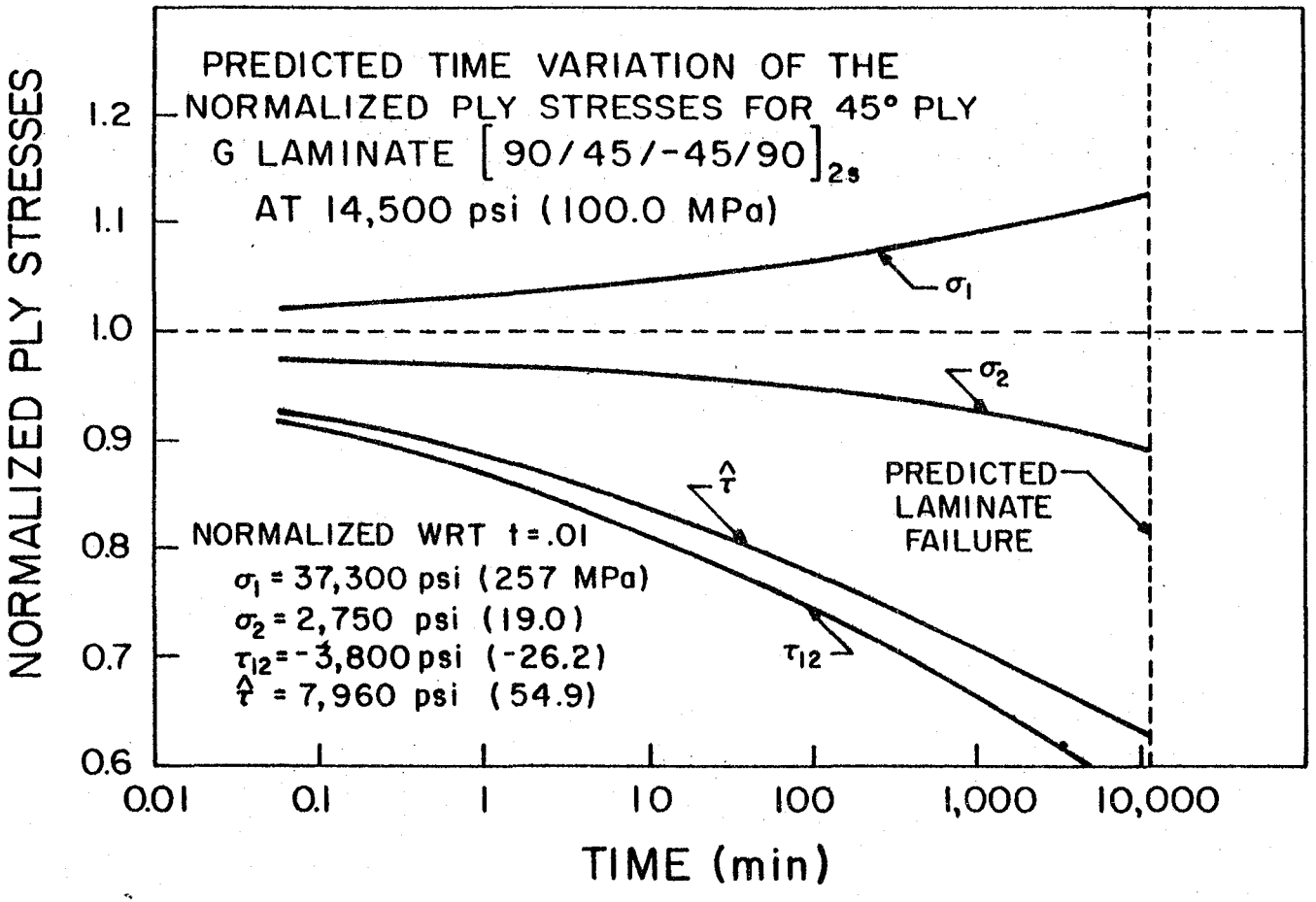

Fig. 7.41 Time variation of the normalized ply stresses for 45° ply laminate G $[90/45/-45/90]_{2s}$ at 14,500 psi.

general rate processes. Approximately 80 dogbone specimens were creep loaded at 167°F (75°C). Fig. 7.42 illustrates the results for the creep tests. The times to yield vary from 1 minute to several days. The data is seen to be nearly linear when plotted stress vs log time. After this creep yield line for a constant load had been established, step-up and step-down tests were conducted to investigate cumulative damage relationships. These tests were designed so that approximately 1/2 of the life to yield was expended at the initial stress level prior to the load change.

Results from the step-down tests show some evidence that the linear damage accumulation may be non-conservative for this type loading scheme. Yield tended to occur when the linear accumulated yield lifetime reached about 0.8 rather than 1.0. Of greater interest, however, was the evidence that predictions for step-up loadings tended to be overly conservative. In fact, it was found that the yield lifetime at a given stress level was actually increased if it was first preloaded at a lower stress level. Specimens loaded at 5750 psi for 25 minutes and then stepped to 6250 psi showed a three-fold increase in lifetime at this high stress level over that of a virgin specimen loaded at 6250 psi. If, however, the specimen was allowed to recover for 25 minutes following the initial load, the lifetime at the high stress level was a fraction of the virgin specimen lifetime. The data taken for these step loads was quite minimal and as a result are not presented in graphical form. More extensive testing should be conducted to verify these indications.

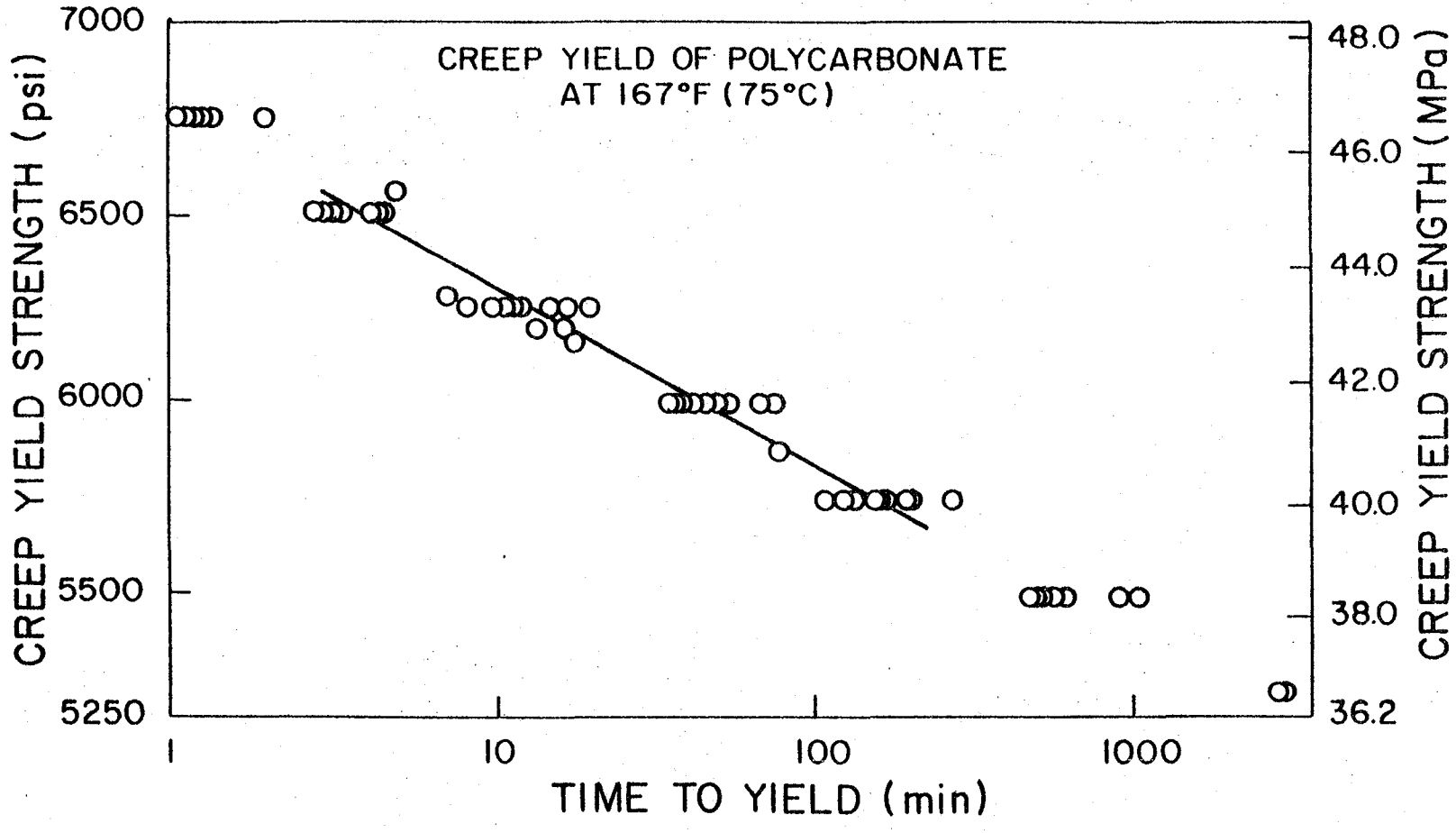

Fig. 7.42. Creep yield of polycarbonate dogbone specimens at 167°F.

The conclusions, however, is that the linear damage accumulation rule is not always appropriate for polycarbonate. The loading sequence can be very important because, apparently, some type of beneficial aging process takes place at the low stress level. Because this improvement is negated when the specimen is allowed to recover prior to applying the high load, this beneficial aging must be a mechanical or stress effect rather than of thermal origin.

Physical Aging Effects in Graphite/Epoxy

Mechanical aging effects similar to those in the polycarbonate have also been observed in the current testing of Gr/Ep specimens. Again it was found that a creep preload tended to increase the ultimate breaking strength of a specimen. If a specimen had not broken under creep loading after about a week, the load was gradually increased by the addition of one pound weights to the weight pan until the specimen broke. This breaking strength was considerably higher than the static strength of a virgin specimen.

The results of the breaking strengths of the specimens for the preloaded specimens are given in Table 7.2. The creep load and its duration are given along with the breaking strength. These strength values are compared with the estimated creep rupture strength of the given laminate at 1 minute. These values were obtained from the best fit lines in the creep rupture figures. As may be seen there was about a 15% increase in static strength of the specimen if it had been preloaded. The K specimens, composed of only two fiber orientations, showed an even greater increase in strength and underwent the largest

TABLE 7.2. Increase in static strength due to mechanical aging of a preload.

SPECIMEN	PRELOAD (KSI)	TIME AT PRELOAD (MIN)	BREAKING STRENGTH (KSI)	R (1 MIN) (KSI)	% INCREASE
E-14	67.0	9850	79.0	70.4	12.2
F-2	44.0	11440	68.0	57.0	19.3
F-11	54.0	10000	64.8	57.0	13.7
F-	54.5	9400	70.8	57.0	24.2
I-8	31.0	9870	38.2	33.0	15.8
J-2	25.7	3100	35.9	31.7	13.2
J-3	27.0	2640	36.2	31.7	14.2
J-4	28.2	2570	38.6	31.7	21.8
J-5	29.0	9837	37.4	31.7	18.0
J-19	29.2	9533	35.2	31.7	11.0
K-6	18.0	11360	26.4	19.4	36.1
K-7	18.8	9790	25.9	19.4	33.5

deformations. This strengthening effect may have been due in part to the smaller fiber angles which result from the scissoring action associated with large deformations.

Strengths tended to approach that of a virgin specimen if the specimens were allowed to recover several days after the initial creep loading.

Despite the major differences between the ductile polycarbonate and brittle epoxy matrix, significant similarities exist between these materials. In particular, the mechanical aging phenomenon in both materials seem to be closely related. Both materials appear to exhibit a reversible strength improvement from a moderate level creep load. Recovery tends to return the material back to a quasi-virgin state.

Accuracy of Predictions

In general the predicted compliance values are considered to be quite promising when compared with the experimental data. The short time compliance predictions are all quite accurate. The compliance predictions at long times are not as correct, perhaps because of errors in the power law model. Except for the erratic results of the E and F laminates, the agreement of the transient nonlinear effect is fair. The predictions for laminate compliances approaching the fiber truss asymptote are significantly in error. This behavior is a characteristic of the lamination theory model used herein. If the approach could be modified to relax the interlaminar shear deformation constraint, better compliance predictions might be obtained without resorting to a more costly finite element analysis procedure. The authors are

encouraged by the accuracy of the results.

The creep rupture strength predictions based on apparent strength properties of the unidirectional material are low for all laminates. Although conservative predictions are good, the current results are often overly conservative. The failure model is believed to be responsible for these discrepancies because of the assumption that a ply ceases to support any σ_2 or τ_{12} stresses once ply matrix failure has occurred. As a result, the laminate loses all predicted load carrying capabilities when the matrix in all plies has broken. The experimental results indicate that this assumption may not be appropriate.

Often the failure of several plies within a general laminate is not felt to necessarily result in total laminate failure. In the current data there are some indications that this is correct. The load-deflection curves for several laminates tested at a constant crosshead speed exhibited plateaus in the load response such as the results for the D laminate which have been illustrated in Fig. 7.43. Jones [48] has indicated such plateaus may represent the failure of certain plies within the laminate and he has idealized such behavior with a laminate model composed of springs in parallel. If each spring represents a particular ply, failure of a certain spring would result in a horizontal shift in the load-deflection curve. The results given in Figs. 7.22 and 7.23 for specimen I indicate probable matrix cracking at the σ_4 stress level, yet the specimen supported an even higher stress at a subsequent load level. The edge view photomicrographs indicated that several laminates were significantly cracked even at

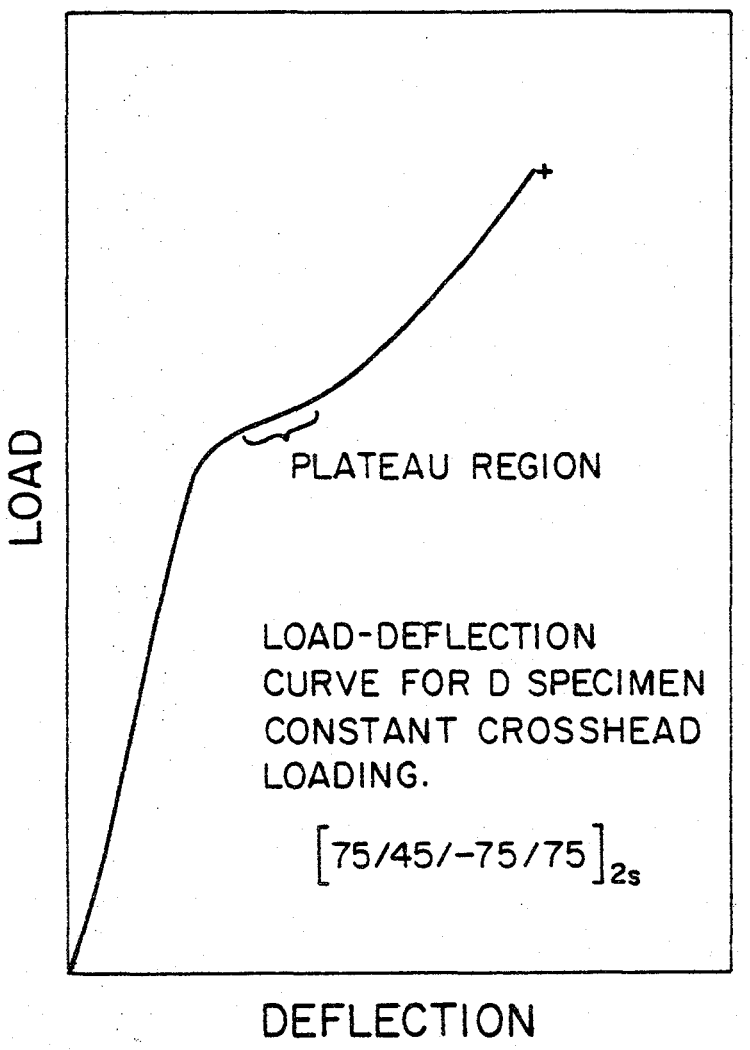

Fig. 7.43 Load-deflection curve for a D specimen ($[75/45/-75/75]_{2s}$) in constant crosshead loading.

large distances from the failure zone. Thus there was substantial evidence that first ply matrix cracking does not necessarily result in immediate failure of the total laminate.

The program predictions for the laminates tested, however, indicated that matrix failure in the plies of a single orientation always resulted in almost immediate global laminate failure following the first ply failure. These predictions were based on eliminating all σ_2 and τ_{12} stiffness contributions from plies in which matrix cracking had been predicted. Based on the experimental evidence, more accuracy may have been obtained by allowing broken plies to remain partially effective. Determination of appropriate methods to achieve this effect, however, could be quite difficult.

The assumption that a laminate could not support any load if all plies had cracked was also not borne out experimentally. Indeed, the individual plies in the J and K laminates are extensively shattered, and yet the laminate continued to support the applied creep load. The failure model does not account for the strength contributions made by the intact regions between the matrix cracks within the plies. Interlaminar shear stresses can continue to support an applied load via a contorted load path. Unless this strength contribution can be accounted for, failure predictions should be expected to be low.

A crack may easily propagate over the cross-sectional area and result in a clean break in unidirectional laminates such as those used to determine the material failure properties. However, a flaw cannot propagate as a smooth break for general laminates. The actual damage region for a general laminate may be quite extensive, as indicated in

the photographs of the laminate failure zones. Flaws must also grow between the plies to provide the delamination necessary for separation contributing to the insensitivity of laminated fiber reinforced materials to internal flaws. There may be inherent difficulties in applying the flaw sensitive unidirectional failure properties to general laminates which are not as susceptible to global failure resulting from a flaw in a single ply.

For these reasons, the laminate failure model used is felt to be overly conservative. Two other aspects tend to make our model non-conservative, but apparently do not completely compensate for the problem. Lamination theory ignores all interlaminar stresses which are known to exist at the free edges and constraint stresses introduced by the grips have also been neglected. These two factors produce stress states that are greater than those accounted for by the lamination theory model. Development of a more accurate failure model to account for all the above effects could be quite difficult.

A prominent discrepancy exists for all laminates between the rate at which the creep rupture strength predictions decrease with time and that indicated by actual creep rupture data. This difference cannot be explained by lamination theory shortcomings. In fact, lamination theory predicts a greater decrease in matrix stresses for laminates near the fiber truss compliance limit than actually occurs. This should have the effect of decreasing the predicted rate of creep rupture strength reduction.

Failure properties determined from non-post-cured unidirectional creep rupture data may have contributed to the rapid decrease of

predicted laminate creep rupture strengths. As obtained from Eqns. 4.6b and 4.6c, the decrease of $Y(t_r)$ and $S(t_r)$ from 1 to 10,000 minutes is 32% as opposed to the 3 to 13% decrease obtained for the general laminates tested, as indicated in Table 7.1. Obviously, the use of Eqns. 4.6b and 4.6c should result in rapidly decreasing strength predictions. Recently Eqn. 4.6b was noticed to have been based on Griffith's [38] best fit line for the 90° specimens at 320°F. This line does not agree with the best fit line drawn in Fig. 4.2. Our best fit line indicates a 26% strength reduction rather than the 32% for the 10,000 minute time span. Use of this corrected best fit line would result in a small improvement over the results obtained using Eqn. 4.6b.

Again, difficulties are apparent for determining functional relationships from a minimal amount of widely scattered data. If the indicated strength reductions for the unidirectional and general laminates are correct, the rate discrepancy between experimental and predicted strengths may allude to errors in the cumulative damage law or the constitutive model. Our lamination program predicts that the ply stresses decrease with time. The polycarbonate creep yield data indicated that the linear cumulative damage law was non-conservative for step-down loading. Although not verified for Gr/Ep, the implication of the latter is that the predicted strengths would decrease more rapidly than the experimental values which is in general agreement with the comparisons previously given in Figs. 7.31 - 7.39.

One other possible explanation for the rate discrepancy is that the unidirectional creep rupture data obtained by Griffith [41] was

for specimens which had not been postcured. Creep ruptures for several postcured 60° specimens were obtained during the current work and have also been illustrated in Fig. 4.2. The best fit line through this postcured data indicates only a 9% decrease in the 60° creep rupture strength over the 10,000 minute time span rather than the 26% decrease for non-postcured specimens. The implication is that the rates of strength reduction may be considerably smaller than for non-postcured specimens. The data scatter prevents substantiation of this claim. Because the failure model was based on no postcure yet the general laminates tested were postcured, this is a possible explanation for the prediction discrepancies.

Interestingly Figs. 7.31 - 7.39 indicate that the curves based on failure at .5% strain are often in better agreement with the creep rupture data than the program predictions. In particular, the slope of the predicted and experimental creep rupture strengths are often quite similar. This was true for all cases except the two-fiber orientation laminates, J and K. One shortcoming of such a procedure is that the creep rupture strength is predicted to decrease more rapidly at larger values of (log t_r). Physically, however, one would expect creep rupture curves to flatten out in order that a zero stress would not result in a finite time to rupture.

Grip Constraint Stresses

Because of the shear coupling effect in unbalanced laminates, an axial stress results in shear as well as normal deformations. A complex shear and bending moment stress state is developed in such

specimens because of the constraints imposed by fixed grips. A static finite element model was used to determine the variation in stress state throughout each laminate but difficulties were encountered in trying to model the boundary conditions. The procedure was abandoned in favor of a closed form solution provided by Pagano and Halpin [56] and based on some simplifying assumptions about the boundary conditions. Their equations were used to predict the axial stresses at the grip on each edge of the specimen. These locations represent the maximum deviations of axial stresses from the nominal value. Normalized results have been given in Table 7.3. A general correlation between large deviations from the nominal stress value and the likelihood of failures near the grip has been noted. Pagano and Halpin have also indicated that the apparent stiffness measurements may be different than the actual stiffness because of the shear coupling. The apparent modulus is given in terms of the actual modulus and a parameter ζ

$$E_{xx}^{*} = E_{xx}\ \zeta$$

Values of ζ have also been tabulated in Table 7.3. The parameter ζ is highly dependent on the specimen aspect ratio. For the specimen length used, the error in the apparent modulus is quite small except for the J laminate. The values in Table 7.3 are based on no lateral motion of the grips. Because of the small lateral constraint on the creep frames, the actual error for our work is considered to be even less than indicated in the table.

TABLE 7.3. Effect of grip constraint on laminate stresses and apparent modulus.

SPECIMEN	$\sigma_{max}/\sigma_{nom}$	$\sigma_{min}/\sigma_{nom}$	ζ
D	.9034	1.091	1.0015
E	.9774	1.022	1.00009
F	.935	1.062	1.00069
H	.9217	1.074	1.00098
I	.8539	1.133	1.0033
J	.6088	1.306	1.0219
K	.7986	1.177	1.0061

Chapter 8

SUMMARY AND RECOMMENDATIONS

An incremental numerical scheme based on lamination theory was developed to predict the time dependent response of general laminates composed of orthotropic laminae. The procedure uses a nonlinear compliance model based on an extension of a technique due to Findley to a biaxial stress state in a fiber reinforced material. The octahedral shear stress, based on the stress state in the matrix, was used as the nonlinearizing parameter in order to provide an interaction effect among the stresses. The time variation of the compliances was assumed to obey the power law for creep. Findley's modified superposition principle was used to determine the strains resulting from a time varying stress state. Also incorporated into the numerical procedure was a plywise failure model based on a modification of the Tsai-Hill criteria which accounts for time dependent creep rupture strengths. Thus, the 90° strength rupture time was assumed to increase exponentially with decreasing applied stress. The shear strength as required for the Tsai-Hill approach was assumed to be a constant fraction of the 90° creep rupture strength. A linear damage accumulation rule was used to determine the life expenditure at each time step. The procedure incremented through time until all plies were determined to have failed. The material properties used in the analysis were determined from tests on unidirectional specimens.

Delayed failures were produced in a variety of different laminates. The specimens ranged from matrix dominated layups to those in

which the load axis was just slightly off-axis from the predominant fiber direction. Both balanced and unbalanced laminates were tested. Creep rupture data indicated that at 320°F stress levels 3 to 13% below the short time strengths could result in delayed failures within one week. Considerable scatter characterized the creep rupture data for several laminates studied. One of the panels used contained plies with crooked fibers and these were believed to have precipitated premature failures. Some specimens exhibited considerable thickness variations and presented difficulty in determining effective cross-sectional areas. Furthermore, particularly in the unbalanced laminates, the stress state varied considerably along the specimen length. These factors could have led to even more significant scatter than that normally observed for creep rupture of homogeneous, isotropic materials.

Based on the failure model developed from uniaxial tests, computer predictions of creep rupture strengths were presented for each laminate tested. In general, the computer strength predictions were lower than the experimental creep rupture data. A possible reason may be due to the assumption that total laminate failure occurred when the matrix in each ply failed. Photomicrographs of the specimen edges indicated that plies could continue to be partially effective although the matrix of each ply was cracked through. Laminates could remain intact and thus continue to support the applied load even after the matrix of each ply had cracked. The conservativeness of this assumption is partially offset by lamination theory's neglect of the effects of interlaminar stresses. Also, the shear and bending stresses induced

by the grip constraints in unbalanced laminates were not considered.

The predicted creep compliance strengths decreased more rapidly with time than was indicated by the experimental data. A possible explanation for this discrepancy is that the failure model was based on creep rupture data of non-postcured unidirectional specimens, whereas the laminates tested were all postcured. Several postcured 60° specimens were tested and the results indicated that the postcure process did not change the basic strength substantially. However, postcured specimens did tend to exhibit a smaller decrease in creep rupture strength with time than those that had not been postcured.

Creep compliance data was taken for several laminates and was compared with predictions made by the lamination program. The assumption that no interlaminar deformations exist, results in an upper bound on the predicted compliances for laminates composed of three or more fiber orientations. The fibers in these laminates produce a triangular truss network which fixes the maximum predicted laminate deformation unless interlaminar displacements are permitted. For laminates which did not possess a limiting compliance value, or for those in which the measured compliances were well below this asymptotic value, the predicted compliances agreed quite well with the experimental values. The upper bound provided by the fiber-truss network, however, proved to be a severe shortcoming of the application of lamination theory to certain laminates. A finite element approach could have avoided this limitation, but, as discussed earlier, would likely have been very costly to implement. If the constraint caused by the assumption that no interlaminar deformation exists could

be partially relaxed, the lamination theory approach might be more successful.

A mechanical aging phenomena has been observed in both Gr/Ep and polycarbonate. Similarities of the rate processes in these two very different materials have been noted, particularly with regard to the mechanical aging phenomenon.

Our investigation has been based on integrating a variety of appropriate concepts into a single procedure to predict the compliance and delayed failures of general laminated composites composed of a fiber reinforced nonlinear viscoelastic matrix. In developing the procedure, aspects have been drawn from a variety of seemingly unrelated areas such as: lamination theory, orthotropic viscoelasticity, static laminate failure, creep of metals, cumulative damage laws, metal plasticity, numerical procedures, and previous experimental data for the unidirectional material. As with any predictive technique, the overall accuracy can be no better than that of its component assumptions. While the predictions have borne out certain trends reasonably well, they have not been acceptable in several ways. In pursuing any future analytical treatment, it is proposed that many of the assumptions used within this work should be verified or modified as more data is obtained.

Experimental Recommendations

The unidirectional properties used in the current analysis were determined from existing data, which was at times widely scattered and even somewhat inconsistent. Most of these results were obtained

prior to the realization that there was a significant postcuring effect. As such, much of the existing data represents a rather haphazard degree of postcuring which of necessity took place during each creep test at elevated temperature. Accurate expressions for material response are essential for developing predictive techniques.

Many aspects concerning the characterization of Gr/Ep have been revealed by the current project during the past several years. With these new concepts in mind, perhaps the time has come to systematically repeat much of the testing. A sufficient quantity of material should be obtained so that all specimens for the foreseeable testing program could be cut from the same batch of material. Care should be taken that all specimens receive the same postcure treatment and contain similar moisture contents. The recommendation is made that mechanical conditioning effect on compliance, as discussed by Lou and Schapery [54], be investigated. Testing should be tailored to provide information required to characterize the most appropriate models for characterizing the various facets of material behavior which contribute to the creep rupture process.

The use of compliance and creep rupture data obtained at several temperatures to predict material response at other temperatures has been advanced in previous work [38,82]. The present work has been conducted primarily at only one temperature. The feeling is held that in developing compliance, creep rupture, and numerical models for the Gr/Ep material studied herein, concentration on a single temperature is the best procedure. Once acceptable techniques have been developed at a particular temperature, generalizations can be made for the

thermal dependence.

Recommendations for the Compliance Model

The Findley approach to nonlinear compliance has been found to be quite appropriate in matching data from unidirectional and general laminates. It is believed that the power law provides an adequate description of the compliance time dependence. Determining the exponent from short term data is not generally valid for predicting long term compliance. The short term data generally dictates a higher value of the exponent than is indicated by long term response. While this points to the inappropriateness of the power law, it is believed that an exponent obtained from long term data can give quite accurate predictions over a very large time span. The power law is not exact, but it is felt to be the best simple approach available at this time. A further problem associated with using short term data to evaluate the exponent is the errors introduced by the singularity problem. There is some evidence that the power law exponent may vary with the applied stress level. It is recommended that week long compliance data be taken for several stress levels on 10° and 90° specimens. This long term data should provide a good base to establish the dependence of the power law exponent on the applied stress level.

It has been assumed that the averaged octahedral shear stress in the matrix serves as the nonlinearizing effect for the compliance. There is no verification for this assumption on the Gr/Ep system studied. More extensive compliance testing at several off-axis angles

could provide information on this or other interaction terms.

The exponents for Griffith's [38] 30° and 60° long term compliance were significantly higher than those for the 10° and 90° tests, as indicated in Chapter 7. The transformation equations cannot predict these differences. It is recommended that these tests be repeated to determine the accuracy of the results. If the previous data is correct, a substantial rework of the compliance model and/or transformation equations would be required. The proposed tests could be the same as indicated in the previous paragraph.

The modified superposition principle used to account for a varying stress level was felt to be adequate for the small stress variations associated with creep loaded laminates. However, this approach is not believed to be accurate for a more general stress variation. Because of its more general nature, the Schapery procedure should provide a better treatment of this aspect. While this technique does require more extensive testing, it could provide a more unified compliance model. The hyperbolic sine terms of the Findley procedure have been found to provide good agreement with the experimental data. Perhaps these terms could be incorporated into the Schapery procedure to assist determination of the stress dependent functions. It has been proposed that multiple step loads be applied to 10° and 90° specimens to determine the appropriateness of the modified superposition procedure used herein. Such information could also prove useful in evaluating the performance of the Schapery procedure for our material system.

Recommendations for the Failure Model

Evaluation of meaningful functional relationships for creep rupture of unidirectional specimens is hampered by the severe data scatter. Accurate property descriptions are imperative when these values will be used to predict failure in other configurations. It is proposed that an extensive testing program be conducted to obtain creep rupture data for the unidirectional material at several off-axis angles. This could establish the appropriateness of the modified Tsai-Hill failure criteria used herein or could lead to the development of a better creep rupture criteria for unidirectional specimens.

The cumulative damage law used is believed to be inaccurate. Cumulative damage in metals is currently supporting a great deal of investigation. Perhaps this technology could provide better analysis procedures. The indications of a mechanical aging phenomena should be investigated as their effects may continue to frustrate applications of cumulative damage laws.

It is possible that other time dependent failure models would prove to be more accurate. Three basic approaches have been widely used in the past to predict delayed yield and rupture. By far the most attention has been given to the stress approach as used herein. The deformation and energy approaches have also been studied. These methods may prove more adaptable to the damage accumulation concept.

Brinson [9] has advocated the use of a deformational failure criterion in a ply by ply fashion to predict delayed failures of general laminates. Specifically, he has postulated that for a unidirectional material, the shape of the creep rupture curve is the same

as that of the inverse of the creep compliance. Short term compliance data at several temperatures could be shifted to obtain a master curve of the creep compliance. The implication of this approach is that this compliance function could be inverted and normalized to obtain a failure master curve. If this procedure could be verified, a substantial reduction in required creep rupture testing would result. A simple extension of this procedure to a general biaxial stress state in a lamina is not apparent, however.

Bruller [10,11,12] has advocated the use of an "energetical limit" in predicting the viscoelastic yield of polymers. His approach is based on the Reimer-Weissenberg Theory which states that viscoelastic yield will occur when the stored deviatoric energy reaches a critical value known as the resilience - a material property. While this approach seems quite accurate for predicting yield in polymers, it is limited to linear viscoelastic materials which can be modeled by a generalized Kelvin element.

One disturbing feature about the approach used herein is that the compliance and failure phenomena are addressed by unrelated models. It would seem advantageous to provide a common basis for these two aspects. Perhaps the use of a deformation failure criteria could unify the treatment. It should be noted that the creep rupture theory indicated by Eqn. 4.2 is a power law similar to that used for the compliance model. With these approaches, however, one has still not properly addressed the superposition effect or cumulative damage of a time-varying stress state. It was originally thought that the Tobolsky-Eyring Reaction Rate Equation could be adapted to treat this

problem. This equation relates the rate at which atomic bonds are broken, and is given by

$$\frac{dN}{dt} = - N \frac{kT}{h} \exp\left(- \frac{F}{RT}\right) 2 \sinh\left(\frac{W}{RT}\right)$$

where

N = number of bonds/unit cross section

ΔF = free energy of activation

T = temperature

k = Boltzmann's constant

h = Planck's constant

R = gas constant

W = work done on a single bond applied by σ.

It has been widely studied by a number of investigators [1,2,3, 42,46]. Because the number of remaining bonds represents a state variable, it is possible that this could provide a unified approach to compliance and failure under a biaxial, time-varying stress state.

Recommendations for the Numerical Procedure

The most significant flaw in the compliance predictions is the upper bound imposed by the fiber truss work. This effect results from the manner in which the individual ply stiffnesses are combined according to lamination theory. By artificially reducing the lateral stiffness, one could relax the constraint imposed by the assumption that normals remain straight and normal. If this does not prove feasible, one may be forced to use a finite element approach.

The computer predictions for strength are low. This could possibly be remedied by allowing "failed" plies to remain partially effective. As illustrated in the damage zone photographs, the failure mechanism for general laminates is quite complex. Accounting for these intricate processes will be very difficult. Some of the procedures used to predict static failures of general laminates are not applicable to delayed failures. Considerable work remains to be done in this area.

It is expected that a finite element approach will eventually be desired to analyze general laminates. More valid models for material response will warrant the improved accuracy afforded by the finite element method. A three-dimensional approach could model the effects of the end constraints as well as the interlaminar stresses. It might be possible to develop a two-dimensional element to represent the specimen cross-section. This could account for the interlaminar stresses without requiring so much storage.

Conclusion

The procedure developed is not the final answer to analyzing time dependent behavior in laminated composites. Nonetheless, it is felt that this work can help pave the way for developing better tools towards this end. The author envisions developing better compliance and failure models which could eventually be incorporated into a more accurate finite element solution scheme.

REFERENCES

1. Akay, A. and E. Saibel, "Fracture of Polymeric Materials Under Tensile Load," Wear, Vol. 37, 1976, pp. 377-381.

2. Akay, A. and E. Saibel, "Fracture Time of Composites Under Tensile Loading," Journal of Composite Materials, Vol. 12, 1978.

3. Akay, A. and E. Saibel, "Fracture Time of Composites Under Time Dependent Loading," ASME Proceedings, Winter Annual Meeting, December 1979.

4. Arridge, R. G. C., Mechanics of Polymers, Clarendon Press, Oxford, 1975.

5. Beaumont, P. W. R., "Fracture Mechanisms in Fibrous Composites," Fracture Mechanics: Current Status, Future Prospects, R. A. Smith (ed), Pergamon Press, 1979.

6. Beckwith, S. W., "Viscoelastic Characterization of a Nonlinear, Glass/Epoxy Composite Using Micromechanics Theory," presented at Annual Meeting of Jannaf, San Francisco, Feb. 1975.

7. Boller, K. H., "Tensile Stress Rupture and Creep Characteristics of Two Glass-Fabric-Base Plastic Laminates," Forest Products Lab Report, Madison, Wisconsin, 1957.

8. Brinson, H. F., "The Viscoelastic-Plastic Behavior of a Ductile Polymer," Deformation and Fracture of High Polymers, Kausch, et al (ed), Plenum Press, 1974.

9. Brinson, H. F., D. H. Morris, and Y. T. Yeow, "A New Experimental Method for the Accelerated Characterization of Composite Materials," Sixth International Conference on Experimental Stress Analysis, Munich, September 18-22, 1978.

10. Bruller, O. S., "Crazing Limit of Polymers in Creep and Stress Relaxation," Polymer, Vol. 19, October 1978.

11. Bruller, O. S., "On the Damage Energy of Polymers in Creep," Polymer Engineering and Science, Vol. 18, No. 1, 1978.

12. Bruller, O. S. and H. H. Schmidt, "On the Linear Viscoelastic Limit of Polymers - Exemplified on Polymethylmethacrylate," Polymer Engineering and Science, 1979.

13. Bui-Quoc, T., "An Engineering Approach for Cumulative Damage in Metals Under Creep Loading," ASME Journal of Engineering Materials and Technology, Vol. 101, 1979.

14. Cartner, J. S. and H. F. Brinson, "The Non-Linear Viscoelastic Behavior of Adhesives and Chopped Fiber Composites," VPI-E-7821, 1978.

15. Cartner, J. S., W. I. Griffith, and H. F. Brinson, "The Viscoelastic Behavior of Composite Materials for Automotive Applications," Composite Materials in the Automobile Industry, ASME, 1978.

16. Chamis, C. C. and J. H. Sinclair, "10° Off-Axis Test for Shear Properties in Fiber Composites," NASA Technical Memorandum NASA TM X-73550, 1977.

17. Chiao, C. C., "An Accelerated Test for Predicting Lifetime of Organic Composites," Proc. of the 3rd Biennial AIME Symposium on Failure Modes in Composites, Las Vegas, Nevada, 1976.

18. Chiao, C. C., R. J. Sherry, and N. W. Hetherington, "Experimental Verification of an Accelerated Test for Predicting the Lifetime of Organic Fiber Composites," J. Composite Materials, Vol. 11, January 1977.

19. Choi, I. and C. O. Horgan, "Saint Venant's Principle and End Effects in Anisotropic Elasticity," Journal of Applied Mechanics, Vol. 44, No. 3, 1977.

20. Christensen, R. M., Theory of Viscoelasticity - An Introduction, Academic Press, New York, 1971.

21. Clauss, F. J., "An Examination of High Temperature Stress-Rupture Correlating Parameters," ASTM Proc., Vol. 60, 1960.

22. Conway, J. B., Numerical Methods for Creep and Rupture Analyses, Gordon and Breach, New York, 1965.

23. Conway, J. B., Stress-Rupture Parameters: Origin, Calculation, and Use, Gordon and Breach, Science Publishers, New York, 1969.

24. Crossman, F. W. and D. L. Flaggs, "Viscoelastic Analysis of Hygrothermally Altered Laminate Stresses and Dimensions," LMSC-D633086. 1978.

25. Darlington, M. W. and S. Turner, "Creep of Thermoplastics," Creep of Engineering Materials, Pomeroy (ed.), Mechanical Engineering Publications Ltd., London, 1978.

26. Davis, C. S. and E. P. Coleman, "The Additivity of Cumulative Damage in the Test or Use Environment," Approved for publication, ASME, 1980.

27. DeRuntz, Jr., J. A. and F. W. Crossman, "Time and Temperature Effects in Laminated Composites," Proc. of Conf. on Computer Simulation for Materials Applications, Gaithersburg, Md., April 1976.

28. Ferry, J. D., Viscoelastic Properties of Polymers, John Wiley & Sons, NY, 1970.

29. Fessler, H. and T. H. Hyde, "Creep Deformation of Metals," Creep of Engineering Materials, Pomeroy (ed.), Mechanical Engineering Publications Ltd., London, 1978.

30. Findley, W. N., C. H. Adams, and W. J. Worley, "The Effect of Temperature on the Creep of Two Laminated Plastics as Interpreted by the Hyperbolic Sine Law and Activation Energy Theory," ASTM Proc., Vol. 48, 1948.

31. Findley, W. N. and G. Khosla, "Application of the Superposition Principle and Theories of Mechanical Equation of State, Strain, and Time Hardening to Creep of Plastics Under Changing Loads," Journal of Applied Physics, Vol. 26, Number 7, 1955.

32. Findley, W. N. and D. B. Peterson, "Prediction of Long-Time Creep with Ten-Year Creep Data on Four Plastic Laminates," ASTM Proc., Vol. 58, 1958.

33. Findley, W. N. and J. S. Y. Lai, "A Modified Superposition Principle Applied to Creep of Nonlinear Viscoelastic Material Under Abrupt Changes in State of Combined Stress," Transactions of the Society of Rheology, Vol. 11, No. 3, 1967.

34. Findley, W. N., U. W. Cho and J. L. Ding, "Creep of Metals and Plastics Under Combined Stresses, A Review," ASME Journal of Engineering Materials and Technology, Vol. 101, 1979.

35. Flugge, Wilhelm, Viscoelasticity, 2nd Ed., Springer-Verlag, New York, 1975.

36. Foye, R. L., "Creep Analysis of Laminates," Composite Reliability, ASTM STP 580, 1975.

37. Gerhards, C. C., "Time-Related Effects of Loads on Strength of Wood," Proc. of Conf. on Environmental Degradation of Engineering Materials, VPI & SU, Oct. 1977.

38. Griffith, W. I., "The Accelerated Characterization of Viscoelastic Composite Materials," Ph.D. Dissertation, VPI & SU, Blacksburg, VA, 1979.

39. Griffith, W. I., D. H. Morris, and H. F. Brinson, "The Accelerated Characterization of Viscoelastic Composite Materials," VPI & SU, Blacksburg, VA, VPI-E-80-15, 1980.

40. Griffith, W. I., D. H. Morris, and H. F. Brinson, "Creep Rupture of Polymer-Matrix Composites," 1980 SESA Spring Meeting, Boston, Massachusetts, May 25-30, (Paper No. R151), 1980.

41. Griffith, W. I., unpublished log books, 1979.

42. Graham, P. H., C. N. Robinson, and C. B. Henderson, "Analysis of Dilatational Failure of Heterogeneous Materials by Reaction Rate Theory," International Journal of Fracture Mechanics, Vol. 5, No. 1, 1969.

43. Grounes, M., "A Reaction-Rate Treatment of the Extrapolation Methods in Creep Testing," Journal of Basic Engineering, Vol. 91, March 1969.

44. Halpin, J. C. and N. J. Pagano, "Observations on Linear Anisotropic Viscoelasticity," Journal of Composite Materials, Vol. 2, No. 1, 1968.

45. Halpin, J. C., "Introduction to Viscoelasticity," Composite Materials Workshop, Tsai, Halpin, Pagano (eds), Technomic, Stamford, 1968.

45a. Heller, R. A., H. F. Brinson, and A. B. Thakker, "Environmental Effects on Fiber Reinforced Composites," IV Interamerican Conference on Materials Technology, Caracas, Venezuela, 1975.

45b. Heller, R. A., A. B. Thakker, and C. E. Arthur, "Temperature Dependence of the Complex Modulus for Fiber-Reinforced Materials," ASTM STP 580, 1975.

45c. Heller, R. A., et al., "Accelerated Characterization of Fiber/Epoxy Composites--Part 1. Viscoelastic Methods," AFML-TR-74-256, 1975.

46. Henderson, C. B., et al., "A Comparison of Reaction Rate Models for the Fracture of Solids," International Journal of Fracture Mechanics, Vol. 6, No. 1, March 1970.

47. Hill, R., "Elastic Properties of Reinforced Solids: Some Theoretical Principles," J. Mech. Phys. Solids, Vol. 11, 1963.

48. Jones, R. M., Mechanics of Composite Materials, McGraw-Hill, New York, 1975.

49. Kargin, V. A. and G. L. Slonimsky, "Mechanical Properties," in Mechanical Properties of Polymers, edited by Bikcles, N. M., Wylie-Intersciences, NY, 1971.

50. Landel, R. F. and R. F. Fedors, "Rupture of Amorphores Unfilled Polymers," Fracture Processes in Polymeric Solids, B. Rosen (ed.), Interscience Publishers, New York, 1964.

51. Lockett, F. J., Nonlinear Viscoelastic Solids, Academic Press, London, 1972.

52. Lohr, J. J., "Yield Master Curves for Various Polymers Below Their Glass Transition Temperature," Transactions of the Society of Rheology, Vol. 9, No. 1, 1965.

53. Lohr, J. J., D. E. Wilson, and F. M. Hamaker, "Accelerated Testing of the Mechanical and Thermal Integrity of Polymeric Materials," private communication.

54. Lou, Y. C. and R. A. Schapery, "Viscoelastic Characterization of a Nonlinear Fiber-Reinforced Plastic," Journal of Composite Materials, Vol. 5, 1971.

55. Morris, D. H., Y. T. Yeow, and H. F. Brinson, "The Viscoelastic Behavior of the Principal Compliance Matrix of a Unidirectional Graphite/Epoxy Composite," VPI&SU, Blacksburg, Va., VPI-E-79-9, February 1979.

56. Pagano, N. J. and J. C. Halpin, "Influence of End Constraint in the Testing of Anisotropic Bodies," Journal of Composite Materials, Vol. 2, No. 1, Jan. 1968.

57. Pindera, J. M. and Herakovich, "Influence of Stress Interaction on the Behavior of Off-Axis Unidirectional Composites," unpublished report.

58. Puppo, A. H. and H. A. Evensen, "Strength of Anisotropic Materials Under Combined Stresses," Journal of AIAA, No. 4, 1972.

59. Roberts, B. W., F. V. Ellis, and J. E. Bynum, "Remaining Creep or Stress-Rupture Life Under Nonsteady Temperature and Stress," ASME Journal of Engineering Materials and Technology, Vol. 101, 1979.

60. Roberts, I., Proc. ASTM, Vol. 51, p. 811, 1951

61. Robinson, E. L., "Effect of Temperature Variation on the Long-Time Rupture Strength of Steels," Journal of Applied Mechanics, Vol. 74, July 1952.

62. Rosen, S. L., Fundamental Principles of Polymeric Materials for Practicing Engineers, Barnes and Noble Inc., NY, 1971.

63. Rotem, A. and H. G. Nelson, "Fatigue Behavior of Graphite/Epoxy Laminates at Elevated Temperatures," NASA TM 81150, 1979.

64. Rowlands, R. E., "Flow and Failure of Biaxially Loaded Composites: Experimental Theoretical Correlation," Inelastic Behavior of Composite Materials, ASME, 1975.

65. Sandhu, R. S., "Ultimate Strength Analysis of Symmetric Laminates," AFFDL-TR-73-137, 1974.

66. Schapery, R. A., "Stress Analysis of Viscoelastic Composite Materials," Journal of Composite Materials, Vol. 1, p. 228, 1967.

67. Schapery, R. A., "Stress Analysis of Viscoelastic Composite Materials," Composite Materials Workshop, Technomic, Stamford, 1968.

68. Schapery, R. A., "On the Characterization of Non-Linear Viscoelastic Materials," Polymer Engineering and Science, Vol. 9, No. 4, 1969.

69. Schapery, R. A., "Deformation and Failure Analysis of Viscoelastic Composite Materials," Inelastic Behavior of Composite Materials, AMD Vol. 13, ASME, 1975.

70. Slonimskii, G. L., A. A. Askadskii, and V. V. Kazantseva, "Mechanism of Rupture of Solid Polymers," Polymer Mechanics, No. 5, 1977.

71. Stinchcomb, et al., "Investigation and Characterization of Constraint Effects on Flaw Growth During Fatigue Loading of Composite Materials," Final Report NASA Grant NSG-1364, 1978.

72. Stratonova, M. M., "Calculation of One-Dimensional Polymer Creep Under Stepped Loading," Polymer Mechanics, Vol. 3, No. 4, 1967.

73. Sturgeon, J. B., "Creep of Fiber Reinforced Thermosetting Resins," Creep of Engineering Materials, Pomeroy (ed.), Mechanical Engineering Publications Ltd., London, 1978.

74. Sumsion, H. T. and D. P. Williams, "Effects of Environment on the Fatigue of Graphite/Epoxy Composites," ASTM STP 569, 1975.

75. Sumison, H. T., "Environmental Effects on Graphite/Epoxy Fatigue Properties," Journal of Spacecraft and Rockets, Vol. 13, No. 3, 1976.

76. Taylor, R. L., K. S. Pister, and G. L. Goudreau, "Thermomechanical Analysis of Viscoelastic Solids," International Journal of Numerical Methods for Engineering, Vol. 2, 1970.

77. Tsai, S. W. and H. T. Hahn, "Failure Analysis of Composite Materials," Inelastic Behavior of Composite Materials, AMD, Vol. 13, ASME, 1975.

78. Weitsman, Y., "Residual Thermal Stresses Due to Cool-Down of Epoxy Resin Composites," Journal of Applied Mechanics, Vol. 46, No. 3, 1979.

79. Woo, H. H., et al., "Creep Rupture Bending Test of 20% Cold-Prestrained Ni-Fe-Cr Alloy Straight Tubes at 1100 F (593C)," ASME Publication 80-C2/PVP-18, 1980.

80. Woodford, D. A., "Creep Damage and the Remaining Life Concept," ASME Journal of Engineering Materials and Technology, Vol. 101, 1979.

81. Wu, E. M. and D. C. Ruhmann, "Stress Rupture of Glass-Epoxy Composites: Environmental and Stress Effects," ASTM STP 580, 1975.

82. Yeow, Y. T., "The Time-Temperature Behavior of Graphite Epoxy Laminates," Ph.D. Dissertation, VPI&SU, Blacksburg, VA, 1978.

83. Yeow, Y. T. and H. F. Brinson, "A Comparison of Simple Shear Characterization Methods for Composite Laminates," Composites, January 1978.

84. Yeow, Y. T., D. H. Morris and H. F. Brinson, "Time-Temperature Behavior of a Unidirectional Graphite/Epoxy Composite," ASTM STP 674, 1979.

85. Zhurkov, S. N., "Kinetic Concept of the Strength of Solids," International Journal of Fracture Mechanics, Vol. 1, 1965.

86. Zienkiewicz, O. C., M. Watson, and I. P. King, "A Numerical Method of Visco-Elastic Stress Analysis," International Journal of Mechanical Science, Vol. 10, 1968, pp. 807-827.

87. Zienkiewicz, O. C., The Finite Element Method, Third Edition, McGraw-Hill, London, 1977.

Appendix A

LEAST SQUARES HYPERBOLIC SINE FIT

The following procedure was used to obtain a least squares fit of a hyperbolic sine function

$$y = a \sinh(x/b)$$

to a given set of data (x_i, y_i) $\quad i = 1,2,\ldots,n$

Let

$$\varepsilon_i = y - y_i = a \sinh(x/b) - y_i$$

and

$$I = \sum_{i=1}^{n} \varepsilon_i^2 = a^2 \Sigma \sinh^2(x_i/b) - 2a \Sigma \sinh(x_i/b)y_i + \Sigma y_i^2$$

Now let

$$a = \Sigma \sinh(x_i/b)y_i / \Sigma \sinh^2(x_i/b)$$

and

$$F(b) = [\Sigma \sinh(x_i/b)y_i][\Sigma \sinh(x_i/b) \cosh(x_i/b)(x_i/b^2)]$$
$$- [\Sigma \sinh^2(x_i/b)][\Sigma \cosh(x_i/b)(x_i/b^2)y_i] = 0$$

Roots to this equation will render I stationary with respect to a and b. Solving for the roots is not as easy task because of the shape of the F function. The secant method (modification of the Newton - Raphson procedure which uses derivatives approximated by successive secants) was tried, but obtaining a starting value which did not result in an overflow or diverge to infinity was quite difficult. Use of the bisection method was found to yield an appropriate initial guess. The combination of these two techniques provided an adequate solution scheme.

Appendix B

EFFECTS OF LEVER ARM OSCILLATION AND ROTATION

In creep rupture testing, the specimen may linger on the verge of failure for some time prior to actually rupturing. When superimposed on the applied load, small additional stresses such as machine vibration may be sufficient to trigger a premature failure. Such oscillations should be minimized to insure accurate results.

Load train oscillation is an annoying feature of the ATS Lever Arm Test Frame at the 20:1 arm ratio. The specimen and load train mass act as a simple spring and mass system to result in the vibration problem. Aside from the friction of the knife edge supports, the only significant attenuation is the internal damping of the specimen. Applying the load by lowering the weight elevator resulted in large oscillations. The load may be applied more gradually by using the variable speed drive for the crosshead while set at a slow rate. This significantly reduces the system oscillation, but does not eliminate them. Measurements were taken to evaluate the dynamic effects. At the 20:1 ratio, a pan load of 150 lbs resulted in a stress of 70,500 psi on specimen E-1. An effective weight for the entire load train was taken to be 165 lbs. A dial indicator mounted on the test frame was used to monitor the weight pan deflection. By using a gradual application of the load as described above, the maximum load displacement did not exceed δ = .01". The oscillation frequency was about 2 Hz. This resulted in a sinusoidal dynamic load of amplitude .34 lbs or a load variation of .22%. Because the stress

levels for our creep ruptures were all within several percents of one another, this may not be a negligible quantity. Care should be taken to minimize any machine vibration.

Occasionally a concern is raised regarding the variation in applied stress of the lever arm creep machines as the specimen elongates and permits the lever arm to droop. Measurements taken on the Budd machine were used to determine the maximum error associated with this aspect. For a specimen elongation of 0.5", the lever arm rotates 10° and the load drops 5". Based on simple geometric considerations, the resulting deviation in the applied stress is only 0.03%--a negligible amount. As the effective lever arm of the applied load decreases with arm rotation, the effective lever arm of the specimen load train decreases by an almost identical proportion.

SECURITY CLASSIFICATION OF THIS PAGE *(When Data Entered)*

REPORT DOCUMENTATION PAGE		READ INSTRUCTIONS BEFORE COMPLETING FORM
1. REPORT NUMBER VPI-E-81-3	2. GOVT ACCESSION NO.	3. RECIPIENT'S CATALOG NUMBER
4. TITLE *(and Subtitle)* Creep and Creep Rupture of Laminated Graphite/ Epoxy Composites		5. TYPE OF REPORT & PERIOD COVERED 6. PERFORMING ORG. REPORT NUMBER
7. AUTHOR(s) Dillard, D. A. Morris, D. H. Brinson, H. F.		8. CONTRACT OR GRANT NUMBER(s)
9. PERFORMING ORGANIZATION NAME AND ADDRESS Department of Engineering Science and Mechanics Virginia Polytechnic Institute and State Univ. Blacksburg, VA 24061		10. PROGRAM ELEMENT, PROJECT, TASK AREA & WORK UNIT NUMBERS
11. CONTROLLING OFFICE NAME AND ADDRESS NASA-Ames Materials Science and Applications Office Ames Research Center, 240-3, Moffett Field, CA 94035		12. REPORT DATE March 1981 13. NUMBER OF PAGES 228
14. MONITORING AGENCY NAME & ADDRESS*(if different from Controlling Office)*		15. SECURITY CLASS. *(of this report)* Unclassified 15a. DECLASSIFICATION/DOWNGRADING SCHEDULE

16. DISTRIBUTION STATEMENT *(of this Report)*

Approved for public release; distribution unlimited.

17. DISTRIBUTION STATEMENT *(of the abstract entered in Block 20, if different from Report)*

Approved for public release; distribution unlimited.

18. SUPPLEMENTARY NOTES

19. KEY WORDS *(Continue on reverse side if necessary and identify by block number)*

Graphite/Epoxy, laminates, non-linear viscoelasticity, creep testing, creep rupture, accelerated characterization

20. ABSTRACT *(Continue on reverse side if necessary and identify by block number)*

Laminated fiber reinforced composite materials such as Graphite/Epoxy are generally designed using elastic consideartions. Although graphite fibers are essentially elastic, the epoxy matrix behaves in a viscoelastic manner. The resulting Graphite/Epoxy composite material exhibits creep and delayed failures. Time dependent processes which are quite slow at room temperature are accelerated by higher temperatures and other factors. Assuming the applicability of the Time Temperature Superposition Principle (TTSP) concept, short term experimental creep compliance and creep rupture data should be useful in

DD FORM 1 JAN 73 1473 EDITION OF 1 NOV 65 IS OBSOLETE

SECURITY CLASSIFICATION OF THIS PAGE *(When Data Entered)*

Item 20 (continued)

predicting the long term behavior of laminates at lower temperatures. Such an accelerated characterization procedure should have an impact on the design of laminated composite structures where combinations of temperature, moisture content, applied stress level, and duration of load application may necessitate the use of a time dependent analysis.

An incremental numberical procedure based on lamination theory is developed to predict creep and creep rupture of general laminates. Existing unidirectional creep compliance and delayed failure data is used to develop analytical models for lamina response. The compliance model is based on a procedure proposed by Findley which incorporates the power law for creep into a nonlinear constitutive relationship. The matrix octahedral shear stress is assumed to control the stress interaction effect. A modified superposition principle is used to account for the varying stress level effect on the creep strain. The lamina failure model is based on a modification of the Tsai-Hill theory which includes the time dependent creep rupture strength. A linear cumulative damage law is used to monitor the remaining lifetime in each ply.

Creep compliance and delayed failure data is presented for several general laminates along with the numerical predictions. Typical failure zone pictures are also given. The compliance predictions for matrix dominated laminates indicate reasonable agreement with the experimental data at various stress levels. Predictions for fiber dominated laminates are erroneously bounded by lamination theory assumptions. Failure predictions are of the right magnitude but are not in exact agreement. Reasons for these discrepancies are presented, along with recommendations for improving the models and the numerical procedure.

End of Document